TÉCNICO LISBOA

UNIVERSIDADE DE LISBOA
INSTITUTO SUPERIOR TÉCNICO

Tuning extracellular cues to regulate epithelial cell phenotype

Maria João Pardelha da Cruz

Supervisor: **Doctor** Cláudia Alexandra Martins Lobato da Silva
Co-Supervisor: **Doctor** Molly Morag Stevens

Thesis approved in public session to obtain the PhD Degree in
Bioengineering

Jury final classification
Pass with Distinction

2020

TÉCNICO LISBOA

UNIVERSIDADE DE LISBOA
INSTITUTO SUPERIOR TÉCNICO

Tuning extracellular cues to regulate epithelial cell phenotype

Maria João Pardelha da Cruz

Supervisor: **Doctor** Cláudia Alexandra Martins Lobato da Silva
Co-Supervisor: **Doctor** Molly Morag Stevens

Thesis approved in public session to obtain the PhD Degree in
Bioengineering

Jury final classification
Pass with Distinction

Jury

Chairperson: Doctor Joaquim Manuel Sampaio Cabral, Instituto Superior Técnico, Universidade de Lisboa

Members of the Committee:
Doctor Molly Morag Stevens, Faculty of Engineering, Imperial College London; UK
Doctor Joaquim Manuel Sampaio Cabral, Instituto Superior Técnico, Universidade de Lisboa
Doctor Lino da Silva Ferreira, Faculdade de Medicina, Universidade de Coimbra
Doctor Cristina Maria Santos Alves de Carvalho Barrias, INEB-Instituto Nacional de Engenharia Biomédica
Doctor Maria Margarida Fonseca Rodrigues Diogo, Instituto Superior Técnico, Universidade de Lisboa

Funding Institution
Fundação para a Ciência e a Tecnologia

2020

Abstract

Epithelial cells form very cohesive sheets that line all surfaces of our bodies and mainly act as a selective barrier, supporting nutrient and water transport while preventing the entry of external insults. In addition, cells can sense and respond to the biophysical and biochemical cues from the surrounding extracellular milieu. In this thesis, the regulation of important aspects of mammary epithelial cell behaviour by different external stimuli is investigated.

A hallmark of invasive carcinomas is the breaching of the basement membrane, in which transformed cells migrate from the epithelial compartment to the interstitial matrix, thereby acquiring the potential to metastasise. In this PhD thesis, human mammary epithelial (MCF10A) cells are exposed to components of the basement membrane, which support epithelial tissue architecture, and to increasing concentrations of stromal collagen in a three-dimensional morphogenesis assay, which lead to a matrix collagen-induced invasive phenotype. Since these phenotypical changes highly resemble a process termed epithelial-mesenchymal transition (EMT), this cellular programme is comprehensively characterised by employing biomolecular tools (gene and protein expression), microscopy and Raman spectroscopy.

Dysregulated EMT can contribute to the development and progression of disease, namely fibrosis and cancer. In this work, MCF10A cells undergoing EMT, in response to transforming growth factor β1 treatment or to stromal collagen, are exposed to a biologically-active fragment from the β1-chain of laminin-111 to investigate whether this cryptic extracellular matrix (ECM) fragment can be used to modulate this cellular process. Exposure of these epithelial cells to this fragment via soluble and biomaterial-based approaches is investigated by measuring EMT gene expression and cell invasion. The interaction between this fragment and potential binding partners is also assessed. Studying the modulation of EMT by using an ECM fragment can provide important insight into molecular mechanisms of this cellular transition in the context of pathogenesis, and potentially open new research avenues that make use of bioactive molecules in the ECM that can be released by proteolysis.

Endogenous electric fields are essential in the physiological processes of all living organisms, namely in controlling fundamental cellular functions, such as morphology, gene expression, proliferation, and migration. However, little is known about the mechanisms that allow cells to sense and respond to an electric field. In this work, the biomechanical response of MCF10A cells exposed to an external electrical stimulation (ES) via a biocompatible, conducting polymer (polypyrrole) is carried out. By

synergistically combining scanning ion conductance microscopy (SICM), atomic force microscopy (AFM) and molecular biology tools, a highly-sensitive characterisation of how mammary epithelial cells sense and respond to ES was carried out. These findings can potentially shed light on how these cells sense and mediate electrical cues, and how ES affect cell fate.

Keywords: mammary epithelial MCF10A cells; extracellular matrix (ECM); epithelial-mesenchymal transition (EMT); laminin fragment; electrical stimulation.

Resumo

As células epiteliais formam camadas coesas que revestem todas as superfícies do nosso corpo e actuam principalmente como uma barreira seletiva, a qual permite o transporte de nutrientes e água, enquanto evita a entrada de agentes nocivos externos. Adicionalmente, as células têm a capacidade de detectar e responder a estímulos biofísicos e bioquímicos provenientes do meio extracelular. Nesta tese, é investigada a regulação de aspectos fundamentais do comportamento de células epiteliais mamárias por manipulação de factores bioquímicos e biofísicos do ambiente extracelular.

Uma das principais características dos carcinomas invasivos é a infiltração da matriz intersticial por parte de células transformadas que provêm do compartimento epitelial, adquirindo assim o potencial de metastatizar. Neste trabalho, células epiteliais mamárias humanas (MCF10A) são expostas a componentes da membrana basal, que fornecem os elementos necessários para a arquitetura adequada do tecido epitelial, e a concentrações incrementais de colagénio estromal num modelo de morfogénese tridimensional, resultando num fenótipo invasivo induzido pela presença do colagénio na matriz. Uma vez que estas alterações fenotípicas se assemelham a um processo denominado por transição epitélio-mesenquimal (EMT), diversas ferramentas biomoleculares para medição da expressão de genes e proteínas, assim como microscopia e espectroscopia Raman, são utilizadas para caracterizar este programa celular.

A desregulação do processo de EMT pode contribuir para o desenvolvimento e progressão de doenças, nomeadamente fibrose e cancro. Neste trabalho, células MCF10A submetidas a EMT, em resposta ao tratamento com *transforming growth factor* β1 (TGF-β1) ou à presença de colagénio estromal, são expostas a um fragmento biologicamente activo da cadeia β1 da laminina-111 para investigar se o mesmo pode ser usado para modular este processo celular. A exposição destas células epiteliais ao fragmento, utilizando diferentes estratégias, como factor solúvel ou imobilizado em biomateriais, é estudada com base na expressão de genes associados ao processo de EMT e na capacidade de invasão celular. A interação entre este fragmento e potenciais ligandos é também avaliada. O estudo da modulação de EMT utilizando o fragmento de laminina pode fornecer informações importantes sobre o mecanismo molecular desta transição celular no contexto de patogénese e, potencialmente, abrir novas vias de investigação que fazem uso de moléculas bioativas que podem ser libertadas pela matriz extracelular por proteólise.

Os campos elétricos endógenos são essenciais aos processos fisiológicos de todos os organismos,

nomeadamente no controlo de aspetos fundamentais do comportamento celular, como morfologia, expressão de genes, proliferação e migração. No entanto, pouco se sabe sobre os mecanismos que permitem que células detectem e respondam a campos electrics. Neste trabalho, é estudada a resposta biomecânica de células MCF10A expostas a uma estimulação elétrica (ES) externa através de um polímero condutor (polipirrol) biocompatível. Ao combinar sinergisticamente técnicas de microscopia de varrimento por conductância iónica (SICM), microscopia de força atómica (AFM) e ferramentas de biologia molecular, é possível alcançar uma caracterização com resolução temporal e espacial de como células epiteliais mamárias recebem e respondem a sinais de ES. Estes resultados poderão ajudar a compreender de que forma a ES altera o comportamento celular aquando da utilização de sinais elétricos em aplicações biomédicas.

Palavras-chave: células epiteliais mamárias MCF10A; matriz extracellular; transição epitélio-mesenquimal; fragmento de laminina; estimulação elétrica.

Acknowledgments

Completing this PhD would not have been possible without the help and support I have received along the way from many people. First, I want to thank Molly and Prof. Cláudia for all the encouragement, support, and trust in my work at every step.

The people within the Stevens group are very special and have made my time in the lab so enjoyable and I will leave with so many amazing memories. Liliana, Valeria, Camille, Arianna, Lucia, Maxine, Marta, Charlotte, Joyce, Alessandra, Håkon, Marco, Michele, and Mike - thank you for everything. I love and admire you all. Not only have I made great friends but I also had the opportunity to work with and learn from many wonderful, talented and incredibly intelligent colleagues. Amongst those, I would like to especially thank Tim, Anika, Spence, Amy, Dan, Isaac, Sahana, Conor, Liliang, James, Jono, Ben and Marta, who have contributed tremendously to this work. I also have to thank TEAtime and BioBio subgroups for all the helpful discussions and suggestions.

My family - my brother, Pedro, my sister in law, Susana, my little nephews, Gabriel and Gustavo, my uncle and aunt, António and Fátima, my cousins, David and Ricardo, and my grandparents, Gertrudes e Dimas - contributed more to this work than they know or can imagine. Thank you for your continuous and unconditional support. I love you more than what I can describe with words.

Luís, my boyfriend, partner, fiancé, and best friend - the words 'thank you' cannot even begin to describe how grateful I am to have you in my life, but I will try to say something. Thank you for your patience. I know it wasn't easy to put up with me during stressful times. Thank you for your support. Thank you for always believing in me - more than I ever did, really. You are the reason I never gave up. You are the reason I am still standing. You are my home. I love you. I also need to thank Nala, our fur baby, for giving me a reason to smile every single day since I laid my eyes on her, even at the end of the most frustrating days in the lab. Thank you for teaching and reminding me every day to appreciate the little things.

Now the hardest part - thanking the two most important people in my life who are not actually here to read this. My parents, Inácia and Zé. Thank you for the life you gave me. Thank you for being my biggest supporters (and critics). I miss you every waking moment. You are always with me in my thoughts. Life is not fair, but it is worth living.

I have no special talent. I am only passionately curious.

Albert Einstein

Contents

List of Figures

List of Tables

List of Abbreviations

2D	Two-dimensional
3D	Three-dimensional
AFM	Atomic Force Microscopy
BLI	Bio-Layer Interferometry
BM	Basement Membrane
BMP	Bone Morphogenetic Protein
Cy5	Cyanine 5
Cys	Cysteine
DBS	Dodecylbenzenesulfonate
DMSO	Dimethyl Sulfoxide
DoF	Degree of Functionalisation
ECM	Extracellular Matrix
EHS	Engelbreth-Holm-Swarm
ELISA	Enzyme-Linked Immunosorbent Assay
EMT	Epithelial-Mesenchymal Transition
EMT-TFs	Epithelial-Mesenchymal Transition Transcription Factors
ES	Electrical Stimulation
FGF	Fibroblast Growth Factor
GelMA	Gelatin Methacryloyl
HEK	Human Embryonic Kidney
Lys	Lysine
LV	Latent Variable

MMP	Matrix Metalloproteinase
MWCO	Molecular Weight Cutt Off
PBS	Phosphate-Buffered Saline
NHS	N-Hydroxysuccinimide
PCA	Principle Component Analysis
PCL	poly(ϵ-caprolactone)
PDMS	Polydimethylsiloxane
PEG	Poly(ethylene glycol)
PLS-DA	Partial Least Square Regression Discriminant Analysis
PPy	Polypyrrole
rBM	Reconstituted Basement Membrane
ROI	Region Of Interest
RS	Raman Spectroscopy
RT-qPCR	Quantitative Reverse Transcription Polymerase Chain Reaction
SICM	Scanning Ion Conductance Microscopy
siRNA	Small Interference RNA
SPAAC	Strain-Promoted Azide–Alkyne Cycloaddition
TGF-β	Transforming Growth Factor β
WB	Western Blotting
WGA	Wheat Germ Agglutinin

1

Introduction

Contents

1.1 Epithelial Cells

The epithelium lines all surfaces of our bodies. The cells that compose the epithelium, epithelial cells, are a specialised component of many organs. Epithelial cells are arranged in cohesive sheets, which mainly function as a selective barrier between the body and its environment. Many of our major organs and tissues (e.g. kidney, lung, liver and breast) contain cavities lined by an epithelial sheet that can be arranged in a monolayer, in the case of simple epithelia, or in stratified layers, that selectively mediate the exchange of nutrients, hormones, ions, gases and cells between different parts of the body. These internal epithelial organs are typically made of two types of units: spherical cysts – also known as lobules in the mammary gland, alveoli in the lung and follicles in the thyroid – and tubules. Albeit differently shaped, cysts and tubules are composed of a polarised, lumen-enclosing monolayer of cells, and together form a complex network of tubular structures (Figure 1.1) [1].

In order to protect the integrity of these organ cavities and tissue compartments, epithelial cells rely on being tightly attached to their neighbouring cells, which is mediated by cell junctions, polarisation along their apicobasal axis, which is accomplished by unique membrane structural and functional domains. The apical membrane domain faces the lumen and contains the proteins that mediate numerous functions including absorption, secretion, transcellular transport, and sensation. The basal membrane domain interacts with the surrounding basement membrane (BM), a specialised subtype of extracellular matrix, and the lateral membrane domain is in direct contact with neighbouring epithelial cells (Figure 1.1). Since many proteins localise to both the basal and lateral domains, these surfaces are commonly collectively referred to as basolateral domain. In the case of stratified epithelial layers, some cells lack one or more surface types, depending whether they border a lumen and/or the BM.

The process of epithelial polarisation is closely associated with the formation of the apical junctional complex, which includes tight junctions (or zonula occludens) and adherens junctions (or zonula adherens) [2–4]. Tight junctions form a complex protein network that consists of transmembrane proteins and peripheral membrane proteins. Transmembrane proteins are composed of three main families: occludins [5], claudins [6] and junctional adhesion molecules [7]. Together, these proteins establish close contacts between epithelial cells, form an important selective barrier to diffusion through the intercellular space, and also prevent intramembrane diffusion of proteins and other macromolecules between the apical and basolateral membrane domains [8, 9]. Adherens junctions are the main contributor to the initiation and stabilisation of cell-cell adhesion between epithelial cells, and these include transmembrane glycoproteins of the classical cadherin superfamily, such as E-cadherin, and the catenin family, namely α and β-catenin [10].

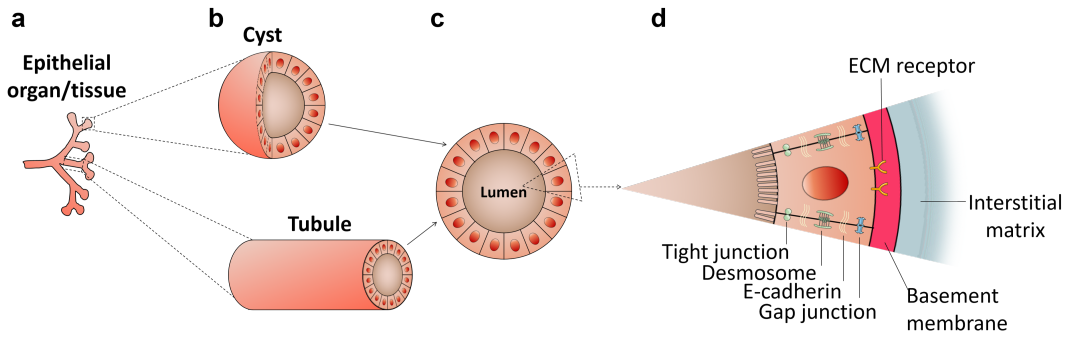

Figure 1.1: Epithelial architecture. **a** Internal epithelial organs typically consist of two types of units: spherical cysts and tubules (**b**). **c** Both structures consist of a polarised, lumen-enclosing monolayer of cells. **d** Each epithelial cell is in tight contact with its neighbouring cells, which is mediated by tight junctions, desmosomes, and E-cadherin interactions, on their lateral membrane domains. The apical membrane, a microvilli-rich domain, faces the lumen. The basal membrane domain faces the BM, which serves as a barrier between the epithelium and the interstitial matrix. Epithelial cells interact with the BM though integrin and non-integrin cell surface receptors. Adapted from [1].

1.2 Extracellular Matrix - Composition and Function

The extracellular matrix (ECM) is a highly dynamic structure that not only functions as a scaffold to provide physical support to the architecture and integrity of all tissues, but also regulates nearly every aspect of cell behaviour, including proliferation, migration, and differentiation. In mammals, the ECM is a complex assembly of around 300 proteins [11, 12], known as the core matrisome, which include collagens, proteoglycans and glycoproteins [13, 14]. The precise composition of the ECM varies from tissue to tissue to provide the appropriate architectural structure, stiffness and biochemical environment.

1.2.1 ECM composition

1.2.1.A Collagen

The main structural proteins of the ECM are collagens, the most abundant protein in mammals. There are 28 different types of collagen in vertebrates, which are classified into fibrillar and non-fibrillar forms. Collagens are composed of three polypeptide α chains and the most common structural feature amongst the members of this protein superfamily is the presence of three stranded helical segments [15]. The properties of each type of collagen will vary due to the arrangement of the triple-helical domains and the segments between, which produces different three-dimensional structures [16]. Collagens differ in the way they form fibres and how these fibres are then organised into net-

works. The type, cross-linking and orientation of collagen molecules vary according to the tissue type. For example, type I collagen molecules form fibrils (around 50 nm in diameter) that have great tensile strength, which are then packed in parallel bundles called fibres, can be found in tendons linking muscles and bones, where they have to withstand strong forces. Conversely, type IV collagen forms a sheet-like network and is one of the main components of the BM [15–17].

1.2.1.B Proteoglycans

Proteoglycans, which include aggrecan, versican, perlecan and decorin, are composed of a core protein domain that is covalently linked to long, negatively charged, linear chains of disaccharide units, called glycosaminoglycans (GAGs) [18]. The main biological function of proteoglycans relies on the biochemical and hydrodynamic characteristics of GAGs, which have a unique ability to bind water, providing hydration and compressive resistance to tissues [19].

1.2.1.C Glycoproteins

Glycoproteins, namely laminins, fibronectin, and vitronectin, consist of a core protein domain covalently bound to bulky, branched carbohydrates (or glycans) [20]. These important components function as connector molecules due to the ability of their functional groups to recognise and bind to other ECM proteins, growth factors and cell surface receptors [19].

1.2.1.D Laminins

Laminins are composed of α, β, and γ chains arranged in a triple α-helical coiled-coil domain towards the C-terminal of each chain, which can form cross-shaped (three arms), Y-shaped (two arms) and rod-shaped (one arm) structures [21]. Laminins are mainly found in the basal lamina of tissues and their primary role is to mediate interactions between cells via cell surface receptors, namely integrins, and various other components of the ECM. Different combinations of chain isoforms generate functional diversity of laminins, which are classified according to their subunit composition [22]. For example, $\alpha1\beta1\gamma1$ and $\alpha3\beta3\gamma2$ are known as laminin-111 (Figure 1.2**a**) and laminin-332, respectively, which exhibit very distinct functions. Whilst laminin-111 forms a meshwork that composes the BM (Figure 1.2**b**), laminin-332 is secreted during wound healing and hair follicle development and undergoes extensive specific proteolytic cleavage [23, 24].

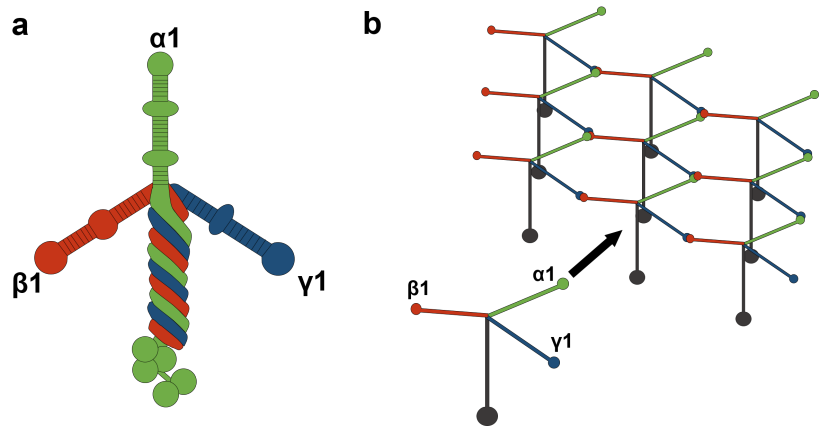

Figure 1.2: Laminin-111 structure and self-assembly. **a** Heterotrimeric laminin-111 is composed of α1, β1, and γ1 chains, which are arranged in a triple α-helical coiled-coil domain towards the C-terminal of each chain. The α1 chain uniquely contains five laminin G-like (LG) domains at its C-terminal. **b** The three-arm interaction model predicts that laminin-111 self-assembles by forming a network by the N-terminal domains of the α1, β1, and γ1 chains. **a** was adapted from [22] and **b** from [24].

1.2.2 ECM organisation

After intracellular synthesis, ECM components are secreted into the extracellular environment. There are two main types of ECM that differ in terms of composition and location in the body: the interstitial connective tissue matrix and the BM. The interstitial connective tissue matrix, which is mainly composed of type I collagen and fibronectin, compose the bulk of the ECM in the body and provides structural scaffolding and mechanical strength to tissues [25, 26]. The BM is a specialised form of sheet-like ECM that separates epithelial cells to underlying connective tissues, and it is mainly composed of type IV collagen, laminins, heparan sulfate proteoglycans and nidogen (or entactin), which are synthesised and secreted by epithelial cells [27–29]. BMs have a pivotal role in regulating epithelial cell behaviour, as they provide signals for apicobasal polarity establishment and maintenance, and for cell differentiation [30].

1.3 Cell-ECM Interactions

Far from being a static structure, the ECM continuously undergoes dynamic remodelling that involves matrix biosynthesis, secretion, assembly, modification and degradation [25]. In turn, the ECM plays a vital role in regulating several aspects of cell behaviour, including differentiation, proliferation, survival, polarity and migration [31]. This establishes a vital bidirectional and dynamic relationship between the cells and the ECM [32]. Both cellular behaviour and the ECM structure are context dependent and respond to biochemical and biophysical cues.

1.3.1 Biochemical cues

Cells attach to the ECM via cell surface receptors, namely integrins, discoidin domain receptors and syndecans [33–35]. Integrins, the major mammalian receptors for cell adhesion to the ECM, are a large family of transmembrane heterodimeric molecules that bind to specific motifs of ECM components and also interact with cytoskeletal proteins [36]. Their heterodimeric nature is due to the noncovalent association between α and β subunits. There are 8 β and 18 α subunits which combine to form a variety of at least 24 integrins, with distinct ligand-binding affinities and tissue specific expression [34, 37]. Both α and β subunits are composed of a large ectodomain, which binds to the ECM proteins, a single transmembrane helix domain and a short cytoplasmic domain, with the exception of β_4, which has a much larger cytoplasmic domain, that mediates interactions with the cytoskeleton [36]. Integrin receptors not only play an important role in mediating cell adhesion to the ECM, but also mediate signalling in two directions: 'outside-in' in which integrins transmit chemical signals into the cell from the extracellular environment, and 'inside-out' (a processed that is also termed activation) in which the affinity of integrins for their extracellular ligands can be increased upon binding of an intracellular activator, such as talin and kindlin, and consequently influence cell migration and ECM remodelling (Figure 1.3) [35–38]. Although these signalling pathways are conceptually defined separately, they are often closely related [39].

1.3.2 Biophysical cues

An ever-growing body of work has demonstrated that cells are capable of sensing external physical cues, such as stiffness and fluid shear stress, and convert them into biochemical signals. This sensing enables cells to adjust their behaviour according to external stimuli (e.g. proliferation, differentiation and migration) by a process commonly known as mechanotransduction [40–44]. Mechanical stim-

uli allosterically modulate the activity and function of 'mechanosensor' proteins inducing biochemical signalling cascades [45]. In 1993, Ning Wang et al. experimentally demonstrated for the first time that ECM integrins and focal adhesions (a multiprotein assembly of clustered integrins and intracellular components connected to the actin cytoskeleton) mediate the transmission of external mechanical forces to the cytoskeleton [46]. It is now well established that integrins and their associated adhesion signalling complexes are mechanosensitive [45, 47, 48]. Integrin-mediated adhesion to the ECM components starts with conformational changes that lead to their activation (aforementioned 'outside-in' signalling), which results in an increased ligand binding affinity [37] (Figure 1.3**a**). Once integrins are activated and bound to their ligands, they cluster (numerous ligands are multivalent, which contributes to integrin clustering) and recruit a multitude of signalling molecules at their cytoplasmic tail to assemble into focal adhesions, commonly termed integrin adhesome [48, 49]. There are three known categories of integrin adaptor proteins [50], although there is significant functional crossover: (1) adaptors that have a primarily structural function, which include talin [51], filamin and tensin [52], bind to F-actin, linking integrins to the cytoskeleton; (2) adaptors that have a scaffolding role by providing additional binding sites to focal adhesion proteins, such as kindlins 2 [53] and 3 [54] and paxillin [55]; and (3) adaptors that have a catalytic activity, namely focal adhesion kinase (FAK) [55, 56] and Src [57], which mediate the signal transduction pathways from the adhesion site. Among integrin-binding adaptor proteins, talins and kindlins are the only ones that have been described to be essential to integrin activation [38]. However, even though a direct interaction between kindlin 2 and F-actin has been shown [58], evidence so far describes an indispensable role for talin in force transmission to integrins, whereas kindlins may serve to stabilise adhesion through the regulation of actin dynamics [38]. Upon direct coupling between ECM components and the cell surface via integrins and focal adhesions, cells are able to channel mechanical information to the nucleus through the LINC (Linker of the Nucleoskeleton and Cytoskeleton) complex and alter gene expression [59].

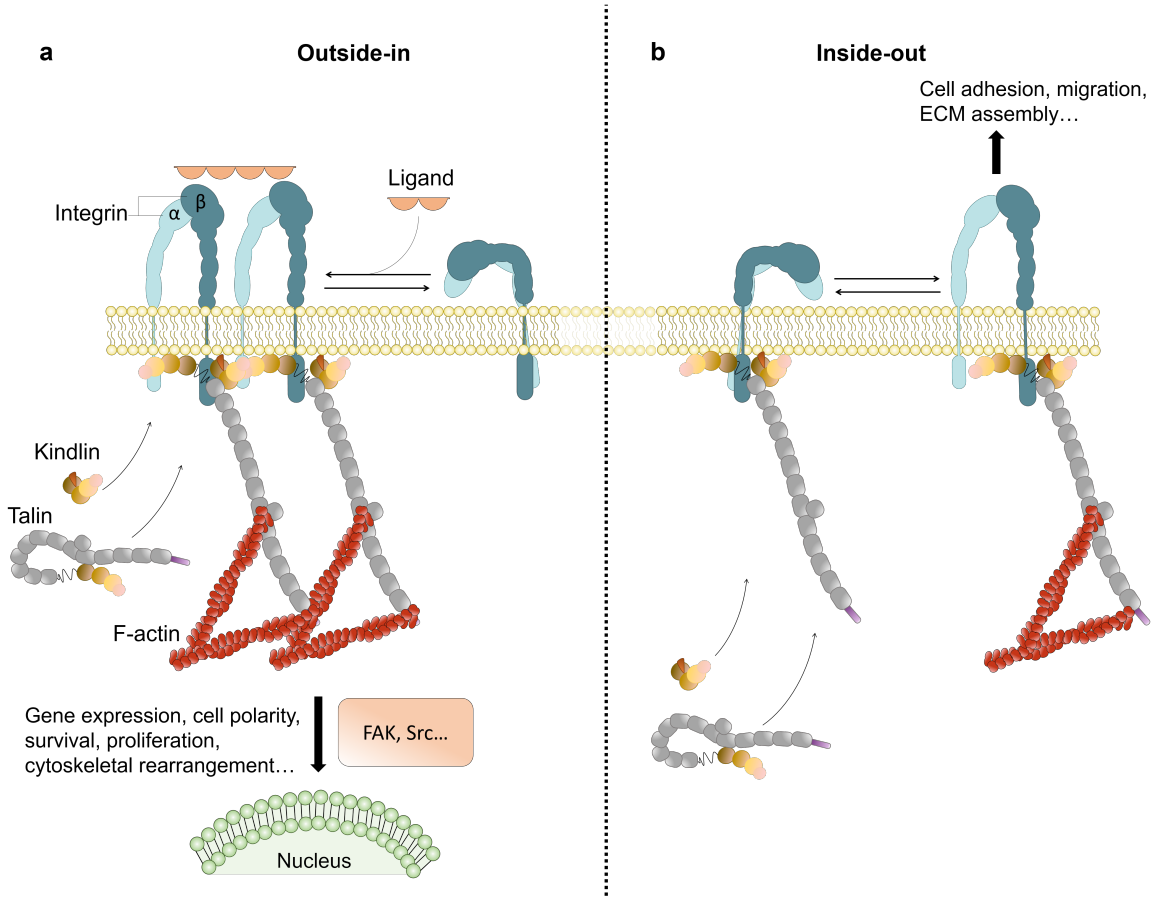

Figure 1.3: Bidirectionality of integrin signalling. Integrins mediate signalling in two directions: **a** 'outside-in' in which binding between ligands and integrins changes their conformation, resulting in their activation and clustering, which leads to the recruitment of integrin adaptor proteins to their cytoplasmic tail to assemble into focal adhesions and consequent transmission of signalling molecules that regulate gene expression, cell polarity, survival, proliferation, and cytoskeletal rearrangement, among others; and **b** 'inside-out' in which integrins can undergo conformational changes and become activated upon binding of an intracellular activator, such as talin and kindlin, to the β-integrin cytoplasmic tail and consequently influence cell adhesion, migration and ECM remodelling. Even though conceptually these signalling processes are defined separately, there is a strong crosstalk between them, as ligand-integrin binding can then result in inside-out signalling, and, conversely, inside-out integrin activation can increase ligand binding affinity. Adapted from [39] and [47]

1.4 ECM remodelling and homeostasis

The ECM is a highly dynamic and complex structure that is vital for organ development, wound healing and tissue homeostasis [31]. Indeed, cells are continuously rebuilding and remodelling the ECM by synthesising, degrading, reassembling and chemically modifying its components [26, 60, 61]. Additionally, the ECM acts as a reservoir of biologically active molecules, such as growth factors, including bone morphogenetic proteins (BMPs), epidermal growth factor (EGF), fibroblast growth factor (FGF), transforming growth factor-β (TGF-β), and other signalling molecules, such as Wnt proteins [26, 31]. It is essential that this dynamic relationship between cells and their surrounding extracellular matrix is tightly controlled. In fact, dysregulated ECM remodelling can result in pathological conditions such as fibrosis and cancer [62–64].

1.4.1 Key players in ECM breakdown

The proteolytic cleavage of ECM components constitutes the main mechanism by which the ECM is remodelled, and it can be carried out by different families of proteases, including matrix metalloproteinases, adamalysins, meprins, among others.

1.4.1.A Matrix metalloproteinases

Initially discovered in a 1962 study of collagen remodelling in tadpole tail during morphogenesis [65], matrix metalloproteinases (MMPs), a family of zinc-dependent endopeptidases [66, 67], are now recognised as the main matrix-degrading enzymes. Humans express 23 MMPs [68] and this family of proteinases, which exist as soluble or membrane-bound, can degrade a wide range of ECM components and other extracellular proteins [60]. All mammalian MMPs have a catalytic domain and a self-inhibitory pro-domain. The latter, located at the amino terminus, contains a conserved Cys residue of the cysteine-switch motif, which, together with the three His residues of the conserved active site motif, chelates the catalytic zinc ion, maintaining enzyme latency [69, 70]. The active site of the catalytic domain becomes available for proteolytic cleavage once the pro-domain is destabilised or removed [71]. Additionally, most MMPs also contain a hemopexin domain (a four-bladed β-propeller structure) connected to the carboxyl terminus by a flexible hinge linker [72]. The hemopexin domain plays an important role in mediating protein-protein interactions and in substrate recognition [73]. Activation of MMPs mainly occurs by proteolytic cleavage by serine proteases, membrane-bound MMPs (for example, latent soluble MMP-2 proenzyme is activated by MT1-MMP) or by other soluble MMPs

(for example, MMP-3 can activate the latent forms of MMP-1 and MMP-9) [74]. In addition to breaking down ECM structural components, MMPs can also cleave cell surface molecules and thus affect several aspects of cell behaviour, including apoptosis [75, 76]. Moreover, MMPs can create space for cells to migrate through the extracellular environment and produce fragments with independent biological activity [77], directly or indirectly alter the activity of signalling molecules and regulate tissue architecture [78]. Due to their pleiotropic nature and proteolytic activity, under normal conditions MMPs are expressed at low levels and the regulation of their localisation and activity is critical [79]. MMP expression and activity becomes elevated in diseased or inflamed tissue, namely in the case of malignant cancer and fibrosis, but also throughout wound healing processes [78].

1.4.1.B Adamalysins

The adamalysins protein family includes ADAMs (a disintegrin and metalloproteinases) [80] (reviewed in [81]) and ADAMTSs (ADAMs with a thrombospondin motif) [82], which, like MMPs, contain a zinc-dependent catalytic active site. ADAMs are membrane-anchored enzymes that modulate cell-cell and cell-ECM interactions by shedding various membrane-bound molecules and thereby releasing the ectodomain of cytokines, growth factors, transmembrane receptors and other adhesion molecules [83, 84]. As opposed to ADAMS, ADAMTSs are secreted enzymes capable of cleaving various extracellular molecules, namely aggrecan, versican and fibrillar procollagens (essential for deposition of normal collagen fibrils onto the extracellular environment in a tissue specific manner) [85]. Dysregulation of expression and function of ADAMs and ADAMTS is also linked with pathological conditions [84, 85].

1.4.1.C Meprins

Meprins are also zinc-endopeptidases that consist of two subunits (α and β) encoded by two separate genes [86]. Meprins can form disulphide-linked homo- or hetero-dimers [87, 88]. Meprin α is constitutively secreted into the extracellular space during its biosynthesis and maturation [89]. Meprin β is expressed as a transmembrane protein and acts as a 'sheddase' at the cell surface [90], but can also be released from the cell membrane by ADAM10 [91]. Meprin metalloproteases have an important role in fibrillar collagen deposition [92], and their overexpression has been associated with cancer and fibrosis [93].

1.4.1.D Metalloproteinase inhibitors

The proteolytic activity of the three families of metalloproteinases mentioned above needs to be tightly regulated in order to maintain tissue integrity. Such regulation can be achieved by the activity of endogenous inhibitors that can inactivate ECM proteases. The tissue inhibitor of metalloproteinases (TIMP) compose a family of four (TIMP1-4) and can reversibly inhibit the activity of MMPs, ADAMs and ADAMTSs [94, 95], but not of meprins. Cystatin C, Fetuin-A and elafin have been identified as endogenous inhibitors of human meprins [91, 96].

1.4.1.E Other enzymes

There are also other enzymes which play an important part in ECM remodelling, such as serine proteases, cathepsins, heparanases and sulphatases. Serine proteases include tissue-type plasminogen activator (tPA) and urokinase-type plasminogen activator (uPA), which catalyse the conversion of plasminogen into plasmin (also a serine protease) that, in turn, will degrade fibrin, fibronectin [97, 98] and laminin [99]. Cathepsins, which include cysteine, serine and aspartic cathepsins, are found both intracellularly, in the lysosomes where they can degrade internalised collagen, and extracellularly where they can degrade ECM proteins [100, 101]. Finally, heparanases and sulphatases are important regulators of the structure and function of heparan sulfate proteoglycans [102].

1.4.2 ECM remodelling in branching morphogenesis

During development, many organs and tissues, namely the lungs and the mammary and submandibular glands, are formed by a process termed epithelial branching morphogenesis (reviewed in [103]), wherein groups of cells increase their surface area by creating cellular or tissue extensions thereby forming tubular networks, which then contributes to establishing tissue architecture.

ECM remodelling plays an indispensable role throughout this process as it provides the necessary structural integrity, and the biochemical and biophysical cues that regulate and mediate cellular behaviours during morphogenesis [26, 60]. For example, in the mammary gland, type I collagen is found primarily around the duct and, before initiation of the branching process, its fibres are oriented to mediate an intracellular reorganization of the actomyosin cytoskeletal networks of epithelial cells [103, 104]. Moreover, the ECM at the tip is much thinner than that around the ducts, which is suggests that the ECM is cleaved at the leading edge of the branching epithelium to create space for cells to migrate [105, 106]. In fact, various types of metalloproteinases are expressed during branching of

the mammary epithelium [107–112]. MMP activity has been shown to be required for branching morphogenesis of primary mammary organoids *in vitro* [113] and defects in primary branching has been observed in *Mmp2-null* mice [114].

Importantly, as the ECM also serves as a ligand reservoir by selectively binding to various growth factors, these signalling molecules can be proteolytically released and thereby affect epithelial cell proliferation, orientation and migration during branching morphogenesis [31]. For example, the FGF signalling is crucial for vertebrate organ development, including the mammary gland [115]. This family of growth factors comprises 22 members and the majority of FGFs functions by binding to heparan sulphate proteoglycans with varying affinity, which regulates different aspects of epithelial morphogenesis [116]. In particular, FGF receptor 2 (FGFR2) expression is essential for regulating mammary gland development, as demonstrated by mammary epithelial cells lacking *Fgfr2* failing to regenerate the gland *in vitro* [117]. The different isoforms of FGFR2 are expressed in a context dependent manner, and FGFR2b has been shown to be preferentially expressed in epithelial tissues [118, 119]. FGF10, which binds to FGFR2b [120], has been identified as a key player in mammary epithelium branch initiation, which relies on properly oriented epithelial cell migration by ECM cleavage [117].

While there is still an increasing body of evidence highlighting the key players in the remodelling of the ECM during branching morphogenesis, there is no doubt that biosynthesis, deposition, orientation and degradation of specific ECM components are essential to generate a functional epithelial branching network.

1.4.3 ECM remodelling and disease

ECM remodelling needs to be tightly regulated, particularly throughout wound healing and developmental processes, in which signalling events and diverse cell behaviours are dynamic and transient [121, 122]. However, despite the existence of several regulatory mechanisms, ECM dynamics and remodelling can go awry and lead to pathological conditions, such as cancer and fibrosis, in which excessive deposition of ECM components is observed [63, 123].

1.4.3.A Fibrosis

In a healthy state, tissue-resident fibroblasts are quiescent, albeit metabolically active and supporting the structure and function of the local tissue. When repair mechanisms are necessary, these fibroblasts are activated and differentiate into myofibroblasts, which are responsible for depositing ECM components that will contribute to contracture and closure of the existing wound [124]. Fibrosis is the

result of a reparative process in response to chronic or severe tissue injuries, in which there is an excessive deposition of ECM components. Progressive fibrotic disease can be caused by a number of conditions, such as persistent infections, chronic inflammation, repeated exposure to toxins, myocardial infarction, amongst others [125]. Importantly, irrespective of the initiating trigger, a common feature of aberrant healing is the activation of hyperproliferating fibroblasts that then differentiate into myofibroblasts, which excessively synthesise and secrete ECM components, like collagen [126]. Excessive ECM deposition and cross-linking can lead to altered biochemical and biomechanical tissue properties (e.g. increased tissue stiffness), resulting in organ failure and, eventually, death.

The TGF-β pathway is likely the most comprehensively studied driver of fibrosis [127]. Early responders to the wound healing process, macrophages, are major contributors to local increase in TGF-β levels [128], which then promote fibroblast-to-myofibroblast transition, further increasing ECM production (Figure 1.4) [129]. TGF-β1 signalling pathway promotes the expression of over 60 ECM genes [130] and is correlated with progressive fibrosis in various organs, including liver, lung, kidney, skin and heart [131]. Moreover, significantly reduced development in fibrosis has been demonstrated by specifically inhibiting this pathway [132]. Besides regulating fibrosis, TGF-β is a ubiquitous cytokine that has a pleiotropic role in various processes that regulate cellular and tissue homeostasis [133].

Interestingly, a fibrotic ECM itself can act as a driver of fibrosis, by stimulating production and secretion of ECM components by myofibroblasts, generating a positive feedback loop [134]. Though traditionally viewed as a result of fibrotic disease, an increasing body of evidence has suggested that ECM stiffness plays a critical role in mediating fibrosis [135]. In fact, it has been shown that fibroblasts are highly sensitive to changes in tissue mechanics [136] and that an increase in matrix stiffness can mechanically activate myofibroblasts, thereby further exacerbating fibrosis [137]. Collectively, these studies demonstrate that ECM components can actively drive fibrosis.

1.4.3.B Cancer

In a balanced and healthy state, the ECM provides the appropriate biochemical and biophysical signals to maintain tissue homeostasis and architecture, which involves maintenance of epithelial cell polarity, and control of cell proliferation and apoptosis. In 2011, a seminal review by Mina J. Bissell and William C. Hines proposed an important role for the extracellular environment in stopping cancer from progressing [138]. They suggested that under normal conditions, the ECM is sufficient to suppress tumorigenesis. In contrast, once the barrier to tumour formation is overcome by various factors (or a combination), such as mutagens, inflammation and abnormally expressed growth factors, the microenvironment can be permissive to tumour growth and cancer progression. For example, studies

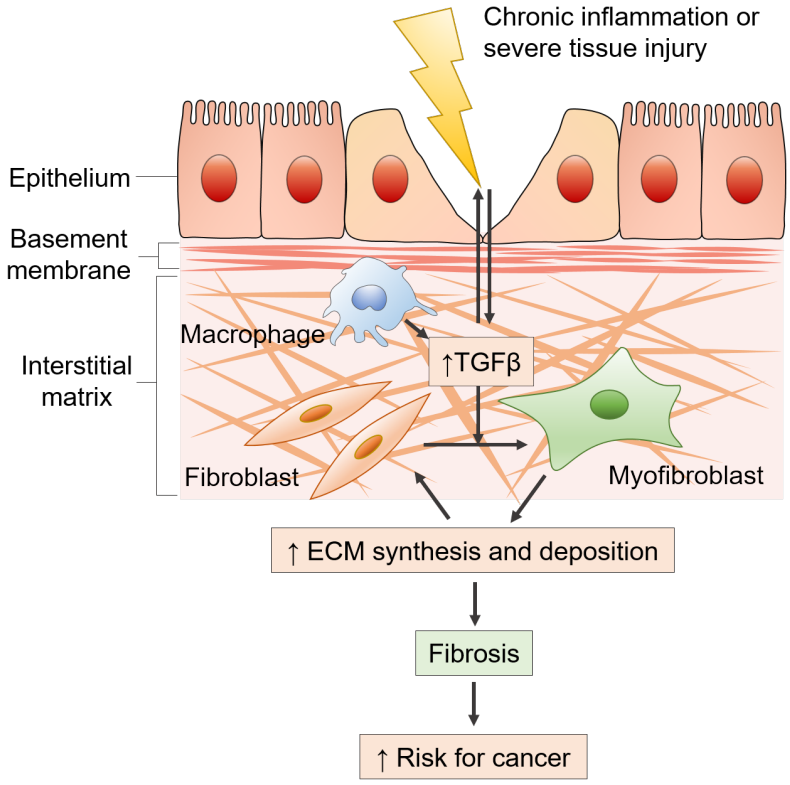

Figure 1.4: Aberrant ECM remodelling can result in pathological conditions, such as cancer and fibrosis. In the event of chronic inflammation or tissue injury, early responders to the wound healing process, macrophages, are major contributors to local increase in TGF-β levels, promoting fibroblast-to-myofibroblast transition, which are the main ECM producers. Excessive ECM production and deposition, through a positive feedback loop, further stimulates fibroblasts, resulting in progressive fibrotic disease, which, in turn, is a major risk for developing cancer. Adapted from [26].

have shown that different types of breast cancer can be classified based on their ECM gene expression signature, which can provide important information for prognosis [139]. This evidence strongly highlights the existence of a link between clinical outcomes and cancer ECM characteristics.

Due to the dynamic and intricate relationship between cells and their surrounding environment, it is not surprising that the ECM, with its plethora of biochemical and biophysical signals, plays a crucial role in cancer progression [140]. Cancer progression is complex and the tumour ECM is continuously remodelled as it develops [141]. It is well established in the cancer field that an abnormal ECM can promote and drive malignancy [142]. However, it is interesting to note that through a positive feedback mechanism cancer cells are capable of utilising and manipulating their microenvironment to enhance survival [143]. For example, ECM stiffness can affect the way the cancer responds to treatment potentially by forming a barrier that limits the access of chemotherapeutic agents [144, 145], and is a driving force in metastasis [146, 147]. ECM stiffening is mainly caused by increased deposition of collagen and its crosslinking, mediated by lysyl oxidase (LOX) and LOX-like enzymes

[148, 149], which drives malignant progression by disrupting tissue architecture [150]. In fact, LOX-mediated collagen crosslinking has been shown to promote invasion and breast cancer progression [151] and, in addition, high LOX expression has been shown to be correlated with poor response to therapy and patient survival [152, 153]. Targeting LOX to inhibit cancer progression seems to be an encouraging therapeutic approach. However, despite promising results from preclinical *in vivo* experiments [154, 155], it still remains unknown whether targeting LOX in human patients can be therapeutic. A first-in-human study has been performed in 2010 that aimed at evaluating how adults with advanced solid tumours tolerated a drug targeting LOX [156], but the results are still unknown. Nevertheless, it is important to keep in mind that targeting a single molecule, when our bodies have compensation mechanisms, might result in drug resistance.

Considering that around 90% of human cancers are derived from epithelia [157], a particularly relevant example to illustrate the cross-talk between ECM composition and cell behaviour is the important of the biochemical signalling provided to epithelial cells by the BM. As previously discussed in this chapter, the BM is crucial for controlling and maintaining apicobasal polarity. Thus, alterations in the composition of the BM can result in alterations of its biomechanical properties, and thereby affecting cell behaviour. In fact, altered spatial distribution of cell-surface receptors has been shown to promote epithelial cell proliferation and tumorigenesis [158]. Subsequently, tumour cells have to be able to cross the BM during metastatic progression, through a process that has long been hypothesised to require ECM degradation by MMPs. However, cells can use both proteolytic and non-proteolytic mechanisms to squeeze and migrate through the ECM [159]. Remarkably, it has been demonstrated that cells that are genotypically tumorigenic can behave in a phenotypically normal way when grown within a normal microenvironment context [160, 161]. Given how actively cancer ECM is remodelled, the idea of targeting the cancer microenvironment, considering both biochemical and biomechanical cues, has gained attention by the bioengineering community and it has opened research avenues that are shedding light into the mechanisms of cancer progression and potentially new therapeutic targets.

1.5 Modelling mammary epithelial cells *in vitro*

As mentioned in Section 1.1, epithelial cells are characterised by an apicobasal polarised morphology, tightly attached to their neighbouring cells by specialised cell-cell adhesive contacts, arranged in cohesive sheets that protect our bodies from external insults, and attached to an underlying BM. This highly organised architecture is essential for tissue homeostasis and when its disruption leads to pathological conditions.

1.5.1 Structure of the mammary epithelium

Normal mammary epithelium is composed of ducts (tubules) that connect the functional glandular units, lobules (or cysts), to the nipple. This now well-established branched organisation of the mammary gland with lobular and tubular structures was first described by the anatomist Sir Astley Paston Cooper in 1840 [162]. These structures are organised in a bilayer: a layer of luminal secretory cells that surrounds a hollow lumen, and a surrounding layer of basal myoepithelial cells that lie in direct contact with the BM [163]. Unlike other tissues in the human body, the mammary branching morphogenesis, which starts during fetal development, pauses after birth and restarts during adolescence in response to oestrogen signalling [164]. In addition, this tissue undergoes extensive remodelling during pregnancy, lactation and involution [165, 166]. Moreover, even though to a lesser extent, modifications to the mammary tissue also occur during the menstrual cycle [167]. Understanding the mechanisms underlying cell behaviour in a healthy, normal context is of utmost importance for understanding of alterations and disruptions that lead to a diseased state. The unique complexity in the development and regulation of the mammary gland, in addition to the fact that breast cancer is the leading cause of cancer related death for women worldwide [168], makes it a good tissue target for the development of new culture systems and devices that can recapitulate the level of structural and biochemical complexity found *in vivo*.

1.5.2 Modelling mammary glandular epithelium

A large body of studies has focused on pathobiology of the breast have been conducted using *in vivo* mouse models [169] and *ex vivo* primary human tissues [170]. These have undoubtedly been instrumental in providing information on the genetic and other mechanistic events in pathogenesis of the mammary glandular epithelium, particularly from a histopathological perspective. However, while using mouse models can capture the physiological complexity found *in vivo*, they might misrepresent

what would happen within the human body due to species-specific differences. In addition, the use of vertebrate animals for scientific research imposes ethical constraints, which can be largely overcome by the use of *in vitro* systems. Finally, both primary human tissues and mouse models are relatively limiting for studying biochemical and cellular mechanisms of disease initiation, particularly when trying to manipulate the microenvironment and cell-ECM interactions. Cell culture models, together with biomaterial systems, can potentially be employed to answer remaining questions, and the development of such techniques is a now a major focus of research.

1.5.2.A Epithelial culture models

Madin-Darby canine kidney cells

Non-transformed epithelial Madin-Darby canine kidney (MDCK) cells [171] are widely used as models for studying epithelia, as they can develop a clear apicobasal polarity, have a fast growth rate, and are a tractable model for studying diverse biological processes and epithelial junctions [172–175]. In addition, these cells have been shown to develop polarised cysts (acini) enclosing a hollow lumen when cultured within matrices containing type I collagen [176, 177], in contrast with other epithelial cells that cannot form acini within fibrillar collagen [178]. Nevertheless, this cell line was also instrumental in demonstrating the importance of a laminin-rich matrix for proper establishment of apicobasal polarity during acini formation [179]. The main disadvantage in using this cell line as an epithelial model is perhaps its canine origin.

MCF10A mammary epithelial cells

The spontaneously immortalised, non-transformed human mammary epithelial cell line MCF10A is likely the most commonly used cell model to study and characterise developmental and pathological events of breast glandular structures. MCF10A cells were derived from a benign proliferative fibrocystic breast tissue of a 36-year-old patient [180]. These cells are a good model to study mammary epithelial cells as, like normal breast epithelium, they are not tumorigenic, grow in an anchorage-dependent manner, need growth factors and hormones for proliferation and survival [180], and express wild-type *p53* [181]. Notably, MCF10A are capable of forming acinar structures when cultured in reconstituted BM, with characteristics that are also found in normal glandular epithelium, namely low proliferation levels, and their acinar dimensions and cell number remain relatively stable in culture [182, 183]. This low proliferation seen in MCF10A acinar structures is extremely important to study morphogenesis and to investigate the effect of introducing genetic alterations, particularly oncogenes. However, it is important to recognise the limitations of using this cell line as a mammary epithelial

model. First, during immortalisation and long-term *in vitro* culture, these cells have lost the architectural signals they received in the *in vivo* tissue and have undergone epigenetic changes [184]. Second, these cells have genetic abnormalities commonly associated with cultured mammary epithelial cells, including deletion of the locus containing *p16* and *p14ARF*, and *MYC* amplification [185–187]. Nevertheless, the formation of acinar structures by MCF10A cells within reconstituted BM makes them an invaluable model to investigate biological properties of the mammary glandular epithelium.

Human mammary epithelial cells

Isolation and culture of Human Mammary Epithelial Cells (HuMEC) was first described in 1980 [188, 189]. Since then, significant efforts towards optimising the protocols and techniques used in isolation, culture and characterisation of these cells have been made [190–195]. Importantly, early cultures derived from reduction mammoplasties (primary breast cancer cells, in contrast, are typically derived from mastectomies) consist of a heterogeneous cell population, including luminal, basal, myoepithelial and stem cells. The differentiated subpopulations of cells have a limited life span before becoming senescent [196]. Therefore, techniques aiming at isolating cell subpopulations based on differential expression of cell surface markers or by functional differences are broadly used [190, 197]. Additionally, HuMEC can also be immortalised so researchers can use them in long-term studies [198–200], however the major drawback of this process is that it induces chromosomal changes, which can generate subpopulations of cells that are no longer representative of the tissue of origin [201].

1.5.2.B *In vitro* culture systems

Since the foundations of cell culture were laid in 1885 by Wilhelm Roux with his work on chick embryos [202] (over 200 years after the term 'cell' was coined and used for the first time by Robert Hooke) and the work of Ross Harrison and colleagues in 1907 establishing cell culture methods for the first time using frog nervous tissue [203], substantial progress has been made in developing and optimising cell and tissue culture techniques that have allowed to uncover an ever-increasing number of biophysical and molecular mechanisms that regulate cell and tissue biology.

Cell culture is a routinely-used and indispensable tool for improving our understanding of cell behaviour in development, homeostasis and disease. Experiments can be conducted using primary cells isolated directly from tissues, or using established cell lines deposited in cell banks [204]. Two-dimensional (2D) cell culture systems have been primarily used to date, but, since we entered the new millennium, a paradigm shift occurred to promote the development and improvement of three-

dimensional (3D) systems to try overcome the shortcomings of 2D culture [205].

2D cultures

In conventional adherent 2D cultures, cells grow as a monolayer on a flat surface, typically in polystyrene culture flasks, plates or Petri dishes (Figure 1.5**a** left). 2D culture platforms are still widely used mainly due to being well established, simple, conceptually easy, convenient, efficient, and fairly inexpensive (when compared to other systems). In addition, experimental assays carried out in 2D are also typically simpler to observe, measure and analyse with most commonly used tools compared to 3D culture methods. However, while they can be extremely useful to investigate certain cell behaviours and suited for high-throughput platforms, it is widely recognised that 2D models do not recapitulate the complex natural structure of tissues (or tumours) [206–213]. When cells are isolated to be grown on a plastic or glass surface as monolayers, the cell-cell and cell-ECM interactions that take place *in vitro* cannot mimic the *in vivo* environment [214, 215]. In addition to the differences in spatial arrangements of cells in 2D or 3D, there are several biological differences that affect diverse aspects of cell behaviour, such as gene expression [216–218], cell shape and polarity [219–222], growth [223–226], motility [227–230] and differentiation [231–233]. Furthermore, the substrate stiffness significantly impacts how cells respond to their microenvironment [234]. Epithelial cells, in particular, characterised by their normal arrangement in cohesive cell sheets by tight cell-cell adhesion contacts and apicobasal polarity, when grown on stiff substrates, lose their typical tissue architecture, as they flatten and lose their differentiation markers [235]. It is possible to employ various techniques to overcome certain limitations of 2D cultures without having to move towards 3D, namely by making use of coatings (biological matrices or synthetic polymers), which can be multi-layered and their stiffness can potentially be tuned [236, 237], and by engineering the 2D surface using micro-patterning techniques to create different topographies, which can also be achieved using various biomaterials [238–240]. Since mammary epithelial cells in the gland are organised as a monolayer contacting the BM, they can potentially be grown on 2D surfaces *in vitro* on a substrate that is similar to the BM, in regards to composition and stiffness, while exhibiting normal and differentiated epithelial cell function [212]. Nevertheless, there is a need to develop and improve 3D culture models that better mimic conditions *in vivo*.

3D cultures

In 1997, a landmark article by Mina J. Bissell's group, a pioneer of 3D culture, was published showing that using integrin blocking antibodies in a 3D culture reverted the malignant phenotype of human breast cancer cells [241]. This outcome has never been observed in 2D cultures. Therefore, with this work, these researchers were able to show how a 3D environment can significantly impact cell

fate and potentially more faithfully replicate the mechanisms occurring *in vivo*. Since then, the work of Mina J. Bissel, Joan S. Brugge and their co-workers have shed light on how ECM composition and stiffness are main regulators of cellular response, in the context of breast epithelial cell culture [178, 213], laying foundations on the importance of developing new approaches and technologies to study the mechanisms underlying development and disease of the mammary glandular epithelium.

Acinar morphogenesis. Normal breast epithelial cells grown in 3D cultures self-organise into structures that resemble the architecture of the glandular epithelium *in vivo* [187], particularly the formation of spherical acini with a hollow lumen and the establishment of apicobasal polarity in the cells that compose these acini [242]. Currently, there are two main methods routinely used to generate acinar structures: in one method epithelial cells are embedded within the ECM, in the second method the ECM is first polymerised into a gel bed and the cells are then seeded onto the gel as single-cell suspension in culture medium (Figure 1.5**a** middle and right, respectively) [178]. MCF10A cells can be cultured in Engelbreth-Holm-Swarm (EHS) tumour-derived reconstituted BM (rBM) to form acinar structures (Figure 1.5**b**) [187]. Within days after seeding the cells within reconstituted BM, two different subpopulations of cells become evident within each acinus – an outer monolayer of polarised cells in direct contact with the BM and an inner subpopulation of cells in the middle of the spherical structure lacking contact with the matrix. Throughout acinar morphogenesis, the apicobasal polarity of the outer monolayer of epithelial cells is maintained. After about a week in culture, the subpopulation of cells in the centre the acini undergo programmed cell death, which results in the formation of a hollow lumen that is maintained thereafter [178]. The methods for growing such structures have been fairly well established and are highly-reproducible.

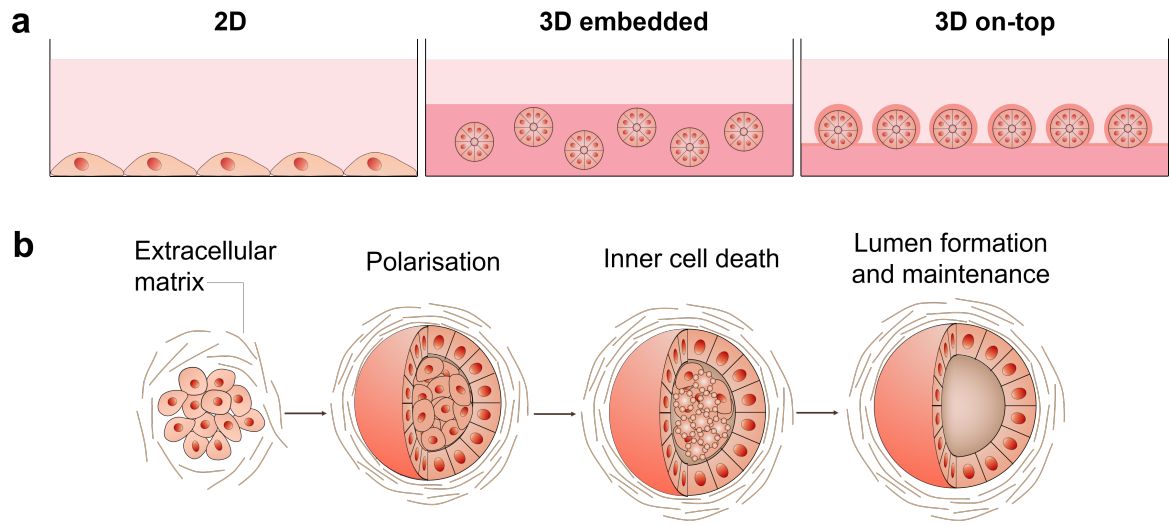

Figure 1.5: Mammary epithelial cells morphology in different culture conditions. **a** Mammary epithelial cells grown as a monolayer on a conventional flat surface, typically in polystyrene culture flasks, plates or Petri dishes (2D, left); epithelial cells form acinar structures when grown embedded within rBM (3D embedded, middle), or onto gelled rBM (3D on-top, right). **b** Acinar morphogenesis of MCF10A cultured in rBM – within days after seeding the cells within reconstituted BM two different subpopulations of cells become evident within each acinus – an outer monolayer of polarised cells in direct contact with the BM and an inner subpopulation of cells in the middle of the spherical structure lacking contact with the matrix. Throughout acinar morphogenesis, the apicobasal polarity of the outer monolayer of epithelial cells is maintained. After about a week in culture, the subpopulation of cells in the centre the acini undergo programmed cell death, which results in the formation of a hollow lumen that is maintained thereafter. **a** was adapted from [243] and **b** from [178].

Spheroids. Spheroids are self-assembled spherical aggregates of poorly organised cells. These spherical 3D culture systems have become very popular in cancer research, because, much like rapidly growing tumours that have poorly vascularised regions that become hypoxic and deprived of nutrients [244], spheroids typically develop a necrotic core, surrounded by quiescent cells, which are, in turn, surrounded by proliferating cells exposed to the surface, because, due to their morphology, nutrient and oxygen transport becomes limited towards the centre (Figure 1.6**a**) [245]. In fact, the fraction of cells in solid tumours that can survive this hypoxic stress are refractory to traditional chemotherapeutic agents and can then exhibit a more invasive phenotype [246–248]. These aggregates can, therefore, be better mimetic systems to study tumour biology and drug resistance that 2D cell cultures. In order to culture cells as spheroids in a scaffold-free environment cells need to preferentially adhere to each other in detriment to the substrate. This can be achieved by numerous methods that have been developed to generate these *in vitro* 3D cell culture systems, namely spinner cultures, rotating wall vessels, hanging drop techniques, liquid overlay techniques (by ultra-low attachment substrates), microfluidics and micro-moulded hydrogels [249]. Spinner cultures prevent

cells from adhering to the flask and promote cell-to-cell collisions by constant stirring, and it has been used to form spheroids with a variety of primary cells, cell lines and different types to form heterotypic spheroids (Figure 1.6**b**) [250–252]. Rotating wall vessels generate a micro-gravity environment that maintains a cell suspension continuously in free fall and promotes cells to aggregate in low shear (Figure 1.6**c**) [253–255]. Hanging drop techniques make use of gravitational forces and the fact that a surface is not available for cell attachment, promoting self-aggregation of cells into spheroids, by using specialised plates with open, bottomless wells where small droplets of medium with cells in suspension can be hanged without being displaced or perturbed during manipulation (Figure 1.6**d**) [256–259]. In turn, the liquid overlay method promotes the formation of spheroids by inhibiting the attachment of cells to the substrate, typically V-shaped or round bottom 96-wells plates, which can be coated with poly(hydroxyethyl methacrylate) (pHEMA) or commercially acquired as ultra-low attachment (Figure 1.6**e**) [260–263]. Finally, microfluidic devices and micro-moulded hydrogels, particularly useful for high throughput platforms, can be fabricated with non-adhesive polymers and then can be used to form spheroids, or microtissues, which shape, size and composition can be easily controlled (Figure 1.6**f**) [264, 265]. Depending on the specific research goals, spheroids can be studied in liquid medium or encapsulated/embedded within 3D matrices, which can be made of biological polymers, semi-synthetic or synthetic hydrogels, namely matrigel [266], collagen [267], agarose [268], gelatin methacrylate (GelMA) [269], and poly(ethylene glycol) (PEG) [270], among others.

Developing better systems. In order to progress in disease modelling, translational research and regenerative medicine, continued development of better 3D *in vitro* epithelial models is needed. Because normal epithelial tissues and tumours are composed of different populations of cells, the use of monotypic 3D has inherent limitations and one promising research avenue is the development of heterotypic 3D culture systems with appropriate ECM composition and architecture. Increasing the complexity of these culture models can potentially offer greater insight into the mechanisms underlying pathobiology. Nevertheless, it is important to maintain a level of complexity that is attainable and manageable in a reproducible fashion for each target application.

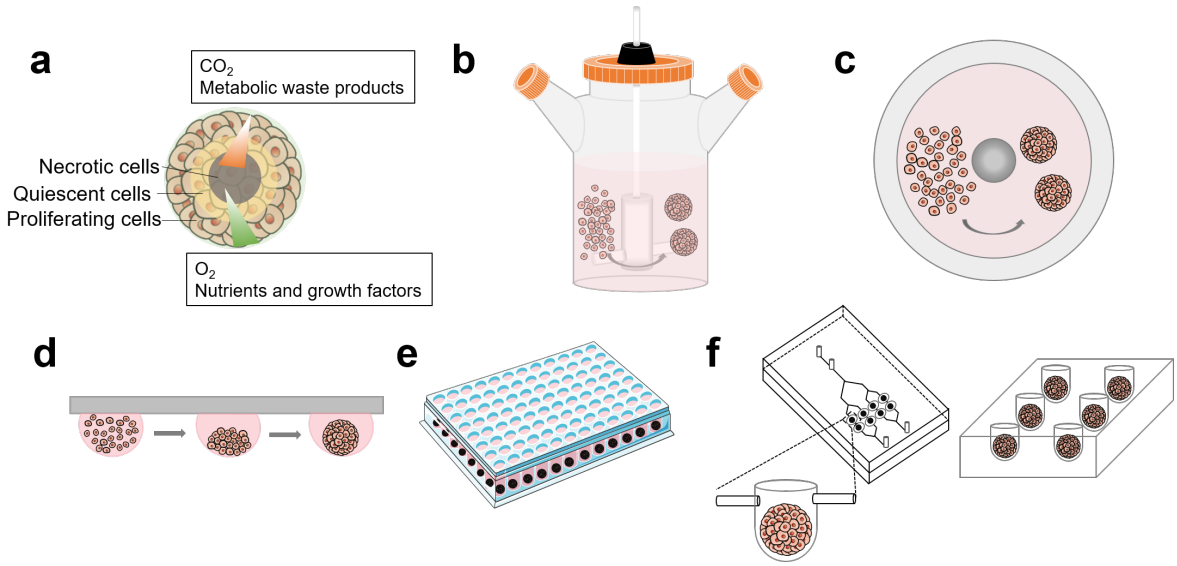

Figure 1.6: Epithelial 3D spheroid cultures. **a** Spheroids typically develop a necrotic core, surrounded by quiescent cells, which are, in turn, surrounded by proliferating cells exposed to the surface. The formation of three cell layers is due to their morphology creating molecular gradient, in which transport of oxygen, nutrients and growth factors becomes limited, and carbon dioxide and waste products accumulate towards the centre. Methods to culture cells as spheroids: **b** spinner cultures, which prevent cells from adhering to the flask and promote cell-to-cell collisions by constant stirring; **c** rotating wall vessels generate a micro-gravity environment that maintains a cell suspension continuously in free fall and promotes cells to aggregate in low shear; **d** Hanging drop technique, which makes use of gravitational forces and the fact that a surface is not available for cell attachment, promoting self-aggregation of cells into spheroids, by using specialised plates with open, bottomless wells where small droplets of medium with cells in suspension can be hanged without being displaced or perturbed during manipulation; **e** liquid overlay method that promotes the formation of spheroids by inhibiting the attachment of cells to the substrate, typically V-shaped or round bottom 96-wells plates, which can be coated with poly(hydroxyethyl methacrylate) (pHEMA) or commercially acquired as ultra-low attachment; and **f** microfluidic devices and micro-moulded hydrogels that can be fabricated with non-adhesive polymers and then can be used to form spheroids, which shape, size and composition can be easily controlled. Adapted from [271]. The microfluidic device schematics in **f** was adapted from [265].

1.6 Scope of the Thesis

This thesis aims to explore and assess the response of epithelial cells, in particular mammary epithelial MCF10A cells, when their extracellular environment is manipulated both biophysically and biochemically.

In Chapter 2, the crosstalk between ECM composition and epithelial-mesenchymal transition (EMT) is investigated using various biomolecular tools, such as gene and protein expression, microscopy and Raman spectroscopy.

In Chapter 3, MCF10A cells undergoing EMT are interfaced with a biologically-active laminin-111 fragment to investigate whether this cryptic ECM fragment can modulate EMT. Different methods of interfacing the fragment and different cell culture methods are assessed.

In Chapter 4, mechanoresponsive elements in electrically-stimulated MCF10A cells are studied using a comprehensive methodology. In this experimental work, the effects of electrical stimulation provided via a biocompatible conductive polymer (polypyrrole) are analysed by assessing the expression of genes involved in mechanotransduction pathways; by looking at the subcellular localisation of key transcription factors, the cytoskeleton organisation and the expression of focal adhesion elements by confocal microscopy; and by measuring single cell elasticity and morphology changes using Atomic Force Microscopy and Scanning Ion Conductance Microscopy.

Finally, Chapter 5 summarises the work in this thesis with concluding remarks and considerations for future research.

2

Interplay between ECM composition and EMT

Contents

2.1 Introduction

2.1.1 Epithelial-mesenchymal transition

Epithelial-mesenchymal transition (EMT) refers to a reversible cellular and molecular programme in which polarised epithelial cells shift towards (quasi-)mesenchymal states [272, 273]. During this process, epithelial cells, which are characterised through their apicobasal polarity and tight cell-cell contact by specialised intercellular junctions, lose their polarity, reorganise their cytoskeleton, alter their morphology and change their expression of adhesion molecules, to gradually acquire a migratory and invasive behaviour (Figure 2.1) [274, 275].

The pioneering work of Gary Greenburg and Elizabeth D. Hay in 1982 experimentally established EMT for the first time when they demonstrated that both embryonic and adult avian epithelial cells from the anterior lens become migratory and acquire invasive fibroblast-like behaviour when embedded in 3D type I collagen matrices [276]. EMT was initially described as a transformation, rather than a transition process from an epithelial to a mesenchymal state [277], which had been described as a binary cellular switch. Later, the term was changed from 'transformation' to 'transition', reflecting on its reversibility and plasticity [278]. Indeed, EMT is a highly dynamic and plastic process that can be considered a spectrum of transitional states, and describing it by the loss and gain of certain molecular and cellular characteristics during the transition between two states is quite reductionist [278]. Most experimental models typically assume that EMT encompasses a drastic change in the expression of epithelial and mesenchymal markers, which are used to characterise this transition: E-cadherin, claudins and occludins for the epithelial state, and N-cadherin, vimentin, SNAIL and SLUG for the mesenchymal [273]. However, more recent work has shed light on EMT transitional states during fibrosis and in metastatic tumour cells, supporting the notion that this process encompasses a spectrum of inter and intracellular modifications, and, importantly, that not all of these molecular and cellular changes necessarily need to be observed during this transition process [273, 278]. Therefore, the oversimplification of this process in experimental work in cultured cells most likely does not reflect what occurs *in vivo* and has potentially contributed to the controversy and debate around EMT and carcinoma progression [279].

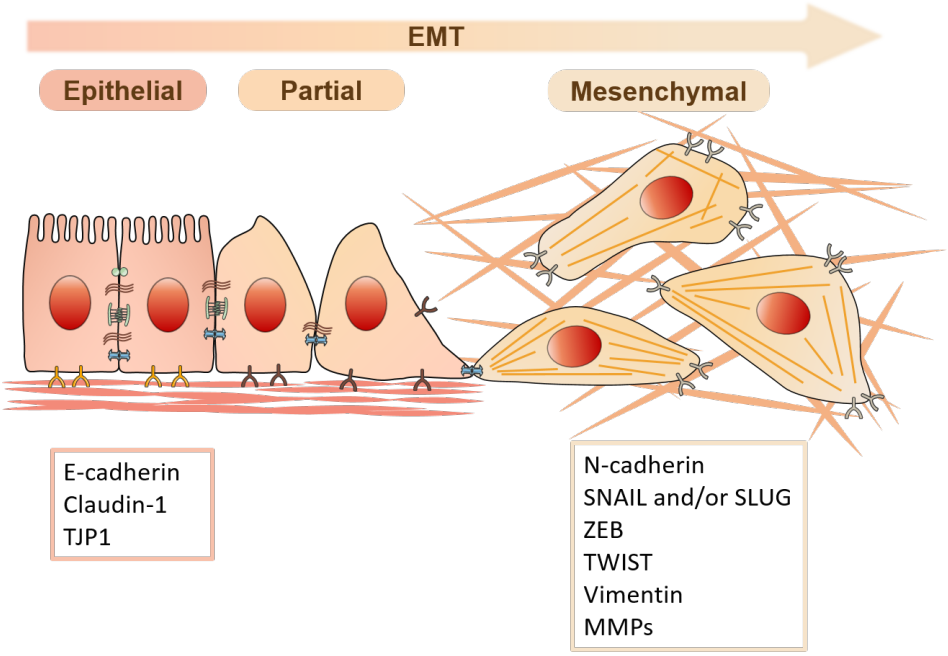

Figure 2.1: EMT spectrum. EMT is a process in which epithelial cells, which are characterised by their apicobasal polarity and tight cell-cell contact by specialised intercellular junctions, lose their polarity, reorganise their cytoskeleton, alter their morphology and change their expression of adhesion molecules, to gradually acquire a migratory and invasive behavior. EMT is a continuum whereby cells can display epithelial, partial and mesenchymal phenotypes. During EMT, expression of EMT-TFs (SNAIL, SLUG, ZEB, TWIST) is upregulated, which inhibits the expression of genes associated with the epithelial state (listed in the box on the left) and upregulates genes associated with mesenchymal state (listed in the box on the right). Adapted from [272, 280].

2.1.2 EMT regulation

EMT is a non-linear cellular programme orchestrated at multiple levels, which encompass complex signalling networks that include transcriptional regulation [281], epigenetic changes [282, 283], protein stability [284], alternative splicing [285–287], and subcellular localisation [287–289]. Cell and tissue culture studies have been instrumental for our understanding of the regulatory mechanisms underlying EMT. However, even though a large body of work has been done towards identifying common EMT regulatory networks in the context of development and disease, it has been suggested that some pathways might be tissue (or tumour subset) specific [278].

In addition, three different EMT programmes have been described and classified according to the biological context in which the transition process takes place [290]. Briefly, type 1 EMT occurs during embryogenesis and organ development, type 2 EMT is associated with tissue regeneration and fibrosis, and type 3 EMT is observed during carcinoma progression and metastasis. It is not clear, however, how different these three types of EMT really are, or whether they are the same cellular

transition process occurring in different biological settings [272, 290].

The regulation of EMT, which, for simplicity, will be referred to as a single programme hereafter, is based on the transcriptional suppression of E-cadherin, an important epithelial marker [291], and the upregulation of specific transcription factors termed EMT-TFs, namely SNAI1 (also known as SNAIL), SNAI2 (also known as SLUG), ZEB1, ZEB2, and the basic helix-loop-helix factors TWIST1 and TWIST2 [292]. There is a negative feedback regulatory mechanism in which SNAI1 and ZEB1 have been described to control EMT by repressing the expression of E-cadherin [293–295]. In effect, early stages of EMT encompass the disruption of epithelial properties, including loss of apicobasal polarity and modifications in the expression of adhesion complexes to favour cell-ECM interactions [296]. In addition to the downregulation of E-cadherin, the loss of tight junctions and cell-cell contacts leads to the supression of expression of claudins and occludins, as well as downregulation of zonula occludens 1 (ZO1; also known as tight junction protein 1, TJP1) [297]. One of the hallmarks of EMT is the increase in the expression of the mesenchymal marker N-cadherin while E-cadherin is downregulated, which is oftentimes referred to as 'cadherin switch' [298]. Moreover, the cytoskeletal reorganisation during EMT is accompanied by an increased expression of vimentin, an intermediate filament that mesenchymal-like cells utilise to facilitate motile and invasive behaviour [299].

2.1.3 Role of MMPs in EMT

The repertoire of molecular and cellular changes that occur during EMT also includes increased expression of proteases, namely matrix metalloproteinases (MMPs; discussed in Chapter 1 Section 1.4.1.A). MMPs play key roles in development, branching morphogenesis and overall tissue homeostasis. In fact, the most comprehensive characterisation of the involvement of MMPs in EMT-related events has been in developmental contexts, namely neural crest delamination, mammary gland branching morphogenesis, and cardiac morphogenesis [300–303]. In the particular case of mammary gland development, the tips of the extending ducts are invasive structures that exhibit an increased expression of EMT markers, namely SNAIL and TWIST [304], along with MMP-2 and MT1-MMP (also known as MMP-14) [114]. In addition, MMP-3 is important for secondary (or side) branching formation in the mammary gland [114] and, importantly, a key substrate of this protease is the cell-cell adhesion protein E-cadherin [305]. Due to their proteolytic activity responsible for degrading ECM components, as well as cell-cell junction proteins, MMPs play an instrumental role in EMT by aiding cell invasion and migration. Not surprisingly, increased and dysregulated expression of these proteases is associated with pathological conditions, namely fibrosis and cancer [306–309].

2.1.4 EMT signalling

EMT can be initiated by several signalling pathways, in which ligands from the extracellular microenvironment bind to epithelial (normal or neoplastic) receptors and can trigger a cascade of molecular and cellular events that result in a transition from an epithelial state to a (quasi-)mesenchymal state. A plethora of signalling pathways have been described to induce EMT in various biological contexts, namely TGF-β [310], NOTCH [311] and WNT/β-catenin [312], which have a pleiotropic nature and play important roles in controlling cell fate decisions. These signalling pathways can individually lead to activation of the EMT programme and they can also work together to do so (reviewed in [272]). TGF-β signalling, in particular, has a very important role in triggering EMT in various tissue types [39]. This pathway consists of a large family of ligands, which includes three different TGF-β isoforms (TGF-β1, 2 and 3), activins and bone morphogenetic proteins (BMPs) [310]. Briefly, TGF-β1, 2 and 3 bind to the same receptor complexes TGF-β receptor type 1 (TGF-βR1) and type 2 (TGF-βR2), leading to activation of SMAD2 and SMAD3 through direct phosphorylation at their C-terminal, which, in turn results in a complex formation with SMAD4 [313]. Once formed, the SMAD complex is transported into the nucleus, where it can act as a transcription factor and, therefore, regulate gene expression [314]. SMAD complexes transcriptionally activate various genes implicated in the transitioning process to a mesenchymal state, such as vimentin [314], and EMT-TFs SNAIL, SLUG, ZEB1 (Figure 2.2) [315]. The EMT-TFs can then work in a positive feedback loop by upregulating the expression of TGF-β ligands, maintaining the cells in a mesenchymal-like state [316]. Furthermore, TGF-β can also induce EMT via non-SMAD signalling through post-transcriptional regulation [317, 318] and post-translational modifications [319]. Additionally, TGF-β can also participate in the activation of the EMT programme via mechanisms of signalling crosstalk with other pathways, namely the WNT signalling pathway [320].

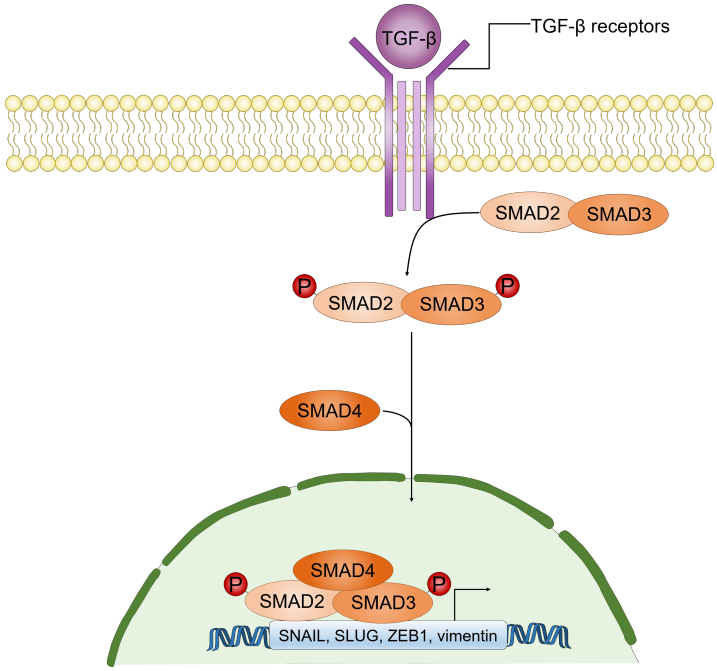

Figure 2.2: TGF-β-activated SMAD pathway during EMT. TGF-β signalling pathway can initiate EMT in various tissue types. The canonical TGF-β pathway involves the binding of TGF-β proteins to the TGF-β family of receptors, leading to activation of SMAD2 and SMAD3 through direct phosphorylation, which, in turn results in a complex formation with SMAD4. Once formed, the SMAD complex is transported into the nucleus, where it can act as a transcription factor and, therefore, regulate gene expression. SMAD complexes transcriptionally activate various genes implicated in the transitioning process to a mesenchymal state, such as vimentin, and EMT-TFs SNAIL, SLUG, and ZEB1. Adapted and modified from [272].

2.1.5 Matrix rigidity and EMT

The ECM regulates cell function and tissue homeostasis through highly dynamic and complex interactions between cells and their microenvironment, which consists of a cohort of biochemical and biophysical signals. Changes to cell-ECM interactions, which can result from abnormal ECM remodelling, are essential in the initiation and progression of EMT. Research on how the EMT programme is activated in different biological contexts has been largely focused on the role of various intra- and inter-cellular biochemical signals on cell behaviour. However, cells can also sense the physical properties of their microenvironment and respond accordingly [321].

A mechanically altered ECM has long been thought to contribute to the development and progression of disease. Excessive production, deposition and crosslinking of ECM components without a balanced turnover results in fibrosis, which significantly increases the risk of cancer development and progression [147, 322]. For example, in the context of breast cancer, the tumour microenvironment is stiffer than normal tissue [323], a characteristic that is normally used for initial screening through

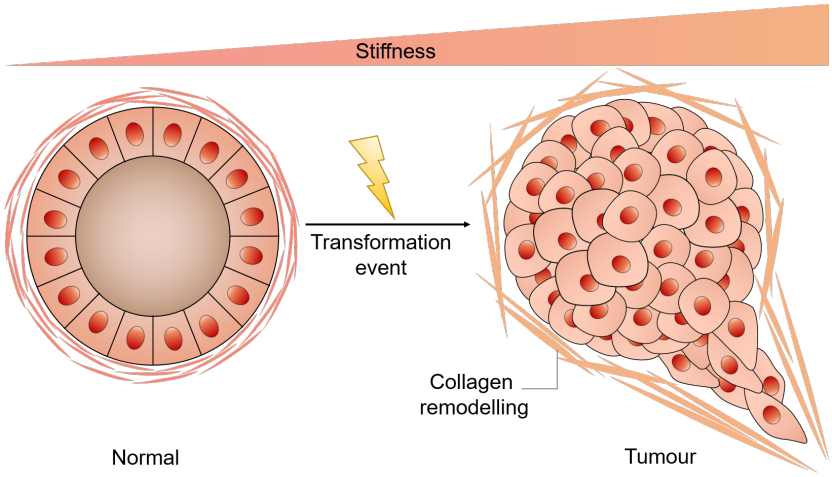

Figure 2.3: Interplay between tissue rigidity and EMT. Normal human mammary epithelial cells form normal polarised acini structures within reconstituted BM (rBM). However, increasing matrix stiffness induces an invasive phenotype when cells sense a rigid matrix. These morphological changes resemble the process of EMT. Adapted and modified from [25].

palpation and mammography [324]. Seminal studies have demonstrated that human mammary epithelial cells, which form acini within reconstituted BM (rBM), show an invasive phenotype in a rigid matrix, with a stiffness that simulates that of breast tumours (Figure 2.3) [151, 325]. These evident morphologic changes that occur as a response to increasing mechanical forces by the ECM resemble the process of EMT. Recent studies have directly linked an increase in matrix stiffness with a transition into a mesenchymal-like phenotype [326, 327]. Additionally, increasing ECM stiffness has also been shown to activate TGF-β signalling, which, as previously discussed, is an inducer of EMT [328]. Together, the evidence suggests that matrix stiffness has an instrumental role in inducing EMT and, importantly, that there is a crosstalk between biochemical and biophysical cues that regulate EMT.

2.1.6 EMT in development, wound healing and disease

EMT is an instrumental process in embryonic development, particularly in gastrulation and tissue morphogenesis, as well as in wound healing events in the adult [274, 329]. It has been known for decades that EMT is essential for epithelial cells to migrate in the embryo, because to do so cells need to acquire a mesenchymal phenotype [330, 331]. The transient and reversible nature of EMT allows the formation of various structures within the developing embryo in a highly organised fashion. In the adult, EMT is also an essential physiological response to injury to achieve tissue regeneration and repair [332]. During wound healing, stationary epithelial cells lose their intercellular adhesions and adopt mesenchymal features to migrate across the wound site [333]. Then, in order to restore the epithelial barrier, cells revert to the epithelial state, during a process known as re-epithelialisation

[334].

Dysregulated EMT results in the disruption of the epithelium and the production of mesenchymal-like cells with an invasive phenotype that can contribute to disease progression, namely fibrosis and cancer [335]. At the cellular and molecular level, pathological and physiological EMT programmes are orchestrated by similar signalling pathways, as well as regulatory and effector molecules [274]. In the context of fibrosis, cell tracing studies have demonstrated that a significant fraction of myofibroblasts are originated from epithelial cells through EMT [336]. It is now well established that epithelial and endothelial cells, as well as hepatocytes and cardiomyocytes can all undergo EMT and significantly contribute to the development and progression of tissue fibrosis [274, 337–340]. There is a large set of evidence linking EMT to cancer progression in various *in vitro* and *in vivo* models [272], but the role of EMT in human cancer has always been rather controversial [279]. As mentioned before, it is important to take into consideration that an EMT programme is not a binary switch between two cellular states, but a series of transitions through different states along an epithelial to mesenchymal spectrum [278]. Research to date suggests that EMT is an integral event of many different types of cancer, including breast [341], pancreatic [342], lung [343], and colorectal [344]. In addition, different reports have suggested that cells that have undergone EMT also become more refractory to several drugs and chemotherapy [345–348]. While it seems clear that targeting EMT is a potential avenue in the treatment of fibrotic diseases, the inherent diversity and complexity of cancer requires caution in the approach of targeting this process for therapeutic purposes. Advances in our understanding of EMT and its transitional states is of pivotal important for the development and improvement of treatment regimens that can eradicate cancer.

2.2 Chapter Aims

Abnormally high expression of type I collagen has been linked with metastasis [349–352] and with elevated mesenchymal gene expression [327]. In this chapter, the behaviour of human mammary epithelial cells (MCF10A) was investigated as they were cultured within rBM with increasing concentrations of type I collagen added to the ECM. This model system was employed to alter epithelial cell phenotype and mimic breaching of the basement membrane (BM), a key step in carcinoma invasion [353]. Since the invasive behaviour induced by the presence of extracellular type I collagen highly resembles EMT, a comprehensive analysis of this cellular transition was carried out.

Ever since the ground-breaking work by Greenburg and Hay in 1982 [276] (Subsection 2.1.1), significant research interest has been focused on detecting and characterising epithelial cells undergoing EMT. Published studies use a collection of criteria at the molecular and cellular levels to characterise EMT: loss of cobblestone shape to adopt spindle-shape morphology accompanied by loss of polarity; migratory and invasive behaviour; cadherin switch (downregulation of E-cadherin and upregulation of N-cadherin); upregulation of at least one EMT-TF (SNAIL, SLUG, ZEB, TWIST); loss of epithelial markers, including ZO1; increased expression of MMPs; and upregulation of intermediate filament vimentin, among others [354]. In this chapter, standard biomolecular tools and techniques, such as imaging, protein expression with Western blot analysis and gene expression with quantitative reverse transcription PCR (RT-qPCR), were used to detect and characterise EMT using the described criteria.

Raman spectroscopy, a powerful and non-destructive vibrational spectroscopic technique that can be utilised to optically interrogate molecular changes within a wide range of biological conditions [355], was used to study different systems of inducing EMT. In addition to investigating the cellular Raman spectra of MCF10A cells cultured within rBM mixed with increasing concentrations of type I collagen, EMT was induced in two additional 2D culture systems to be studied: in one cells were exposed to exogenous TGF-β signalling, and in the other cells were culture at different densities (confluent and sparse conditions). This experimental work was conducted to understand whether this vibrational spectroscopic technique has the potential of probing biomolecular changes of cells that have undergone EMT and how the different *in vitro* systems compare to each other.

Studies have reported that cells reduce their intracellular stiffness after undergoing EMT potentially to facilitate migratory and invasive behaviour [356]. To study cell stiffness, scanning ion conductance microscopy (SICM) was used to measure MCF10A cell stiffness after being cultured within rBM mixed with different concentrations of type I collagen to test the hypothesis that mesenchymal-like cells are softer than their epithelial counterparts.

2.3 Materials and Methods

2.3.1 General Cell Culture

MCF10A cells were obtained from American Type Culture Collection (ATCC) and cultured under standard cell culture conditions in humid incubators at 37℃ and 5% CO_2 atmosphere. These cells were cultured in Dulbecco's Modified Eagle Medium/Nutrient Mixture F-12 (DMEM/F-12, Gibco, Life Technologies), supplemented with 5% (v/v) Horse Serum (Gibco, Life Technologies), 5% (v/v) Penicillin Streptomycin (Gibco, Life Technologies), 20 ng/ml Epidermal Growth Factor (EGF, Peprotech), 0.5 mg/ml hydrocortisone (Sigma-Aldrich), 100 ng/ml Cholera toxin (Sigma-Aldrich), 10 µg/ml insulin (Sigma-Aldrich) [187]. Before being added to DMEM/F-12, all supplements were pre-mixed and filtered through a sterile 0.2 µm syringe filter. MCF10A cells were expanded in T-75 flasks and medium was changed every 2-3 days until 80-90% confluency was reached. For passaging, as well as for seeding at specific cell densities for experimental assays, cells were detached from the tissue flask after one rinse in sterile Phosphate Buffered Saline (PBS) and incubation at 37℃ with TripLE Express Enzyme (Thermo Fisher Scientific). Once detached, cells were centrifuged at 300 x*g* for 5 minutes and the TrypLE Express-containing supernant was discarded each time. Fresh complete medium was used to resuspend the pellet and cells were counted with trypan blue (Thermo Fisher Scientific) with a 1:1 (v/v) ratio.

2.3.2 Collagen Extraction and Reconstitution

The extraction and reconstitution of collagen I from rat tail tendons was performed by myself and Dr Jennifer Puetzer as previously described [357]. The procedure was carried out under sterile conditions. Briefly, the rat tails were initially submerged in 70% (v/v) ethanol and allowed to completely thaw. Both ends of each tail were cut and a superficial incision was made along the tails in order to peel the skin and have the tendon bundles visible. Tendons were then placed in 70% (v/v) ethanol until extraction was complete. Following, tendons were suspended in 0.1% (v/v) acetic acid at 150 ml/g of tendon for at least 48 hours at 4℃ to allow collagen to solubilise. Next, the collagen solution was centrifuged for 90 minutes at 2,500 x*g*. The supernatant was then collected and lyophilised for 48 hours, whilst the pellet containing unsolubilised collagen, blood, and muscle tissue, amongst other components, was discarded. Lastly, the lyophilised collagen was weighed and reconstituted in 0.1% (v/v) acetic acid at a concentration of 10 mg/ml and stored at 4℃.

2.3.3 Cell Culture on Matrigel/Collagen I Gels

During the preparation of the gels, all reagents, tubes and plates were kept on ice (approximately 4℃). Stock collagen I from rat tail tendon (see previous Subsection 2.3.2) was prepared at a concentration of 10 mg/ml, dissolved in 0.1% (v/v) acetic acid. Acid-solubilized collagen I needs to be neutralised in order to polymerise, which was achieved by adding 1N sodium hydroxide (NaOH) and Hank's Balanced Salt Solution (HBSS, Sigma-Aldrich). Calculations were made as described in Table 2.1.

Table 2.1: Calculations to obtain the necessary volume of each component to make Matrigel/Collagen I gels.

Component	Calculations to obtain the necessary volume
Collagen I	$\frac{\text{(final gel volume)x(desired collagen I concentration)}}{\text{Collagen-I stock concentration}}$
1N NaOH	Volume of collagen I x 0.023
10X HBSS	$\frac{\text{(volume of collagen I)+(volume of NaOH)}}{10}$
1X HBSS	(final gel volume)-[(collagen I volume)+(NaOH volume)+(10X HBSS volume)]

Collagen I solutions were prepared to the desired final concentrations by pipetting and mixing the components in the following order: HBSS 1X, HBSS 10X, 1N NaOH and, lastly, collagen I from stock solution. Positive displacement pipettes were used for transferring viscous stock collagen solution. After preparing the different concentrations of collagen I, they were mixed with equal volume of Matrigel (LDEV-free, Corning). For Raman imaging on these gels, phenol-red free Matrigel was used (LDEV-free, Corning) in order to remove noise signal. Matrigel and Collagen I mixtures were prepared under sterile conditions and the gels were polymerised at 37℃ for at least 30 minutes, prior to seeding the cells. Throughout this thesis, these gels are referred by using the concentration of collagen prepared before mixing with Matrigel.

2.3.4 RNA Isolation, cDNA synthesis and RT-qPCR

2.3.4.A RNA Isolation

The expression of EMT-related genes was studied by quantitative reverse transcription polymerase chain reaction (RT-qPCR). Cells were seeded at 15,000 cells/cm^2 on Matrigel/Collagen I gels in 48-well plates and cultured for 1 week before RNA collection. For EMT models on 2D cultures, cells were cultured at an initial cell density of 15,000 cells/cm^2 for sparse conditions and TGF-β1 assay and 150,000 cells/cm^2 for confluent conditions (on 10 mm diameter MgF_2 windows fitted in 48 well plates). Cells on sparse and confluent conditions were collected 24 hours post seeding. For TGF-β1

assay, cells received treatment (10 ng/ml in complete media from a TGF-β1 stock concentration of 50 µg/ml) 24 hours post seeding and were collected 24 hours post treatment. At the time of collection, conditioned medium was aspirated from each well. Cells on gels were lysed in 700 µl TRIzol reagent (Life Technologies) per well and frozen immediately at -80℃ until further analysis. Cells in TRIzol reagent were thawed and transferred to PCR clean DNA LoBind Eppendorf tubes. Next, 140 µl of chloroform (molecular biology grade, Acros Organics) was added to each tube, which were shaken vigorously by hand. The samples were left incubating for 3 minutes at room temperature, followed by a centrifugation step at 12,000 x*g* for 15 minutes at 4℃. This step results in phase separation and the top RNA-containing aqueous phase was transferred into a new PCR clean DNA LoBind Eppendorf tube. In the case of cells on MgF_2 windows, TRIzol reagent was not used. Instead, cells were washed once with sterile ice-cold PBS and 100 µl of RLT buffer (Qiagen) was added to each well. The extracts from 4 wells were then pooled for each condition. Next, an equal volume of 70% ethanol (molecular biology grade, Fisher Bioreagents) was added to each sample (for both TRIzol and RLT collection procedures) and mixed well by pipetting. For the final steps of RNA isolation, the instructions from the RNeasy Mini Kit (Qiagen) were followed. For each sample a volume of up to 700 µl at a time was transferred to a spin column placed in a 2 ml collection tube and centrifuged for 30 seconds at 10,000 x*g* at room temperature. If the samples contained more than 700 µl, multiple centrifugations were carried out. Next 700 µl of buffer RW1 was added to each spin column followed by a centrifugation at 10,000 x*g* for 30 seconds at room temperature. Subsequently, 500 µl of buffer RPE was added to each tube for a final wash, which were centrifuged for 2 minutes at 10,000 x*g* at room temperature, followed by another centrifugation with no buffer added to ascertain that no traces of ethanol were left in the samples. In every step, the flow-through from the spin column was discarded. Finally, 30 µl of RNase-free water (Life Technologies) was added to each spin column to collect the purified RNA from each sample with a last step of centrifugation for 30 seconds at 10,000 x*g* at room temperature. The RNA concentration was then measured using NanoDrop 2000c (Thermo Fisher Scientific). Once RNA samples from all biological replicates were collected and isolated for subsequent use, RNase-free water was added to each tube in adequate amounts to ensure that all samples were at the same RNA concentration.

2.3.4.B cDNA synthesis

Complementary DNA (cDNA) was synthesised from each RNA sample using Applied Biosystems High-Capacity cDNA Reverse Transcription kit (Thermo Fisher Scientific). After allowing the kit components to thaw on ice, the reverse transcription master mix was prepared, which contained, per reaction, 2 µl RT buffer, 0.8 µl dNTP mix, 2 µl RT random primers, 1 µl multiscribe reverse transcrip-

tase and 3.2 µl nuclease-free water. Following, 10 µl of each RNA sample was added to a 0.5 ml PCR tube and mixed with 10 µl of reverse transcription master mix. Each tube was quickly vortexed, spun down and placed in the thermal cycler (LifePro, Bioer) to go through the following cycle: 10 minutes at 25℃, 120 minutes at 37℃ and 5 minutes at 85℃.

2.3.4.C RT-qPCR

After reverse transcription, the cDNA was diluted with nuclease-free water to be used in RT-qPCR, which was carried out using TaqMan Fast Advanced Master Mix (Thermo Fisher Scientific), FAM-MGB conjugated TaqMan probes listed in Table 2.2 (Thermo Fisher Scientific), and run on a StepOnePlus™ machine (Applied Biosystems). Components were prepared on 96-well reaction plates (Thermo Fisher Scientific): 5 µl of TaqMan Fast Advanced Master Mix, 0.5 µl of TaqMan probe, 0.5 µl of nuclease-free water, and 4 µl of cDNA for each sample (10-20 ng of cDNA per reaction). The RT-qPCR programme settings were as follows: step 1 50℃ for 2 minutes, step 2 95℃ for 20 seconds, and step 3 40 cycles of PCR that comprised a denaturing step at 95℃ for 1 second and a annealing/extending step at 60℃ for 20 seconds. Cycles-to-threshold (Ct) values were automatically obtained by the Thermo Fisher Scientific StepOnePlus™ software. Subsequently, these values were exported to Microsoft Excel and manually processed to obtain fold change expression values. Ct values of each gene of interest were normalised to the Ct values of the housekeeping gene (*Gapdh*) within each respective sample. $2^{-\Delta\Delta Ct}$ values were obtained by normalising to the internal control sample (in this case, the epithelial-like state). Three biological replicates (two technical replicates each) are reported.

Table 2.2: FAM-MGB conjugated TaqMan probes for housekeeping and EMT-related genes. List of primers used for RT-qPCR gene expression studies in this chapter. *Gapdh* was used as housekeeping gene and all others were for genes of interest related with EMT.

Target	TaqMan Assay ID
Gapdh	Hs02758991_g1
Cdh1	Hs01023895_m1
Cdh2	Hs00983056_m1
Snail	Hs00195591_m1
Slug	Hs00161904_m1
Vim	Hs00958111_m1
Tjp1	Hs01551861_m1
Mmp2	Hs01548727_m1

2.3.5 Cell lysis and protein isolation

For protein collection, MCF10A cells were grown on Matrigel/Collagen I gels with an initial density of 15,000 cells/cm^2 (48-well plate) and cultured for 1 week. Then, cells were lysed using RIPA buffer (New England Biolabs) with phosphatase and protease inhibitors (Roche). Cell lysates were then transferred to Protein LoBind Eppendorf tubes and kept on ice. Next, samples were sonicated (using a probe sonicator) on ice for 20 seconds at 20% amplitude and then incubated for 1 hour at 4℃ on a shaker. Lysates were subsequently centrifuged for 10 minutes at 16,000 x*g* at 4℃. Lastly, supernatants were transferred to clean Protein LoBind Eppendorf tubes and stored at -80℃ until further use.

2.3.6 Measuring protein concentration

Protein concentration was determined by the Micro BCA^{TM} Protein Assay Kit (Thermo Fisher Scientific). First, the Bovine Serum Albumin (BSA) standards were prepared by serial dilution using a diluent similar to the sample buffer (UltraPure water or PBS) in sufficient amounts to use three replicates of each dilution. Following, the Micro BCA working reagent was prepared by mixing 25 parts of reagent MA, 24 parts of reagent MB and 1 part of reagent MC. Next, 150 µl of each solution of BSA standard and diluted samples was transferred into a 96-well clear bottom plate in triplicate. The absorbance was then measured at 562 nm using a SpectraMax M5 plate reader. The standard curve

was drawn by plotting the average absorbance reading of each BSA standard and its concentration. Finally, the protein concentration for each sample was then calculated by linear interpolation of the standard curve and by accounting the dilution factor used during sample preparation.

2.3.7 Western blotting

Relative levels of EMT-related proteins were measured by Western blotting (WB). Whole cell extracts were separated by SDS-PAGE, transferred to polyvinylidene difluoride (PVDF) membranes and analysed by WB. Briefly, protein samples were prepared, before being separated according to their molecular weight by electrophoresis, by mixing 15 or 30 µg of protein with XT Reducing Agent (20X, Bio-Rad) and XT Sample Buffer (Bio-Rad) to a volume of 15 µl per lane. These samples were then incubated at 100℃ for 3 minutes and then cooled down to room temperature. Prepared samples and protein ladder were then loaded on 4–12% Criterion XT Bis-Tris Protein Gels (26 well, 15 µl each, Bio-Rad) and protein separation was performed in XT MOPS Running Buffer (Bio-Rad) at 80 mA (when running 2 gels) for 2 to 2.5 hours, on ice. Following, proteins separated in the gels were transferred to a 0.45 µm PVDF membrane (Immobilon-FL PVDF, Merck) using the Criterion™ Blotter (Bio-Rad). Immunoblotting sandwiches were prepared using Whatman® filter paper. Transfer was then conducted on ice at 100 V for 30 minutes in Tris/Glycine buffer (Bio-Rad). Next, efficient transfer of proteins into the PVDF membranes was confirmed by Ponceau staining (0.1% (w/v) in 5% (v/v) acetic acid, Sigma) staining and after membranes were washed in TBS-T (TBS, Bio-Rad, with 0.1% (v/v) Tween20, Sigma-Aldrich) until no red coloured bands were visible. Membranes were then blocked with 5% skimmed milk (Sigma-Aldrich, in TBS-T) for at least 1 hour at room temperature on a shaker. Membranes were then thoroughly washed in TBS-T before being incubated with primary antibody against Vimentin (Sigma-Aldrich, rabbit monoclonal SAB5500191) diluted (1:500) in 5% BSA (Sigma-Aldrich) in TBS-T at 4℃ overnight on a shaker. The following day, membranes were incubated with secondary antibody (anti-rabbit 800CW, Licor) diluted in a ratio of 1:10,000 in TBS-T for 1 hour at room temperature with gentle orbital shaking. Membranes were then washed and imaged using the Licor system and image studio. Subsequently, membranes were incubated with loading control antibody against GAPDH (Santa Cruz Biotechnology, mouse sc-32233) diluted in a ratio of 1:500 in 5% BSA in TBS-T for at least 1 hour at room temperature with gentle orbital shaking. Membranes were then washed in TBS-T and incubated with secondary antibody (anti-mouse 680RD, Licor) diluted at a factor of 1:10,000 in TBS-T for 1 hour at room temperature with gentle orbital shaking. Finally, membranes were thoroughly washed and imaged using the Licor system and image studio. Image processing and analysis was performed using Image Studio Lite Ver 5.2.

2.3.8 Imaging

MCF10A cells were cultured on Matrigel/Collagen I gels at an initial density of 5,000 cells/cm^2 and cultured for 1 week on 8 chamber slides (ibidi) for fluorescent imaging. Cells on gels were fixed in a solution of 4% (v/v) paraformaldehyde (methanol-free, 16% (w/v), Thermo Fisher Scientific) and 1% (v/v) glutaraldehyde (50% (v/v), Electron Microscopy Sciences) in PBS for 15 minutes at room temperature. Samples were then washed three times in PBS. Cells were permeabilised with 0.5% Triton X-100 (Sigma-Aldrich) in PBS for 10 minutes at room temperature. Following, samples were rinsed 3 times in Glycine Buffer (Table 2.3) at room temperature. To block non-specific binding, samples were then incubated in 10% (v/v) goat serum in IF Buffer (Table 2.3) for 1 hour at room temperature. AlexaFluor 488 Phalloidin (Thermo Fisher Scientific, 1:500 in PBS) and DAPI (Sigma-Aldrich, 1:1,000 in PBS) were then used to label the actin cytoskeleton and nucleus of cells, respectively, by incubating the samples with this solution for 40 minutes at room temperature. Finally, samples were washed 3 times with PBS and stored at 4 ℃ in Fluoromount-G™ (Thermo Fisher Scientific) mounting medium.

Table 2.3: Buffers for imaging MCF10A cells on gels.

Component	**Final concentration**
Glycine Buffer	
NaCl	130 mM
Na_2HPO_4	7 mM
NaH_2HPO_4	3.5 mM
Glycine	100 mM
IF Buffer	
NaCl	130 mM
Na_2HPO_4	7 mM
NaH_2HPO_4	3.5 mM
NaN_3	7.7 mM
BSA	0.1% (w/v)
Triton™ X-100	0.2% (v/v)
Tween-20®	0.05% (v/v)

Imaging was performed on a Leica SP8 inverted confocal microscope, using a HC PL APO 10x/0.40 CS2 objective. Brightfield images were acquired on a EVOS XL Core Imaging System using a 4x long working distance phase contrast objective. After image acquisition, images produced were processed with the image analysis software FIJI.

2.3.9 Rheology

Characterisation of the rheological properties of Matrigel/Collagen I gels was performed using a AR2000ex rheometer (TA Instruments, New Castle, DE) fitted with a 25 mm parallel plate and temperature controlled peltier plate. Gel samples were prepared immediately before rheological testing following the procedure in Section 2.3.3. Before loading each sample, the temperature of the peltier plate was set to be at 10℃, a temperature at which the rate of gelation is negligible for ECM hydrogels [358, 359]. The samples were then placed in the centre of the peltier plate, then the parallel plate was lowered to a gap of 500 µm. To minimise evaporation, mineral oil was distributed around the sample-plate interface. Three oscillatory rheological procedures were conducted in sequence for each sample: a time sweep, a frequency sweep and a strain sweep. The oscillatory time sweep step was performed at 37℃ using a 0.2% constant strain (within the linear viscoelastic region) and at a frequency of 3.14 rad/s to study the gelation kinetics of the gels. Gelation occurs by increasing the temperature to 37℃. Immediately after the time sweep step, samples were subjected to a frequency sweep step to determine their viscoelastic properties over an angular frequency range (0.1 to 100 rad/s), while applying a 0.2% oscillatory strain at 37℃. Following this step, a strain sweep test was performed to determine the crossover point of each sample over a range of strain (0.01 to 100%), at a frequency of 3.14 rad/s at 37℃. Each sample was tested in triplicate.

2.3.10 Scanning Ion Conductance Microscopy

Scanning Ion Conductance Microscopy (SICM) uses a nanopipette filled with an electrolyte containing aqueous medium as the probe. As shown in Figure 2.4, a voltage is applied between two electrodes, one in the nanopipette and a reference electrode in the sample medium, which results in a closely monitored ionic current flowing in and out of the nanopipette opening. The movement of the nanopipette is controlled through a piezoelectric stage and, when the probe approaches the sample, the ionic flux becomes restricted, so the ion current drops and the z-position of the probe is recorded [360]. This technique can be used to obtain cell stiffness measurements [361, 362] by exploiting the fact that as the probe approaches a soft substrate (in this case a cell or a group of cells) the current drop occurs much more slowly than with stiff substrates [361]. It is worth noting that the absolute values obtained by this method should not be used for comparison with stiffness values obtained using other techniques (personal communication from Dr Pavel Novak, Queen Mary University), but rather to be compared with the measurements acquired from other samples using SICM in the same conditions. The non-contact probe-sample interaction that takes place is sufficient to cause cell surface deformation, and the distance alteration between the probe and the sample can be used to map the

mechanical properties of biological samples [361].

2.3.10.A Sample and Imaging Equipment Preparation

A custom polydimethylsiloxane (PDMS) mould was designed to seed cells on Matrigel/Collagen I gels in 35 mm Petri dishes. To produce PDMS, silicone elastomer and curing agent (SYLGARD® 184 Elastomer Kit, Dow Corning) were mixed with a ratio of 10:1 (w/w) with vigorous stirring. Following, 3 ml of this mix was poured into 35 mm Petri dishes, which were then placed in a 60℃ oven for at least 16 hours. Once cured, these were peeled off of the Petri dishes and the wells were manually formed with a hollow punch (16mm diameter, Boehm). Moulds were sterilised by autoclaving and placed in sterile 35 mm Petri dishes inside a laminar flow hood. Before cell culture, well-shaped moulds in Petri dishes were incubated with complete cell medium for at least 16 hours in a humidified cell culture incubator (37℃, 5% CO_2). Cells were seeded at a density of 15,000 cells/cm^2 on 0 and 4 mg/ml Collagen I gels and, after 1 week in culture, samples were washed in sterile PBS and imaged in Leibovitz's L-15 medium (Gibco). A P-2000 CO_2 laser puller (Sutter Instruments, Novato, CA) was used to pull borosilicate glass (outer diameter 1 mm, inner diameter 0.5 mm, Intracel, Cambridge, UK) pipettes, which parameters for temperature and velocity were optimised to obtain a tip inner diameter of approximately 100 nm and ion currents of approximately 1 nA. The ion current was measured using Axopatch 200B amplifiers (Molecular Devices, Wokingham, UK). After pulling, the pipette was backfilled with sterile PBS and an Ag/AgCl electrode was inserted inside the pipette. The ion current flowing through the pipette was measured with an applied bias potential of 200 mV. The current traces were acquired and analysed using pClamp 10 (Molecular Devices).

2.3.10.B Hopping Probe Ion Conductance Microscopy

SICM operation was carried out by myself together with Sahana Gopal. To operate in hopping mode the pipette filled with PBS and containing the electrode was placed on the inverted microscope to approach the sample vertically. Next, the sample in a 35 mm Petri dish was positioned and an Ag/AgCl electrode was submersed in the Leibovitz's L-15 liquid medium. Once the pipette was immersed and a current of approximately 1 nA was detected, the piezo controller was utilised to approach the sample, which was determined by a 0.3-0.6% drop in the current, compared to the reference (maximum) current. Due to gels being transparent, it was possible to align the microscope camera with the pipette tip, and scanning areas on top of the cells were selected. Importantly, in order to map cellular stiffness scanning areas did not cover any section of ECM (cells were cultured as 3D on top). Subsequently, the selected areas were scanned at a high resolution. Stiffness maps were

obtained by simultaneously acquiring three topographical images using multiple set-points, at a fall rate of 40 nm/ms. Topography map of samples was acquired at a set-point of around 0.3% of ion current drop. In each point, the nanopipette was consecutively lowered to set-points of 0.6% and 3%, and the distances between the nanopipette and the deformed samples were recorded and stored in separate scan maps (one for each set-point). Due to the tridimensional aspect of the acini and other structures formed by the cells , a pre-scan hop size of 60 µm was used to avoid collision between the pipette and the sample when scanning the cells. Two separate experimental replicates were carried out, and at least 3 scan areas (10x10 µm or 20x20 µm) were obtained for each sample.

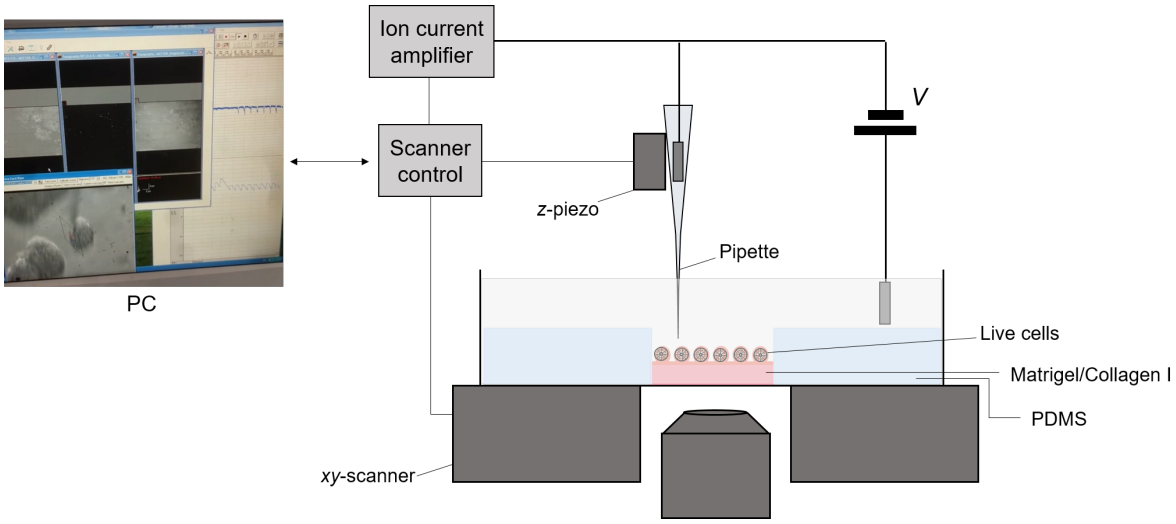

Figure 2.4: Schematics of SICM experimental set-up. A nanopipette filled with an electrolyte containing aqueous medium is used as the probe. A voltage is applied between two electrodes, one in the nanopipette and a reference electrode in the sample medium, which results in a closely monitored ionic current flowing in and out of the nanopipette opening. The movement of the nanopipette is controlled through a piezoelectric stage and, when the probe approaches the sample, the ionic flux becomes restricted, so the ion current drops and the z-position of the probe is recorded. The non-contact probe-sample interaction that takes place is sufficient to cause cell surface deformation, and the perturbation in the distance between the probe and the sample can be used to map the mechanical properties of biological samples. Map scans can be visualised in real-time in the computer connected to the closed system.

2.3.10.C Image processing

Cell stiffness maps were analysed using SICM image viewer software developed by Dr. Pavel Novak, Queen Mary University of London. With this software, 5 µm regions of interest (ROIs) were selected in each image and stiffness measurements were obtained with Clarke's method [361].

2.3.11 Raman Spectroscopy

2.3.11.A Sample Preparation

PDMS moulds (see Subsubsection 2.3.10.A) were used to prepare Matrigel/Collagen I for MCF10A 3D morphogenesis assay. To minimise acquisition of noise in the Raman spectra, phenol red-free Matrigel and DMEM/F-12 were used to culture MCF10A cells on gels. For 2D EMT models, cells were cultured on MgF_2 windows. Prior to cell culture, MgF_2 windows were treated by oxygen plasma (0.5 mbar, power 5.0, 10 minutes, Plasma Prep 5, Gala Instrumente) to increase their hydrophilicity and incubated with complete cell medium for at least 16 hours in a humidified cell culture incubator (37℃, 5% CO_2) to improve cell adhesion. Cells were seeded at a density of 15,000 cells/cm^2 on Matrigel/Collagen I gels (Subsection 2.3.3), and for cells on MgF_2 windows seeding was carried out at densities of 15,000 cells/cm^2 for sparse conditions and TGF-β1 assay, and 150,000 cells/cm^2 for confluent conditions. MgF_2 windows (10 mm diameter) were placed in 48 well plates.

At experimental endpoint, MCF10A on Matrigel/Collagen I gels were fixed with 4% (v/v) paraformaldehyde (methanol-free, 16% (w/v), Thermo Fisher Scientific) and 1% (v/v) glutaraldehyde (50% (v/v), Electron Microscopy Sciences) in PBS for 15 minutes at room temperature. Cells on MgF_2 windows were fixed with 4% (v/v) paraformaldehyde (methanol-free, 16% (w/v), Thermo Fisher Scientific) in PBS for 15 minutes at room temperature. Cells were washed in PBS and then stored at 4℃ until imaging.

2.3.11.B Raman Imaging

Raman imaging of MCF10A cells was performed by Conor Horgan and Fergus O'Brien using a confocal Raman microscope (alpha300R+, WITec, GmbH, Germany). A 532 nm laser light source at 35 mW power output was applied through a 63x/1.0 NA water-immersion microscope objective lens (W Plan-Apochromat, Zeiss, Germany). Inelastically-scattered light was collected through the objective and directed via a 100 µm diameter silica fibre, acting as a confocal pinhole, to a high-throughput imaging spectrograph (UHTS 300, WITec, GmbH, Germany) with a 600 groove/mm grating and equipped with a thermoelectrically cooled (-60℃) back-illuminated charge-coupled device (CCD) camera. Raman spectra were acquired in the range from 0 to 3700 cm^{-1} with a spectral resolution of 11 cm^{-1}. Chemically fixed cells on MgF_2 windows and on gels were imaged with a 2 µm resolution and 1 second integration time. For each sample, ten 40 x 40 µm distinct regions of cells were imaged.

2.3.11.C Data Processing

Initial spectral image processing was performed in collaboration with Conor Horgan using Witec ProjectFOUR software. Briefly, spectra were first cropped to remove laser contribution. Background subtraction was performed using a 'shape' background filter with parameter size 500 to remove autofluorescence spectral contributions and spectra normalised to the area under the curve.

Further image processing was performed by myself and Conor Horgan in MATLAB (2016a, Mathworks) using custom in-house scripts. Briefly, data were imported from Witec ProjectFOUR and a k-means analysis was used to exclude non-cell spectra. The remaining cell spectra were then normalised to the area under the curve. Next, cosmic ray peaks present in the spectra were then removed and the spectra were smoothed using a 1st order Savitzky-Golay filter with a frame length of 7. Principal component analysis (PCA) and partial least squares-discriminant analysis (PLS-DA) statistical analyses were then performed on normalised, mean-centred data in PLS_Toolbox (Eigenvector Research) in MATLAB. Venetian blinds cross-validation was used to test each model.

2.3.12 Statistical Analysis

Statistical analyses were carried out using GraphPad Prism 6.0. For RT-qPCR, three independent biological replicates were collected for each sample in study, and two technical replicates were measured and analysed in each RT-qPCR assay plate. In the case of 2D EMT models, in which MCF10A were grown on MgF_2 windows (to match the same experimental conditions used to obtain Raman spectra) cell extracts from at least 4 wells were pooled for RNA isolation and subsequent gene expression analysis. To determine whether data were normally distributed, Komogorov–Smirnov and Shapiro–Wilk tests were performed. Differences in gene expression on 2D models were tested by paired *t*-tests. When data were not normally distributed, Wilcoxon tests were performed. Differences in gene expression of cells on Matrigel/Collagen I gels were tested by One-way ANOVA. For the latter sample group, when data were not normally distributed, Kruskal-Wallis tests were performed. All hypothesis tests were considered two-tailed.

Statistical analysis of specific Raman spectra peaks that resulted from the visual inspection of the computed difference spectra was carried out by Dr Isaac Pence. Differences between experimental groups were tested using ordinary least-squares regression based on Generalized Linear Models in the statistical software R using the rms package. The data was then modelled as the dependent variable, and regression coefficients were calculated for independent variables for each EMT model. To account for different levels of response due to variability between biological replicates, generalised

estimating equations were used to enable clustering of measurements obtained from samples derived from a single biological replicate [363–366]. The generated regression coefficients were compared. Heteroscedasticity in the data set was addressed by using the robust covariance function created in the rms package (“robcov”) to adjust the standard errors. Finally, to compare groups, a one-way ANOVA was performed on the generated GLM regression coefficients from the developed regression model, which were represented with p-values calculated based on multiple comparisons via Holm correction. All hypothesis tests were considered two-tailed.

For SICM, mean stiffness values of each ROI were plotted and statistically analysed. To determine whether data were normally distributed, Komogorov–Smirnov and Shapiro–Wilk tests were performed. Data were tested with a two-tailed unpaired *t*-test with Welch’s correction.

In all cases, *$p<0.05$;**$p<0.01$;***$p<0.001$;****$p<0.0001$.

2.4 Results

2.4.1 Stromal collagen upregulates mesenchymal phenotype

A 3D morphogenesis assay was used to study the interplay between matrix composition and mammary epithelial cell behaviour. Here, Matrigel – EHS mouse tumour-derived matrix mainly composed of laminin-111 and collagen IV – was used as rBM to support 'normal' laminin-dependent mammary acini morphogenesis in culture. To investigate the role of type I collagen, one of the main components of the interstitial matrix that malignant tumour cells encounter when breaching the BM, human mammary gland cells (MCF10A) were exposed increasing concentrations of rat tail tendon type I collagen (with constant amounts of rBM). In the present study, MCF10A cells were cultured using the 3D on-top method, as discussed in Chapter 1, Section 1.5.2.B.

2.4.1.A Matrix type I collagen results in an invasive epithelial phenotype

As expected from previous studies [187], a matrix composed exclusively of rBM supported the formation of hollow acinar structures by MCF10A cells after a week in culture (Figure 2.5**a**, 0 mg/ml Collagen I). However, increasing concentration of type I collagen in the matrix with constant rBM resulted in an invasive epithelial behaviour (2.5**a**). Notably, lower concentrations of type I collagen (0.5 and 1 mg/ml) supported the formation of misshapen spherical structures. Higher concentrations of stromal type I collagen (2mg/ml and, especially, 4mg/ml) were conducive of an invasive phenotype in MCF10As, which consistently did not permit the formation of acinar structures.

2.4.1.B Matrix type I collagen upregulates mesenchymal gene expression

The invasive phenotype and the morphological changes that occur in response to increasing concentrations of type I collagen in the matrix highly resemble the process of EMT. Hence, in order to better understand whether these changes in matrix composition were consistent with a type of EMT programme, the expression of certain EMT markers was investigated using WB and RT-qPCR. Increasing concentration of type I collagen in the matrix resulted in a higher expression of intermediate filament vimentin, as observed by WB (Figure 2.5**b**). Interestingly, an overall upregulation of mesenchymal gene expression, relative to samples with no type I collagen, was observed by RT-qPCR (Figure 2.5**c**), but with varying degrees depending on the concentration of type I collagen.

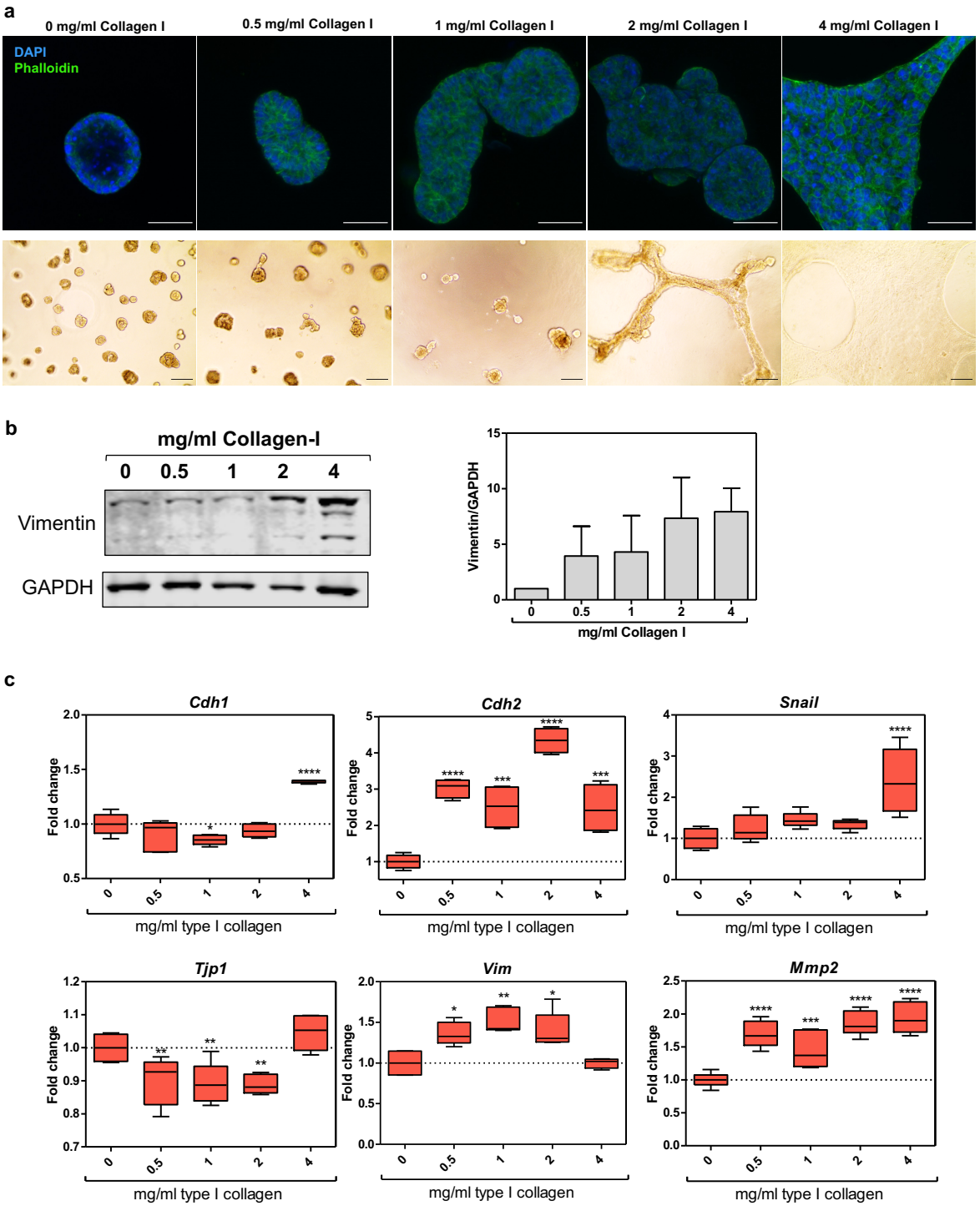

Figure 2.5: Matrix type I collagen upregulates invasive phenotype that resembles EMT. a Brightfield and fluorescent images of MCF10A cells on rBM and type I collagen after 1 week in culture. Scale bars: 50 μm on brightfield and 500 μm on fluorescent images. **b** Representative Western blot of MCF10A cells on rBM and type I collagen after 1 week in culture and respective quantification on the bar graph, N=2. **c** EMT gene expression of MCF10A cells on rBM and type I collagen after 1 week in culture measured by RT-qPCR and normalized to *GAPDH* and to sample 0 mg/ml Collagen (rBM only). *y* axis: $2^{-\Delta\Delta Ct}$. Data are shown on Tukey box and whiskers plot. *p<0.05;**p<0.01;***p<0.001;****p<0.0001.

Expression of *Cdh1* (E-cadherin) was downregulated in the presence of lower concentrations of type

I collagen, particularly at 1 mg/ml, but showed a significant upregulation at 4 mg/ml collagen. Regardless, *Cdh2* (N-cadherin) expression was upregulated in all matrices that contained type I collagen and a peak was observed at 2 mg/ml. Remarkably, the overexpression of both E-cadherin and N-cadherin at a 4 mg/ml collagen concentration somewhat challenges the long-standing idea of a cadherin switch happening with EMT. Consistent with the gene expression of epithelial marker E-cadherin, *Tjp1* (ZO-1) expression significantly decreased in the presence of collagen, with the exception of 4mg/ml. Moreover, *Snail* (EMT-TF SNAIL) expression was upregulated at 4 mg/ml collagen. In addition, an increased expression of *Vim* (vimentin) was observed up until a collagen concentration of 2 mg/ml, and, surprisingly, no significant alteration was observed at 4 mg/ml, even though a clear increase in vimentin protein expression was observed in response to stromal collagen. Finally, *Mmp2* (MMP-2) expression was consistently upregulated in the presence of type I collagen in the matrix. Together, the collected data confirm that the presence of stromal collagen in the extracellular environment promotes mesenchymal gene and protein expression, but also shed light on the complexity of the transitional states in the EMT programme.

2.4.1.C Effects of extracellular type I collagen on the stiffness of mammary epithelial cells

The extracellular microenvironment controls cell behaviour [31]. Cells can sense their biochemical and biophysical environment, including the stiffness of the surrounding matrix [234]. Importantly, it has been shown by atomic force microscopy studies on human breast biopsies that cancer cells surrounded by a stiffer ECM appear to be softer than normal cells in healthy tissues [367]. Considering that the matrices built in the present study composed of interpenetrating networks of rBM and type I collagen are stiffer with increasing amounts of fibrillar collagen (Figure A.1 Appendix B and Figure 2.6**a**), it was hypothesised that MCF10A cells that exhibit an invasive phenotype in the presence of collagen are softer than their acinar counterparts in rBM alone. To investigate this, scanning ion conductance microscopy (SICM), a scanning probe microscopy technique that can be used to obtain surface topography and to map the stiffness of living cells [360], was employed to measure the stiffness of cells grown on these gelled matrices. Mean stiffness values acquired a week post-seeding from MCF10A cells grown on rBM (0 and 4 mg/ml Collagen I) are shown on Figure 2.6**b**. Results showed that MCF10A cells grown on rBM and type 1 collagen (4 mg/ml) are stiffer than acinar structures grown on rBM alone, which refutes the initial hypothesis.

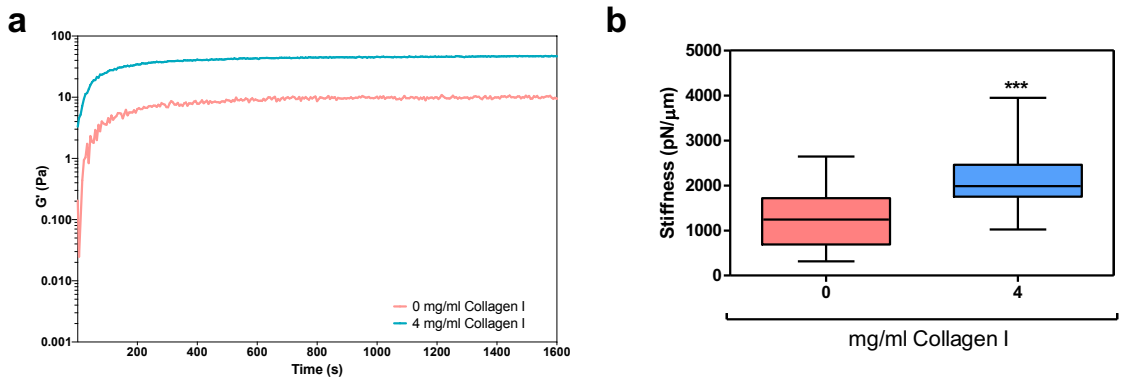

Figure 2.6: Rheological measurements of matrices composed for rBM and type I collagen and stiffness of MCF10A cells on those matrices measured by SICM. a 0 and 4 mg/ml Collagen gels (with rBM) were characterised by rheology. Plot shows a oscillatory time sweep that was performed at 37℃ using a 0.2% constant strain (within the linear viscoelastic region) and at a frequency of 3.14 rad/s. *y* axis: shear modulus G' in Pa. n = 3. **b** Stiffness measurements of MCF10A cells on matrices composed for rBM alone and rBM and 4 mg/ml Collagen. SICM measurements were carried out with the help of Sahana Gopal. *y* axis: Stiffness in pN/μm. Data is shown on Tukey box and whiskers plot. ***p$<$0.0001. N = 2, n = 3.

2.4.2 Using Raman spectroscopy (RS) to characterise EMT

2.4.2.A EMT induction via different methods

In addition to having the 3D EMT model described above, two 2D EMT models were used in the study by RS. In one of the 2D models, MCF10A were cultured at two different cell densities, as it has been shown that these cells exhibit mesenchymal-like features when cultured in low cell density [368]. In the second method, TGF-β1 treatment was also used to induce EMT changes in MCF10A in 2D, given that it is an extensively used EMT model *in vitro* [369].

As expected, MCF10A grown in sparse conditions showed a decrease in the expression of *Cdh1* and an increase in the expression of mesenchymal genes *Cdh2*, *Snail*, *Slug*, and *Vim*, with the exception of *Mmp2*, which expression was not significantly altered in these conditions (Figure 2.7**a** and **b**). Following TGF-β1 treatment, the expression levels of all mesenchymal genes measured were increased, but the expression of epithelial marker *Cdh1* was also increased relative to cells that were not exposed to TGF-β1 (Figure 2.7**c** and **d**). Again, at the transcriptional level, an E- to N-cadherin switching in EMT is not observed, and this result also challenges the idea of TGF-β1 functioning as a transcriptional repressor of E-cadherin [370–372]. Together, these observations confirm that human mammary epithelial MCF10A cells exhibit a mesenchymal-like phenotype when cultured at low density and that they undergo EMT in response to TGF-β1 treatment.

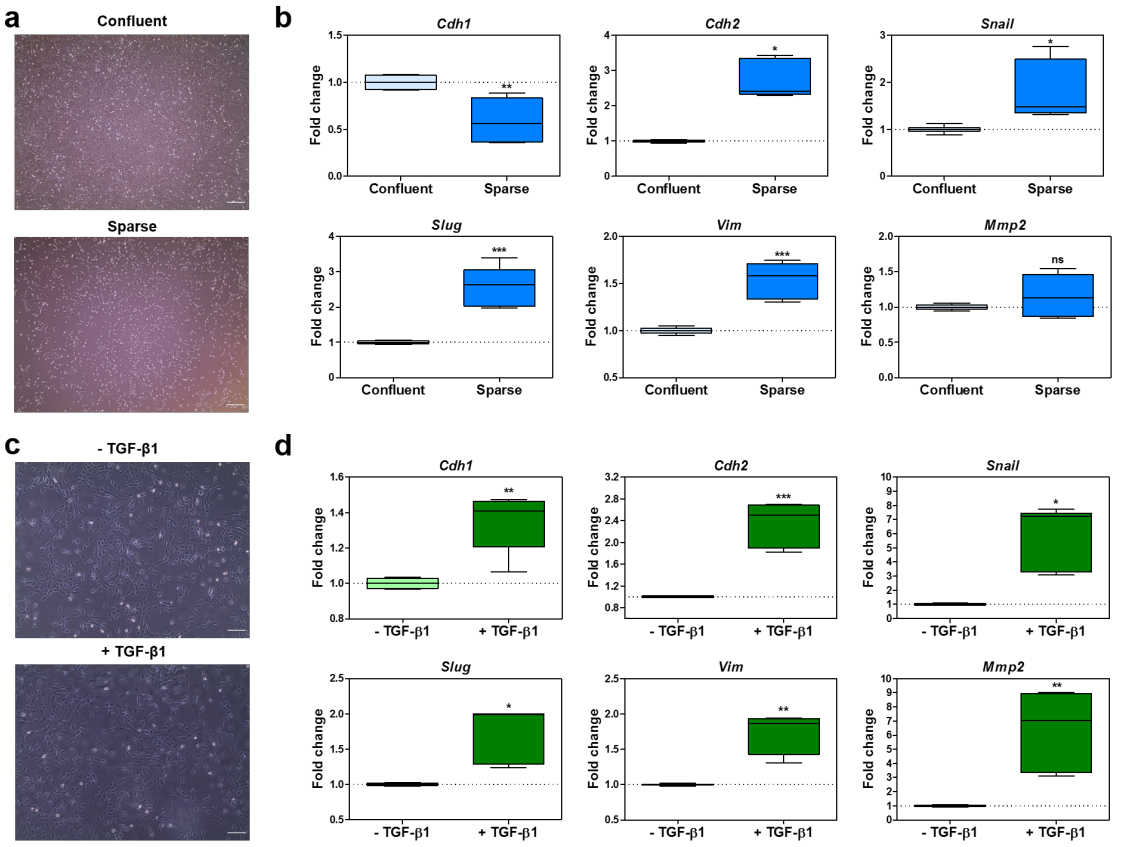

Figure 2.7: Changes in EMT in 2D culture Human mammary epithelial MCF10A cells exhibit a mesenchymal-like phenotype when cultured at low density and undergo EMT following TGF-β1 treatment. **a** Brightfield images of MCF10A in 2D culture 24 hours post seeding. High density (confluence) top and low density (sparse) bottom. **b** EMT gene expression of MCF10A cells at different densities (sparse and confluent) 24 hours post seeding by RT-qPCR and normalized to *GAPDH* and confluent cells. **c** Brightfield images of MCF10A in 2D culture 24 hours post TGF-β1 treatment and 48 hours post seeding (same cell density). Cells that received TGF-β1 treatment on top and without treatment on bottom. **d** EMT gene expression of MCF10A cells 24 hours post TGF-β1 treatment and 48 hours post seeding by RT-qPCR and normalized to *GAPDH* and to cells that did not receive TGF-β1 treatment. **a,c**.Scale bars 200 μm. **b,d** *y* axis: $2^{-\Delta\Delta Ct}$. Data is represented as Tukey box and whiskers plot. *p<0.05;**p<0.01;***p<0.001.

2.4.2.B RS can be used to separate epithelial from mesenchymal-like states

Raman spectra of all conditions that generated either an epithelial or a (quasi-)mesenchymal phenotype were acquired in the Raman shift fingerprint region, 600 to 1800 cm^{-1}. Figure 2.8 (**a**,**c** and **e**) shows the mean Raman spectra for each condition within each EMT system after background subtraction, area normalisation and multiple scattering correction. Spectral data was then processed using multivariate methods. After a k-means analysis to exclude non-cell spectra, PCA was performed to achieve data compression. Next, PLS-DA, a commonly used supervised classification method, was performed to build models for the different sample groups. Figure 2.8 (**b**, **d** and **f**) shows 3D latent variable plots from the PLS-DA models that were generated within each EMT group. The constructed

models were subjected to venetian blinds cross-validation to test the accuracy of each model, which was over 90% in all cases (Table 2.4). These data show that it is possible to differentiate the spectra from EMT conditions that were directly compared against each other.

To further investigate the process of EMT occurring on the 3D morphogenesis assay with interpenetrating networks of rBM and type I collagen, a multiclass PLS-DA was built using Raman spectra of MCF10A cells on 0, 0.5, 2 and 4 mg/ml Collagen I gels. The Raman spectra of cells on 1 mg/ml Collagen I gels were excluded from this particular analysis due to their heterogeneity and variability. With the 3D latent variable plot produced from this PLS-DA model it is possible to visualise a separation between the cells on gels with lower amounts (or none) of type I collagen (0 and 0.5 mg/ml, with more epithelial-like morphological features) and on gels with higher concentrations of type I collagen (2 and 4 mg/ml, with more mesenchymal-like morphological features) (Figure 2.9**a**). The multiclass PLS-DA model displayed on Figure 2.9**a** was cross-validated and its accuracy is of 94.02%. Following, a binary (two-class) PLS-DA model was generated to separate Raman spectra of MCF10A cells on rBM (0 mg/ml Collagen) and of cells on the matrix with rBM and the highest concentration of type I collagen (4 mg/ml). Here the separation is visually evident as shown on Figure 2.9**b**.

All Raman spectra obtained from 2D EMT models were plotted (Figure 2.10**a**) and a multiclass PLS-DA model was built to separate the epithelial (confluent and TGF-β1-) from the (quasi-)mesenchymal states (sparse and TGF-β1+) (Figure 2.10**b**), which was accomplished with an accuracy of 81.9%. Finally, the 2D and 3D EMT models in this study were compared and separated by multiclass PLS-DA. This last model shown in Figure 2.11 was built to separate all epithelial (confluent, TGF-β1- and 0 mg/ml Collagen) from the (quasi-) mesenchymal states (sparse, TGF-β1+ and 4 mg/ml Collagen), with an accuracy of 79.6%. To have a clearer training set for the classification method and to better evaluate the prediction model, samples 0.5, 1 and 2 mg/ml Collagen were excluded from this analysis. 2D latent variable (LV) plots show a clear separation between 2D and 3D EMT models (Figure 2.11**a** and **b**), but it is also possible to see a separation between a more epithelial-like state and a more mesenchymal-like state (Figure 2.11**a**). From observing the 3D LV plot the separation between 2D and 3D EMT models is clear from the gap that can be seen in the middle of the plot (Figure 2.11**c**) and the separation between a more epithelial-like state and a more mesenchymal-like state can also be seen (Figure 2.11**c**).

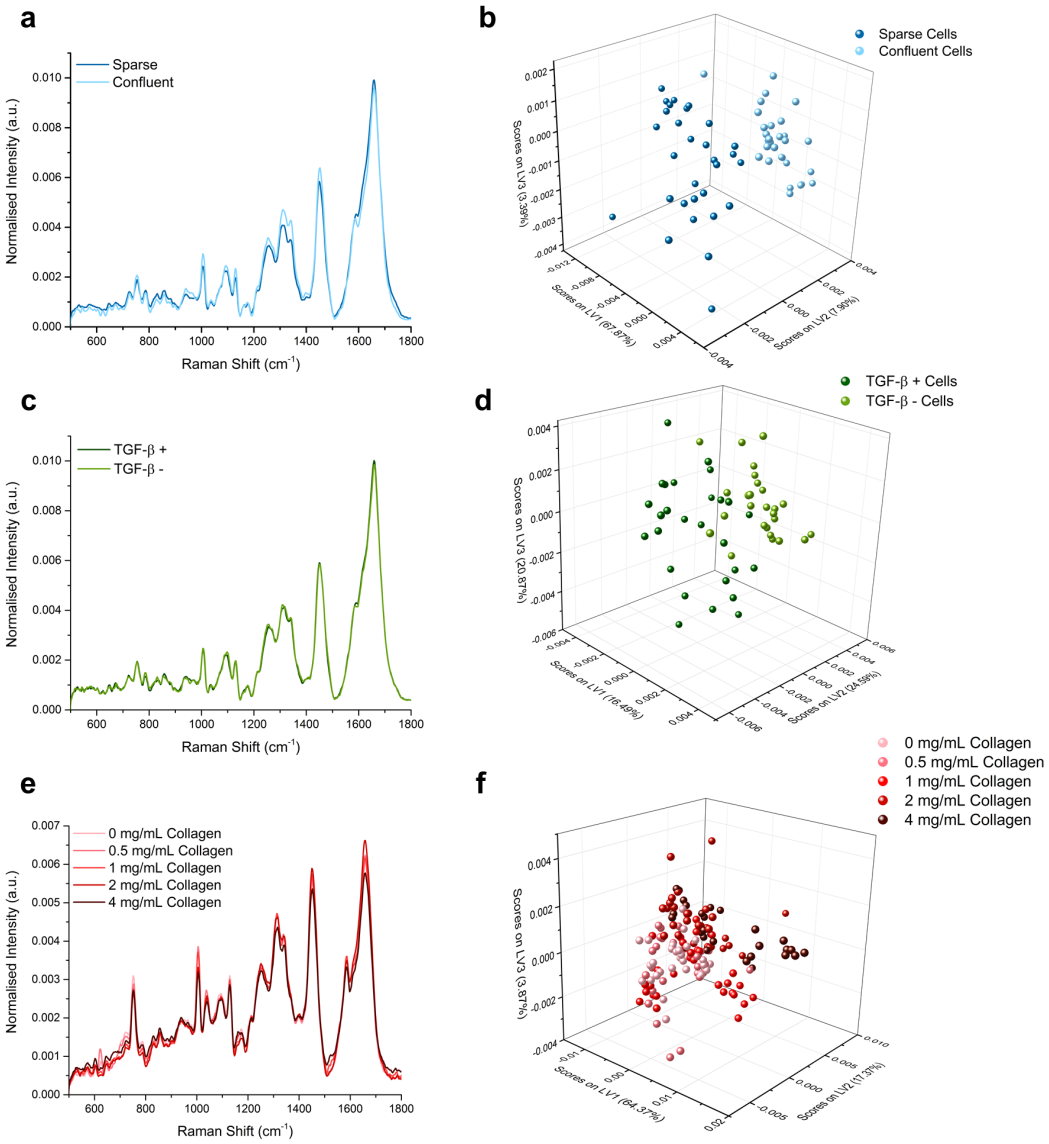

Figure 2.8: Raman spectra and PLS-DA of all EMT samples. **a** Raman spectra and b PLS-DA model from MCF10A cells cultured at different densities (sparse and confluent) 24 hours post seeding. **c** Raman spectra and **d** PLS-DA model from MCF10A cells cultured with and without TGF-β1 24 hours post treatment, 48 hours post seeding. **e** Raman spectra and **f** multiclass PLS-DA model from MCF10A cells on rBM and type I collagen after 1 week in culture. **a,c,e** RS after background subtraction, area normalisation and multiple scattering correction. The colour sets represent different models: in blue is the sparse and confluent model, in green the response to TGF-β1 treatment, and in different shades of red the 3D EMT model. **b, d, f** Each PLS-DA model was subjected to venetian blinds cross-validation and the accuracies are presented in Table 2.4. Raman spectra were collected by Conor Horgan and Fergus O'Brien.

Table 2.4: Accuracy values obtained for PLS-DA models in Figure 2.8 with venetian blinds cross-validation test. Table is displayed in the same colour codes as in Figure 2.8. Venetian blinds cross-validation test results refer to each model separately.

Condition	Accuracy (%)
Confluent	96.6
Sparse	96.6
TGF-β1 -	93.2
TGF-β1 +	93.2
0 mg/ml Collagen	95.8
0.5 mg/ml Collagen	95.8
1 mg/ml Collagen	97.9
2 mg/ml Collagen	95.8
4 mg/ml Collagen	97.9

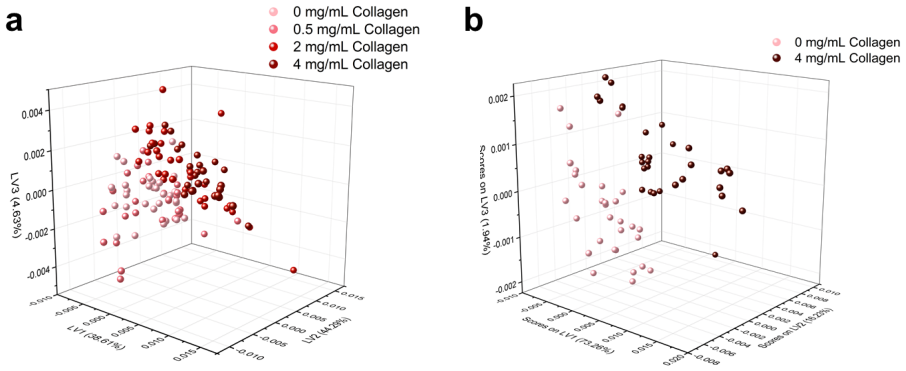

Figure 2.9: PLS-DA models of EMT on 3D morphogenesis assay. **a** Multiclass PLS-DA from the Raman spectra of MCF10A cells on 0, 0.5, 2 and 4 mg/ml Collagen I gels (cells on 1 mg/ml Collagen I gels was excluded from this particular analysis due to its inherent heterogeneity and variability). **b** Two-class PLS-DA from the Raman spectra of MCF10A cells on 0 and 4 mg/ml Collagen I gels.

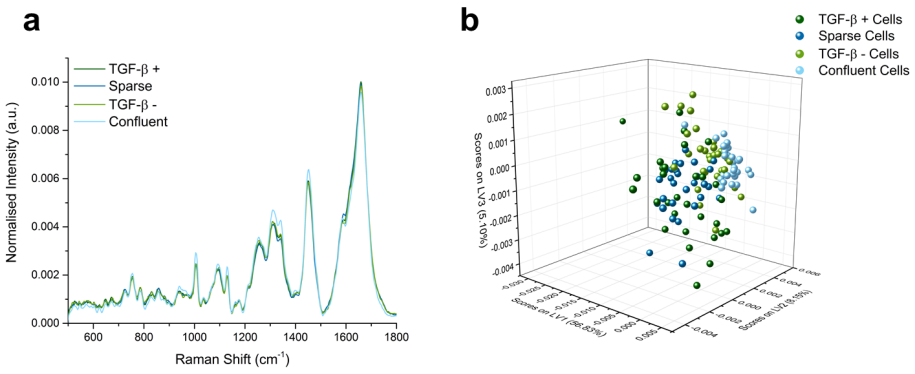

Figure 2.10: Raman spectra and PLS-DA models of EMT on 2D models. **a** Raman spectra of MCF10A cells on 2D culture - sparse *versus* confluent (different shades of blue) and TGF-β1 treatment (different shades of green) and **b** multiclass PLS-DA model built from these spectra to separate the epithelial (confluent and TGF-β1-) from the (quasi-)mesenchymal states (sparse and TGF-β1+). Raman spectra were collected by Conor Horgan and Fergus O'Brien.

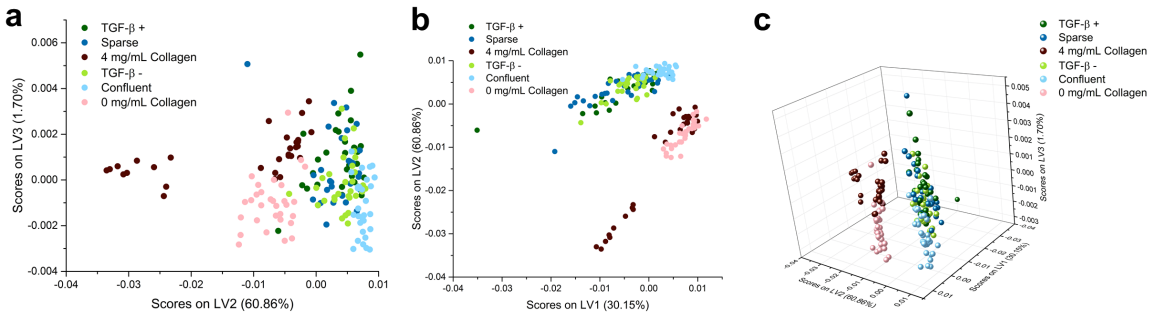

Figure 2.11: PLS-DA models of EMT on 2D and 3D models together. Multiclass PLS-DA model to separate all epithelial (confluent, TGF-β1- and 0 mg/ml Collagen) from the (quasi-) mesenchymal states (sparse, TGF-β1+ and 4 mg/ml Collagen), with an accuracy of 79.6%. For simplicity, 0.5, 1 and 2 mg/ml Collagen samples were excluded from this analysis. **a** 2D LV plot shows a separation between 2D and 3D EMT models and between a more epithelial-like state and a more mesenchymal-like state. **b** 2D LV plot shows a separation between 2D and 3D EMT models. **c** 3D LV plot shows the separation between 2D and 3D EMT models (from the gap that can be seen in the middle) and the separation between a more epithelial-like state and a more mesenchymal-like state can also be seen.

In order to determine distinguishing features between epithelial-like and mesenchymal-like states, the difference between the Raman spectra (Figure 2.8**a**, **c** and **e**) were computed and plotted as shown in Figure 2.12 **a**, **b** and **c**. This allowed for a visual inspection of spectroscopic signal differences, and, consequently, the identification of prominent peaks. Raman databases [355, 373] were used as a tool to identify which biomolecules possess groups that vibrate at those specific frequencies. All of the analysed peaks in the confluent *versus* sparse group (Figure 2.12**d**) were found to be significantly different between the two samples. The Raman frequencies seem to correspond to differences in nucleic acids (751 and 1344 cm^{-1}), phenylalanine (an aminoacid that is part of the structure of various proteins, including collagen; 1008 cm^{-1}), lipids (functional group amide; 1129 and 1634 cm^{-1}), and proteins (1455 cm^{-1}, which has also been attributed to lipids). In turn, from the TGF-β assay the two significantly different peaks have been previously assigned to proteins (1103 cm^{-1}, which has also been attributed to lipids) and lipids (functional group amide; 1681 cm^{-1}). Finally, from the selected peaks in the 3D EMT model with the rBM/Collagen matrix, only one was found to be significantly different and it has been assigned to phenylalanine (1002 cm^{-1}).

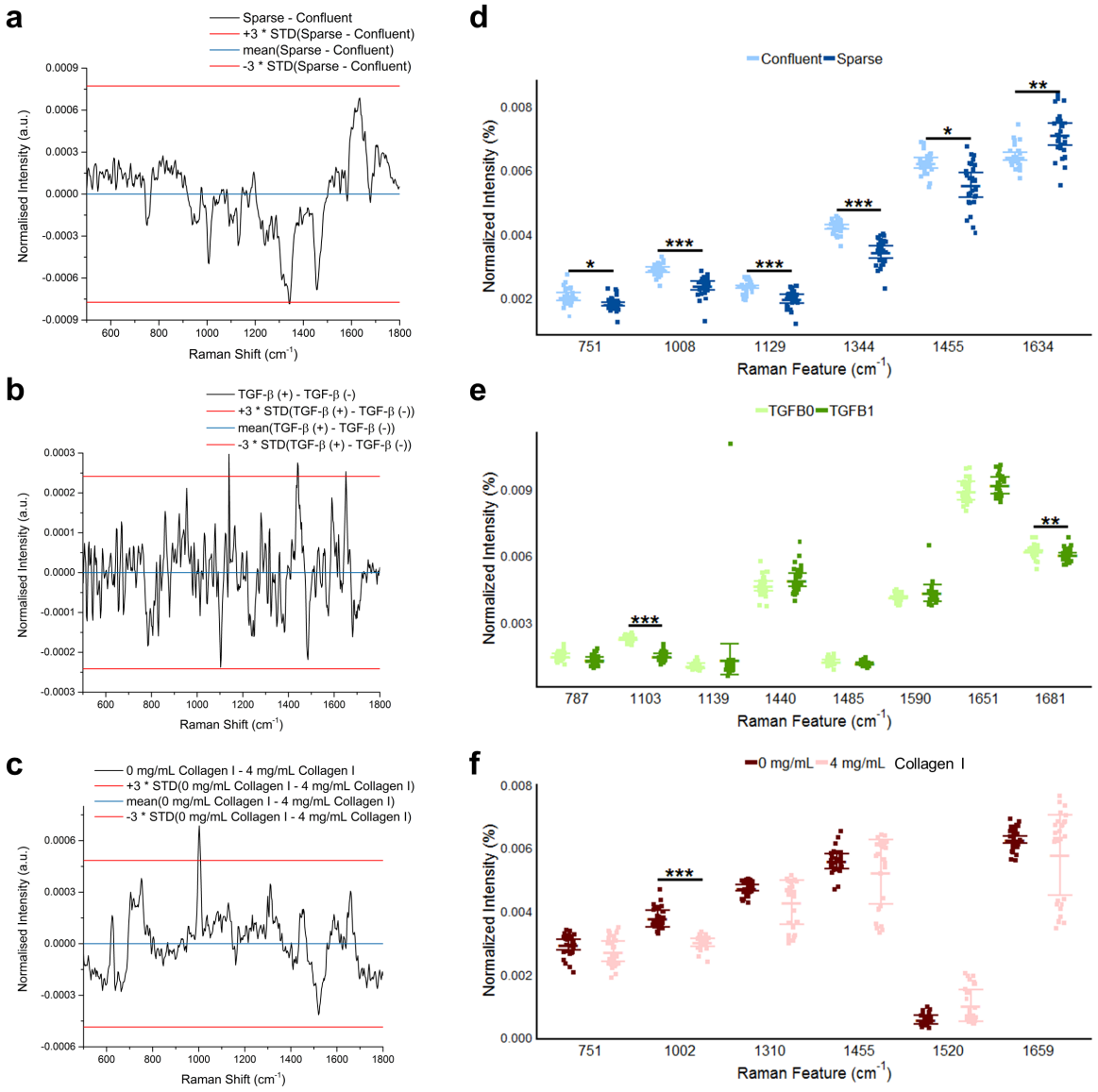

Figure 2.12: Difference spectra from EMT models. Differences between the spectroscopic signals were computed to visualise the most prominent peaks from the Raman spectra presented in Figure 2.8: **a** confluent *versus* sparse cells, **b** TGF-β1 treatment, and **c** cells on 0 and 4 mg/ml Collagen. Spectral values that corresponded to each prominent peak (10 samples per biological replicate, and so a total of 30 points per condition) were plotted and statistically analysed to understand if these differences were of any mathematical significance: **d** confluent *versus* sparse cells, **e** TGF-β1 treatment, and **f** cells on 0 and 4 mg/ml Collagen. *p$<$0.05;**p$<$0.01;***p$<$0.001.

2.5 Discussion

Breaching of the basement membrane, which occurs when cells are able to migrate from the epithelial compartment to the interstitial matrix, is one of the hallmarks of malignant carcinomas [353]. The overall objective of this work was to model and investigate the breaching of the basement membrane by human mammary epithelial cells utilising biological components cells encounter *in vivo*. The epithelium is tightly organised and maintained by the BM, which is a thin sheet-like layer of specialised ECM primarily composed of collagen IV and laminin. In turn, stromal ECM, comprised predominantly of type I collagen, surrounds the BM [104]. The epithelial microenvironment is instrumental to maintain tissue homeostasis and to control epithelial cell phenotype, including cell polarity and controlled levels of proliferation and apoptosis [26]. Importantly, increased expression, deposition and crosslinking of type I collagen have been implicated in cancer progression both *in vitro* and *in vivo* [374]. In this chapter, it is shown that exposure of non-transformed human mammary epithelial MCF10A cells to increasing concentrations of type I collagen in the matrix results in an invasive phenotype (Figure 2.5**a**). This provides a direct evidence that an imbalance in the ECM composition can result in a dysregulated epithelial phenotype, which is consistent with previous reports [151, 325, 327, 375].

The morphological and behavioural changes observed here highly resemble EMT, a process in which epithelial cells lose their apicobasal polarity and become migratory. Indeed, increased expression of mesenchymal marker vimentin with increased concentration of type I collagen is observed by WB (Figure 2.5**b**). Vimentin is expressed in EMT-related events during embryonic development [376–379]. Importantly, increased vimentin expression has also been reported in metastatic breast carcinoma and is associated with poor prognosis [380–382]. The protein expression pattern of vimentin observed in the present work seems to be in agreement with what is found in the literature in the context of breast carcinoma, but it should be noted that the use of vimentin as an EMT marker has been met with some controversy in the context fibrosis [354]. Furthermore, RT-qPCR measurements (Figure 2.5**c**) show an overall upregulation of mesenchymal gene expression induced by the presence of type I collagen. It is interesting to note that, even though cells seem to lower their expression of *Cdh1* in the presence of Collagen I in the matrix (up to 2 mg/ml), this epithelial gene was found to be significantly upregulated in the matrix with the highest concentration of Collagen I studied (4 mg/ml). This observation was somewhat surprising, as in this condition cells exhibit an invasive phenotype and overexpress other mesenchymal markers, namely *Cdh2*, *Snail* and *Mmp2*, and E-cadherin has long been described as a tumour invasion suppressor gene [383]. However, after a week in culture, MCF10A in Matrigel:4 mg/ml Collagen I proliferate and populate most of the gel area, bringing cells in close contact with each other, which can explain this relative increase in expression. Furthermore, it has been reported that loss of E-cadherin is not necessary for EMT in human breast cancers, and

that basal-like cells (a group in which MCF10A are included) *in vitro* do not always stop expressing *Cdh1* after undergoing EMT [384]. Similarly to *Cdh1*, the expression pattern of *Tjp1* (ZO-1) shows a decrease in the presence of Collagen I in the matrix (up to 2 mg/ml), except with highest concentration (4 mg/ml) in which it shows no difference to control (0 mg/ml). Like with E-cadherin, the reasoning behind this might be the overpopulation of the most rigid matrix by these cells, but *Tjp1* seems to be regulated differently to *Cdh1*. Expression of mesenchymal markers *Cdh2* (N-cadherin) and *Mmp2* (MMP2) is upregulated in the presence of collagen I, even in the lowest concentration (0.5 mg/ml). Increased expression of N-cadherin in EMT has been well established [297] and it has also been strongly associated with metastatic carcinomas [344, 385]. The fact that an upregulation of both E- and N-cadherins is observed in the model of EMT used in this work, at the timepoint chosen, seems to challenge the notion that the expression of N-cadherin upon EMT is accompanied by loss of E-cadherin (the cadherin switch). This evidence implies that a cadherin switch does not occur in all EMT events. Nevertheless, it would be important to study the expression of these homotypic cell-cell adhesion molecules at the protein level, as gene expression measurements do not always reflect what is actually happening in terms of synthesis and maintenance of proteins [386]. Interestingly, co-expression of E- and N-cadherins has been reported in developmental studies [387], which leads to the question whether such phenomenon could happen in a different context, such as cancer. In turn, upregulation of MMP2, a matrix protease capable of degrading BM collagen IV [388] and interstitial matrix collagen I [389, 390], is consistent with studies that report an increased expression of MMPs, in particular MMP2, after induction of EMT in MCF10A cells [391, 392]. It has been shown, however, that cells do not necessarily require matrix-degrading proteases to migrate, as long as the porosity of the ECM allows for cellular deformation [159]. Moreover, EMT-TF *Snail* (SNAIL) was found to be significantly upregulated at the highest concentration of type I collagen, even though no change resulted at lower concentrations. The role of this zinc-finger transcriptional repressor in EMT has been well established [297] and previous studies have indicated that SNAIL may contribute to this event by supressing *Cdh1* and other epithelial-related genes [293, 294, 393]. These reports have shown strong evidence of repression of E-cadherin expression by SNAIL at the protein level, which leads to believe that it would be important to investigate whether the same happens using the rBM/collagen I morphogenesis assay in the present work. Finally, an increased expression of mesenchymal gene *Vim* was detected in the presence of collagen I, except at 4 mg/ml. This latter finding is particularly surprising given the Western blotting data (Figure 2.5**b**) that show an increased expression of this protein, but it is possible that this is due to the intrinsic variability in this system.

One of the key messages in this chapter is that the presence of type I collagen in a matrix with rBM shifts cells towards a mesenchymal phenotype. The cells used in this work (see Chapter 1 Section 1.5) offer a great model to study transitional events between healthy and pathological states, particu-

larly the initial steps of malignancy in breast carcinoma. As previously discussed, the importance, or even existence, of EMT in cancer is still controversial, but this debate is more an issue of semantics than of biological mechanisms [279]. EMT should be looked at as a complex phenomenon that involves multiple transitional states and underlying mechanisms, as opposed to a binary cellular switch. To metastasise, cells need to acquire features that allow them to migrate and invade other sites in the body, and there is compelling evidence that the process of partial or complete EMT is what allows cells to do so [291]. Studying EMT in the context of disease is of utmost importance and the development of physiologically relevant systems, particularly in 3D, is needed.

The system used in this work, however, has caveats that should be recognised. One of the main limitations of using increasing concentrations of type I collagen in the ECM to increase matrix stiffness is that it is not possible to decouple biophysical from biochemical effects. In fact, type I collagen is known to bind various cell surface receptors, namely integrins, thereby activating distinct signalling pathways and controlling cell fate independently of matrix mechanics [104, 394, 395]. In addition, in an *in vivo* situation it is likely that not all mammary epithelial cells would breach the basement membrane to encounter stromal collagen [374]. An interesting strategy that has been used is to pre-form acinar structures and then culture them in collagen I matrices to examine cellular behaviour [327, 396]. Moreover, the range of stiffness that can be achieved with an rBM/collagen I system is considerably limited and it becomes challenging to physically manipulate pre-gelled collagen I at high concentrations. One strategy that can be utilised to increase ECM stiffness without having to increase collagen concentration is to make use of non-enzymatic glycation with ribose [397], which increases collagen crosslinking [398]. This approach can potentially also overcome the issue of increasing the number of collagen binding sites that could activate different pathways, as all conditions would have the same amount of collagen. Finally, since one of the limitations that can be noted about using Matrigel as rBM and collagen I as the driver of increasing stiffness is that biophysical and biochemical effects cannot be decoupled, the development and use of (semi-)synthetic systems can be of pivotal importance.

Furthermore, as previous *ex vivo* studies have demonstrated that breast cancer cells are softer than their healthy counterparts [367] and *in vitro* studies have shown evidence to support that induction of EMT reduces intracellular stiffness [356], it was hypothesised that MCF10A cells grown on more rigid matrices that exhibit a mesenchymal-like phenotype could decrease their stiffness compared to the ones that form acinar structures in rBM alone. The mechanical properties of MCF10A cells on rBM/Collagen matrices were then investigated by SICM. To the best of found knowledge, it was the very first time this technique was employed on cells grown on such soft substrates. These measurements were aimed at assessing cell stiffness changes when matrix composition (and stiffness) is

altered. Even though it would be important to carry out more measurements from at least one more biological replicate, the results obtained indicate that the intracellular stiffness of MCF10A increase when these exhibit a mesenchymal-like phenotype on matrices with type I collagen (4 mg/ml; Figure 2.6**b**), which refuted the working hypothesis. It is clear from the collection of studies found in the literature that cellular mechanics is altered with EMT, but it seems the changes in cell stiffness are not so linear as previously stated. In fact, studies using Atomic Force Microscopy have reported an increase in cellular stiffness upon TGF-β treatment of kidney [399], lung [400], and mammary [401] epithelial cells. In addition, a study that investigated the stiffness of pancreatic cancer cells reported that stiffer cells exhibited a more invasive behaviour [402], which also seems to challenge the idea that decreased cellular stiffness is a phenomenon directly associated with metastatic behaviour.

In addition, Raman spectroscopy (RS) was employed to further characterise the biochemical fingerprint of epithelial-like and mesenchymal-like phenotypes in different models of EMT. RS is a vibrational technique that produces a spectrum, of which the bands represent the vibrational frequencies of different functional groups within the biomolecules that compose the sample under study. It has emerged as a promising technique to study biological specimens in various contexts [355, 403]. Raman spectra of cells have an underlying high level of complexity due to the amount of information on a vast number of biomolecules, but the ability to obtain the biochemical fingerprint of cells in different conditions makes RS a potential technique to be instrumental when studying various pathobiological systems. Few studies using RS to study EMT have been published to date [404–406]. Considering the inherent complexity of the 3D model used, 2D models of EMT typically used *in vitro* were analysed for comparison. Figure 2.7**a** shows that there is a shift towards mesenchymal gene expression in sparse MCF10A cells compared to confluent. This model was previously studied using RS by Marro et al. [406] to monitor EMT, which led to its use in this thesis for comparison. Figure 2.7**b** displays the gene expression response to TGF-β1 treatment to induce EMT, which resulted in an upregulation of mesenchymal genes in the presence of TGF-β1, alongside an upregulation of epithelial *Cdh1*. A previous study by Brown et al. [407] showed the varying phenotypes of multiple healthy epithelial and carcinoma cell lines, including HuMEC and MCF10A cells, in response to a treatment with 5 ng/ml TGF-β1 for 48 hours and reported that these two human mammary epithelial cells do not lose E-cadherin expression. This is contrary to the suppressive effect that TGF-β has on the expression of E-cadherin shown in other studies [371, 372].

To the best of found knowledge, this exploratory work is the first of its kind to analyse the Raman spectra of cells undergoing EMT via different *in vitro* methods. While RS is a powerful technique that can be used to acquire the biochemical fingerprint of a sample, which can then be used to obtain important biological information, to date there is no gold standard method of analysing and

processing Raman spectra from biological data. In any case, a central part of data processing is the conversion of each spectrum into variables that allow for interpretation of meaningful biological information. Each spectral profile contains a vast amount of information and multivariate analytical methods have become instrumental to reduce the complexity of the dataset and allow for extraction of information [408]. PLS-DA is a multivariate method that allows for comparison of multiple spectra simultaneously, while identifying particular features that separate different sample groups [408–410]. Importantly, this analytical method has been successfully employed to characterise the lipid content of different breast cancer cells [411]. Here, it was demonstrated that PLS-DA models can be built for different EMT models to classify each phenotype within the EMT spectrum into distinct groups with high accuracy (Figure 2.8 and Table 2.4).

In order to more closely examine the spectral differences between the phenotypes in the 3D morphogenesis assay and to assess whether it was possible to build a multiclass PLS-DA model that can separate morphologically epithelial-like (0 and 0.5 mg/ml Collagen) from mesenchymal-like (2 and 4 mg/ml Collagen) states. As previously mentioned, 1 mg/ml Collagen sample was not included in this particular analysis due to its heterogeneity and variability. Indeed, the PLS-DA model that was built and is displayed in Figure 2.9**a** had an accuracy of 94.02%, which means that it is possible to separate these groups as they are in fact biochemically different. This distinction between morphologically epithelial-like and mesenchymal-like states in the 3D assay was even more pronounced when a two-class PLS-DA model was built to classify 0 mg/ml and 4 mg/ml Collagen samples (Figure 2.9**b**). As the main goal of this part of the experimental work was to make use of this data analysis tool to find spectral differences between EMT phenotypes, more complex multiclass models were built to achieve classification of samples across different combinations of EMT models to understand whether it was possible to distinguish epithelial-like from mesenchymal-like phenotypes (Figures 2.10 and 2.11). Unsurprisingly, these combinatorial models had lower accuracies than the ones displayed on Table 2.4. It is clear that the Raman spectral profiles from samples in the 3D model were strikingly different from the ones on 2D models, which might be explained by the fact that cell behaviour can be markedly different in 2D systems than in 3D systems, which can potentially better mimic the *in vivo* environment [412]. Overall, the data presented in this work supports the ever-growing number of studies [413–415] that show that RS can be a promising tool to distinguish cell phenotypes (even from the same cell source) in the context of EMT, with particular relevance in cancerous and fibrotic pathologies.

Moreover, in an attempt to better understand the spectral differences between phenotypes within EMT models, the difference between spectra (spectral plots in Figure 2.8**a**, **c** and **e**) was computed and plotted (Figure 2.12**a**, **b** and **c**). By visual inspection of the plots, the most prominent peaks were selected for statistical analysis. As seen in Figure 2.12**d**, **e** and **f** the identified peaks were

different for each EMT group. Importantly, biological samples, in particular, consist of a vast number of different molecules that can have similar Raman signatures. RS cannot usually be used to identify individual molecules, rather the bonds that are common to those molecules. Thus, the chemical structure of different molecules can be evaluated using different peak frequencies [355], but peak assignment is still a challenging task. Raman features associated with lipid content were found to be altered in the 2D EMT models, where intensities were lower in the mesenchymal-like state - 1008 and 1129 cm^{-1} in the sparse *versus* confluent model, and 1103 and 1681 cm^{-1} in response to TGF-β1 treatment. This is in agreement with reports that demonstrate that lipid metabolism is changed with EMT as *de novo* lipid synthesis seems to be reduced in a mesenchymal-like state [416]. In the 3D model, which is intrinsically more complex than the other two, the only Raman frequency that is significantly different has been assigned to phenylalanine, an important amino acid that composes several proteins, including collagen. The intensity of phenylalanine peak is lower at 4 mg/ml collagen relative to control. However as not much is known in regards to the role of this aromatic aminoacid in EMT.

2.6 Concluding Remarks and Future Work

In summary, the experimental work presented in this chapter shows a comprehensive study using various state-of-the-art techniques to better understand the biochemical and biophysical response of cells undergoing EMT, as well as the crosstalk with ECM composition.

Here, evidence showing that the presence of type I collagen in the matrix results in an invasive phenotype and an overall shift towards the expression of mesenchymal markers was presented. These results are in agreement with previous studies [151, 327]. While using matrices with natural ECM components, such as collagen, has the benefit of generating more physiologically relevant structures, it would be instrumental to develop (semi)synthetic systems to decouple biochemical from biophysical effects when studying such changes in cell behaviour. Synthetic materials, such as polyacrylamide (PA) [151] and polyethylene glycol (PEG) [417], semi-synthetic (or hybrid) materials, namely hyaluronic acid (HA) [418] and gelatin-methacryloyl (GelMA) [419] and more natural materials, like alginate [375, 420, 421], have been used in a wide range of cell culture applications and, in particular, to better control the mechanical properties of the matrix, including stiffness. It is important that these systems recapitulate relevant aspects of native tissues, but some of these materials might not properly support cellular adhesion, proliferation or migration. In order to study the effect of stiffness independently of biochemical cues, synthetic or natural (ones that are not found in mammalian organisms, such as alginate) systems offer a great potential. Particularly when studying epithelial tissues, like the mammary gland, it is necessary to provide cells with BM components, namely laminin, which are essential for acini formation. Matrigel (used in this study), a protein mixture secreted by EHS mouse sarcoma cells, is commonly used in *in vitro* studies to recapitulate BM in culture. It has been an instrumental tool in epithelial cell culture, but its use carries known disadvantages, including lot-to-lot variability and ill-defined composition [422]. One promising way of overcoming this would be to use tissue-specific recombinantly produced laminin, particularly in studies where is it crucial to utilise xeno-free components [423].

Moreover, the mechanical characterisation of MCF10A on rBM/collagen matrices in this study suggests that these cells increase their stiffness when exhibiting an invasive phenotype (at 4 mg/ml collagen). Even though this refuted the initial working hypothesis, there is also evidence in the literature that supports an increase in cellular stiffness after EMT, as mentioned in the Discussion (Section 2.5). However, due to the challenge of eliminating matrix effects using SICM, methods like microrheology with microbeads delivered intracellularly [424] or Brillouin microscopy [425] could potentially be employed to better resolve this research question.

Finally, it was shown in this chapter that the multivariate PLS-DA method can be successfully em-

ployed to classify each phenotype within the EMT spectrum into distinct groups with high accuracy. It should be noted that, even though fairly similar trends in terms of expression of EMT markers was observed, the RS analyses in this study show that the biomolecular differences between EMT states, particularly from different EMT models, are far more complex than what standard gene and protein expression studies lead to believe. For future research, it would be interesting to carry out proteomic studies and utilise novel optical probes (e.g. Raman tags) to better track these biochemical changes.

3

Towards modulating EMT using a cryptic ECM fragment

Contents

3.1 Introduction

3.1.1 Basement membrane structure and function

All epithelial tissues are lined by a specialised and sheet-like type of extracellular matrix (ECM) – the basement membrane (BM). BMs play an instrumental role in providing proper mechanical support and architecture to tissues, while functioning as a barrier that controls transport of solutes between them [426]. Much of the knowledge about BMs comes from studies using the matrix of mouse Engelbrecht Holm–Swarm (EHS) sarcoma tumour, which is rich in BM components and can be easily isolated [427]. The dense sheet-like structure of the BM comprises mainly two highly crosslinked polymeric networks – one of laminin and one of type IV collagen [29].

Laminins are highly glycosylated heterotrimers, whose size can vary approximately between 400 and 800 kDa [428], formed by one of each of five α, four β and three γ chains assembled in tertiary structures [429]. Theoretically, these twelve chains could form 60 different trimeric combinations, but to date only 16 laminin isoforms have been identified [430]. Laminin trimers interact with each other via ternary nodes formed by the N-terminal region of one α, one β and one γ chain [24], resulting in a dense meshwork. Despite considerable homology between different laminin isoforms [431], their tissue distribution and functional roles differ in both healthy and diseased states [428]. At least four different isoforms have been described to be present in the mammary gland: laminin-111, -322, -511 and -521[432].

Type IV collagen forms a covalently crosslinked network that is also crucial for BM stability and assembly [433]. This collagenous BM component comprises a family of six genetically distinct α-chain polypeptides (α1 to α6) that assemble into heterotrimers [434, 435]. These α-chains are composed of three main domains: a 7S domain located at the amino-terminal, a triple-helix domain in the middle, and a globular non-collagenous (NC)-1 domain at the carboxy-terminal [434]. The type IV collagen network in BMs is formed and stabilised by covalent links, including disulphide and sulfilimine bonds [435, 436].

The two independent laminin and collagen networks are then interconnected by additional ECM proteins (Figure 3.1), including glycoprotein nidogen and heparan sulfate proteoglycan perlecan [29]. The composition of BMs varies between tissues, and its diversity arises from the different possible combinations of type IV collagen and laminin isoforms, as well as a plethora of BM-associated proteins that are involved in tissue-specific functions [429].

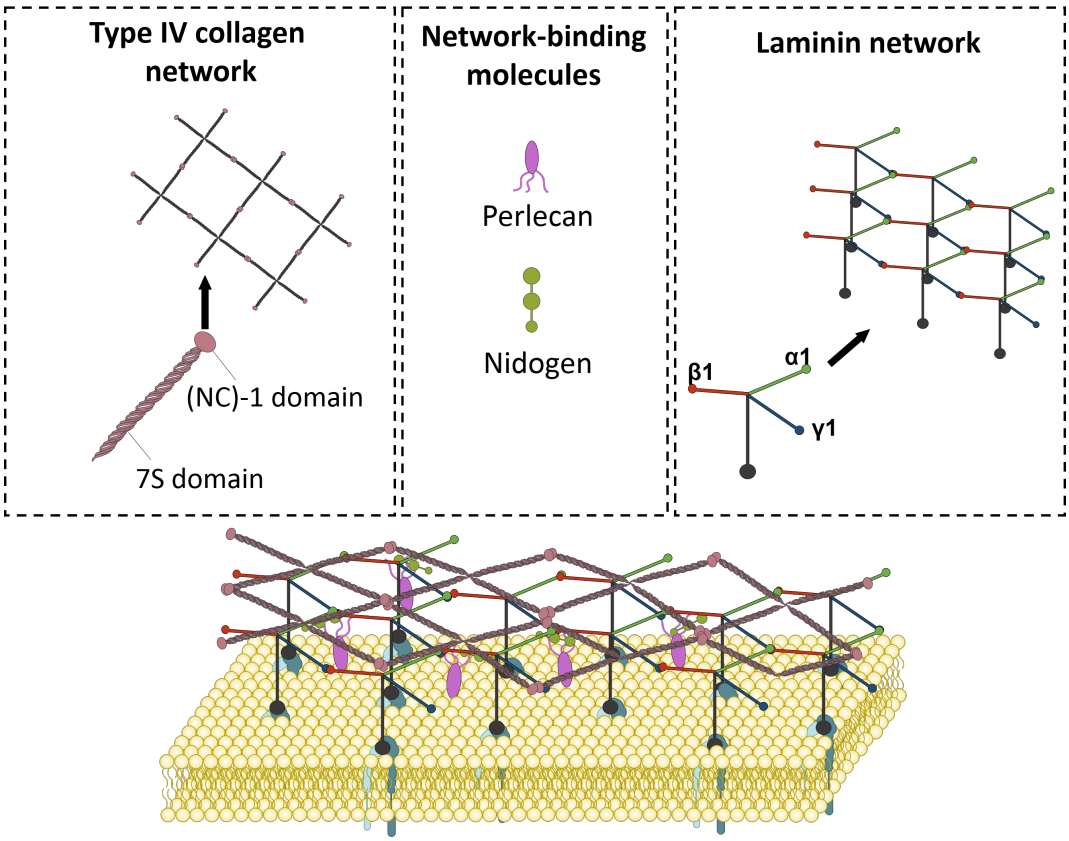

Figure 3.1: BM composition. The self-assembly of the two independent laminin and collagen networks provide BMs with their main structural composition and architecture. In turn, these two main networks are interconnected by additional proteins, including glycoprotein nidogen and heparan sulfate proteoglycan perlecan. Adapted from [426, 437].

In addition, the BM also serves as a reservoir of growth factors, including bone morphogenetic proteins (BMPs), fibroblast growth factor (FGF) and transforming growth factor β (TGF-β), which play crucial roles in cell proliferation, migration and survival [438]. BMs are dynamic ECM structures that interact with cell surface receptors and lipids to orchestrate signalling pathways and to control different aspects of cell behaviour, including cell polarity [426, 437].

Integrins, particularly β1-integrins (α1β1, α2β1, α3β1, α6β1 and α7β1), which are widely expressed in epithelial cells, are the main cell surface receptors that have been described to interact with laminin and type IV collagen [439, 440]. Laminin-integrin interactions are largely mediated by the LG domains at the C-terminus of the α chain, but the β and γ chains, which are described to serve primarily a structural role, have also been described to modulate binding to cell receptors [437] (Figure 3.1). Laminin-111, -511 and -521 have been shown to bind to integrins α3β1, α6β1 and α6β4, and laminin-322 to integrins α3β1 and α6β4 [432]. The dynamic interaction between cells and the BM controls various fundamental aspects of cell behaviour and its tight regulation is of prime importance for tissue homeostasis. Epithelial cells are thus dependent on the regulatory signalling from the BM components

that constitute their natural surrounding [441]. Changes in BM-integrin interactions, particularly during remodelling events, can result in loss of cell polarity and ultimately develop into pathological conditions [442]. In the context of cancer, malignant cells can promote the overexpression of specific ECM components or change the pattern of their integrin expression to survive [441]. In fact, carcinoma cells have been shown to overexpress some isoforms of laminins, in detriment of others. For example, breast cancers often overexpress laminin-332 (in over 70% of triple negative breast cancers) [443] or laminin-511 [444], and downregulate the expression of laminin-111 [242].

3.1.2 Basement membrane breaching during EMT

One of the main functions of the BM is to act as a barrier that controls the transport of molecules and migration of cells. Different types of cells are, however, capable of breaching the BM, which is regulated in a cell and tissue-specific manner [445]. For example, during gastrulation epithelial cells lose their apicobasal polarity and cell-cell junctions to acquire mesenchymal features and migrate through the BM to then form the mesoderm [446]. In addition, leukocytes can also pass through the BM to reach an inflamed tissue, a process termed trans-endothelial migration [447].

During tumorigenesis, the BM prevents cell invasion by confining cancer cells within its physical constraints. However, as the tumour progresses, a combination of events can eventually result in BM breaching by migratory and invasive cancer cells, a hallmark of malignant carcinomas [448]. The mechanisms underlying this acquisition of invasive behaviour are still largely unclear, but existing evidence suggests that, at the cellular level, there is a loss of polarity, loss of tight cell-cell adhesions, and architectural rearrangement of the cytoskeleton, all of which are hallmarks of epithelial-mesenchymal transition (EMT) [449]. The mechanisms underlying EMT are described in Chapter 2 Section 3.1.

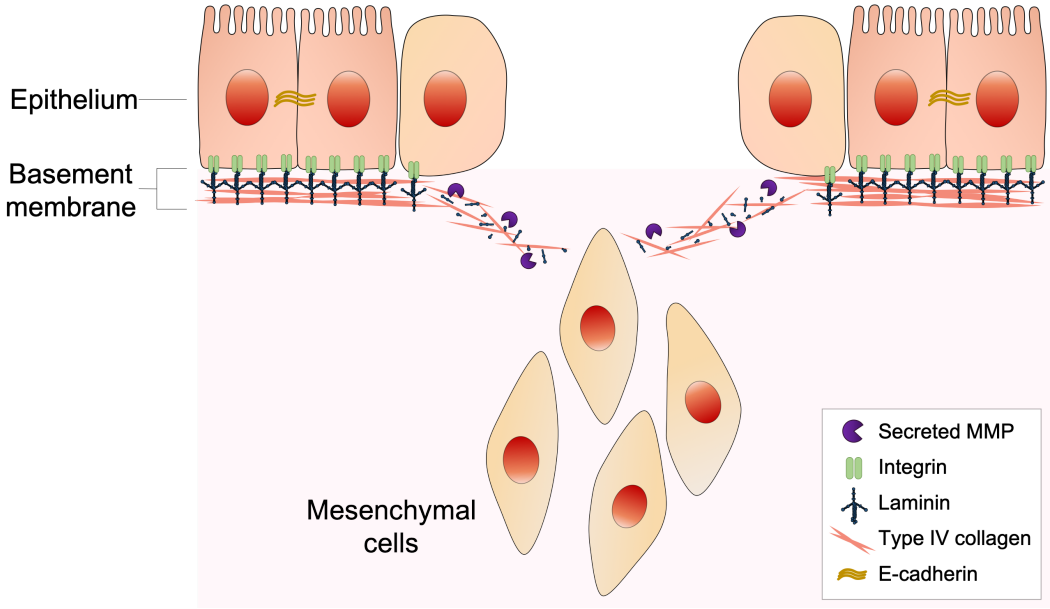

Figure 3.2: BM breaching during EMT. A combination of events can lead to the acquisition of an invasive phenotype, in which there is a loss of polarity, loss of tight cell-cell adhesions, and architectural rearrangement of the cytoskeleton, all of which are hallmarks of epithelial-mesenchymal transition (EMT). During EMT, the BM is degraded by enzymes like matrix metalloproteinases (MMPs). The processing of BM components by MMPs releases laminin and type IV collagen fragments into the extracellular environment. Adapted from [450].

3.1.3 MMP-mediated release of bioactive fragments from the BM

To date, the mechanisms that regulate BM breakdown and invasive cell behaviour are still elusive and most of what has been described results from *in vitro* studies, given the difficulty in investigating the cell-BM crosstalk *in vivo* [451]. Three main mechanistic events have been proposed to be involved in the breaching of the BM: 1) proteolytic degradation of the BM by matrix-degrading proteases, such as matrix metalloproteinases (MMPs; discussed in Chapter 1 Subsection 1.4.1.A) [452]; 2) local rearrangement of the BM by mechanical forces [453]; and 3) abnormal synthesis and deposition of BM components [454].

During remodelling, proteolytic processing of ECM macromolecules, such as laminin and collagen, by MMPs releases protein fragments into the extracellular space (Figure 3.2). These fragments have a cryptic nature, as their release uncovers neoepitopes, and their bioactivity can greatly differ from the parent protein [455]. Table 3.1 lists various reported biologically active fragments that result from the proteolytic cleavage of BM components.

Table 3.1: Biologically active fragments that result from the proteolytic cleavage of BM components.

Parent protein	Fragment	References
Collagen IV	Arresten (α1 chain)	[456–458]
	Canstatin (α2 chain)	[459–461]
	Tumstatin (α3 chain)	[462–465]
	Tetrastatin (α4 chain)	[466, 467]
Laminin-332	γ2x (γ2 chain cleaved by MMP-2)	[468–470]
	γ2' (γ2 chain cleaved by MT1-MMP)	[469–471]
	γ2 DIII (γ2 chain cleaved by MMP-2 and MT1-MMP)	[471]
	β3 chain	[472]
Laminin-111	β1	[473, 474]
Laminin-511	α5	[475]

Cleavage and release of bioactive fragments during remodelling events add another layer of complexity to the relationship between BM components and cell surface receptors. Major biological processes, like angiogenesis, wound healing, fibrosis, cancer progression and metastasis, may be regulated by ECM fragments [476]. In addition, these bioactive fragments may act alone or synergistically with other molecules, whose mechanisms can be mediated by different cell surface receptors [476].

Proteolytic processing of ECM components to release bioactive fragments has been mainly performed and assessed *in vitro*, where proteases and different isoforms of collagen or laminin are incubated, and the cleavage products subsequently analysed [450, 477]. The bioactivity of such cryptic ECM fragments can hold a great therapeutic potential, either alone or with other drugs, but their translation into the clinics has been challenging [478]. In fact, some bioactive fragments can have opposing effects depending on the biological contexts [479, 480], or even exhibit a biphasic response profile [481, 482], which can significantly complicate the determination of an optimal treatment dose. In addition, these fragments can carry more than one cryptic site that may exhibit opposing activities [478, 483].

3.1.4 Bioactive laminin β1 fragment

Horejs et al. [473] demonstrated for the first time that a biologically active fragment can be derived from the cleavage of the N-terminal of the β1 chain of laminin-111 (Figure 3.3, in red) by MMP-2. It was reported that this 60 kDa laminin fragment can modulate EMT *in vitro* via $\alpha3\beta1$ inte-

grin/EMMPRIN (CD147) in mouse and human embryonic stem cells [473], and in mammary epithelial mouse cells (NMuMG) undergoing EMT in response to TGF-β1 treatment [474], by triggering changes in the expression of EMT-related genes, including EMT-TFs SNAIL and SLUG, as well as MMP-2 and 9. This effect in EMT modulation is not seen when cells are interfaced with full length laminin-111 [473, 474], which highlights the cryptic nature of the fragment. Notably, this cryptic fragment has been shown to decrease the expression and activity of EMT-associated MMP-2, which suggests that its release works in a negative feedback mechanism to regulate this protease [473].

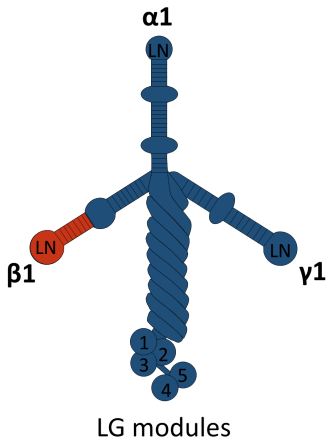

Figure 3.3: Bioactive laminin β1 fragment. Schematic representation of heterotrimeric laminin-111, which is composed of α1, β1, and γ1 chains, arranged in a triple-helical coiled-coil domain towards the C-terminal of each chain. The α1 chain uniquely contains five laminin G-like (LG) domains at its C-terminal. The laminin β1 fragment is shown in red. Adapted from [473].

Importantly, this bioactive laminin β1 fragment has also been utilised via a functionalised poly(ϵ-caprolactone) (PCL) membrane to rescue integrity of peritoneal tissue undergoing fibrosis upon treatment with TGF-β1 both in explants and in an *in vivo* mouse model [474]. Altogether, these results have shown great potential for using this BM cryptic fragment in regenerative medicine as part of a strategy to modulate EMT, particularly by regulating the expression and activity of MMPs, which is extremely relevant in pathological conditions like fibrosis and cancer.

3.2 Chapter Aims

The acquisition of mesenchymal features by epithelial cells through EMT, which then allows them to penetrate the BM and physically interact with the interstitial matrix, is an essential developmental program in pathological conditions like fibrosis and carcinoma invasion. Roughly 90% of cancer-related deaths are caused by the metastatic invasion of vital organs. However, to date, despite significant efforts having been put into understanding the underlying mechanisms and the key events that result in invasion, there are limited therapeutic approaches to prevent, limit or even reverse metastatic tumour progression [484]. Even though there are different molecular and cellular mechanistic views on how metastasis is initiated, at some point in its evolution, a subset of cells from a carcinoma, which is physically confined to the epithelium and separated from the stroma, acquire the ability to breach the BM and invade other tissues.

Evidence to date strongly suggests that individual carcinoma cells undergo an EMT program in order to migrate and invade, although it is still controversial whether EMT is an essential necessity for metastases to occur. Notwithstanding, tumour cells undergoing EMT not only acquire the ability to disseminate to distant sites, but also acquire cancer stem-like properties and become resistant to apoptosis and anticancer therapeutic agents [485, 486]. Therefore targeting EMT is a promising strategy for anticancer chemotherapeutics to prevent, inhibit or reverse metastasis, and, consequently, improve prognosis [487].

In this chapter, strategies to assess the effects of interfacing the recombinantly produced bioactive laminin β1 fragment (Subsection 3.1.4) with human mammary epithelial MCF10A cells undergoing EMT were employed. Two different *in vitro* EMT models were used – TGF-β1 treatment and 3D morphogenesis assay with type I collagen – and two methods to interface the laminin β1 fragment were applied – as a soluble factor and as tethered to a hydrogel. The latter approach aimed to investigate the effects of the fragment covalently bound to a gel system whilst avoiding off-target effects that can occur when using soluble compounds. In this work, EMT-related gene expression and gelatinase activity were studied. In addition, the development of a semi-synthetic hydrogel platform whereby chemical modification is utilised to tether the fragment is shown. Furthermore, the interaction between the fragment and other biomolecules, as well as the epithelial cells used in this work, was investigated to potentially shed light on the mechanisms underlying the effects of this cryptic laminin fragment.

3.3 Materials and Methods

3.3.1 General Cell Culture

MCF10A cells were obtained from American Type Culture Collection (ATCC) and cultured under standard cell culture conditions in humid incubators at 37℃ and 5% CO_2 atmosphere. These cells were cultured in Dulbecco's Modified Eagle Medium/Nutrient Mixture F-12 (DMEM/F-12, Gibco, Life Technologies), supplemented with 5% (v/v) Horse Serum (Gibco, Life Technologies), 5% (v/v) Penicillin Streptomycin (Gibco, Life Technologies), 20 ng/ml Epidermal Growth Factor (EGF, Peprotech), 0.5 mg/ml hydrocortisone (Sigma-Aldrich), 100 ng/ml Cholera toxin (Sigma-Aldrich), 10 µg/ml insulin (Sigma-Aldrich) [187]. Before being added to DMEM/F-12, all supplements were pre-mixed and filtered through a sterile 0.2 µm syringe filter. MCF10A cells were expanded in T-75 flasks and medium was changed every 2-3 days until 80-90% confluency was reached. For passaging, as well as for seeding at specific cell densities for experimental assays, cells were detached from the tissue flask after one rinse in sterile Phosphate Buffered Saline (PBS) and incubation at 37℃ with TripLE Express Enzyme (Thermo Fisher Scientific). Once detached, cells were centrifuged at 300 x*g* for 5 minutes and the TrypLE Express-containing supernant was discarded each time. Fresh complete medium was used to resuspend the pellet and cells were counted with trypan blue (Thermo Fisher Scientific) with a 1:1 (v/v) ratio.

3.3.2 Collagen Extraction and Reconstitution

The extraction and reconstitution of collagen I from rat tail tendons was performed by myself and Dr Jennifer Puetzer as previously described [357]. The procedure was carried out under sterile conditions. Briefly, the rat tails were initially submerged in 70% (v/v) ethanol and allowed to completely thaw. Both ends of each tail were cut and a superficial incision was made along the tails in order to peel the skin and have the tendon bundles visible. Tendons were then placed in 70% (v/v) ethanol until extraction was complete. Following, tendons were suspended in 0.1% (v/v) acetic acid at 150 ml/g of tendon for at least 48 hours at 4℃ to allow collagen to solubilise. Next, the collagen solution was centrifuged for 90 minutes at 2,500 x*g*. The supernatant was then collected and lyophilised for 48 hours, whilst the pellet containing unsolubilised collagen, blood, and muscle tissue, amongst other components, was discarded. Lastly, the lyophilised collagen was weighed and reconstituted in 0.1% (v/v) acetic acid at a concentration of 10 mg/ml and stored at 4℃.

3.3.3 Cell Culture on Matrigel/Collagen I Gels

During the preparation of the gels, all reagents, tubes and plates were kept on ice (approximately 4℃). Stock collagen I from rat tail tendon (see previous Subsection 3.3.2) was prepared at a concentration of 10 mg/ml, dissolved in 0.1% (v/v) acetic acid. Acid-solubilized collagen I needs to be neutralised in order to polymerise, which was achieved by adding 1N sodium hydroxide (NaOH) and Hank's Balanced Salt Solution (HBSS, Sigma-Aldrich). Calculations were made as described in Table 3.2.

Table 3.2: Calculations to obtain the necessary volume of each component to make Matrigel/Collagen I gels.

Component	Calculations to obtain the necessary volume
Collagen I	$\frac{\text{(final gel volume)x(desired collagen I concentration)}}{\text{Collagen-I stock concentration}}$
1N NaOH	Volume of collagen I x 0.023
10X HBSS	$\frac{\text{(volume of collagen I)+(volume of NaOH)}}{10}$
1X HBSS	(final gel volume)-[(collagen I volume)+(NaOH volume)+(10X HBSS volume)]

Collagen I solutions were prepared to the desired final concentrations by pipetting and mixing the components in the following order: HBSS 1X, HBSS 10X, 1N NaOH and, lastly, collagen I from stock solution. Positive displacement pipettes were used for transferring viscous stock collagen solution. After preparing the different concentrations of collagen I, each was mixed with equal volume of Matrigel (LDEV-free, Corning). Matrigel and Collagen I mixtures were prepared under sterile conditions and the gels were polymerised at 37℃ for at least 30 minutes, prior to seeding the cells. Throughout this thesis, these gels are referred to by using the concentration of collagen prepared before mixing with Matrigel.

3.3.4 Spheroid Cell Culture

MCF10A cell spheroids were formed by seeding 10,000 cells/well on 96-well round bottom ultra-low attachment plates (Corning), in complete media (as described in Subsection 3.3.1) with 2.5% (v/v) Matrigel (LDEV-free, Corning). Immediately after seeding, plates were spun down for 10 minutes at 800 x*g*. Within 24 hours spheroids were formed.

3.3.5 Recombinant laminin fragment production, isolation and purification

3.3.5.A Transient 293F transfection

Human Embryonic Kidney (HEK) 293-F cells, obtained from Thermo Fisher Scientific, were used for production of recombinant laminin fragment. The cells were cultured in shaker flasks on an orbital shaker platform at 125 rpm, in FreeStyle 293 Expression Medium (Gibco, Life Technologies). 293F cells were subcultured when a density of 1-3x10^6 cells/ml was reached and diluted to 0.1-0.3x10^6 viable cells/ml. Cells were transfected between passage 5 and 10 with the expression vector (Figure B.1, Appendix B) using 293fectin Transfection Reagent (Thermo Fisher Scientific). Briefly, for each transfection sample 35 µg of plasmid DNA (pDNA) was mixed with 70 µl of 293fectin Transfection Reagent in Opti-MEM (Thermo Fisher Scientific) to a total volume of 2 ml. To ensure formation of lipid-DNA complexes, this mix was gently homogenized and incubated at room temperature for 30 minutes. Following, 2 ml of pDNA-293fectin complexes was added to each shake flask that contained 1x10^6 viable cells/ml to a total volume of 30 ml. Transfected HEK 293-F cells were cultured for 72 hours before harvesting. Conditioned media containing recombinant laminin fragment was collected by centrifuging the cell suspensions from each shake flask at 400 x*g* for 5 minutes at room temperature. Supernatants were then transferred into Amicon ultra-15 centrifugal filter units with ultracel-10 membranes 10 kDa MWCO (Merck Millipore) and centrifuged at 4,000 x*g* for 30 minutes at 4℃ to concentrate the recombinant fragment in solution.

3.3.5.B Isolation and purification

Recombinant laminin fragment was purified using 3 ml HisPur™ Ni-NTA Spin Columns (Thermo Fisher Scientific). First, concentrated conditioned media was mixed with an equal volume of Equilibration Buffer (10 mM imidazole in PBS, pH 7.4). Next, HisPur Ni-NTA Spin Columns were prepared by centrifugation at 700 x*g* for 2 minutes to remove storage buffer and by adding 6 ml of Equilibration Buffer, followed by vigorous hand mixing to ensure that the buffer completely entered the resin bed. To remove Equilibration Buffer, HisPur Ni-NTA Spin Columns were centrifuged at 700 x*g* for 2 minutes. Following, the conditioned media mixed with Equilibration Buffer was added to the HisPur Ni-NTA Spin Columns and allowed to interact with the resin bed for 30 minutes at 4℃ on a shaker. Recombinant laminin fragment-bound HisPur Ni-NTA Spin Columns were then centrifuged at 700 x*g* for 2 minutes. Resin was then washed three times with 6 ml of Wash Buffer (25 mM imidazole in PBS, pH 7.4), which was removed each time by centrifuging spin columns at 700 x*g* for 2 minutes. Next, His-tagged recombinant laminin fragment was eluted from the nickel resins by adding 3 ml of

Elution Buffer (250 mM imidazole in PBS, pH 7.4) and mixing vigorously. Purified laminin fragment was collected after centrifuging HisPur Ni-NTA Spin Columns at 700 x*g* for 2 minutes. This step was repeated twice. Eluted sample was then concentrated using Amicon ultra-15 centrifugal filter units with ultracel-10 membranes 10k MWCO (Merck Millipore) for 10 minutes at 4,000 x*g* at 4℃. In order to exchange buffer, twice the volume of PBS was added to the same Amicon ultra-15 centrifugal filter units with ultracel-10 membranes, which were further centrifuged for 10 minutes at 4,000 x*g* at 4℃. Concentration of purified recombinant laminin fragment was determined by BCA assay (see Subsection 3.3.10) or A280 method on NanoDrop 2000c (Thermo Fisher Scientific). Protein purification was monitored by SDS-PAGE and immunoblotting.

3.3.5.C Cellular metabolic activity assay

The Cell Counting Kit-8 (CCK-8, Sigma-Aldrich) was performed to measure cellular metabolic activity. Cells were seeded at an initial density of 8,000 cells/cm^2 in a 96-well plate. After 24 hours, cells were treated with different concentrations of laminin fragment (0, 0.5, 1 and 10 µg/ml). Following 72 hours of treatment, cells were gently washed once with sterile PBS and received fresh medium. The following day, 10 µl of CCK-8 were added to each well and left incubating for 1 hour and 30 minutes at 37℃. Wells with media without cells were also incubated and used blanks (negative control). The absorbance was then measured at 450 nm using the SpectraMax M5 plate reader. The blank absorbance from the medium was subtracted from the measured absorbance from the wells seeded with cells.

3.3.6 Laminin-111 digestion by MMP-2

Full length laminin-111 from Engelbreth-Holm-Swarm murine sarcoma basement membrane (Sigma-Aldrich) and human recombinant laminin-111 (BioLamina) were digested by active MMP-2 (Sigma-Aldrich, SRP3118) at a ratio of 1:10 (w/w) in 50 mM Tricine, 10 mM $CaCl_2$, 50 mM NaCl, 20 µM $ZnCl_2$ and 0.05% (w/v) Brij35 (pH adjusted to 7.5) to a total volume of 100 µl each. Mouse and human laminin were separately incubated with MMP-2 for 24 hours at 37℃. Digestion products were then analysed by SDS-PAGE using 4–12% Criterion XT Bis-Tris Protein Gels (Bio-Rad) under native and denatured conditions, which were then stained with QC Colloidal Coomassie Blue (Bio-Rad) or analysed by immunoblotting.

3.3.7 Gene Knockdown Mediated by Small Interference RNA (siRNA)

In order to knockdown *Itga3* gene and to study the interaction between MCF10A cells and the recombinant laminin fragment, these cells were seeded at a density of 8,000 cells/cm^2 on 12-well tissue culture plates for RT-qPCR and at a density of 4,000 cells/cm^2 on 8 chamber slides (ibidi) for fluorescence imaging. Cells were cultured for 24 hours before siRNA transfection, with out without concomitant treatment with 10 ng/ml TGF-β1 and/or 10 µg/ml recombinant laminin fragment for RT-qPCR, or 10 µg/ml Cy5-labelled laminin fragment for fluorescence imaging. Briefly, for each sample to be transfected, a 1:1 volume ratio mixture of Lipofectamine RNAiMAX Transfection Reagent (Invitrogen) and SMARTpool: Accell ITGA3 siRNA (Dharmacon) was prepared in Opti-MEM and incubated at room temperature for 20 minutes before adding or not recombinant laminin fragment and/or TGF-β. Separate wells with cells that were treated with transfection reagent but no *ITGA3* siRNA to serve as negative controls.

3.3.8 RNA Isolation, cDNA synthesis and RT-qPCR

3.3.8.A RNA Isolation

The expression of EMT-related genes was studied by quantitative reverse transcription polymerase chain reaction (RT-qPCR). Cells were seeded at 15,000 cells/cm^2 on Matrigel/Collagen I gels in 48-well plates and cultured for 1 week before RNA collection. Cells undergoing TGF-β-induced EMT were cultured at density of 8,000 cells/cm^2 in 96 well plates. TGF-β1 treatment was administered at 10 ng/ml in complete media (from a stock concentration of 50 µg/ml) 24 hours post seeding, together with recombinant laminin fragment prepared at different concentrations (0, 0.5, 1 and 10 µg/ml) and RNA collection was performed 24 hours post treatment. Cells treated with siRNA against *Itga3* were cultured as described in subsection 3.3.7. RNA from GelMA-encapsulated spheroids was collected 3 days after encapsulation. At the time of collection, conditioned medium was aspirated from each well. Cells on/in gels were lysed in 700 µl TRIzol reagent (Life Technologies) per well and frozen immediately at -80 ℃. Cells in TRIzol reagent were thawed and transferred to PCR clean DNA LoBind Eppendorf tubes. Samples with spheroids encapsulated within GelMA had to be submitted to an additional step of high-speed shaking with sterile metal beads using a TissueLyser II (Qiagen), at a frequency of 30 s^{-1} for, at least, 5 minutes, to disrupt the structure of the hydrogels. Next, 140 µl of chloroform (molecular biology grade, Acros Organics) was added to each tube, which were shaken vigorously by hand. The samples were left incubating for 3 minutes at room temperature, followed by a centrifugation step at 12,000 x*g* for 15 minutes at 4 ℃. This step results in phase separation and the

top RNA-containing aqueous phase was transferred into a new PCR clean DNA LoBind Eppendorf tube. In the case of cells grown on tissue culture plastic, TRIzol reagent was not used. Instead, cells were washed once with sterile ice-cold PBS and 100 µl or 350 µl of RLT buffer (Qiagen) was added to each well on a 96-well or a 12-well plate, respectively. When using 96-well plates, the extracts from 4 wells were pooled for each condition. Next, an equal volume of 70% ethanol (molecular biology grade, Fisher Bioreagents) was added to each sample (for both TRIzol and RLT collection procedures) and mixed well by pipetting. For the final steps of RNA isolation, the instructions from the RNeasy Mini Kit (Qiagen) were followed. For each sample a volume of up to 700 µl at a time was transferred to a spin column placed in a 2 ml collection tube and centrifuged for 30 seconds at 10,000 x*g* at room temperature. If the samples contained more than 700 µl, multiple centrifugations were carried out. Next 700 µl of buffer RW1 was added to each spin column followed by a centrifugation at 10,000 x g for 30 seconds at room temperature. Subsequently, 500 µl of buffer RPE was added to each tube for a final wash, which were centrifuged for 2 minutes at 10,000 x*g* at room temperature, followed by another centrifugation with no buffer added to ascertain that no traces of ethanol were left in the samples. In every step, the flow-through from the spin column was discarded. Finally, 30 µl of RNase-free water (Life Technologies) was added to each spin column to collect the purified RNA from each sample with a last step of centrifugation for 30 seconds at 10,000 x*g* at room temperature. The RNA concentration was then measured using NanoDrop 2000c (Thermo Fisher Scientific). Once RNA samples from all biological replicates were collected and isolated for subsequent use, RNase-free water was added to each tube in adequate amounts to ensure that all samples were at the same concentration.

3.3.8.B cDNA synthesis

Complementary DNA (cDNA) was synthesised from each RNA sample using Applied Biosystems High-Capacity cDNA Reverse Transcription kit (Thermo Fisher Scientific). After allowing the kit components to thaw on ice, the reverse transcription master mix was prepared, which contained, per reaction, 2 µl RT buffer, 0.8 µl dNTP mix, 2 µl RT random primers, 1 µl multiscribe reverse transcriptase and 3.2 µl nuclease-free water. Following, 10 µl of each RNA sample was added to a 0.5 ml PCR tube and mixed with 10 µl of reverse transcription master mix. Each tube was quickly vortexed, spun down and placed in the thermal cycler (LifePro, Bioer) to go through the following cycle: 10 minutes at 25℃, 120 minutes at 37℃ and 5 minutes at 85℃.

3.3.8.C RT-qPCR

After reverse transcription, the cDNA was diluted with nuclease-free water to be used in quantitative reverse transcription PCR (RT-qPCR). RT-qPCR was carried out using TaqMan Fast Advanced Master Mix (Thermo Fisher Scientific), FAM-MGB conjugated TaqMan probes listed in Table 3.3 (Thermo Fisher Scientific), and run on a StepOnePlus™ machine (Applied Biosystems). Components were prepared on 96-well reaction plates (Thermo Fisher Scientific): 5 µl of TaqMan Fast Advanced Master Mix, 0.5 µl of TaqMan probe, 0.5 µl of nuclease-free water, and 4 µl of cDNA for each sample (10-20ng of cDNA per reaction). The RT-qPCR programme settings were as follows: step 1 50℃ for 2 minutes, step 2 95℃ for 20 seconds, and step 3 40 cycles of PCR that comprised a denaturing step at 95℃ for 1 second and a annealing/extending step at 60℃ for 20 seconds. Cycles-to-threshold (Ct) values were automatically obtained by the Thermo Fisher Scientific StepOnePlus™ software. Subsequently, these values were exported to Microsoft Excel and manually processed to obtain fold change expression values. Ct values of each gene of interest were normalised to the Ct values of the housekeeping gene (*Gapdh*) within each respective sample. $2^{-\Delta\Delta Ct}$ values were obtained by normalising to the internal control sample (in this case, the epithelial-like state). Three biological replicates (two technical replicates each) are reported.

Table 3.3: FAM-MGB conjugated TaqMan probes for housekeeping, EMT-related genes and integrin α3. List of primers used for RT-qPCR gene expression studies in this chapter. *Gapdh* was used as housekeeping gene, *Itga3* was used to study expression of integrin $\alpha 3$ and all other probes were used to assess expression of genes of interest related with EMT.

Target	TaqMan Assay ID
Gapdh	Hs02758991_g1
Cdh1	Hs01023895_m1
Cdh2	Hs00983056_m1
Snail	Hs00195591_m1
Vim	Hs00958111_m1
Mmp2	Hs01548727_m1
Itga3	Hs01076879_m1

3.3.9 Cell lysis and protein isolation

For protein collection, MCF10A cells were seeded in a 12-well plate at a density of 8,000 cells/cm^2 and treated with soluble laminin fragment at different concentrations (0, 0.5, 1 and 10 µg/ml) 24 hours

post-seeding. Then, cells were lysed using RIPA buffer (New England Biolabs) with phosphatase and protease inhibitors (Roche) 24 hours post-treament with fragment. A cell scraper was used to help detach cells and cell debris from the tissue culture plastic. Cell lysates were then transferred to Protein LoBind Eppendorf tubes and kept on ice. Next, samples were sonicated on ice for 20 seconds at 20% amplitude and then incubated for 1 hour at 4℃ on a shaker. Lysates were subsequently centrifuged for 10 minutes at 16,000 x*g* at 4℃. Lastly, supernatants were transferred to clean Protein LoBind Eppendorf tubes and stored at -80℃ until further use.

3.3.10 Measuring protein concentration

Protein concentration was determined by the Micro BCA^{TM} Protein Assay Kit (Thermo Fisher Scientific). First, the Bovine Serum Albumin (BSA) standards were prepared by serial dilution using a diluent similar to the sample buffer (UltraPure water or PBS) in sufficient amounts to use three replicates of each dilution. Following, the Micro BCA working reagent was prepared by mixing 25 parts of reagent MA, 24 parts of reagent MB and 1 part of reagent MC. Next, 150 µl of each solution of BSA standard and diluted samples was transferred into a 96-well clear bottom plate in triplicate. The absorbance was then measured at 562 nm using the SpectraMax M5 plate reader. The standard curve was drawn by plotting the average absorbance reading of each BSA standard and its concentration. Finally, the protein concentration of each sample was then calculated by linear interpolation of the standard curve and by accounting for the dilution factor used during sample preparation.

3.3.11 Subcellular fractionation

In order to investigate the interaction between the laminin fragment and MCF10A cells and its subcellular location, these cells were exposed to the fragment and then the subcellular protein content was fractionated according to the Subcellular Protein Fractionation Kit for Cultured Cells (Thermo Fisher Scientific). First, 8,000 cells/cm^2 were seeded on 12-well tissue culture treated plates and cultured for 24 hours before adding recombinant laminin fragment at a concentration of 10 µg/ml. Cells grown on separate wells not exposed to the laminin fragment were used as negative controls. Cells were harvested 24 hours post-treatment with TrypLE Express Enzyme (Thermo Fisher Scientific) incubation at 37℃ followed by a centrifugation at 500 x*g* for 5 minutes. Cell pellets were then washed with ice-cold sterile PBS and transferred to Protein LoBind Eppendorf tubes and centrifuged at 500 x*g* for 3 minutes. The supernatant was then discarded, the cell pellets were suspended in ice-cold cytoplasmic extraction buffer (CEB) containing 1:100 Halt protease inhibitor cocktail, and incubated for 10 minutes

at 4℃ with gentle mixing. Following, protein samples were centrifuged at 3,000 x*g* for 5 minutes. These supernatants (cytoplasmic fraction) were immediately transferred to clean pre-chilled Protein LoBind Eppendorf tubes. Next, ice-cold membrane extraction buffer (MEB, containing 1:100 Halt protease inhibitor cocktail) was added to the pellet, vortexed on the highest speed setting for 5 seconds and incubated at 4℃ for 10 minutes with gentle mixing. Samples were then centrifuged at 3,000 x*g* for 5 minutes and the supernatants (membrane fraction) were transferred to clean pre-chilled Protein LoBind Eppendorf tubes. Following, ice-cold nuclear extraction buffer (NEB, containing 1:100 Halt protease inhibitor cocktail) was added to the pellets, which were vortexed on the highest setting for 15 seconds, and incubated for 30 minutes at 4℃ with gentle mixing. This was followed by a centrifugation at 5,000 x*g* for 5 minutes and the supernatants (soluble nuclear fraction) were transferred to clean pre-chilled Protein LoBind Eppendorf tubes. Subsequently, room temperature chromatin-bound extraction buffer (NEB, containing 1:100 Halt protease inhibitor cocktail, 5 mM $CaCl_2$ and 300 units of Micrococcal Nuclease) was added to the pellets, vortexed on the highest speed setting for 15 seconds and incubated at room temperature for 15 minutes. Following this incubation, tubes were vortexed on the highest setting for 15 seconds and centrifuged at 16,000 x*g* for 5 minutes. The supernatants (chromatin-bound nuclear fraction) were transferred to clean pre-chilled Protein LoBind Eppendorf tubes. Finally, room temperature pellet extraction buffer (PEB containing 1:100 Halt protease inhibitor cocktail) was added to the pellets, vortexed on the highest setting for 15 seconds and incubated at room temperature for 10 minutes. Tubes were then centrifuged at 16,000 x*g* and the supernatants (cytoskeletal fraction) were collected into clean pre-chilled Protein LoBind Eppendorf tubes. Once all fractions were collected, samples were stored at -80℃ until further use. Before samples were analysed by immunoblotting (see Subsection 3.3.12), protein concentration was determined by Micro BCA Protein Assay (see section Subsection 3.3.10).

3.3.12 Western Blotting

Fragment interacting with MCF10A cells and the product of MMP-2 processing of full length laminin-111 were analysed by Western blotting. Whole cell extracts and MMP-2 digestion samples were separated by SDS-PAGE, transferred to polyvinylidene difluoride (PVDF) membranes and analysed by Western Blotting. Briefly, protein samples were prepared, before being separated according to their molecular weight by electrophoresis, by mixing 15 or 30 µg of protein with XT Reducing Agent (20X, Bio-Rad) and XT Sample Buffer (Bio-Rad) to a volume of 15 µl per lane. These samples were then incubated at 100℃ for 3 minutes and then cooled down to room temperature. Prepared samples and protein ladder were then loaded on 4–12% Criterion XT Bis-Tris Protein Gels (26 well, 15 µl each, Bio-Rad) and protein separation was performed in XT MOPS Running Buffer (Bio-Rad) at

80 mA (when running 2 gels) for 2 to 2.5 hours, on ice. Following, proteins separated in the gels were transferred to a 0.45 µm PVDF membrane (Immobilon-FL PVDF, Merck) using the Criterion Blotter (Bio-Rad). Immunoblotting sandwiches were prepared using Whatman®filter paper. Transfer was then conducted on ice at 100 V for 30 minutes in Tris/Glycine buffer (Bio-Rad). Next, efficient transfer of proteins into the PVDF membranes was confirmed by Ponceau staining (0.1% (w/v) in 5% (v/v) acetic acid, Sigma) staining and after membranes were washed in TBS-T (TBS, Bio-Rad, with 0.1% (v/v) Tween20, Sigma-Aldrich) until no red coloured bands were visible again. Membranes were then blocked with 5% skimmed milk (Sigma-Aldrich, in TBS-T) for at least 1 hour at room temperature on a shaker. Membranes were then thoroughly washed in TBS-T before being incubated with primary antibody. For samples with whole cell extracts with different concentrations of fragment, membranes were first incubated with primary antibody against the His-tag (mouse, Abcam ab18184) diluted (1:1000) in 5% BSA (Sigma-Aldrich) in TBS-T at 4℃ overnight on a shaker. The following day, these same membranes were incubated with secondary antibody (anti-mouse 800CW, Licor) diluted in a ratio of 1:10,000 in TBS-T for 1 hour at room temperature. Membranes were then washed and imaged using the Licor Odyssey system and image studio. Subsequently, these were incubated with primary antibody against the laminin fragment (rabbit, custom-made) diluted (1:1000) in 5% BSA (Sigma-Aldrich) in TBS-T at 4℃ overnight on a shaker. The following day, they were incubated with secondary antibody (anti-rabbit 680RD, Licor) diluted in a ratio of 1:10,000 in TBS-T for 1 hour at room temperature. Membranes were then washed and imaged using the Licor system and Image Studio software. Next, membranes were incubated with loading control antibody against GAPDH (mouse, Santa Cruz Biotechnology sc-32233) diluted in a ratio of 1:500 in 5% BSA in TBS-T for at least 1 hour at room temperature with gentle orbital shaking. Membranes were then washed in TBS-T and incubated with secondary antibody (anti-mouse 680RD, Licor) diluted at a factor of 1:10,000 in TBS-T for 1 hour at room temperature with gentle orbital shaking. Finally, membranes were thoroughly washed and imaged using the Licor system and image studio. In the case of samples from MMP-2 processing of full length laminin-111, membranes were incubated with primary antibody against the laminin fragment (rabbit, custom-made) diluted (1:1000) in 5% BSA (Sigma-Aldrich) in TBS-T at 4℃ overnight on a shaker. The following day, they were incubated with secondary antibody (anti-rabbit 800CW, Licor) diluted in a ratio of 1:10,000 in TBS-T for 1 hour at room temperature. Membranes were then washed and imaged using the Licor system and Image Studio software. Image processing and analysis was performed using Image Studio Lite Ver 5.2.

3.3.13 Gelatin zymography

Activity of gelatinases in conditioned media was investigated with gelatin zymography. Immediately after collection from tissue culture plates, samples were snap frozen in liquid nitrogen followed by storage at -80℃. To proceed with this technique, samples were then thawed on ice and then concentrated using amicon ultra-2 centrifugal filter units with ultracel-10 membranes 10k MWCO (Merck Millipore) at 4,000 x*g* for 30 minutes at 4℃. Protein concentration was measured using the A280 method on NanoDrop 2000c (Thermo Fisher Scientific confirm the equipment). Following, 10 µl of each concentrated sample was mixed with 10 µl of Novex Tris-Glycine SDS Sample Buffer (2X, Invitrogen) and loaded on a Novex 10% Zymogram (Gelatin) Protein Gel (Invitrogen). Proteins were then resolved by running the gels in Tris-Glycine SDS running buffer (Invitrogen) at 125V for 2 hours. After electrophoresis, gels were incubated in Novex Zymogram Renaturing Buffer (Invitrogen) for 45 minutes at room temperature on an orbital shaker. Next, gels were incubated in Novex Zymogram Developing Buffer (Invitrogen) overnight at 37℃ on a shaker. Gels were then stained with QC Colloidal Coomassie Blue (Bio-Rad) for 1 hour at room temperature with gentle agitation, and washed for at least 4 hours in Milli-Q water at room temperature. Gelatin gels were imaged and densitometric analysis was performed using ImageJ.

3.3.14 Laminin Fragment Chemical Modification

The recombinant laminin fragment was chemically modified by Dr Daniel Richards using a strain-promoted azide–alkyne cycloaddition (SPAAC) chemical reaction strategy. Two different approaches to add strained alkyne functionalised handles were carried out: one cysteine selective and the other lysine selective. Briefly, the recombinantly expressed laminin fragment (400 µl, 36.6 µM, in PBS, pH 7.4) was incubated with tris(2-carboxyethyl)phosphine hydrochloride (TCEP) (7.32 µl, 20 mM in PBS, pH 7.4, 10 equivalents) for 30 minutes at 37℃. Following, samples were split into two tubes (2 x 200 µl) to proceed with the two different chemical modification approaches. One was reacted with a cysteine selective bromopyridazinedione with a strained alkyne functionalised handle (14.64 µl, 20 mM in DMSO, 20 equivalents), the other was reacted with lysine selective NHS ester-PEG_4-DBCO (14.64 µl, 20 mM in DMSO, 20 equivalents; Jena Bioscience). These reactions occurred at room temperature overnight (approximately 16 hours). Subsequently, the samples were purified using VivaSpin 0.5 ml 10 kDa MWCO spin filters in PBS (pH 7.4). This step was repeated 5 times using a volume of 500 µl. The volume of the purified samples was then adjusted to 100 µl for UV-Vis analysis using Nanodrop 2000c in cuvette mode at 280 nm. The concentration of the chemically modified laminin fragments was determined using a theoretically calculated extinction coefficient (ϵ), based

on the amino acid sequence, with ExPASY ProtParam tool (in this case, ϵ_{280}=61290 cm^{-1} M^{-1}). The chemically modified versions of the recombinant laminin fragment used for biolayer interferometry studies and to tether onto GelMA hydrogels were used as prepared until this step. However, in order to fluorescently visualise the fragment using confocal microscopy a Cy5 dye was clicked onto the two versions of laminin fragment with strained alkyne handles. To do so, each of the fragment samples (30 µl, 40 µM, in PBS, pH 7.40) was reacted with Cy5-azide (0.9 µl, 20 mM in DMSO, 15 equivalents) at room temperature for 8 hours. Since the Cy5 dye was not compatible with the VivaSpin filters, the reacted samples were then purified using 7 kDa MWCO ZebaSpin columns, following the manufacturer's protocol twice to ensure purity. Samples were stored in PBS and analysed by UV-Vis using Nanodrop 2000c in cuvette mode and by SDS-PAGE using a 16% gel. Fluorescence imaging of the gels was performed using LI-COR Odyssey machine and the Coomassie staining was done using QC Colloidal Coomassie Blue (Bio-Rad).

3.3.15 Gelatin Methacryloyl (GelMA) modification

3.3.15.A GelMA synthesis

Gelatin Methacryloyl (GelMA) was synthesised by Dr Liliang Ouyang as described in [488]. In short, 50 g of gelatin (Sigma-Aldrich) was soaked in UltraPureTM Distilled Water (Invitrogen) to a final concentration of 10% (wt/vol) at room temperature and stirred for 40 minutes. While stirring moderately, the mixture was heated and kept at 50℃ in a water bath until gelatin was fully dissolved. Following, while stirring vigorously, 0.6 g of methacrylic anhydride (Sigma-Aldrich) per 1 g of getalin was added slowly to the mixture, which was vigorously stirred for the following 2 hours. After this reaction period, the solution was transferred into 50 ml tubes and centrifuged at 3,500 x*g* for 3 minutes at room temperature to remove unreacted methacrylic anhydride. GelMA-containing supernatant was then transferred into a 500 ml glass beaker and diluted with two volumes of pre-heated (40℃) Milli-Q water. Subsequently, the solution was transferred to a dialysis membrane with a 12 kDa MWCO. The dialysis was carried out at 40℃ against a large volume of Milli-Q water for 5 to 7 days in a chemical safety fume hood. Milli-Q water was changed at least once a day. Following dialysis, the pH was adjusted to 7.4 with 1M $NaHCO_3$. Under a sterile environment, GelMA solution was then filtered using 0.2 µm filter units, aliquoted into 50 ml tubes and snap frozen in liquid nitrogen. Without thawing, the sterile solutions in 50 ml tubes were transferred to a freeze-dryer to lyophilise for 4 to 7 days. Lyophilised GelMA was then stored at -20℃, protected from light and moisture, until further usage. The characterisation of GelMA functionalisation was performed using a fluoraldehyde assay (see Subsubsection 3.3.15.C). The datapoints and respective linear fit can be found in Figure B.4,

Appendix B. It was determined that the degree of functionalisation of the batch of GelMA used in this study was approximately 80%, which means that 20% of the amino groups in the gelatin structure did not react with methacrylic anhydride and were free to react with an NHS ester group, described in the following subsection.

3.3.15.B Azide-modified GelMA synthesis

GelMA was modified with Azido-PEG_4-NHS ester (Jena Bioscience), in oil form and was dissolved in dimethylsulfoxide (DMSO, Sigma-Aldrich) to a concentration of 100 mg/ml. Briefly, 200 mg GelMA were dissolved in 1.9 ml borate buffered saline (pH 8.0) in a small glass vial and 100 µl of Azido-PEG_4-NHS ester was added. This solution was heated to 50℃ and stirred for 2 to 3 hours. The mixing ratio estimation was based on the amount of primary amino groups left unreacted after the GelMA synthesis process. Following, to prevent it from gelling the solution was diluted with five volumes of PBS. Next, the azide-modified GelMA solution was transferred to a dialysis membrane with a 6-8 kDa MWCO. The dialysis was done at 40℃ against a large volume of Milli-Q water for 3 days. Milli-Q water was changed at least twice a day. Following dialysis, the azide-modified GelMA solution was transferred to a 50 ml tube and frozen at -80℃. Next, the tube was transferred to a freeze-dryer to lyophilise for 5 days. Lyophilised azide-modified GelMA was then stored at -20℃, protected from light and moisture, until further use.

3.3.15.C Fluoraldehyde assay to determine the degree of functionalisation

A fluoraldehyde assay was carried out to determine the degree of functionalisation (DoF) of azide-modified GelMA. First, azide-modified GelMA solution was prepared in PBS at 0.5 mg/ml. Next, unmodified GelMA solutions were prepared in PBS at different concentrations (0.05, 0.1, 0.2, 0.5 and 1 mg/ml) in order to obtain a linear calibration curve. Subsequently, 300 µl of each GelMA solution was mixed with 600 µl of room temperature Fluoraldehyde™o-Phthaldialdehyde (OPA) Reagent Solution (Thermo Fisher Scientific) in separate tubes. A mixture of 300 µl of PBS and 600 µl of fluoraldehyde reagent solution was also prepared to be used as a control. Following, 250 µl of each solution was pipetted in triplicate into a black-walled, clear-bottom 96-well plate. The fluorescence intensity was then measured at 450 nm using an excitation wavelength of 360 nm, using the SpectraMax M5 plate reader. The fluorescence from the PBS control was subtracted from the measured fluorescence from the sample and standard solutions. A calibration curve was drawn using the standards and a linear equation was obtained (Figure B.5 Appendix B). Then, with the fluorescence intensity of the azide-modified GelMA sample, the corresponding unmodified GelMA concentration X was obtained. Lastly,

the DoF was calculated as (0.5 – X)/0.5 x 100%.

3.3.15.D Laminin fragment-tethered GelMA synthesis via a click reaction

In order to tether the recombinant laminin fragment to the semi-synthetic hydrogel, azide-modified GelMA was mixed with strained alkyne handle-bearing laminin fragment (see Subsection 3.3.14) at a molarity ratio of 1:1 (laminin fragment to azide groups) in PBS to a total volume of 2 ml (100 mg azide modified GelMA, which corresponds to 0.06 µmol azide, with 0.06 µmol laminin fragment). Two separate solutions were prepared: one with cysteine-modified and another with lysine-modified laminin fragment. The mixtures were left stirring at room temperature for around 16 hours to ensure the click reaction occurred. The two versions of fragment-tethered GelMA solutions were then filtered through 0.2 µm syringe filters and stored at 4℃ protected from light.

3.3.16 Preparation of GelMA precursor solutions

Firstly, the photo-initiator stock solution was prepared by dissolving 2-Hydroxy-4'-(2-hydroxyethoxy)-2-methylpropiophenone (Sigma-Aldrich) in sterile PBS to a concentration of 0.5% (w/v) and filtered through a 0.2 µm syringe filter. For all formulations of GelMA (with or without tethered fragment), the required amount of lyophilised GelMA was weighed to obtain a final concentration of 5% (w/v), dissolved in sterile PBS and 0.05% (w/v) photo-initiator. In order to facilitate dissolution, this solution was incubated at 37℃ for approximately 10 minutes and then centrifuged at 400 x*g* for 5 minutes to remove the bubbles that were formed at the surface.

3.3.17 Mechanical testing of GelMA-based hydrogels

Mechanical testing of GelMA-based hydrogels in this experimental worked was carried out by myself and Dr Liliang Ouyang. Each formulation of 5% (w/v) GelMA precursor solution, prepared as described above, was transferred into a 1 ml syringe, whose tip had been cut and removed, and placed in a vertical position. GelMA-based hydrogels were cross-linked under a UV light unit at 365 nm for 5 minutes. Each hydrogel was tested by unconfined mechanical compression using the ElectroForce® 32mm instrument (TA Instruments), with a 250 g loading sensor and a loading speed of 0.01 mm/s. The compressive moduli of all formulations of GelMA-based hydrogels were then calculated by measuring the slope of the 0.1 – 0.2 mm/mm strain linear region of the stress-strain curve. Each GelMA formulation was measured in triplicate.

3.3.18 Histology and immunofluorescence staining of GelMA sections

For immunofluorescence staining of all formulations of 5% (w/v) GelMA-based hydrogels (normal, lys-1800 and cys-1800; where 1800 is the concentration in µg/ml), 50 µl of each respective precursor solution was cross-linked under UV light at 365 nm for 5 minutes, in a syringe whose tip had been cut, as described above, and then submersed in PBS. Following, GelMA hydrogels were chemically fixed with 4% (v/v) paraformaldehyde for 15 minutes at room temperature and washed three times in PBS. Next, hydrogels were paraffin embedded and cut into 5 µm thick sections using Superfrost Plus slides (Thermo Scientific). Then, each section was incubated twice in Histo-Clear (National Diagnostics) for 4 minutes each time to get deparaffinised. Sections were then dehydrated using 100% (v/v) ethanol for two consecutive incubations for 2 minutes each and 70% ethanol for one incubation for 2 minutes, all at room temperature. GelMA sections were then washed in de-ionised water for 2 minutes at room temperature. For immunostaining, sections were incubated in 10% (v/v) goat serum (prepared in PBS) for 1 hour at room temperature, and left incubating overnight at 4℃ with primary antibody (custom-made to detect the laminin fragment) diluted to a 1:200 ratio in 10% (v/v) goat serum prepared in PBS. Next, GelMA sections were washed with PBS three times, incubated in secondary antibody solution (Goat anti-Rabbit IgG (H+L) Cross-Adsorbed, Alexa Fluor® 555) diluted in a 1:200 ratio in PBS, and washed with PBS three time. For each GelMA formulation, a staining control, to which no primary antibody solution was added, was also prepared. Stained hydrogel samples were mounted in Fluoromount-G™ (Invitrogen) and imaged using a EVOS™ Digital Color Fluorescence Microscope (Invitrogen).

3.3.19 Spheroid encapsulation in GelMA

MCF10A spheroids (see Subsection 3.3.4) were collected one by one into Eppendorf tubes from the 96-well round bottom ultra-low attachment plates by pipetting. Each spheroid precipitated to the bottom of the Eppendorf tube and the supernatant was aspirated and discarded. Next, each spheroid was gently resuspended in 50 µl of GelMA precursor solution and transferred into a 1 ml syringe, which tip had been cut and removed, placed in a vertical position. Following, the encapsulated spheroid-hydrogel precursor solution was photo-cross-linked under a UV unit at 365 nm for 5 minutes. Each MCF10A spheroid encapsulated within the cross-linked GelMA hydrogel was then transferred to a well in a 96-well round bottom ultra-low attachment plate with 100 µl medium. Depending on the experimental conditions, media was supplemented with 10 µg/ml soluble laminin fragment and/or 10 ng/ml TGF-β1.

3.3.20 Bio-layer interferometry

Analyses using bio-layer interferometry (BLI) were conducted by myself and Ben Miller (London Centre for Nanotechnology, University College London). BLI was employed to study the interactions between the recombinant laminin fragment (with different chemical modifications) and different potential binding partners, recombinant human $\alpha3\beta1$ integrin (R&D Systems), recombinant mouse $\alpha3\beta1$ integrin (R&D Systems) and recombinant human transforming growth factor-$\beta1$ (TGF-$\beta1$, PeproTech, AF-100-21C-2), using the instrument Octet ®RED96 (Pall FortéBio). All steps were carried out at room temperature. Streptavidin (SA) biosensors (Pall FortéBio) were hydrated before use in kinetics buffer (KB, Pall FortéBio) diluted ten times in PBS. All steps, baseline, loading and association, were carried out in KB, with the exception of the association steps with the integrins, which were performed in integrin buffer (20 mM Tris, 150 mM NaCl, 1mM $MgCl_2$, 1 mM $CaCl_2$, 0.02% (v/v) Tween20, 0.1% (w/v) BSA, pH 7.4). To reduce background signal in the association steps with the integrins due to changes in buffer conditions, an additional baseline step was done after the laminin fragment was loaded. After the first baseline, each SA biosensor was loaded with 20 µg/ml biotinylated anti-6X His-tag antibody (Abcam, ab27025), which was followed by a loading with 25 µg/ml recombinant laminin fragment (for all chemical modifications). For association, mouse and human integrin $\alpha3\beta1$ were added at 20 µg/ml and human TGF-$\beta1$ was added at 1.6 µg/ml. For negative controls, separate sensors loaded with laminin fragment bound to biotinylated anti-6X His-tag antibody were submersed in binding buffer (integrin buffer or KB, depending on the ligand).

3.3.21 Enzyme-Linked Immunosorbent Assay

Enzyme-Linked Immunosorbent Assays (ELISAs) were carried out, in collaboration with Dr Marta Broto, to investigate the interactions between the recombinant laminin fragment and different potential binding partners, recombinant human $\alpha3\beta1$ (R&D Systems), recombinant mouse $\alpha3\beta1$ (R&D Systems) and recombinant human transforming growth factor-$\beta1$ (TGF-$\beta1$, PeproTech). Plates (Corning 96 Well EIA/RIA Assay Microplate) were coated with either 1 µg/ml human $\alpha3\beta1$, 1 µg/ml mouse $\alpha3\beta1$ or 0.5 µg/ml TGF-$\beta1$ in coating buffer (200 mM H_3BO_3, 100 mM NaOH, 34.5 mM HCl, pH 7.8), for 4 hours at room temperature. Following, plates were washed three times in PBST (0.05 % (v/v) Tween20 in PBS). Recombinant laminin fragment was then added at a concentration of 1 µg/ml in PBST to interact with $\alpha3\beta1$ integrins (human and mouse) and TGF-$\beta1$, and incubated for 30 minutes at room temperature. Plates were then washed three times in PBST and incubated with the primary antibody against the laminin fragment (1:6,000; prepared in PBST) for 30 minutes at room temperature. Next, plates were washed three times in PBST and incubated with anti-rabbit HRP sec-

ondary antibody (1:6,000; prepared in PBST) for 30 minutes at room temperature. Again, plates were washed three times in PBST and then incubated in substrate buffer (50 mM sodium citrate, pH 5.5, 0.01% (w/v) TMB, 0.004% (v/v) H_2O_2) for 30 minutes at room temperature. Lastly, in order to stop the reaction, 50 µl of 8M H_2SO_4 was added to each well. The absorbance was then measured at 450 nm using the SpectraMax M5 plate reader.

3.3.22 Imaging and Image Analysis

3.3.22.A Brightfield Live Cell Microscopy

GelMA-encapsulated spheroids imaging was performed using a Zeiss Axio Observer Inverted Widefield Microscope with transmitted light, a 10X magnification objective and a Hamamatsu camera. Each well contained a GelMA-encapsulated spheroid, which positions were stored as scenes in the ZEN software for image acquisition. In order to maintain the cells alive during imaging, the microscope incubation chamber was utilised to maintain the temperature at 37℃ and the CO_2 levels at 5%.

Cell migration analysis was performed using the image software FIJI. Briefly, regions of interest (ROIs) were manually drawn at selected time points (days 0, 3, 4 and 6) and their areas were measured. To obtain migrated areas, measured area of the ROI at day 0 was subtracted from all timepoints within each biological sample. For each condition, three biological replicates were assessed.

3.3.22.B Confocal Microscopy

MCF10A cells exposed to Cy5-labelled laminin fragment or free Cy5 were on 8 chamber slides (ibidi GmbH) for fluorescence imaging at an initial cell density of 5,000 cells/cm^2. Treatment with 10 µg/ml of labelled fragment was performed 24 hours post-seeding, and were then fixed 24 hours post-treatment. For siRNA-mediated knockdown experiments, cells were cultured as described in Subsection 3.3.7 and were fixed 24 and 48 hours post-siRNA treatment. Chemical fixation was performed in a solution of 4% (v/v) paraformaldehyde (methanol-free, 16% (w/v), Thermo Fisher Scientific) prepared in PBS for 15 minutes at room temperature. Samples were then washed three times in PBS. Cells were permeabilised with 0.5% Triton X-100 (Sigma-Aldrich) in PBS for 10 minutes at room temperature, which was followed by three washes in PBS. Following, a solution with AlexaFluor 488 Wheat Germ Agglutinin (Invitrogen, 1:200) and DAPI (Sigma-Aldrich, 1:1,000) in PBS was used to label the membranes and nuclei of cells, respectively, by incubating the samples with this solution for 20 minutes at room temperature. Finally, samples were washed 3 times with PBS and stored at 4℃ in Fluoromount-G™

(Thermo Fisher Scientific) mounting medium. For each condition, three biological replicates were assessed.

Imaging was performed on a Leica SP8 inverted confocal microscope. *Z*-stacks were collected with a HC PL APO 63x/1.40 NA oil CS2 objective lens and a zoom factor of 2, 16 bit depth and an average 500 nm step size. After image acquisition, images produced were processed with the image analysis software FIJI. For quantification of cell-associated Cy5-labelled fragment, *z* projections with maximum intensity were obtained and ROIs were created by manually drawing around the perimeter of each cell. Following, the Cy5 channel images were duplicated and the background was subtracted for each one. New ROIs that corresponded to the Cy5-labelled fragments were found by setting a threshold, which was then used for all image analyses. The ROIs contained within the cells were then analysed and the fluorescence intensity was obtained from the integrated density provided by the software.

3.3.23 Statistical Analysis

Statistical analyses were carried out using GraphPad Prism 6.0. For RT-qPCR, three independent biological replicates were collected for each sample in study, and two technical replicates were measured and analysed in each RT-qPCR assay plate. To determine whether data were normally distributed, Komogorov–Smirnov and Shapiro–Wilk tests were performed. Differences in gene expression and in gelatinase activity were tested with one-way ANOVA using Dunnet's multiple comparisons tests. Paired t tests were conducted to evaluate statistical difference between samples that were exposed to soluble fragment (cells treated with TGF-β1 and grown within 4mg/ml collagen I). When data were not normally distributed, Kruskal-Wallis tests were performed. To compare fluorescence intensity of cell-associated Cy5-labelled fragment, outliers of each sample data group were identified and removed. Sample data was then compared using unpaired nonparametric Mann-Whitney tests. All hypothesis tests were considered two-tailed.

In all cases, $p<0.05$;**$p<0.01$;***$p<0.001$;****$p<0.0001$.

3.4 Results

3.4.1 MMP-2 cleaves full-length laminin-111 and the laminin β1 fragment interacts with human MCF10A cells

The proteolytic activity of matrix metalloproteinases (MMPs) is instrumental during ECM remodelling events. Here, the processing of both human and mouse full-length laminin-111 by active MMP-2 was examined. Figure 3.4**a** shows that MMP-2 cleavage of laminin-111 produces a fragment with a molecular weight of approximately 60 kDa. This resulting 60 kDa fragment can be detected by Coomassie blue staining from the processing of both human and mouse laminin-111 (Figure 3.4**a** lanes 2 and 3). Analysis by Western blotting confirms that the fragment resulting from MMP-2 proteolysis of mouse laminin-111 is specific to the custom antibody previously developed to bind the laminin β1 fragment (Figure 3.4**a** lane 6). However, no band can be observed in the lane that corresponds to the digestion of human laminin-111 (Figure 3.4**a** lane 5). Figure 3.4**b** shows that treating MCF10A cells with soluble recombinant fragment (up to a concentration of 10 µg/ml) does not negatively affect their metabolic activity.

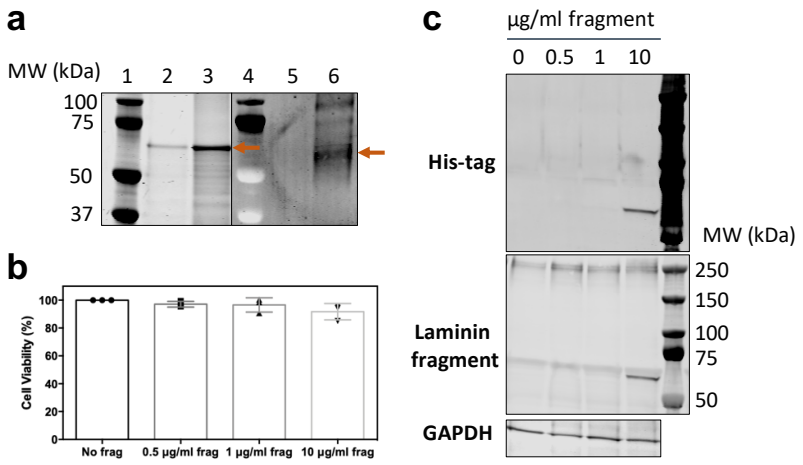

Figure 3.4: MMP2 cleaves full-length laminin-111 and the laminin β1 fragment interacts with human MCF10A cells. **a** Processing of both human and mouse full-length laminin-111 by active MMP-2. Lanes 1 and 4 show molecular weight markers. Lanes 2 and 3 show Coomassie blue-stained denatured a 60 kDa band (orange arrow) generated from the processing of human and mouse laminin by MMP-2, respectively. Lanes 5 and 6 show the immunoblot, using an antibody against the laminin β1 fragment, from the processing of human and mouse laminin by MMP-2, respectively. Only the cleavage of mouse laminin (lane 6) was detected by the antibody (orange arrow). **b** Metabolic activity of MCF10A cells exposed to increasing concentrations of soluble recombinant fragment, measured using CCK8 assay. The metabolic activity is normalised to control with no fragment. **c**. Detection of recombinant laminin fragment in whole cell extracts by Western blotting, using antibodies against the His-tag and the laminin fragment.

In order to determine whether this laminin β1 fragment, which has previously been used in studies using cells of murine origin [473, 474], interacts with human mammary epithelial cells, MCF10A protein extracts were collected 24 hours post-treatment with recombinant fragment and analysed by Western blotting. Figure 3.4**c** shows that a band of approximately 60 kDa can be detected when cells are treated with 10 µg/ml of recombinant fragment. It is likely that the treatment with lower concentrations is below the detection limit of the performed analysis. It is important to note that the use of the anti-His tag antibody confirms that the observed 60 kDa band corresponds to the exogenous fragment used to treat the cells, as it is recombinantly produced as an His-tag fused peptide (Figure B.1, Appendix B). Further analysis to determine the subcellular localization of the fragment was performed using subcellular fractionation and Western blotting (Figure B.2 Appendix B). However, a positive signal for laminin fragment (using both antibodies against the laminin fragment and the His-tag) was found in both experimental and control samples.

3.4.2 Recombinant laminin β1 fragment alters the expression of EMT-related genes and gelatinase activity

Human mammary epithelial MCF10A cells undergoing EMT were treated with the fragment as a soluble factor added to the medium, to study its effects on EMT events. This was achieved by employing two *in vitro* EMT models (both investigated in Chapter 2): one where these cells are grown in 2D culture conditions and treated with TGF-β1 for 24 hours; and a second one, where the process of EMT occurs due to the presence of extracellular type I collagen in a 3D morphogenesis assay.

3.4.2.A Laminin fragment alters EMT events induced by TGF-β1

The expression of EMT-related genes was assessed and, in agreement with previous data, the exposure to TGF-β1 results in an upregulation of mesenchymal genes *Cdh2*, *Snai1*, *Vim* and *Mmp2*, as well as epithelial gene *Cdh1* (Figure 3.5). Strikingly, however, an increase in the expression of the same mesenchymal genes is also observed in conditions where cells were exposed to soluble laminin fragment and no TGF-β1 (Figure 3.5). Figure 3.6 shows changes in expression of EMT-related genes in conditions of concomitant treatment, with increasing concentrations of laminin fragment, to better visualise the effects of the fragment on EMT gene regulation in the presence of TGF-β1. Interestingly, the evidence shows that, in the presence of EMT inducer TGF-β1, the expression of mesenchymal genes *Snai1*, *Vim* and *Mmp2* is slightly downregulated when cells are treated with 10 µg/ml of laminin fragment.

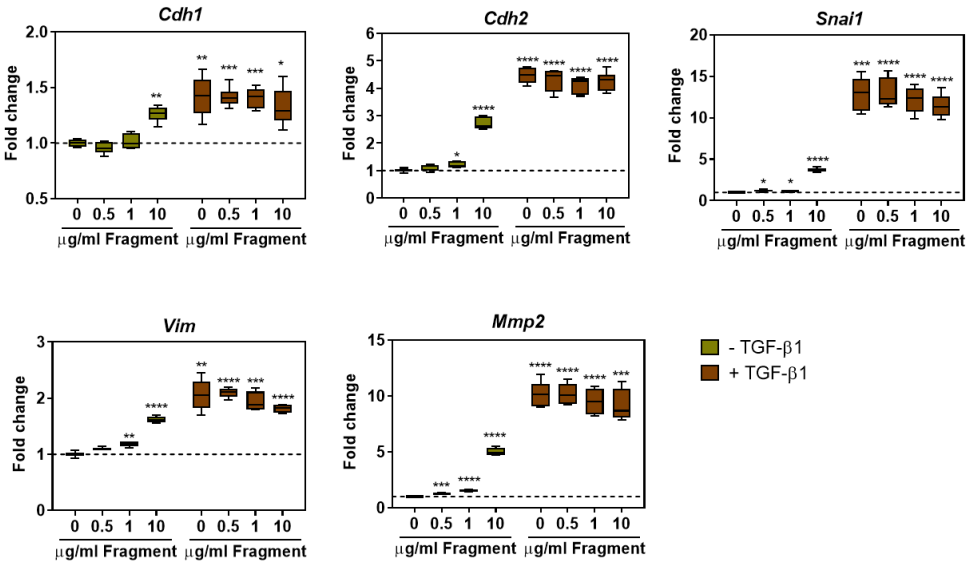

Figure 3.5: Changes in expression of EMT-related genes by TGF-β1 treatment and soluble laminin fragment. EMT gene expression of MCF10A cells exposed to increasing concentrations of laminin fragment in the culture medium, with and without EMT-inducing TGF-β1 (10 ng/ml) treatment measured by RT-qPCR. Normalized to *GAPDH* and to sample with no fragment and no TGF-β1. *y* axis: $2^{-\Delta\Delta Ct}$. Data is shown on Tukey box and whiskers plot. Statistical tests compared all conditions with the control group (no TGF-β1 and no fragment). *p$<$0.05;**p$<$0.01;***p$<$0.001;****p$<$0.0001.

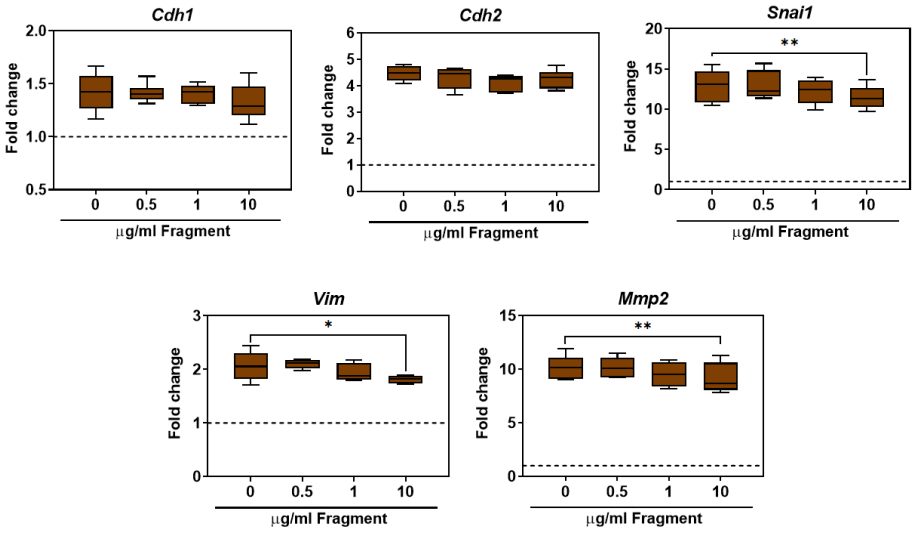

Figure 3.6: Changes in expression of EMT-related genes by increasing concentrations of laminin fragment to MCF10A cells treated with TGF-β1. EMT gene expression of MCF10A cells exposed to increasing concentrations of laminin fragment in the culture medium, with EMT-inducing TGF-β1 treatment (10 ng/ml) measured by RT-qPCR. Normalised to *GAPDH* and to sample with no fragment and no TGF-β1. *y* axis: $2^{-\Delta\Delta Ct}$. Data is shown on Tukey box and whiskers plot. Statistical tests compared specific conditions with the one treated with TGF-β1, but no fragment. *p$<$0.05;**p$<$0.01.

Moreover, gelatin zymography analysis (Figure 3.7) showed that gelatinase activity is increased when cells are treated with TGF-β1. In agreement with gene expression data, it is also observed that gelatinase activity increases with increasing concentration of laminin fragment, when no TGF-β1 is added to the cell culture medium. No significant effect on gelatinase activity was observed with concomitant treatment.

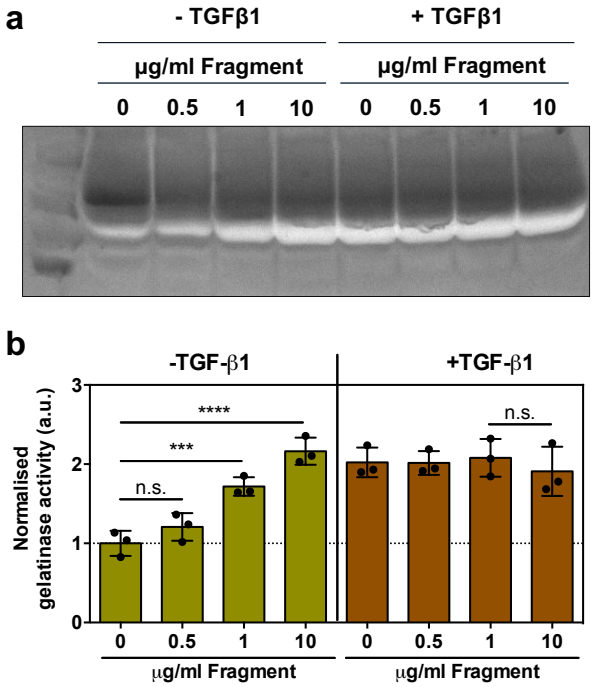

Figure 3.7: Changes in gelatinase activity by TGF-β1 treatment and soluble laminin fragment. a Representative zymogram of conditioned media of MCF10A cells exposed to increasing concentrations of laminin fragment in the culture medium, with and without EMT-inducing TGF-β1 treatment (10 ng/ml). **b** Corresponding densitometric analysis. Data are normalised to sample with no fragment and no TGF-β1. ***p$<$0.001;****p$<$0.0001. n.s.- not significant.

3.4.2.B Laminin fragment alters EMT events induced by 3D type I collagen

Changes in EMT gene expression triggered by the laminin fragment are also observed on MCF10A in a 3D morphogenesis assay with Matrigel and type I collagen, as shown in Figure 3.8. Consistent with results obtained with TGF-β1 treatment, the presence of laminin fragment as a soluble factor in the medium drives an upregulation of mesenchymal gene expression, even in epithelial conditions where cells are grown within Matrigel and no type I collagen. Figure 3.9 shows that when MCF10A cells are grown within Matrigel and 4 mg/ml type I collagen, where they already exhibit a mesenchymal phenotype (as shown in Chapter 2), the upregulation of mesenchymal genes *Cdh2*, *Snai1*, *Vim* (except at 10 µg/ml) and *Mmp2* is further exacerbated with increasing concentrations of soluble laminin

fragment.

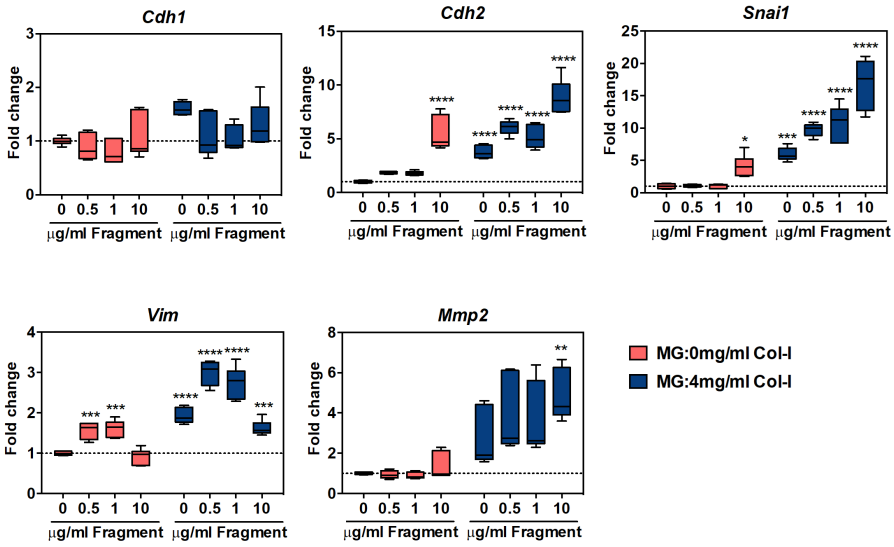

Figure 3.8: Changes in expression of EMT-related genes by extracellular type I collagen and soluble laminin fragment. EMT gene expression of MCF10A cells exposed to increasing concentrations of laminin fragment in a Matrigel/Collagen I 3D morphogenesis assay measured by RT-qPCR. Normalized to *GAPDH* and to sample on Matrigel alone and no fragment. *y* axis: $2^{-\Delta\Delta Ct}$. Data is shown on Tukey box and whiskers plot. Statistical tests compared all conditions with the control group (0 mg/ml collagen I and no fragment). *p<0.05;**p<0.01;***p<0.001;****p<0.0001.

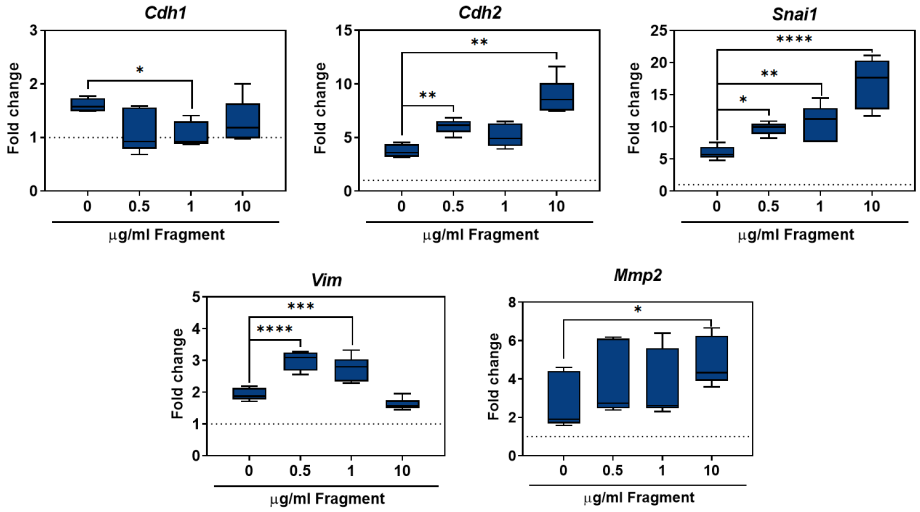

Figure 3.9: Changes in expression of EMT-related genes by soluble laminin fragment in the presence of extracellular type I collagen. EMT gene expression of MCF10A cells exposed to increasing concentrations of laminin fragment in a Matrigel/Collagen I 3D morphogenesis assay measured by RT-qPCR. Normalized to *GAPDH* and to sample on Matrigel alone and no fragment. *y* axis: $2^{-\Delta\Delta Ct}$. Data is shown on Tukey box and whiskers plot. Statistical tests compared specific conditions with the one where cells were grown in 4 mg/ml collagen I, but did not receive fragment treatment. *p<0.05;**p<0.01;***p<0.001;****p<0.0001.

Gelatinase activity in these conditions was assessed by zymography (Figure 3.10). Here, evidence suggests that the presence of type I collagen in the extracellular matrix increases gelatinase activity, but the presence of soluble laminin fragment at the highest concentration studied of 10 µg/ml has no significant effect on this kind of proteolytic activity.

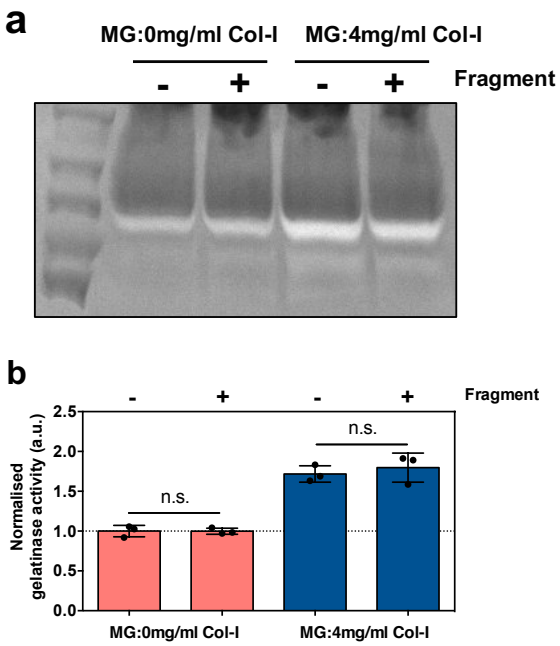

Figure 3.10: Changes in gelatinase activity by extracellular type I collagen and soluble laminin fragment **a** Representative zymogram of conditioned media of MCF10A cells on a Matrigel/Collagen 3D morphogenesis assay exposed to 10µg/ml of laminin fragment in the culture medium. **b** Corresponding densitometric analysis. Data are normalised to sample on Matrigel alone and no fragment. n.s.- not significant.

3.4.3 Modulation of epithelial cell phenotype using the laminin fragment tethered to a gel system

In order to investigate whether this laminin β1 fragment can modulate epithelial cell phenotype while circumventing potential off-target effects, a problem that has prevailed in studies using EMT-inhibiting soluble compounds [489, 490], in this chapter a hydrogel system in which we can have the laminin fragment covalently tethered was developed.

3.4.3.A Synthesis and characterisation of azide modified gelatin methacryloyl (GelMA) with tethered laminin fragment

Using semisynthetic GelMA-based hydrogels, which result from the chemical functionalisation of gelatin with methacryloyl groups, for 3D cell culture offers the benefits associated with the use of natural polymers, including cell-binding and protease cleavage sites, and the advantages of synthetic materials, namely the ability to control their mechanical and biochemical properties. Figure 3.11**a** illustrates a schematic overview of the approach employed in this work, from the GelMA production to the encapsulation of MCF10A spheroids within cross-linked hydrogels.

To achieve the desired formulation of a GelMA-based hydrogel covalently functionalised with laminin fragment, first an approach to chemically modify the recombinant fragment while retaining its bioactivity was developed. The strategy here chosen to bind the fragment to the hydrogel is a strain-promoted azide–alkyne cycloaddition (SPAAC) chemical reaction. This type of copper-free click reaction is particularly convenient when preparing biomaterials, as it can occur through the mixing of compounds containing alkyne and azide groups within an aqueous solution with no interference from other biomolecules present in the mixture. In addition, one of the biggest advantages of this chemical strategy is its lack of toxicity as it does not require a metal catalyst. Here, strained alkyne handles were added to the chemical structure of the recombinant laminin fragment and GelMA precursors were functionalised with azide groups.

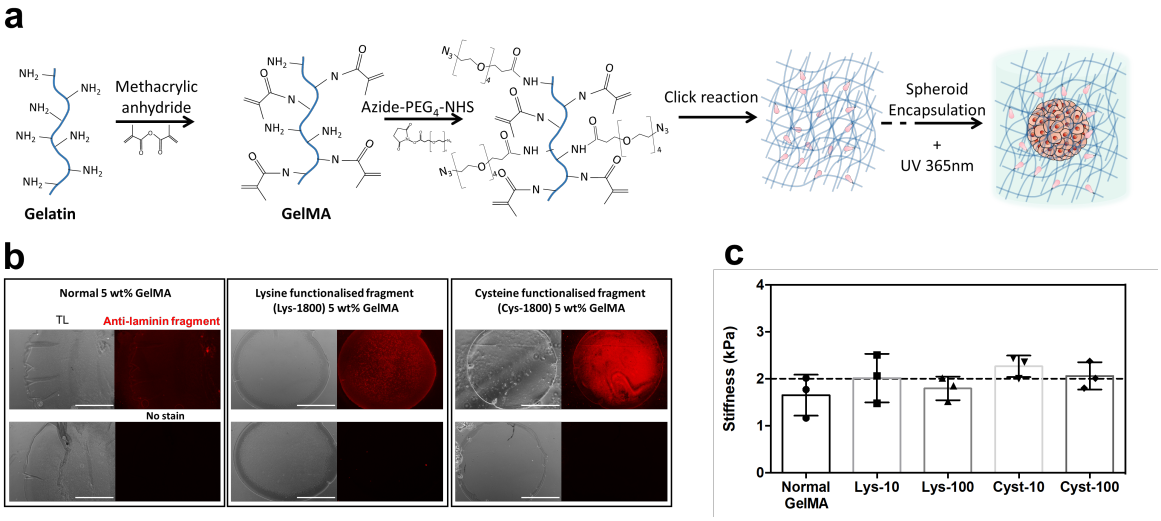

Figure 3.11: Employed strategy to tether the laminin fragment to a GelMA-based hydrogel. a Schematic overview of the approach employed in this study from the GelMA production, to the functionalisation of lysine amino groups with azide groups, to the "click" addition of fragment to the structure of the hydrogel, to the encapsulation of MCF10A spheroids within crosslinked hydrogels. **b** Fluorescence microscopy images showing laminin fragment-tethered GelMA sections (fragment concentration of 1.8 mg/ml). Scale bars: 1000 µm.**c** Compressive moduli of all GelMA formulations used for cell culture in this work. Mechanical testing of GelMA-based hydrogels was conducted by myself together with Dr. Liliang Ouyang.

During synthesis, the ratio of methacrylic anhydride to gelatin was designed such that around 20% of amino groups were left unreacted (Figure B.4, Appendix B). The existence of these amino groups was exploited to functionalise the GelMA structure with azide groups using an NHS ester chemistry (Figure 3.11**a**). Two different strategies to add strained alkyne functionalised handles to the fragment were employed: one cysteine selective and the other lysine selective (Figure B.3**a**, Appendix B). Consequently, two formulations of GelMA-based hydrogels covalently functionalised with laminin fragment were prepared. Figure B.5 in Appendix B shows the resulting final degree of functionalisation (DoF). Fluorescence signal due to the presence of laminin fragment tethered to the GelMA structure was observed (fragment concentration of 1.8 mg/ml, Figure 3.11**b**).

In this work, all formulations of GelMA-based hydrogels for 3D cell culture experiments were prepared at a concentration of 5% (w/v) and the ones functionalised with laminin fragment, both cysteine and lysine modifications, were prepared to have the fragment at 10 µg/ml, as previously reported in [474], and at 100 µg/ml. Importantly, mechanical testing of all formulations of GelMA for cell culture confirmed that tethering the fragment at the studied concentrations did not significantly change the stiffness of the hydrogels (Figure 3.11**c**).

3.4.3.B Effect of the laminin fragment on EMT gene expression when tethered to a gel system

The effects of the fragment functionalisation of GelMA-based hydrogels on EMT gene expression of encapsulated MCF10A spheroids was evaluated. Figure 3.12**a** shows that expression of epithelial gene *Cdh1*, and mesenchymal genes *Vim* and *Mmp2* is not significantly changed by the presence of tethered fragment. However, when GelMA-encapsulated spheroids where exposed to concomitant treatment with fragment and TGF-β1, a significant decrease in *Mmp2* expression in the presence of soluble fragment was observed, even though no significant changes were found with tethered fragment (Figure 3.12**b**). Moreover, gelatinase activity was assessed with zymography. As shown in Figure 3.13, the data suggests that the fragment does not substantially alter the activity of gelatinases in the experimental conditions of this study. The significant increase that was observed in gelatinase activity is most likely due to TGF-β1 treatment.

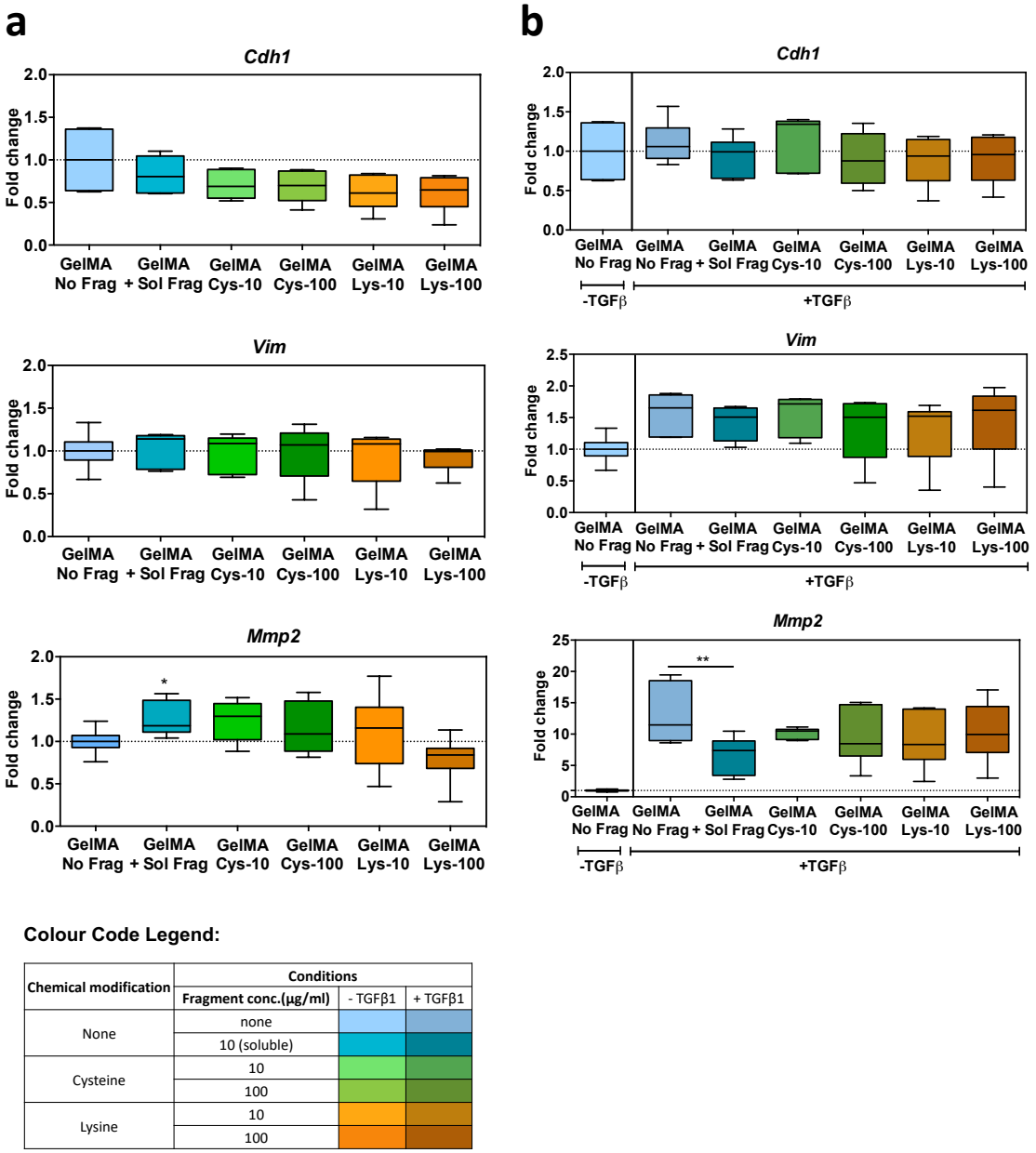

Figure 3.12: Changes EMT gene expression by different strategies to expose the laminin fragment to MCF10A GelMA-encapsulated spheroids. EMT gene expression of MCF10A cells exposed to soluble or tethered laminin fragment without (**a**) or with (**b**) TGF-β1 treatment (10 ng/ml) measured by RT-qPCR. Normalized to *GAPDH* and to unmodified GelMA-encapsulated spheroids with no fragment and no TGF-β1. *y* axis: $2^{-\Delta\Delta Ct}$. Data is shown on Tukey box and whiskers plot. *p$<$0.05;**p$<$0.01. A table with the colour code can be found at the bottom of this figure to facilitate interpretation of plots.

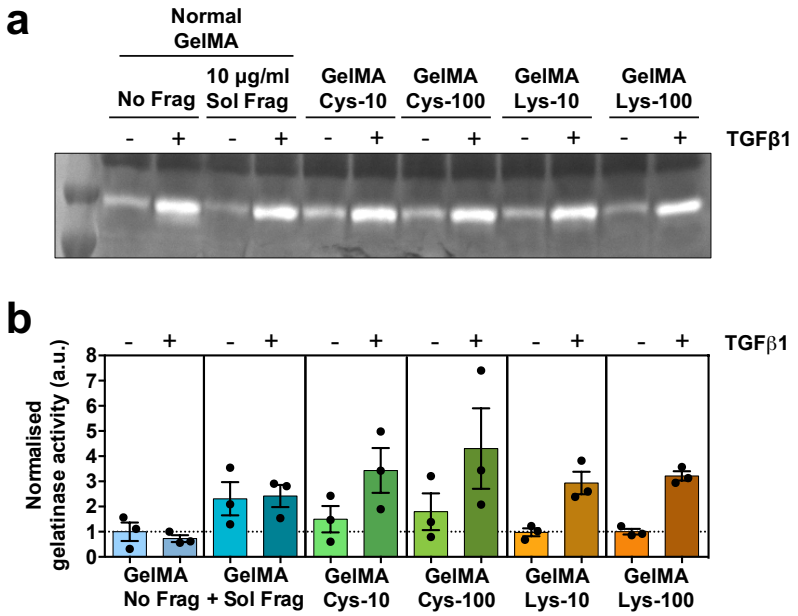

Figure 3.13: Changes in gelatinase activity by different strategies to expose the laminin fragment to MCF10A GelMA-encapsulated spheroids, with and without TGF-β1 treatment. a Representative zymogram of conditioned media of GelMA-encapsulated MCF10A spheroids exposed to soluble or gel tethered laminin fragment, with or without EMT-inducing TGF-β1 treatment (10 ng/ml). **b** Corresponding densitometric analysis. Data are normalised to unmodified GelMA-encapsulated spheroids with no fragment and no TGF-β1.

3.4.3.C Effect of the laminin fragment on invasion when tethered to a gel system

In addition, the effect of fragment functionalisation on cell invasion from encapsulated spheroids into GelMA-based hydrogels was investigated. An overall increase in migrated area was observed over a period of 6 days post-encapsulation (Figure 3.14). Interestingly, the quantification here performed showed that on day 6 three sample clusters were formed in regards to migrated area: unfunctionalised GelMA (two shades of blue in Figure 3.14**b**), GelMA functionalised with 10 µg/ml of fragment (lighter shades of green and orange), and GelMA functionalised with 100 µg/ml of fragment (darker shades of green and orange). Albeit not to a statistically significant degree, it seems that functionalising GelMA with a higher concentration of fragment can potentially inhibit invasion, whereas the lower concentration induces it.

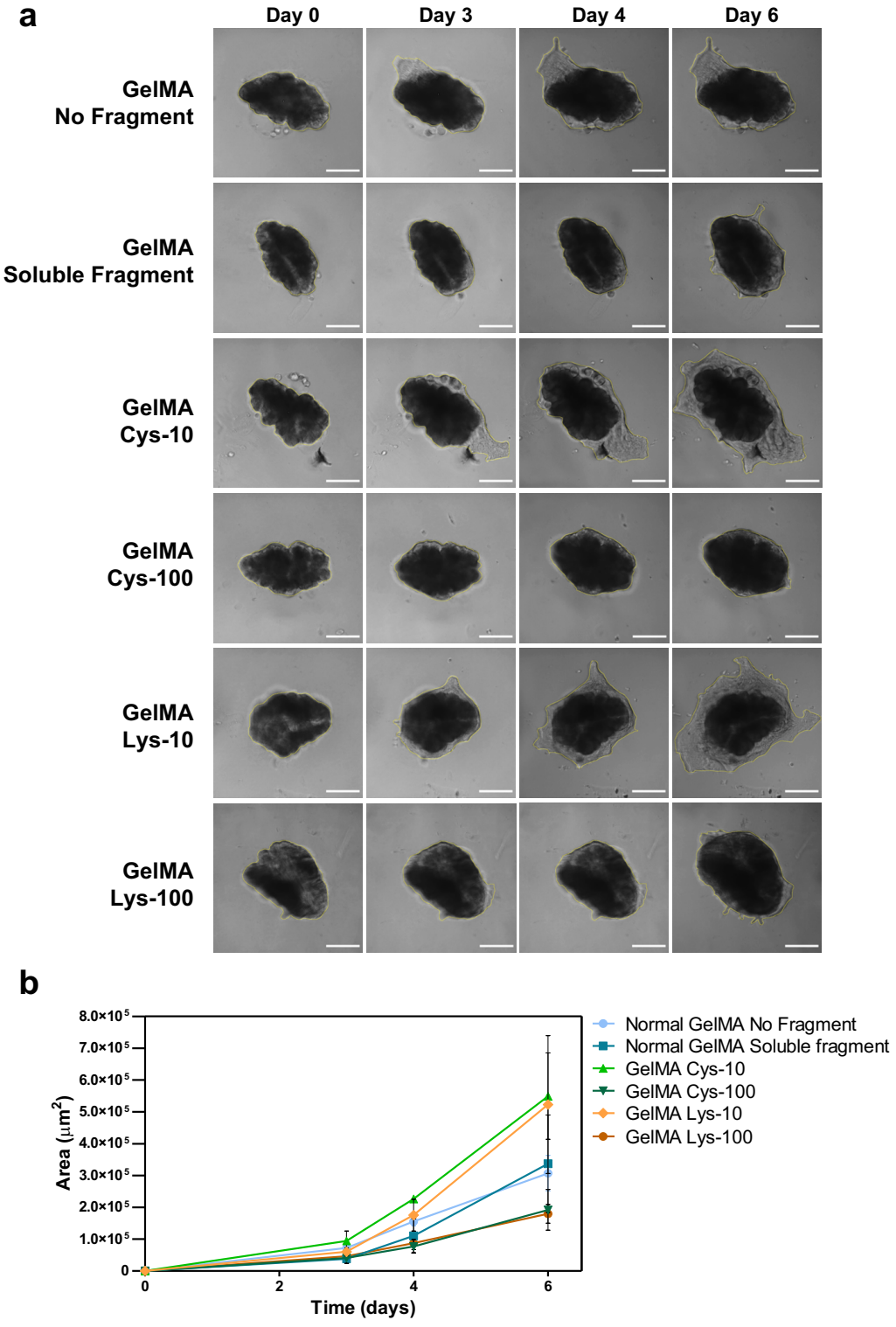

Figure 3.14: Cell invasion from GelMA-encapsulated spheroids exposed to laminin fragment via different strategies. a Representative images of encapsulated MCF10A spheroids 3D invasion into GelMA-based hydrogels, where these cells were exposed to soluble or tethered laminin fragment, over the course of 6 days. Scale bars: 500 µm. **b** Quantification of cell invasion area around the spheroids.

3.4.4 Biomolecular and cellular interactions with the laminin fragment

3.4.4.A Laminin fragment interacts with α3β1 integrin and TGF-β1

Previous studies reported that this recombinant laminin β1 fragment interacts with integrin α3β1 derived from mouse [473, 474]. Using bio-layer interferometry (BLI), a label-free method to optically monitor biomolecular interactions in real-time [491], interactions between the laminin fragment, or the two chemically modified versions with strained alkyne handles (cysteine and lysine), and integrin α3β1 integrin, both of mouse and human origins, were measured. As it can be observed in Figure 3.15**a**, mouse α3β1 integrin interacts with laminin fragment immobilised in the BLI sensor (all versions of the fragment produce a similar binding curve). In turn, negligible interaction was seen between human α3β1 integrin and laminin fragment using BLI.

In addition, due to the potential effect of the laminin fragment in reducing mesenchymal gene expression with concomitant TGF-β1 treatment, as seen in Figure 3.6, the interaction between the fragment and TGF-β was assessed. Importantly, this could shed light on the fragment's mechanism of action. Figure 3.15**c** shows that there is indeed a binding response when TGF-β is in contact with all versions of the immobilised laminin fragment.

Moreover, to complement these data, the interactions between the laminin fragment and the three aforementioned ligands, mouse and human α3β1 integrins and TGF-β1, were assessed with ELISA, a more commonly used method to analyse biomolecular interactions. This assay confirmed that the fragment interacts with mouse α3β1 integrin and with TGF-β1 (Figure 3.15**d**). Interestingly, this assay also detected a specific interaction between the fragment and human α3β1 integrin, as opposed to what was detected using BLI.

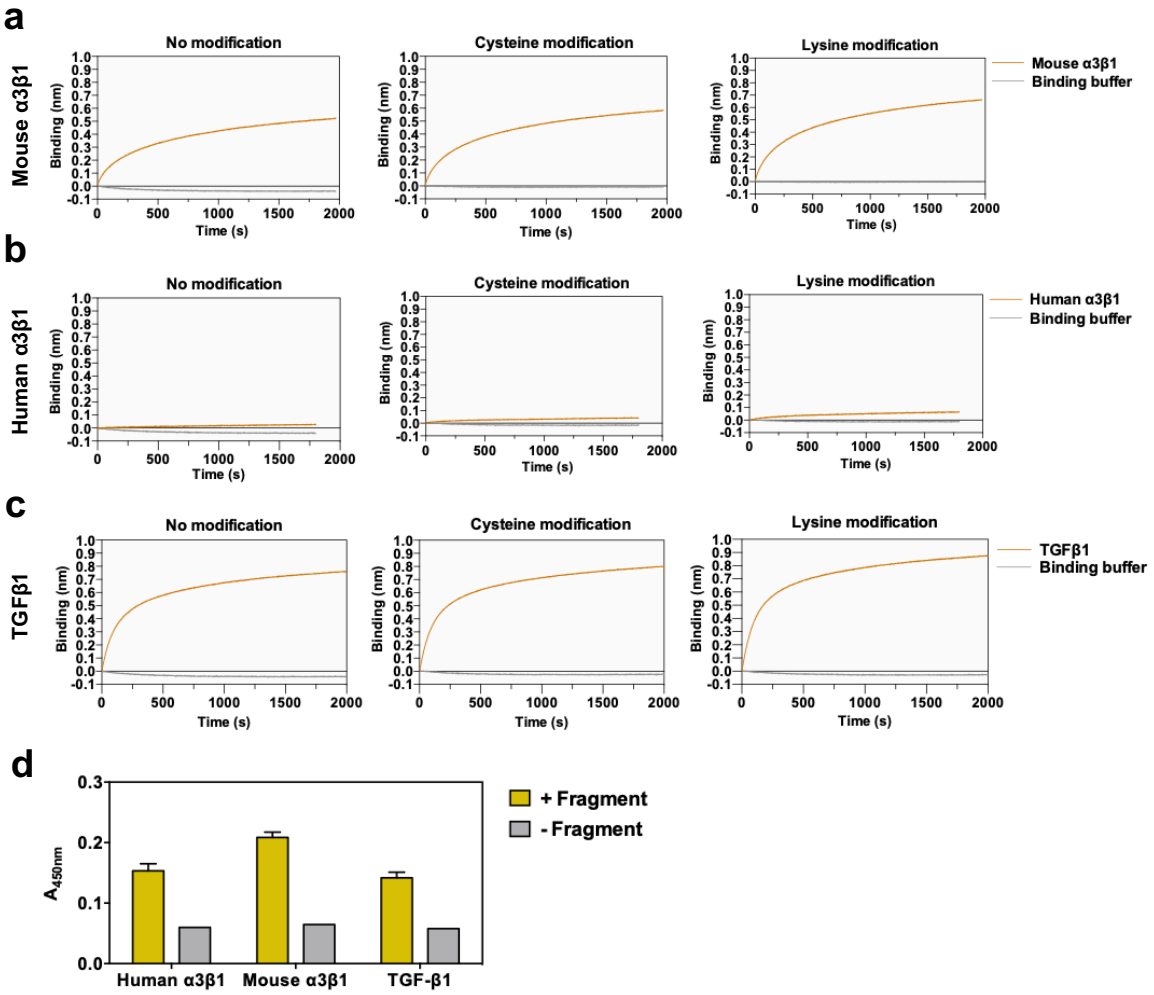

Figure 3.15: Laminin fragment interacts with α3β1 integrin and TGF-β1. Real-time BLI binding response curves of mouse α3β1 (**a**), human α3β1 (**b**), and TGF-β1 (**c**). BLI measurements were carried out together with Ben Miller. **d** Binding of laminin fragment to human α3β1, mouse α3β1 and TGF-β1 by ELISA. ELISA assays were performed with Dr. Marta Broto's collaboration. Bars are presented as mean with SD.

3.4.4.B Cy5-labelled laminin fragment is internalised by MCF10A cells

Fluorescence labelling of the laminin β1 fragment was carried out to study its interaction with MCF10A cells. Using the previously mentioned SPAAC chemical reaction strategy, two versions of the chemically modified fragment (lysine and cysteine) were labelled with Cy5 (Figure B.3, Appendix B). Figure 3.16 shows that Cy5-labelled fragment, both via lysine and cysteine, is incorporated by these human mammary epithelial cells in 2D culture. Orthogonal views of confocal microscopy z-stacks clearly reveal that the fragment is internalised by the cells at the time point studied (24 hours post-treatment).

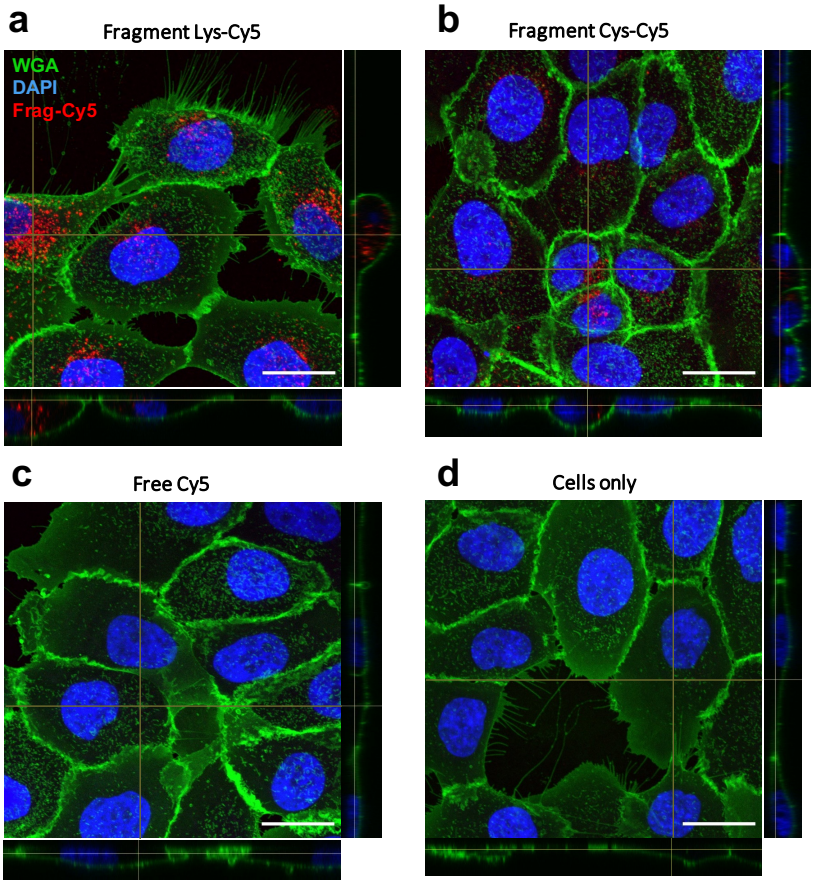

Figure 3.16: Cy5-labelled laminin fragment is uptaken by MCF10A cells *in vitro*. Representative immunofluorescence images of MCF10A cells cultured for 24 hours with fragment labelled via lysine (**a**), fragment labelled via cysteine (**b**), free Cy5 (**c**), with no treatment (**d**). Both labelled versions of the fragment and free Cy5 were added to the cell culture medium at a concentration of 17 nM. WGA staining- green; DAPI staining- blue; Cy5- red. Scale bars: 20 µm.

3.4.4.C siRNA-mediated silencing of integrin α3

Previously reported data [473, 474] suggest that the laminin β1 fragment interacts with epithelial cells directly or indirectly via integrin α3β1. Here, we investigated whether inhibiting the synthesis of integrin α3 can affect the interaction between the Cy5-labelled fragment and MCF10A cells. Figure 3.17 shows that there a significant decrease in the fluorescence intensity of cell-associated Cy5-labelled fragment, particularly the one with lysine modification (Figure 3.17**b**), both 24 hours and 48 hours post-treatment, when integrin α3 is knocked-down via siRNA.

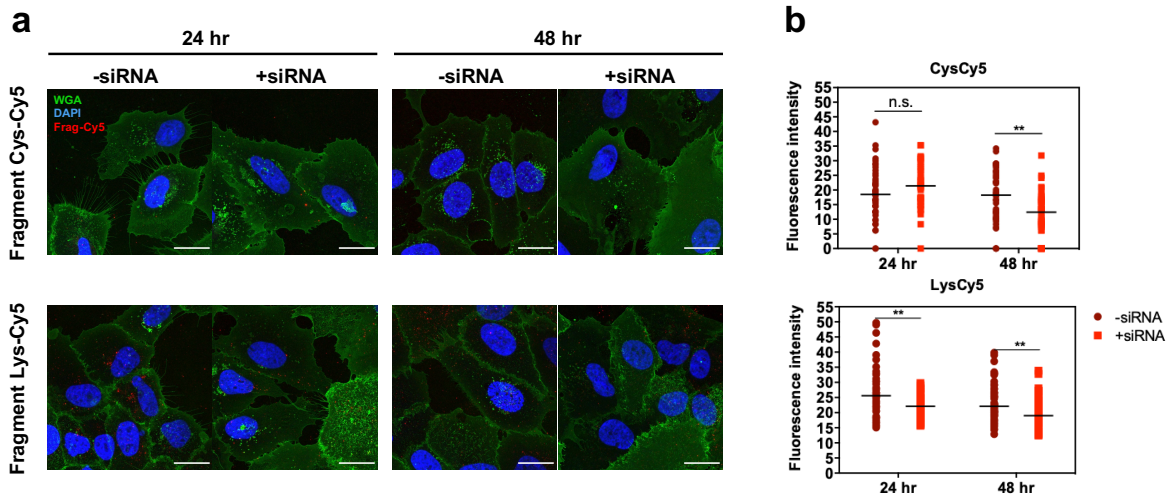

Figure 3.17: Fluorescence intensity of cell-associated Cy5-labelled fragment is reduced when expression of α3 integrin is silenced by siRNA. a Representative immunofluorescence images of MCF10A cells cultured with fragment labelled via cysteine (top) and fragment labelled via lysine (bottom), when treated with *Itga3* siRNA for 24 (left) and 48 hours (right). Both labelled versions of the fragment were added to the cell culture medium at a concentration of 17 nM. WGA stainig- green; DAPI staining- blue; Cy5- red. Scale bars: 20 µm. **b** Corresponding quantification of fluorescence intensity of Cy5-labelled fragment via cysteine (top plot) and via lysine (bottom plot). Data are presented as aligned dot plots, line at median. **p$<$0.01. n.s.- not significant.

Moreover, the influence of siRNA-mediated silencing of integrin α3 on the expression of EMT-related genes (Figure 3.18) with (right side panel of each plot) or without (left side panel of each plot) TGF-β1 treatment was assessed. These results confirm that integrin α3 is not being expressed in the presence of siRNA. In addition, it shows that the expression of the studied genes is not significantly affected, with the exception of *Itga3*, when TGF-β1 is not added to the medium. In contrast, in the presence of TFG-β1, expression of *Cdh1* is upregulated and *Snai1* is downregulated. In these conditions, the presence of the laminin β1 fragment did not alter the expression of the studied genes.

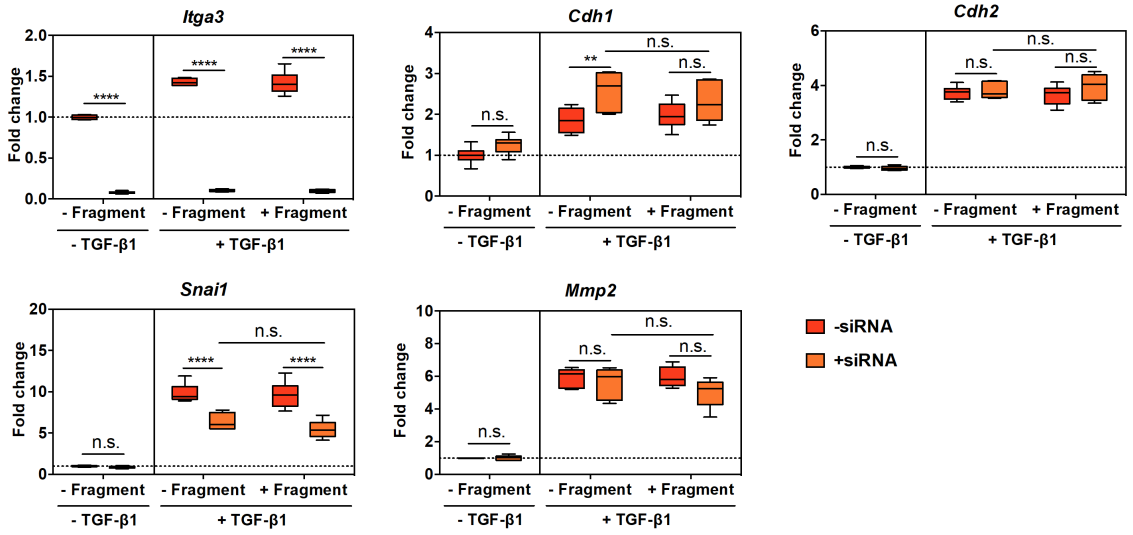

Figure 3.18: Changes in EMT gene expression of MCF10A cells treated with *Itga3* siRNA, TGF-β1 and laminin fragment. EMT gene expression of MCF10A cells treated with siRNA to knockdown integrin α3 and to soluble laminin fragment without (left side of each plot) or with (right side of each plot) TGF-β1 treatment (10 ng/ml) measured by RT-qPCR. Normalized to *GAPDH* and to MCF10A cells in culture without any treatment. *y* axis: $2^{-\Delta\Delta Ct}$. Data is shown on Tukey box and whiskers plot. *p<0.05;**p<0.01;***p<0.001;****p<0.0001. n.s.-not significant.

3.5 Discussion

In this chapter, the potential of exposing human mammary epithelial MCF10A cells with cryptic ECM information via two different strategies – as a soluble factor and as tethered to a hydrogel system – to modulate EMT-like events was investigated. From the data collected here, there is evidence that this non-cytotoxic fragment (at the concentrations used throughout this work, Figure 3.4**b**) directly interacts with these cells, as it can be collected and detected by Western blotting from cell extracts (Figure 3.4**c**). Subcellular fractionation and Western blotting analysis were carried out to investigate the localisation of the fragment within these cells. However, the subcellular fractionation led to inconclusive results because a positive signal for laminin fragment (using both antibodies against the laminin fragment and the His-tag) was found in both experimental and control samples (Figure B.2, Appendix B). Endogenous production of laminin can explain the signal observed in the fractions of the control samples using the custom-made antibody against the fragment. However, the antibody against the His-tag was utilised to confirm the presence of the exogenous recombinant fragment added to the cell culture medium, and a non-specific signal was also found in the control samples. Non-specific detection of endogenous proteins using an antibody against His-tag has been previously reported [492] and the human transcription regulator YY1, which contains 11 consecutive histidine residues (amino acids 70 to 80), has been identified as the protein detected by the anti-His-tag antibody [493]. It is possible that the same transcription regulator was identified during the analysis of the subcellular fractionation of MCF10A cells with and without laminin fragment, but this was not confirmed. These results, in addition to the cited reports, emphasise the need for caution when interpreting data using antibodies against His-tags, particularly using immunoblotting against whole cell extracts and immunofluorescence staining of cells.

The work presented in Section 3.4.2 of this chapter demonstrates that treatment with the laminin β1 fragment as a soluble compound on its own drives upregulation of mesenchymal gene expression, both in 2D or 3D *in vitro* culture (Figures 3.5 and 3.8, respectively), and increases gelatinase activity in 2D (Figure 3.7). In the 3D assay, it is the presence of extracellular type I collagen, not the recombinant fragment, that increases the activity of gelatinases (Figure 3.10). However, when cells are treated with EMT inducer TGF-β1 in 2D, the highest concentration of soluble fragment (10 µg/ml) seems to slightly decrease expression of mesenchymal genes *Snai1*, *Vim* and *Mmp2* (Figure 3.6). The upregulation of mesenchymal gene expression driven by the addition of soluble fragment without TGF-β1 treatment was not in accordance with the data previously published for a mouse model [473, 474], which leads to postulate that its function might be cell type- or even species-dependent. A previous report showed that this fragment, as a soluble compound or as adsorbed onto a polydopamine-coated PCL membrane, interacts with mouse epithelial cells undergoing EMT induced by TGF-β treatment

and prevents EMT-related events, as seen by the decrease in expression and activity of MMP-2 [474]. It seems plausible to hypothesise that the pathway by which this fragment can potentially modulate EMT in certain biological contexts involves a direct or indirect interaction with TGF-β1.

Furthermore, the development of a laminin β1 fragment functionalised GelMA-based hydrogel to study EMT-related gene expression and gelatinase activity, as well as matrix invasion by human mammary gland MCF10A cells grown as encapsulated spheroids is shown. Tethering of the laminin fragment to the semisynthetic hydrogel system was carried out via a SPAAC copper-free click chemistry, a convenient and promising strategy to synthesise biomaterials for various applications, including *in vitro* cell culture and *in vivo* tissue regeneration [494–496]. Importantly, fragment-tethered 5% (w/v) GelMA hydrogels exhibit similar mechanical properties to their non-functionalised counterparts (Figure 3.11), ensuring that the physical properties of the biomaterials do not interfere with the effect of the fragment.

The presence of laminin fragment covalently tethered to GelMA did not substantially affect the expression of epithelial gene *Cdh1* and mesenchymal genes *Vim* and *Mmp2* (Figure 3.12), or gelatinase activity (Figure 3.13), when comparing the different experimental conditions with or without TGF-β1 treatment. In fact, addition of TGF-β1 was the factor that caused the largest change in expression and activity of these biomolecular markers. However, hydrogel invasion analysis from day 6 shows encouraging data when using highest concentrations of tethered fragment (GelMA Cys-100 and Lys-100, Figure 3.14). Further research should focus on longer timepoints and varied concentrations of tethered fragment to fully understand its impact on cell invasion. Even though gene expression and gelatinase activity data analyses did not show significant effects caused by the presence of tethered fragment within cell laden hydrogels, the possibility of inhibition of invasion of MCF10A from spheroids into the semisynthetic matrix harnesses therapeutic potential that should be further explored.

Moreover, data presented in this work demonstrates that the recombinant laminin fragment interacts with mouse $\alpha3\beta1$ integrin, as shown by BLI and ELISA (Figure 3.15 **a** and **d**), supporting previous reports [473, 474]. Importantly, it should be noted that neither chemical modification strategy – via cysteine or via lysine – affects binding capacity between the fragment and the ligands studied here. Interaction between the fragment and human $\alpha3\beta1$ integrin was also evaluated, not only because cells of human origin were used in this thesis, but also because the therapeutic potential of this recombinant laminin fragment can only be fully harnessed when used within a human biological context. BLI data shows a negligible interaction between the fragment and human $\alpha3\beta1$ integrin, as opposed to ELISA data that shows a specific interaction between these two biomolecules (Figure 3.15 **b** and **d**). It is likely that these two biomolecules can specifically interact, as shown by ELISA, but the experimental conditions carried out in real-time BLI are suboptimal for human $\alpha3\beta1$. Furthermore, both BLI and ELISA confirmed that this recombinant fragment can also interact with TGF-β1, potentially explaining

the opposing effects on EMT gene expression in the presence or absence of added TGF-β1 to the culture medium seen in Figures 3.5 and 3.6. It is plausible that this cryptic fragment can modulate EMT events and decrease MMP-2 expression as a soluble compound, in biological contexts where it can act as a TGF-β inhibitor.

In addition, this work demonstrates the use of SPAAC copper-free click chemistry to covalently label the recombinant fragment with Cy5, both via cysteine and via lysine, to visualise its interaction with the cells used in this work. To date, this was the first successful strategy carried out to label and visualise the interaction between the laminin β1 fragment and human mammary epithelial cells *in vitro*. Results displayed in Figure 3.16 show that Cy5-labelled fragment, both via cysteine and lysine, is internalised by MCF10A cells. Of note, no specific signal is detected when equivalent concentrations of free Cy5 is added to the culture medium.

As it has been previously proposed that the molecular mechanism underlying EMT modulation by this recombinant fragment involves a direct or indirect interaction with α3β1 integrin, interaction between the fragment and these epithelial cells when expression of integrin α3 is silenced via siRNA knockdown was assessed. Analysis of these data shows that fluorescence intensity of cell-associated labelled fragment, particularly the one chemically modified via lysine, is reduced 24 and 48 hours post-transfection with *Itga3* siRNA (Figure 3.17). Even though this particular experiment does not investigate any particular functional or mechanistic role, these results further corroborate the existence of an interaction between this recombinant fragment and α3 integrin. It should be noted that silencing of β1 subunit was not investigated because it is the most commonly found subunit in integrin heterodimers [497] and its knockdown would likely lead to mechanistic effects outside the scope of this thesis.

Interestingly, siRNA-mediated silencing of α3 integrin also increased the expression of epithelial adhesion molecule E-cadherin and decreased the expression of mesenchymal marker Snail, in experimental conditions where MCF10A cells were treated with EMT-inducer TGF-β1 (Figure 3.18). This is in accordance with substantial evidence to date that has suggested an important role for integrin α3β1 in promoting basal mammary tumorigenesis and metastasis [498–500], and its suppression has been shown to inhibit basal tumour development [501–503]. However, it is important to note that downregulation of integrin α3β1 in HER2-driven (luminal) breast cancer was reported to promote tumour progression and invasiveness [504]. Such findings highlight the complexity of these regulatory mechanisms and indicates that the role of integrin α3β1 in breast cancer is most likely tumour type specific.

3.6 Concluding Remarks and Future Work

To summarise, the work presented in this chapter demonstrated the use of a laminin β1 fragment with cryptic activity to modulate EMT-like events in human mammary gland epithelial cells. The use of this fragment on its own as a soluble compound led to increased mesenchymal gene expression in the experimental conditions studied. However, when these cells were exposed to EMT-inducer TGF-β1, the fragment showed a modest potential to downregulate the expression of some mesenchymal genes. It is also shown in this chapter that this fragment can interact with TGF-β1, by two independent methods (BLI and ELISA). It is possible that this laminin fragment can have an EMT-inhibiting potential when it can act as a TGF-β1 inhibitor.

The functionalisation of GelMA-based hydrogels with covalently tethered laminin fragment, using a copper-free SPAAC click chemistry, was also shown. The highest concentration of fragment tethered to this 3D culture GelMA-based hydrogel platform showed encouraging potential to inhibit invasion of cells from spheroids. However, these results were not statistically significant. Future work should investigate the effects of increasing the concentration of tethered fragment and longer time-points should be evaluated. It should also be noted that the click chemistry strategy employed in this chapter to tether the fragment to a semi-synthetic hydrogel system can be employed to functionalise other biomaterial with any biomolecule, as long as their structures allow the addition of alkynes or azide groups, potentially enabling the development of platforms that can be used for high-throughput screening of novel therapeutics.

Here, it is also confirmed that the fragment interacts with α3β1 integrin, both of human and of murine origin. However, the mechanistic aspects of this interaction still remain elusive. It is shown that silencing integrin α3 via siRNA reduces the signal of cell associated Cy5-labelled fragment, which further implicates its role in the way the fragment interacts with cells, but further research is necessary to fully understand this biomolecular relationship. Moreover, it is also known that several integrins regulate TGF-β1-mediated signal transduction [505]. Therefore, given that this fragment can potentially act as a TGF-β1 inhibitor and can directly or indirectly interact with α3β1 integrin, it would be important to further elucidate the molecular mechanisms and signalling pathways in which this fragment is involved, so its therapeutic potential can be fully harnessed and applied in the correct biological context.

The BM functions as a barrier that not only controls the transport of various molecules, but also of migrating cells, preventing tumour progression [437]. The amount and type of components that compose the BM are tissue specific, but also dependent on its developmental stage [428, 431]. Laminin-111 has an essential role in assembling the BM and promoting cell attachment during embryogenesis [506],

but later in development its expression is downregulated [507]. Laminin-111 protein therapy has been used for muscle regeneration [508–510], but before using full-length laminin-111 for clinical applications it is important to consider that some of its domains have been shown to promote malignancy [511, 512] and induce immune responses [513]. Numerous active sites have been identified within laminin-111, using recombinant and proteolytic fragment and synthetic peptides [512, 514, 515]. Remarkably, various of these identified active sites, particularly small peptide sequences, have been shown to have opposing phenotypic effects, with some promoting tumour growth and metastasis and other inhibiting these behaviours [515]. The knowledge gained from these previous studies is instrumental when designing therapeutic strategies that aim to use cryptic fragments from naturally occurring proteins, in particular from the ECM. With a molecular weight of around 60 kDa, the laminin β1 fragment used in this thesis is a fairly big protein that harbours various active sites [515], which might have opposing effects. Hopefully the work presented in this chapter will encourage a more comprehensive characterisation at the molecular level of biologically-active ECM fragments to avoid unwanted effects. There is a clear potential for cryptic fragments from ECM components to be used for clinical applications, particularly for regenerative medicine. However, it is important to understand the phenotypes that these promote in a tissue-specific manner. Synergistically combining well-characterised cryptic ECM information with novel biomaterials has a great potential to provide an integrative and, hopefully, more effective approach to therapeutic applications for regenerative medicine.

4

Towards characterising the mechanoresponse of electrically-stimulated epithelial cells

Contents

4.1 Introduction

4.1.1 Mechanotransduction - how do cells respond to external forces?

Cells within tissues are continuously exposed to mechanical stimuli from their surrounding extracellular matrix (ECM) and neighbouring cells. The ability to convert external physical cues into specific biochemical signals, a mechanism collectively known as mechanotransduction [516, 517], is crucial for cells to adapt to their constantly changing, dynamic microenvironment. Over the last few decades significant progress has been made towards understanding how cells can sense and regulate mechanical forces from the ECM [518, 519]. However, only recently have the molecular mechanisms underlying the process of mechanotransduction started being elucidated and much still needs to be learnt [520]. Indeed, key aspects of homeostasis and pathobiology can only be fully understood when the mechanisms of how cells can transform physical stimuli into particular biological responses are known. Therefore, advancing the understanding of how cells orchestrate the numerous molecular mechanisms and pathways at play to generate a concerted and timely response to external mechanical cues is of utmost importance.

Recent work has shown that cells perceive and convert external mechanical stimuli via different mechanisms, utilising a plethora of mechanosensitive molecules and subcellular structures, serving as mechanosensors or mechanotransducers. Sensing of external mechanical stimuli occurs primarily at the plasma membrane, the interface between the cell and its surroundings, where specific receptors are used to perceive and transfer these signals from the extracellular milieu into the cell. Amongst others, cells have been shown to activate mechanotransduction pathways through integrins, stress-activated ion channels, G protein coupled receptors, membrane lipids, focal adhesion complexes, and transmembrane proteins, which mediate cell-cell and cell-ECM interactions [517, 518, 521]. Integrins, in particular, can mechanically link the ECM signals to the cytoskeleton via focal adhesions, comprising various actin-associated proteins, including talin, vinculin, paxillin, and zyxin [522, 523]. It has been shown that the multitude of proteins that compose focal adhesions are organised into nanoscale domains: a membrane-associated integrin signalling layer that includes the cytoplasmic tails of integrins, focal adhesion kinases and paxillin; a force-transduction intermediate layer comprising talin and vinculin; and an actin-regulatory layer containing zyxin and α-actinin [524] (Figure 4.1). Vinculin, for example, one of the main components of the focal adhesion core, is recruited by a direct interaction with phosphorylated paxillin and then works in concert with talin, in turn activated by physical stimuli [525]. In fact, vinculin shuttling and activation has been directly correlated with force applied on focal adhesions [526].

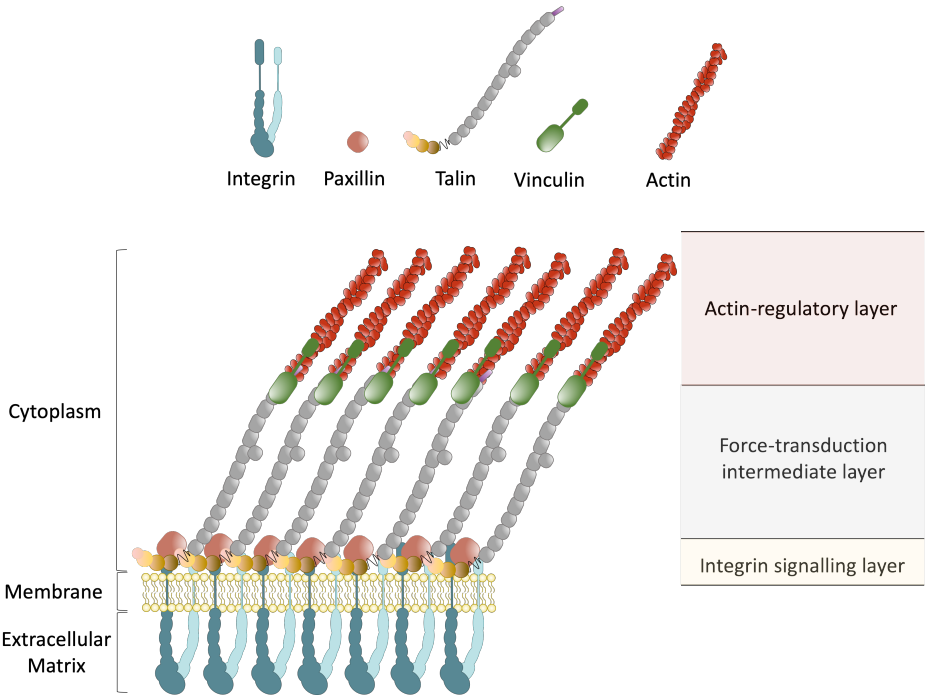

Figure 4.1: Stimuli sensing through focal adhesions. The proteins that compose mature focal adhesions are spatially organised into nanoscale domains: a membrane-associated integrin signalling layer that includes the cytoplasmic tails of integrins, focal adhesion kinases and paxillin; a force-transduction intermediate layer comprising talin and vinculin; and an actin-regulatory layer. Vinculin, for example, one of the main components of the focal adhesion core, is recruited by a direct interaction with phosphorylated paxillin and then works in concert with talin, maintaining its extended conformation. Adapted from [525].

4.1.2 Cytoskeleton-mediated transmission of mechanical stimuli

The cytoskeleton, a highly dynamic and adaptive structure that controls cell shape, motility and tension, as well as subcellular compartment organisation, provides a framework that continuously couples the external biochemical and biophysical cues to the intracellular space [527]. Three main components form the cytoskeleton: microtubules, intermediate filaments and actin microfilaments. Each of these polymer networks is a highly organised structure with a crucial role in arranging and maintaining the integrity of the subcellular organelles [528–530].

Microtubules, the largest, with a diameter of about 25 nm, and stiffest of the three main components of the cytoskeleton [527, 531], play a crucial role in fundamental biological processes, including cell polarity [532], mitotic spindle formation [533] and intracellular cargo transport [534]. Microtubules have been shown to be mechanoresponsive as their persistence length (measurement of polymer stiffness) increases with extracellular stiffness and significantly contribute to how cells handle large-scale compressive forces [535].

Intermediate filaments are flexible and stable polymers, more so than microtubules and actin filaments, that also play an important in regulating mechanotransduction events [536, 537]. Intermediate filament networks undergo significant structural reorganisation and increase their stiffness in the cell cortex in response to shear stress [538–540]. However, the mechanism by which intermediate filaments can sense physical stimuli is not yet well understood.

The actin cytoskeleton is the most well-studied component of this structural system, and has been shown to be instrumental in regulating cell shape, motility and internal organisation of cell compartments [530]. Bundles of F-actin filaments and motor protein myosin, cross-linked by α-actinin, forming the so-called stress fibers, play a central role in conferring cells the ability to generate contractile forces [541]. In addition, stress fibers can propagate physical cues from and to the extracellular environment by connecting to the cell-ECM interface through focal adhesions, which contain various actin binding proteins, including zyxin and paxillin [542]. In turn, these actin-binding proteins can regulate actin cytoskeleton dynamics in response to internal or external signals. For example, it has been demonstrated that zyxin is mobilised from focal adhesion sites to actin stress fibers upon sensing mechanical stress, promoting the reinforcement of stress fibers and, consequently, increasing cytoskeletal tension [543, 544].

4.1.3 Getting mechanical information into the nucleus

Focal adhesions and cytoskeletal polymer networks are not only structural proteins and mechanosensors, but also crucial in the propagation of signals to the intracellular space. Propagated signals impact the expression of mechanosensitive genes, consequently generating a biological response [545]. It is now evident that the nucleus, which is both functionally and structurally complex, is linked to the extracellular space via signal transduction pathways. In 1995, a study by Farshid Guilak demonstrated a connection between the nucleus and the cell membrane, where the first contact with external signals occurs, after nuclei deformation and structural reorganisation was observed upon application of compression forces. In addition, disruption of the actin cytoskeleton affected the relationship between compression and nuclear deformation, implying an important role for the cytoskeleton in this mechanosensing mechanism [546]. This nuclear-cytoskeleton coupling is important for the transmission of signals so cells can adapt and timely respond to the stimuli. The connection between the cytoplasmic cytoskeleton and the nucleoskeleton is enabled by the LINC (Linker of Nucleoskeleton and Cytoskeleton) complex [547, 548].

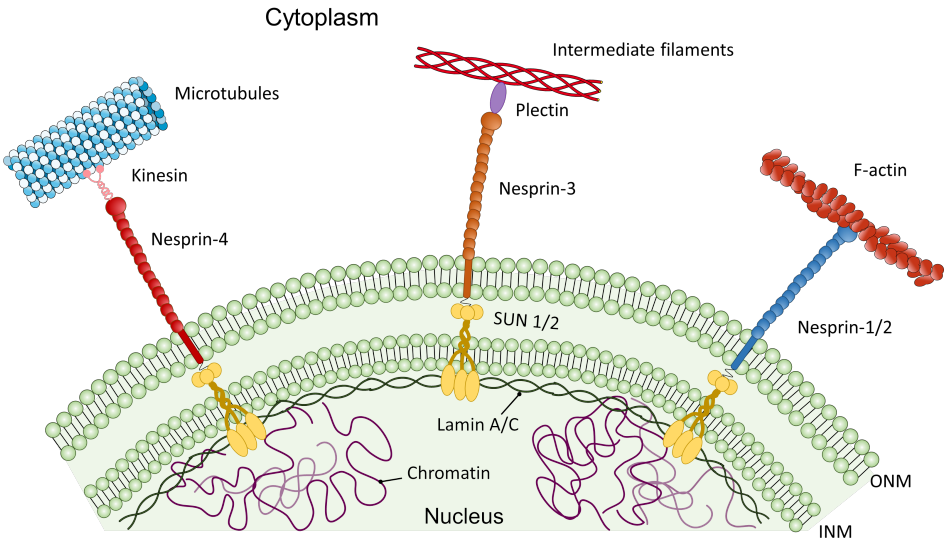

Figure 4.2: The LINC complex connects the cytoskeleton to the nucleoskeleton. Different nesprin isoforms (1 to 4) that reside at the cytoplasmic side of the LINC complex can directly interact with the actin cytoskeleton via a CH domain at their N-terminal, or indirectly interact with microtubules through linker proteins kinesin and dynein, or with intermediate filaments via plectin. The C-terminal binds to SUN proteins in the perinuclear space. SUN proteins, in turn, span the inner nuclear membrane interacting with nesprins at their C-terminal (SUN domain) and with the inner lamin A/C network, which provide shape and mechanical stability to the nucleus, at their nucleoplasmic N-terminal. SUN nucleoplasmic domain and lamin A/C can also interact with chromatin and potentially alter gene expression. INM - inner nuclear membrane; ONM - Outer nuclear membrane. Adapted from [520].

The LINC complex (Figure 4.2) is composed of proteins across the inner and the outer nuclear membranes, including nesprins, SUN proteins, emerin, and inner lamin A/C nucleoskeletal network [549]. Different nesprin isoforms (1 to 4) reside at the cytoplasmic side of the LINC complex, where they can directly interact with the actin cytoskeleton via a CH domain (identical to the one found in the structure of α-actinin) at their N-terminal, or indirectly interact with microtubules through linker proteins kinesin and dynein, or with intermediate filaments via plectin [550]. The C-terminal of nesprins consists of a transmembrane domain that crosses the outer nuclear membrane and ends in a highly conserved Klarsicht, ANC-1, Syne Homology (KASH) domain, which binds to SUN proteins in the perinuclear space [551]. SUN proteins, in turn, span the inner nuclear membrane interacting with nesprins at their C-terminal (SUN domain) and with the inner lamin A/C network, which provide shape and mechanical stability to the nucleus, at their nucleoplasmic N-terminal [552]. SUN nucleoplasmic domain and lamin A can also interact with chromatin and potentially alter gene expression, which further extends and highlights the importance of this close interaction in mechanically coupling the nucleus with the cytoskeleton. Importantly, impaired nucleo-cytoskeletal coupling due to disruptions to the LINC complex have been shown to result in defects in actin cytoskeleton organisation, nuclear positioning, cell

polarisation and migration [553]. However, even though mounting evidence shows the importance of this structural protein bridge connecting the nucleus to the signal perceiving plasma membrane, the molecular mechanisms by which the nucleus responds to different mechanical stimuli are still very elusive. In fact, a study recently showed that deforming the nucleus directly with an atomic force microscopy (AFM) cantilever is sufficient for the nuclear translocation of a mechanosensitive transcriptional activator through the nuclear pores, even in the absence of the LINC complex [554].

4.1.4 Nucleocytoplasmic shuttling of YAP/TAZ in mechanotransduction

To date, the molecular mechanisms that regulate gene expression in response to mechanical cues are still largely unknown. Recent studies have identified Yes-associated protein (YAP) and transcriptional coactivator with PDZ-binding motif (TAZ), also known as WWTR1, henceforth referred to as YAP/TAZ, as molecular sensors and nuclear transducers of cell mechanoresponse [555, 556]. YAP and TAZ are transcriptional co-activators best known as downstream effectors of the Hippo pathway, which regulates proliferation, differentiation, survival and overall homeostasis [557]. However, in recent years, it has become clearer that the Hippo pathway is part of a broader regulatory framework, in which YAP/TAZ can be regulated in a Hippo-dependent or -independent manner [558]. The identification of YAP/TAZ as sensors of a broad range of external signals that transduce them into biological responses in a stimuli- and cell-type dependent way has helped starting to understand the molecular mechanisms at gene expression level underlying mechanoresponse [559].

Regulation of YAP/TAZ as mechanotransducers occurs through their subcellular location, as these transcriptional co-activators are shuttled to the nucleus in response to stimuli, becoming activated and thereupon can regulate gene expression [560]. As an example of this YAP/TAZ regulatory subcellular distribution (Figure 4.3), when epithelial cells are grown on softer ECM (0.7kPa) or a small adhesive area (300 μm^2) YAP/TAZ locate to the cytoplasm, whereas on stiffer ECM (40 kPa) or larger surface areas ($>$300 μm^2) cells experience higher cytoskeletal tension and YAP/TAZ accumulate in the nucleus [555]. Importantly, YAP/TAZ activation requires integrity and stability of the actin cytoskeleton, as it has been demonstrated in studies where actin [554] or myosin [555] were inhibited. Nevertheless, the molecular mechanisms by which YAP/TAZ are regulated by cell mechanics remain elusive and more research in the field is needed to continue filling the gap.

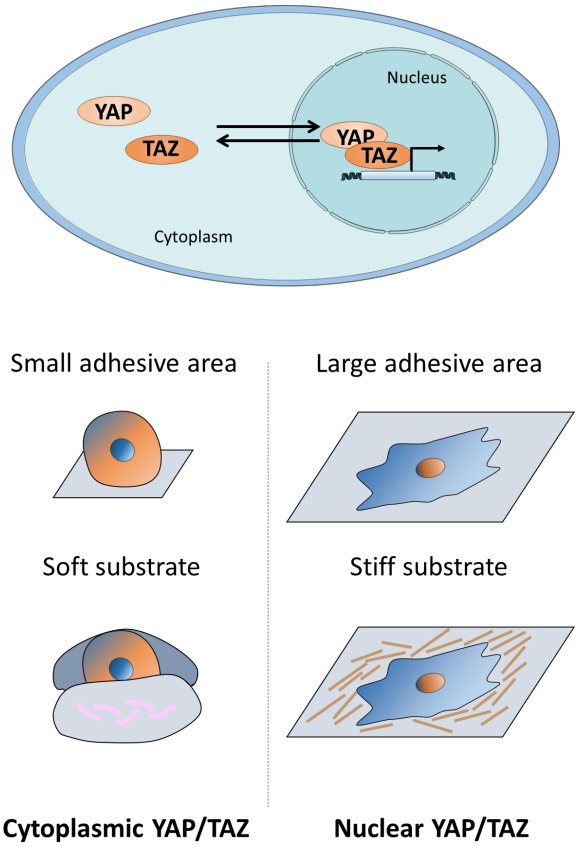

Figure 4.3: Schematic representation of YAP/TAZ mechanoregulation - nucleocytoplasmic shuttling. YAP/TAZ (represented in shades of orange) locate to the cytoplasm when epithelial cells are grown on a small adhesive area or softer substrates (illustrated by a predominantly orange cytoplasm; left hand-side of the schematics), whereas these transcriptional co-activatores accumulate in nucleus, where they can activate specific transcriptional programs, when cells are grown larger surface areas or stiffer substrates (represented by a predominantly orange nucleus; right hand-side of the schematics). Adapted from [559].

4.1.5 Electrical stimulation to study mechanotransduction

Epithelial cells line all surfaces in our bodies and they continuously sense external chemical (ligands) and physical (mechanical, electrical) signals from their surroundings. Electrical signalling, in particular, plays a crucial role in maintaining physiological homeostasis [146]. Through the maintenance of an unequal distribution of ions across the plasma membrane by specialised transmembrane channels, voltage differences are created between the intra and the extracellular space, establishing what is known as the membrane potential [561]. In the epithelium, naturally occurring electric gradients exist due to the spatial organisation of ion channels throughout the plasma membrane, where the apical domain is enriched in Na^+ channels and Cl^- transporters, and the basolateral domain in Na^+-K^+ pumps [562]. Highly polarized epithelial cells with specific ion channels in different domains create

and maintain an endogenous ion gradient. This gradient is known as the transepithelial electrical potential, which in normal breast epithelium is +30 mV [561, 562]. Importantly, breast epithelial cells also harbour mechanosensitive ion channels in their plasma membrane [563].

Similarly to mechanotransduction mechanisms mediated by integrin receptors, mechanosensory ion channels can affect cytoskeletal arrangement and subsequent cell behaviour [521]. Importantly, electrical stimulation has been shown to induce cell-type dependent changes in cellular elasticity and cytoskeleton regulation [564]. In addition, another study has shown that human mesenchymal stem cells reorganise their actin cytoskeleton according to the direction of the electrical field [565]. These studies showing changes in cytoskeletal reorganisation and in cellular elasticity provide evidence to hypothesise that cells activate mechanotransduction pathways upon sensing electrical signals, which may be the same pathways involved in sensing extracellular stiffness. However, the molecular mechanisms underlying cellular mechanoresponse upon electrical stimulation (ES) are largely unexplored.

4.1.5.A Conducting polymers for substrate-mediated ES

Due to the importance of bioelectric fields *in vivo* for homeostasis, extensive research making use of electroactive biomaterials to study how various cell types respond to electrical stimuli has been done over the years [566]. Among these electroactive biomaterials, conducting polymers have become popular materials to be used as substrates to deliver evenly distributed electrical stimuli to cells [567, 568]. Conducting polymers are a class of materials with electrical and optical properties very similar to those of metals and semiconductors, but have great control of electrical stimulus, flexibility and ease of production. Additionally, they may be made biocompatible, biodegradable, and porous, which is why these are so commonly used as electroactive materials [568]. The key for these polymers to become highly conductive is the doping process, which introduces charge carriers to their structure [569, 570]. Doped polypyrrole (PPy) is perhaps the most thoroughly studied conducting polymer for biomedical research applications, due to its great stability and good conductivity under physiological conditions [571], and its *in vitro* and *in vivo* biocompatibility [572, 573], in addition to being easily synthesised in large quantities at room temperature in a broad range of solvents, including water [574]. PPy has been used to electrically stimulate a wide variety of cells in culture, including human primary osteoblasts [575], mesenchymal stem cells [576], cardiac progenitor cells [577], epithelial Madin-Darby Canine Kidney (MDCK) cells [578], and primary pre-frontal cortical (PFC) neurons [579].

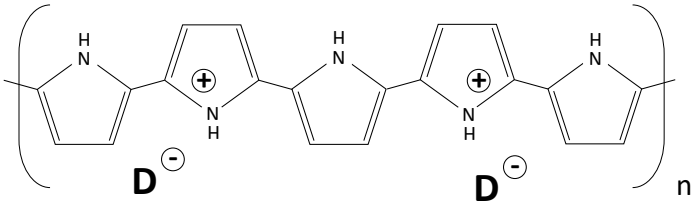

Figure 4.4: Structure of doped polypyrrole (PPy). The incorporation of a dopant (counter ion D^-) renders this polymer highly conductive.

4.2 Chapter Aims

The molecular mechanisms that cells utilise to respond in a timely manner and adapt to external physical stimuli are not yet fully understood. The recent findings that identified transcriptional co-activators YAP/TAZ as sensors and transducers of mechanical cues have shed light on the understanding of how cells perceive and respond to their microenvironment, at the molecular and transcriptional level. In addition, the mechanistic crosstalk between cytoskeletal organisation and YAP/TAZ activation is recognised to have a determinant impact on various mechanoresponsive events [558], but is still largely unexplored.

In this chapter, direct ES was used to expose human mammary epithelial MCF10A cells to external physical signals (in this case, electrical). Here, these cells were electrically stimulated via a biocompatible, conducting PPy substrate on which they are cultured, and their mechanoresponse was studied. AFM and Scanning Ion Conductance Microscopy (SICM) were employed to directly measure single cell elasticity changes caused by the applied direct ES. In addition, the expression of YAP/TAZ-regulated genes, ankyrin repeat domain 1 (*ANKRD1*), connective tissue growth factor (*CTGF*) and Cysteine-rich angiogenic inducer 61 (*CYR61*), was investigated by RT-qPCR. Confocal imaging was also used to further investigate changes in expression and localisation of vinculin, in YAP nucleocytoplasmic shuttling, and in actin cytoskeleton organisation.

4.3 Materials and Methods

4.3.1 Preparation of polypyrrole doped with DBS

To synthesise PPy, pyrrole was electrochemically polymerised on gold coated mylar sheets in a 3-electrode electrochemical cell, using Ag/AgCl as a reference electrode [580]. This procedure was conducted together with Dr Amy Gelmi. Firstly, gold coated mylar sheets were washed with iso-propanol and Milli-Q water. Next, an aqueous solution of 0.1M pyrrole monomer (filtered through Aluminium oxide to remove oligomers) and 0.1M dopant DBS (dodecylbenzenesulfonate) was prepared and placed in ultrasonic bath for 5 minutes to ensure solubilisation. PPy substrates were grown at a constant voltage of 0.6 V (EDaq potentiostat) for 15 minutes. After growth, they were washed with Milli-Q water, dried and placed in Petri dishes until further use. Before cell culture, the substrates were sterilised under UV light for at least 30 minutes. Following, they were rinsed in sterile PBS three times, washed with 70% (v/v) ethanol twice and rinsed again in sterile PBS.

4.3.2 General Cell Culture

MCF10A cells were obtained from American Type Culture Collection (ATCC) and cultured under standard cell culture conditions in humid incubators at 37℃ and 5% CO_2 atmosphere. These cells were cultured in Dulbecco's Modified Eagle Medium/Nutrient Mixture F-12 (DMEM/F-12, Gibco, Life Technologies), supplemented with 5% (v/v) Horse Serum (Gibco, Life Technologies), 5% (v/v) Penicillin Streptomycin (Gibco, Life Technologies), 20 ng/ml Epidermal Growth Factor (EGF, Peprotech), 0.5 mg/ml hydrocortisone (Sigma-Aldrich), 100 ng/ml Cholera toxin (Sigma-Aldrich), 10 µg/ml insulin (Sigma-Aldrich) [187]. Before being added to DMEM/F-12, all supplements were pre-mixed and filtered through a sterile 0.2 µm syringe filter. MCF10A cells were expanded in T-75 flasks and medium was changed every 2-3 days until 80-90% confluency was reached. For passaging, as well as for seeding at specific cell densities for experimental assays, cells were detached from the tissue flask after one rinse in sterile Phosphate Buffered Saline (PBS) and incubation at 37℃ with TripLE Express Enzyme (Thermo Fisher Scientific). Once detached, cells were centrifuged at 300 x*g* for 5 minutes and the TrypLE Express-containing supernant was discarded each time. Fresh complete medium was used to resuspend the pellet and cells were counted with trypan blue (Thermo Fisher Scientific) with a 1:1 (v/v) ratio.

4.3.3 Substrate-mediated ES

MCF10A cells were seeded on PPy or gold coated mylar substrates in teflon blocks at a density of 12,500 cells/cm^2, and cultured for 2 days before ES protocols were initiated. Direct ES was applied to live cells at 1 Hz, 1 ms pulses and a voltage of -0.3 or -1 V, for 1 hour at 37℃, 5% CO_2. This procedure was conducted in collaboration with Dr Amy Gelmi.

4.3.4 RNA Isolation, cDNA synthesis and RT-qPCR

4.3.4.A RNA Isolation

The expression of YAP/TAZ-regulated genes was studied by quantitative reverse transcription polymerase chain reaction (RT-qPCR). At the time of collection, conditioned medium was aspirated from each well. Next, cells were washed once with sterile ice-cold PBS and 350 µl of RLT buffer (Qiagen) were added. Following, an equal volume of 70% ethanol (molecular biology grade, Fisher Bioreagents) was added to each sample and mixed well by pipetting. The following RNA extraction steps were performed as per the manufacturer's instructions (RNeasy Mini Kit, Qiagen). For each sample, a volume of up to 700 µl at a time was transferred to a spin column placed in a 2 ml collection tube and centrifuged for 30 seconds at 10,000 x*g* at room temperature. If the samples contained more than 700 µl, multiple centrifugations were carried out. Next 700 µl of buffer RW1 was added to each spin column followed by a centrifugation at 10,000 x*g* for 30 seconds at room temperature. Subsequently, 500 µl of buffer RPE was added to each tube for a final wash, which were centrifuged for 2 minutes at 10,000 x*g* at room temperature, followed by another centrifugation with no buffer added to ascertain that no traces of ethanol were left in the samples. In every step, the flow-through from the spin column was discarded. Finally, 30 µl of RNase-free water (Life Technologies) was added to each spin column to collect the purified RNA from each sample with a last step of centrifugation for 30 seconds at 10,000 x*g* at room temperature. The RNA concentration was then measured using NanoDrop 2000c (Thermo Fisher Scientific). Once RNA samples from all biological replicates were collected and isolated for subsequent use, RNase-free water was added to each tube in adequate amounts to ensure that all samples were at the same concentration.

4.3.4.B cDNA synthesis

Complementary DNA (cDNA) was synthesised from each RNA sample using Applied Biosystems High-Capacity cDNA Reverse Transcription kit (Thermo Fisher Scientific). After allowing the kit com-

ponents to thaw on ice, the reverse transcription master mix was prepared, which contained, per reaction, 2 µl RT buffer, 0.8 µl dNTP mix, 2 µl RT random primers, 1 µl multiscribe reverse transcriptase and 3.2 µl nuclease-free water. Following, 10 µl of each RNA sample was added to a 0.5 ml PCR tube and mixed with 10 µl of reverse transcription master mix. Each tube was quickly vortexed, spun down and placed in the thermal cycler (LifePro, Bioer) to go through the following cycle: 10 minutes at 25℃, 120 minutes at 37℃ and 5 minutes at 85℃.

4.3.4.C RT-qPCR

After reverse transcription, the cDNA was diluted with nuclease-free water to be used in quantitative reverse transcription PCR (RT-qPCR). RT-qPCR was carried out using SYBR Green master mix (Applied Biosystems, Life Technologies) and run on a StepOnePlus^{TM} machine (Applied Biosystems). Components were prepared on 96-well reaction plates (Thermo Fisher Scientific): 5µl of SYBR Green master mix, 0.5µl of primers, 0.5µl of nuclease-free water, and 4µl of cDNA for each sample (2-10 ng of cDNA per reaction). The RT-qPCR programme settings were as follows: 95℃ for 20 seconds, followed by 40 cycles of denaturation at 95℃ for 3 seconds and annealing at 60℃ for 30 seconds. Melt curves were obtained from all reactions to ensure that a single amplicon was produced for each target gene. Cycles-to-threshold (Ct) values were automatically obtained by the Thermo Fisher Scientific StepOnePlus^{TM} software. Subsequently, these values were exported to Microsoft Excel and manually processed to obtain fold change expression values. Ct values of each gene of interest were normalised to the Ct values of the housekeeping gene (*RPL13A*) within each respective sample. $2^{-\Delta\Delta Ct}$ values were obtained by normalising to the internal control sample (in this case, the epithelial-like state). Three biological replicates (two technical replicates each) are reported. Custom primers (Invitrogen) are listed in Table 4.1.

Table 4.1: Primers for YAP/TAZ-regulated genes. List of primers used for RT-qPCR gene expression studies in this chapter. *RPL13A* was used as housekeeping gene; *CTGF*, *ANKRD1* and *CYR61* were used to measure expression of genes associated with YAP/TAZ activation.

Target	Primer Sequence
RPL13A	Forward: AAGTACCAGGCAGTGACAG
	Reverse: CCTGTTTCCGTAGCCTCATG
CTGF	Forward: AGGAGTGGGTGTGTGACGA
	Reverse: CCAGGCAGTTGGCTCTAATC
ANKRD1	Forward: AGTAGAGGAACTGGTCACTGG
	Reverse: TGGGCTAGAAGTGTCTTCAGAT
CYR61	Forward: AAGGAGCTGGGATTCGATGC
	Reverse: CATTCCAAAAACAGGGAGCCG

4.3.5 Atomic Force Microscopy

AFM measurements of live MCF10A cells elasticity, pre- and post-ES, were performed by Dr. Amy Gelmi. Elasticity of MCF10A cells growing on electrically conductive materials (PPy or gold coated mylar) for 2 days were measured with AFM before, during (each ES protocol lasted 1 hour), and immediately after (1 hour time window) application of ES. This was conducted using a Nanoworld PNP-TR-TL cantilever decorated with a 5 µm colloidal sphere with a 0.05 N/m spring constant. The AFM tip could be accurately moved using the closed-loop feedback system controlling the X–Y piezos. The force versus distance curves were converted to force versus indentation curves and then fitted by the Hertz model to quantify the elastic modulus (E) [581]. The same cantilever tip was used for all measurements, to reduce variations in the tip radius and shape to give a relative comparison between the obtained moduli values.

4.3.6 Scanning Ion Conductance Microscopy

SICM was also used to obtain stiffness maps of live electrically stimulated and unstimulated MCF10A cells. This technique uses a nanopipette filled with an electrolyte containing aqueous medium as the probe. A voltage is applied between two electrodes, one in the nanopipette and a reference electrode in the sample medium, which results in a closely monitored ionic current flowing in and out of the nanopipette opening. The movement of the nanopipette is controlled through a piezoelectric stage and, when the probe approaches the sample, the ionic flux becomes restricted, so the ion current drops and the z-position of the probe is recorded [360]. This technique can be used to obtain

cell stiffness measurements [361, 362] by exploiting the fact that as the probe approaches a soft substrate (in this case a cell) the current drop occurs much more slowly than with stiff substrates [361]. It is worth noting that the absolute values obtained by this method should not be used for comparison with stiffness values obtained using other techniques (personal communication from Dr Pavel Novak, Queen Mary University), but rather to be compared with the measurements acquired from other samples using SICM in the same conditions. The non-contact probe-sample interaction that takes place is sufficient to cause cell surface deformation, and the distance alteration between the probe and the sample can be used to map the mechanical properties of biological samples [361].

4.3.6.A Sample and Imaging Equipment Preparation

MCF10A cells growing on electrically conductive materials (PPy or gold coated mylar) for 2 days were then analysed with SICM immediately after (1 hour time window) ES was applied. Unstimulated cells were used as controls. Firstly, cells were washed in sterile PBS and CO_2-independent medium Leibovitz's L-15 (Gibco) was used to maintain cell viability during scanning. A P-2000 CO_2 laser puller (Sutter Instruments, Novato, CA) was used to pull borosilicate glass (outer diameter 1 mm, inner diameter 0.5 mm, Intracel, Cambridge, UK) pipettes, which parameters for temperature and velocity were optimised to obtain a tip inner diameter of approximately 100 nm and ion currents of approximately 1 nA. The ion current was measured using Axopatch 200B amplifiers (Molecular Devices, Wokingham, UK). After pulling, the pipette was backfilled with sterile PBS and an Ag/AgCl electrode was inserted inside the pipette. The ion current flowing through the pipette was measured with an applied bias potential of 200 mV. The current traces were acquired and analysed using pClamp 10 (Molecular Devices).

4.3.6.B Hopping Probe Ion Conductance Microscopy

SICM operation was carried in collaboration with Sahana Gopal. To operate in hopping mode the pipette filled with PBS and containing the electrode was placed on the inverted microscope to approach the sample vertically. Next, the sample in a 35 mm Petri dish was positioned and an Ag/AgCl electrode was submersed in the Leibovitz's L-15 liquid medium. Once the pipette was immersed and a current of approximately 1 nA was detected, the piezo controller was utilised to approach the sample, which was determined by a 0.3-0.6% drop in the current, compared to the reference (maximum) current. Due to the opacity of the substrates, cells were located by using the feedback mechanism of the piezo controller, which withdrew in the z-direction when the pipette was moved in the x- and y-directions. Next, a quick low-resolution scan was carried out in order to confirm the presence of

cells. Subsequently, the desired area was selected and scanned at a high resolution. Stiffness maps were obtained by simultaneously acquiring three topographical images using multiple set-points, at a fall rate of 40 nm/ms. Topography map of samples was acquired at a set-point of around 0.3% of ion current drop. In each point, the nanopipette was consecutively lowered to set-points of 0.6% and 3%, and the distances between the nanopipette and the deformed samples were recorded and stored in separate scan maps (one for each set-point). A pre-scan hop size of 20 µm was used to avoid collision between the pipette and the sample when scanning the cells. One experimental replicate was carried out, and at least 3 50x50 µm scan areas were obtained for each sample.

4.3.6.C Image processing

Cell stiffness maps were analysed using SICM image viewer software written by Dr. Pavel Novak, Queen Mary University of London. With this software, median stiffness measurements were obtained for each image by applying a mask that excluded the substrate and by using Clarke's method [361].

4.3.7 Immunofluorescence staining

At experimental endpoint, cells to be imaged by confocal microscopy were chemically fixed with 4% (v/v) paraformaldehyde in PBS for 15 minutes at room temperature and washed three times in PBS. Next, samples were permeabilised with 0.25% (v/v) Triton X-100 (Sigma-Aldrich) in PBS for 10 minutes at room temperature, and then washed three times in PBS. Following, cells were blocked in freshly prepared 1% (v/v) donkey serum in PBS for 1 to 2 hours at room temperature, and then washed three times in PBS. AlexaFluor 488 Phalloidin (Thermo Fisher Scientific, 1:500 in PBS) and DAPI (Sigma-Aldrich, 1:500 in PBS) were then used to label the actin cytoskeleton and nucleus of cells, respectively, by incubating the samples with this solution for 40 minutes at room temperature. Next, cells were incubated with primary antibody (listed in Table 4.2) diluted in 1% (v/v) donkey serum in PBS overnight at 4℃. Following, cells were washed three times in PBS and incubated with secondary antibodies (listed in Table 4.2) in 1% (v/v) donkey serum in PBS for 1 hour at room temperature. Samples were then washed three additional times in PBS, before being mounted in Fluoromount-G™ (Invitrogen).

Table 4.2: List of antibodies used for immunofluorescence staining. Names of each antibody (target), and the respective dilution factor, host and source, used for immunofluorescence staining.

Antibody	Dilution	Host	Source and Cat. no
YAP	1:500	Mouse	Santa Cruz, sc-101199
Vinculin	1:400	Mouse	Sigma-Aldrich, V9131
Anti-Mouse Alexa Fluor 647	1:500	Donkey	Invitrogen, A-31571

4.3.8 Imaging and Image Analysis

Imaging was performed on a Leica SP5 inverted confocal microscope with a HCX PL APO 40x 1.25-0.75 OIL CS objective lens, 16 bit depth. After image acquisition (at least five images per experimental condition), images produced were processed with the image analysis software FIJI. In order to visualise the orientation of actin fibres in all experimental conditions, the software package OrientationJ was employed to generate HSB (Hue – local orientation; Saturation – coherency; Brightness – original image) colour coded images with the orientation of the actin fibres. For quantification of cytoplasmic and nuclear YAP/TAZ, the DAPI and Phalloidin channels were used to create a nuclear and a cell mask, respectively. Cellular and nuclear regions were then generated and fluorescence intensity (integrated density) was measured. Cytoplasmic YAP content was obtained by subtracting the nuclear YAP content from the total YAP content, which was produced by the cell mask. Percentages of nuclear and cytoplasmic YAP were then calculated for each image. For quantification of vinculin, the Phalloidin channel was used to obtain a cell mask and vinculin fluorescence intensity was measured within that region. Vinculin fluorescence intensity values are presented as ratio between the value of integrated density and the area of region for each sample.

4.3.9 Statistical Analysis

Statistical analyses were carried out using GraphPad Prism 6.0. To determine whether data were normally distributed, Komogorov–Smirnov and Shapiro–Wilk tests were performed. For AFM force measurements, one-way ANOVA using Kruskal-Wallis multiple comparisons test was performed. For RT-qPCR, three independent biological replicates were collected for each sample in study, and two technical replicates were measured and analysed in each RT-qPCR assay plate. Differences in gene expression were tested with one-way ANOVA using Dunnet's multiple comparisons tests. To compare fluorescence intensity (YAP and vinculin staining), Kruskal-Wallis multiple comparisons test was performed. All hypothesis tests were considered two-tailed.

In all cases, *p<0.05;**p<0.01;***p<0.001;****p<0.0001.

4.4 Results

4.4.1 Effect of electrical stimulation on mammary epithelial cell elasticity

SICM was employed to map epithelial cell stiffness immediately after direct electrical stimulation was applied to live MCF10A cells via a conducting polymer substrate, either polypyrrole or gold Mylar, at 1 Hz, 1 ms pulses and -1 V. Figure 4.5**a** shows the stiffness maps obtained by SICM for unstimulated cells (control) and cells immediately after stimulation (up to 1 hour after the ES protocol was carried out), for both conducting substrates. These maps were then analysed to extract cell elastic moduli (E) using a mask that excluded the substrate. As shown in Figure 4.5**b**, an increase in cell stiffness was observed upon electrical stimulation via either conducting substrate.

Moreover, measurements of MCF10A cellular elasticity before, during and after direct electrical stimulation were also carried out by AFM. However, AFM force measurements require the use of a laser beam to monitor cantilever deflection, and, due to gold being reflective, it was only feasible to conduct these measurements on cells growing on PPy. Direct electrical stimulation via PPy was applied to live cells at 1 Hz, 1 ms pulses and -1 V. Force measurements were carried out before, during (1 hour), and up to 1 hour after application of ES. The elastic moduli of the cells was then calculated from Hertzian fits to the obtained force versus indentation curves. In agreement with SICM, AFM measurements showed an increase in cellular tension after electrical stimulation (Figure 4.6).

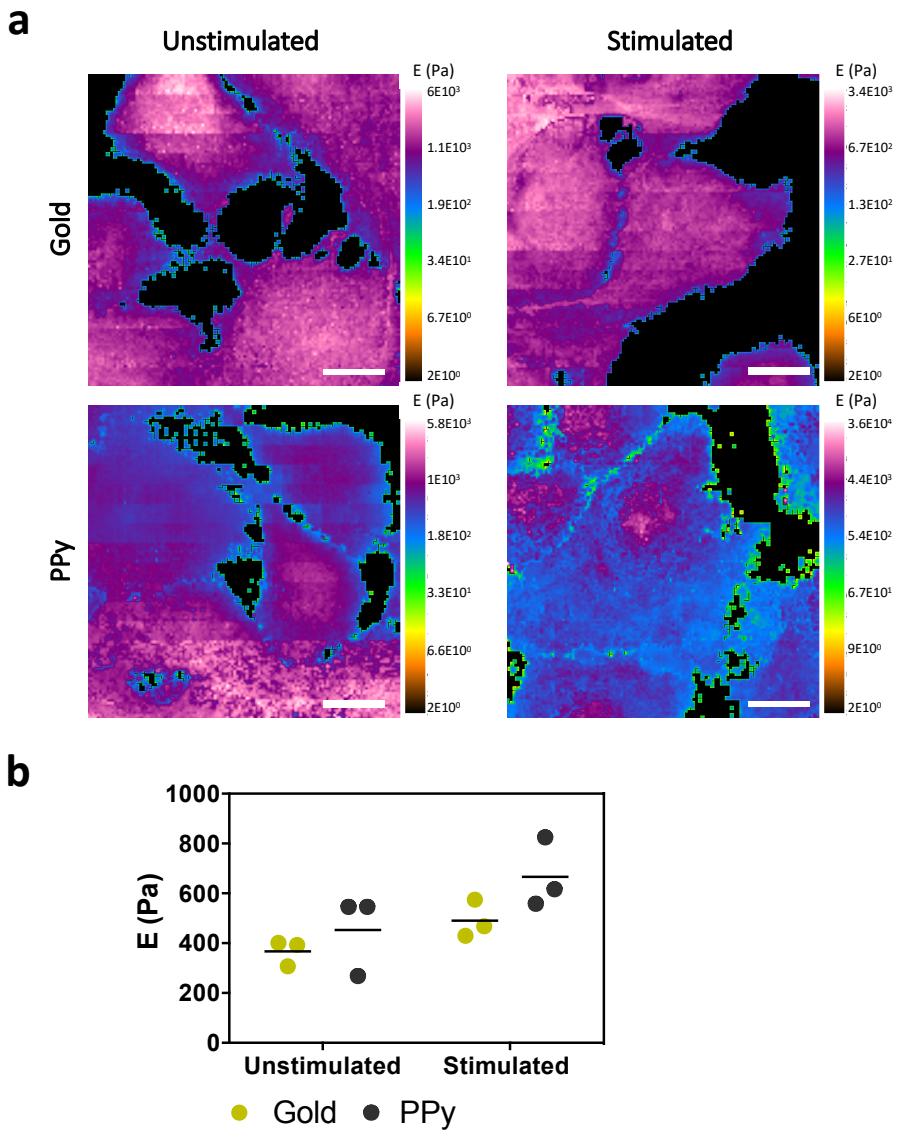

Figure 4.5: Stiffness mapping of live cells immediately after direct ES using SICM. ES protocols were conducted at -1V for 1 hour. SICM measurements were carried out together with Sahana Gopal. **a** Representative images of stiffness maps for unstimulated cells (control) and cells immediately after stimulation, for both gold coated mylar and PPy. Scale bars: 10 µm. **b** Plot of the median values of cell elasticity, calculated from the obtained stiffness maps, shows a trend of increasing cytoskeletal tension upon electrical stimulation. N = 1, n = 3. *y* axis: Elastic modulus in Pa. Data are shown on floating bars (minimum to maximum).

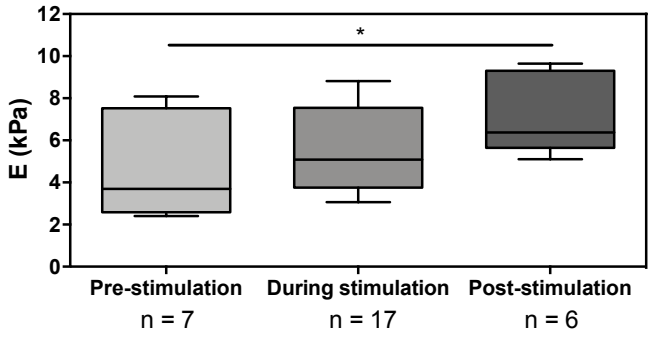

Figure 4.6: Temporal measurements of cellular elasticity in response to direct ES by AFM. Cell elasticity AFM measurements were conducted by Dr. Amy Gelmi before, during and after ES (-1V applied for 1 hour). *y* axis: Elastic modulus (E) in kPa. n - number of measurements per condition. Data are shown on box and whiskers (minimum to maximum) plots. *$p<0.05$.

4.4.2 Effect of electrical stimulation on YAP regulation and activity

When there is an increase in cytoskeletal tension, YAP/TAZ localise to the nucleus to activate their transcriptional program [555]. For this reason, the expression of YAP/TAZ-regulated genes *ANKRD1*, *CTGF* and *CYR61* was assessed. The expression of these genes was highly variable within each condition and did not show to be significantly affected by the application of direct electrical stimulation, via gold or PPy, at -0.3V or -1V, for both timepoints studied (0 and 24 hours post-stimulation), as shown in Figure 4.7.

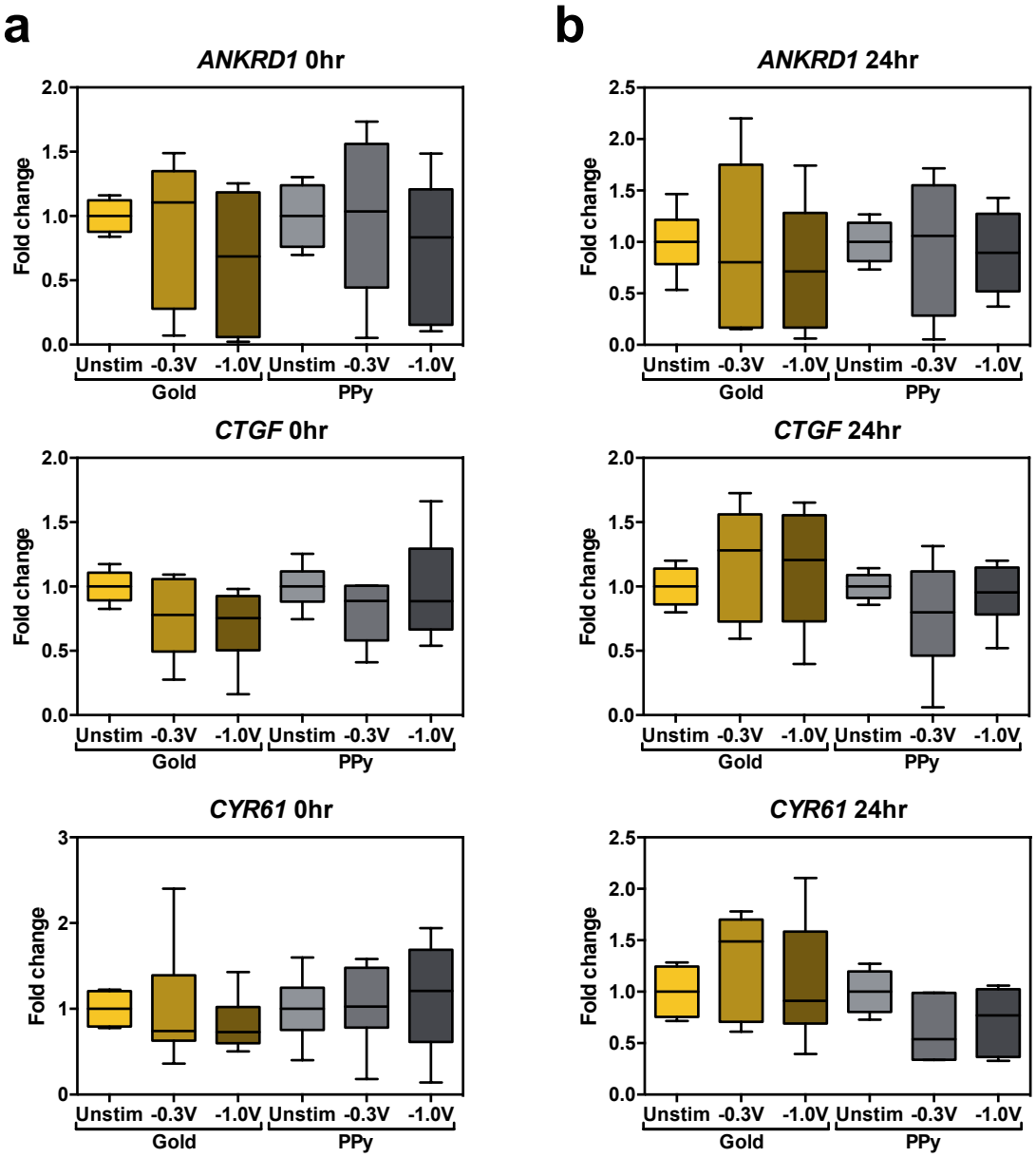

Figure 4.7: Gene expression of YAP target genes. RT-qPCR analysis of three YAP-regulated genes, *ANKRD1*, *CTGF* and *CYR61*, 0 (**a**) and 24 hours (**b**) post-stimulation (-1V or -0.3V for 1 hour). Unstimulated cells were used as controls. *y* axis: $2^{-\Delta\Delta Ct}$. Data are normalised to controls on the same substrate material and shown on Tukey box and whiskers plots. N = 3, n = 2.

Since regulation of YAP/TAZ as mechanotransducers occurs through their subcellular location, YAP immunostaining and imaging was carried out to study its nucleocytoplasmic presence. A decreasing trend in nuclear YAP was observed on cells immeadiately after gold-mediated ES (Figure 4.8**b**, left plot, 0 hr). Conversely, a trend in increasing nuclear YAP was observed on cells electrically stimulated via PPy, 24 hours post-stimulation, at -0.3V and -1V, when compared to their unstimulated counterparts (Figure 4.8**b**, right plot).

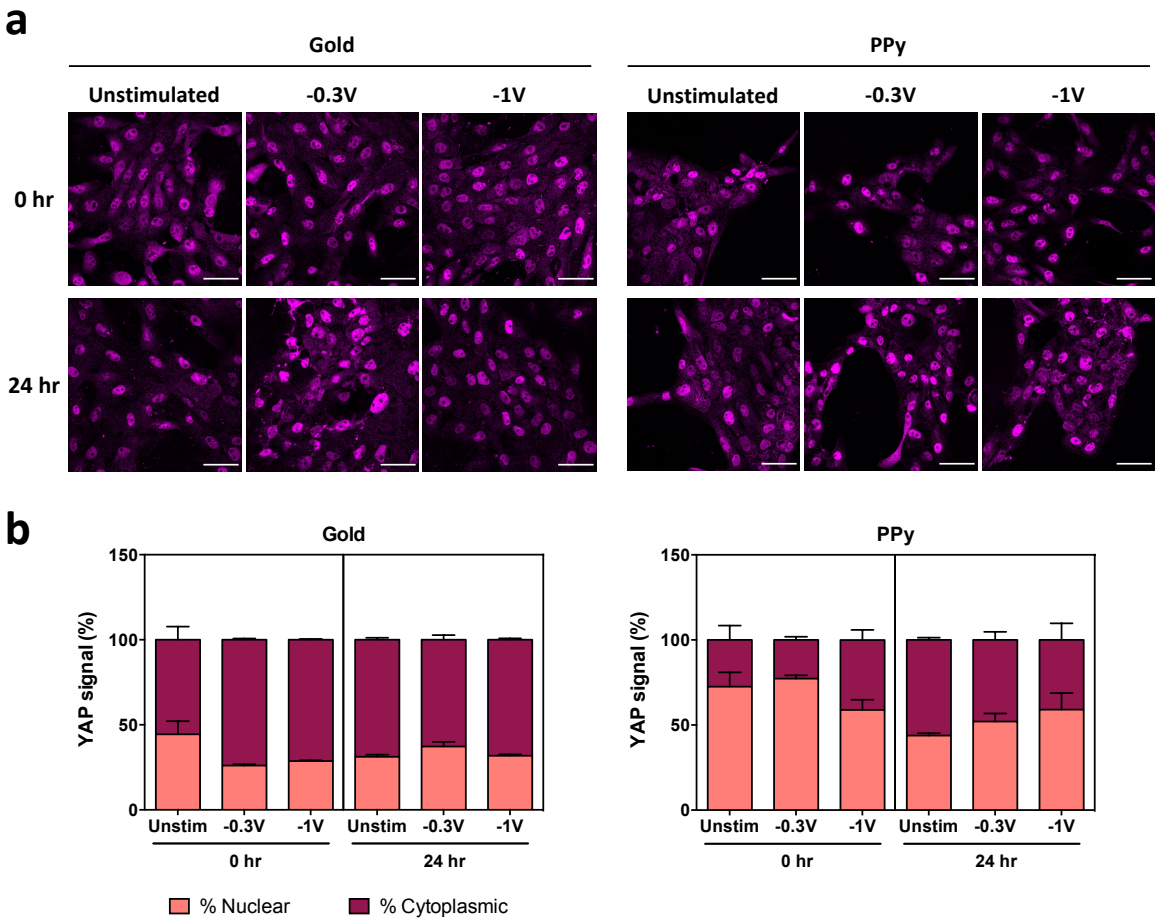

Figure 4.8: YAP subcellular localisation. YAP staining analysis on MCF10A exposed to direct ES for 1 hour at -0.3V or -1V, 0 and 24 hours post-stimulation. **a** Representative images from confocal microscopy showing YAP subcellular localisation. Scale bars: 50 µm.**b** Image analysis quantification of nuclear and cytoplasmic YAP signal, shown in percentage. Unstimulated cells were used as controls.

4.4.3 Effect of electrical stimulation on actin cytoskeleton

The increase in cellular tension upon direct electrical stimulation prompted an investigation into the actin cytoskeleton organization. By visual inspection of actin fibers (Figure 4.9), direct electrical stimulation via gold or PPy, both at -0.3V or -1V, did not seem to significantly change actin fibre density or the cortical-to-central actin ratio. The variety of colours in the representative images in Figure 4.9 shows that most actin fibres seem to have a cortical location and electrical stimulation (in all conditions tested) does not seem to have a significant effect on the arrangement of the actin cytoskeleton (angle distribution histograms can be seen in Figure C.1 in Appendix C).

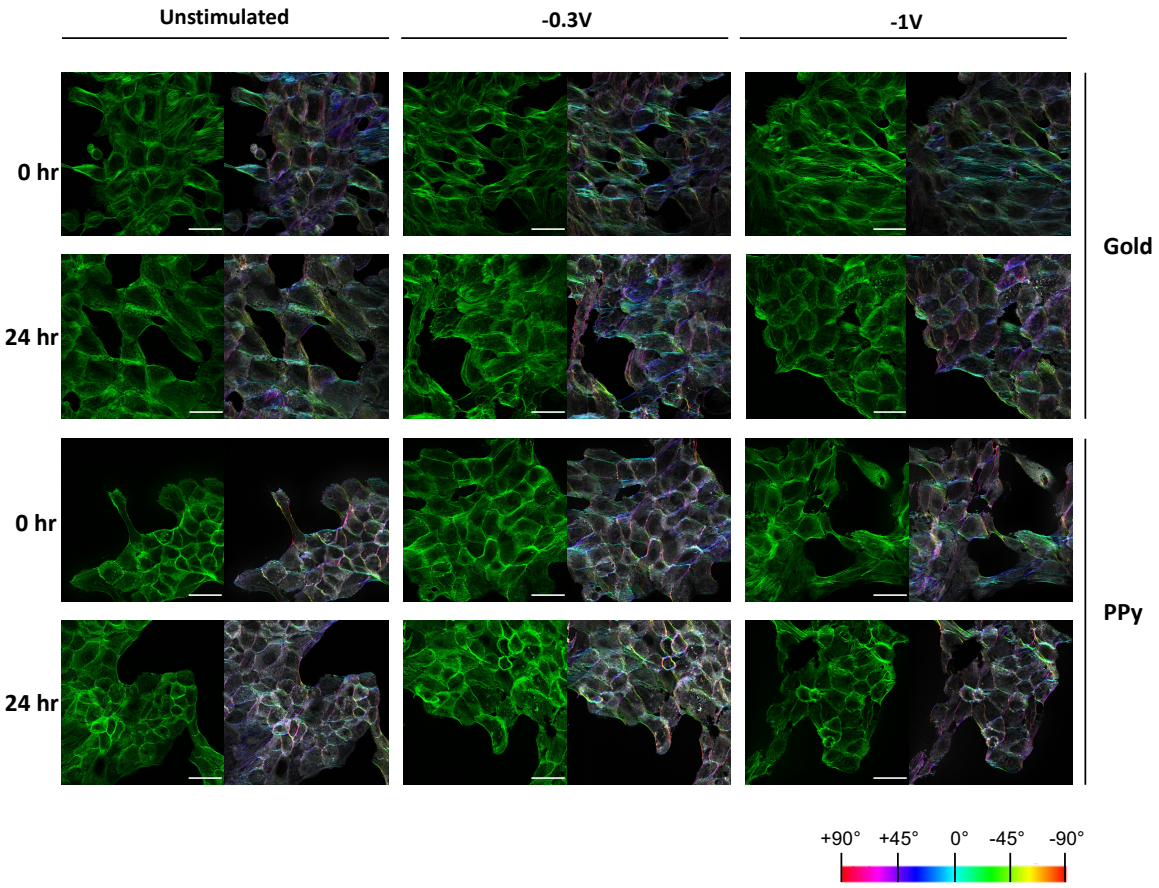

Figure 4.9: Actin cytoskeleton of electrically stimulated epithelial cells. Representative images from confocal microscopy showing the actin cytoskeleton (Phalloidin staining) of MCF10A cells exposed to direct ES (1 hour at -0.3V or -1V) 0 and 24 hours post-stimulation. The distribution of orientations of actin fibres is shown colour coded images (obtained from OrientationJ). Colour coding is presented on the bottom right corner of the figure. Scale bars: 50 µm.

4.4.4 Effect of electrical stimulation on focal adhesion protein vinculin

Vinculin is a key component of focal adhesions and it has an instrumental role in regulating the cell's mechanosensory machinery [582]. Here, MCF10A grown on gold exhibited denser vinculin staining then those grown on PPy (Figure 4.10 **a**). Remarkably, opposing expression patterns were observed between the two conducting substrates after electrical stimulation. Indeed, a significant decrease in vinculin fluorescence intensity was observed 24 hours after electrical stimulation via gold coated mylar (both at -0.3V and -1V); whereas a significant increase was observed on the cells electrically stimulated via PPy, immediately after stimulation, at -1V, 0 and 24 hours after stimulation for both ES protocols (Figure 4.10 **b**).

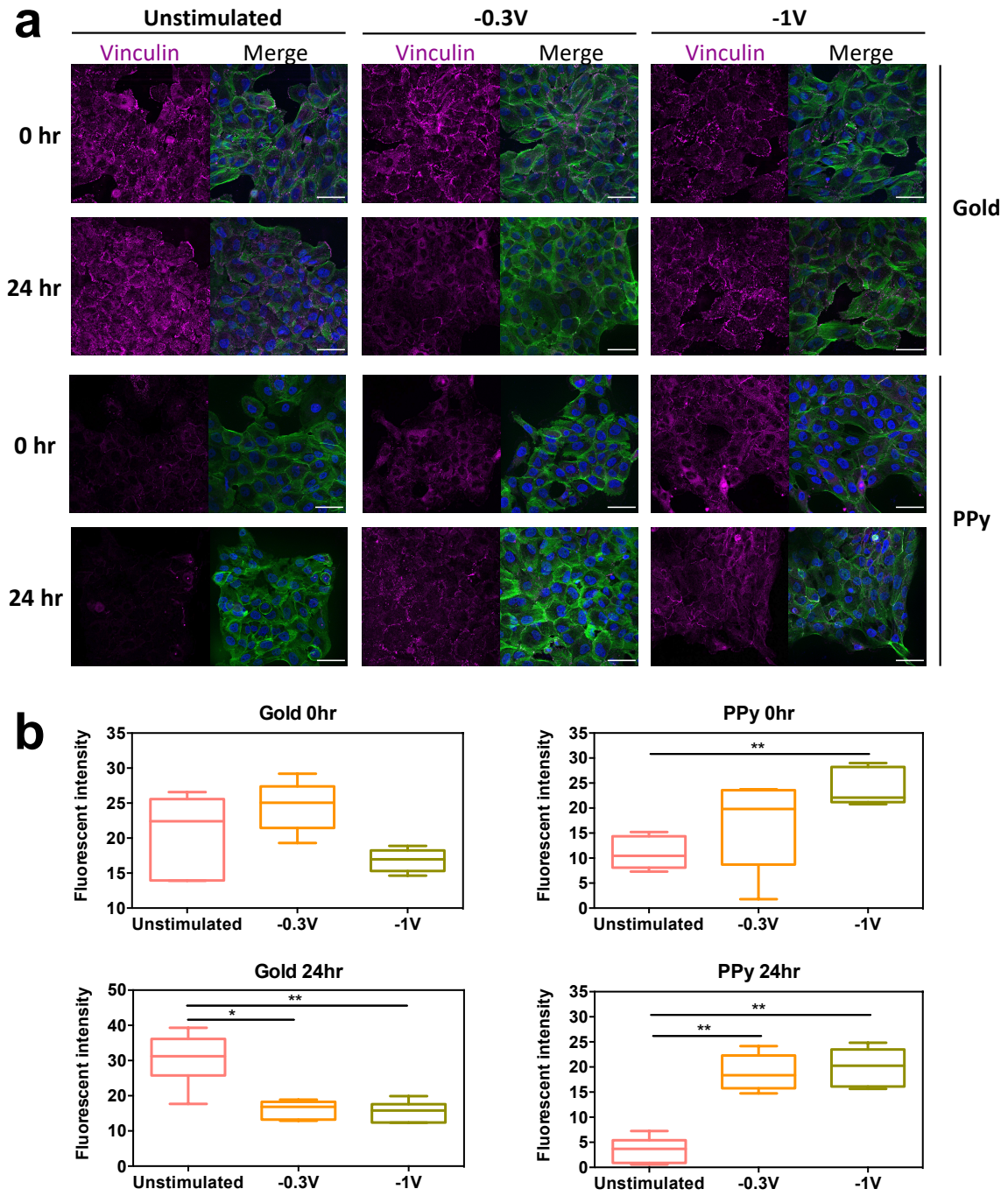

Figure 4.10: Effects on key focal adhesion component vinculin by substrate-mediated ES. a Representative images from confocal microscopy showing vinculin staining on MCF10A cells exposed to direct ES (at -0.3V or -1V for 1 hour) 0 and 24 hours post-stimulation. Magenta - vinculin; Blue - DAPI; Green - Phalloidin. Scale bars: 50 µm. **b** Image analysis quantification of vinculin's fluorescence signal. Data are shown as box and whiskers plots. *$p<0.05$ and **$p<0.01$

4.5 Discussion

In this chapter, an exploratory work towards charactering the mechanoresponse of electrically stimulated human mammary epithelial cells is presented. Here, a method to directly apply electrical stimuli to living cells via a biocompatible, conducting PPy substrate was developed to then investigate how these cells convert electrical into biological signals.

The results from two independent microscopic techniques – SICM and AFM – show that human mammary epithelial MCF10A cells increase their apparent stiffness in response to direct ES (Figures 4.5 and 4.6). In both cases, measurements were carried out right after cells were exposed to a ES protocol of -1V for 1 hour. Even though more biological replicates should be analysed using SICM, the results obtained by AFM provide support to this evidence, as the elastic moduli of cells 1 hour post-stimulation is significantly higher than the one of cells that have not yet been exposed to ES. Interestingly, AFM force measurements conducted while these cells were being electrically stimulated depicted a slight increase in cellular stiffness, albeit not statistically significant. Since apparent cell stiffness, measured using AFM, is strongly correlated with the stiffness of the cell's actin cytoskeleton [583], it is likely that this observed increase in stiffness is a result of an increase in cytoskeletal tension.

Regulation of mechanotransducers YAP/TAZ occurs via their nucleocytoplasmic transport, being activated when they accumulate in the nucleus, where specific transcriptional programs to respond to physical stimuli can be initiated. It has been shown that when cells experience higher cytoskeletal tension, YAP/TAZ are translocated into the nucleus and become activated [555]. For that reason, the expression of YAP-regulated genes *ANKRD1*, *CTGF* and *CYR61*, was studied (Figure 4.7). However, even though the expression of these genes was not significantly altered, when YAP expression and localisation was analysed by immunofluorescence staining, opposing results were obtained for the two substrates. A slight, not statistically significant decrease in nuclear YAP was observed in cells electrically stimulated via gold coated mylar (0 hr, Figure 4.8**b**). Yet, PPy-mediated ES resulted in a slight increase in nuclear YAP, 24 hours post-stimulation (Figure 4.8**b**). It is possible that YAP/TAZ do play a central role in regulating transcriptional machinery in response to electrical stimulation, but their role is still elusive from the data obtained here. The opposite trends observed on the two different substrates indicate the conducting materials might influence cells differently when electrically stimulated. Nevertheless, investigating the expression of only three YAP target genes was limiting and, in the future, it would be important to carry out transcriptome-wide analyses, such as RNA sequencing, to get a more comprehensive understanding of the regulatory networks involved in the response of epithelial cells to electrical stimulation.

Due to the observed increase in cellular stiffness, the actin cytoskeleton was analysed by fluorescence

microscopy. Under normal conditions, actin filaments in epithelial cells are organized into cortical thin bundles [584]. The analysis performed using OrientationJ, as an attempt to understand whether these cells, upon being electrically stimulated, would rearrange their actin cytoskeleton and produce more central actin fibres. This analysis, however, did not show any significant change in the organisation of actin filaments after electrical stimulation (Figure 4.9 and Figure C.1 in Appendix C). Central actin stress fibers were observed in various conditions, including unstimulated ones. It should be noted that the substrates used in this work offer an unnaturally stiff extracellular environment for these cells, which *per se* affects the way they would normally arrange their actin cytoskeleton. In addition, the application of electrical stimulation via the substrates evenly distributed the electrical signal, thereby not providing a specific electrical gradient that has previously been shown to stimulate epithelial cell migration [585], a phenomenon known as galvanotaxis (or electrotaxis). Moving forward, it would be important to conduct a more in-depth analysis to understand the undergoing alterations to the cytoskeletal arrangement of these cells, namely morphometric methodologies that utilise high-content cytoskeletal imaging and computational modelling to identify and extract important morphological features that become significantly altered between experimental conditions [586].

The degree of response to electrical stimulation at the focal adhesion level was assessed by investigating the expression of vinculin. This protein is not only a key component of focal adhesions, but it has also been shown to have a key role in mechanotransduction events [587]. Vinculin has been reported to stabilise focal adhesions when there is an increase in tension [582] and it is required in adhesion-dependent cellular stiffening [588]. Interestingly, the results here presented show that ES alters expression of this bipolar protein, which binds to both talin and F-actin, in a substrate-dependent manner (Figure 4.10). When MCF10A cells are electrically stimulated directly via gold coated mylar, vinculin expression is lowered when compared to unstimulated counterparts, 24 hours post-stimulation. Contrarily, PPy-mediated ES leads to an increased expression of vinculin compared to unstimulated cells grown on the same substrate, both 0 and 24 hours post-stimulation. These results further indicate that the conducting materials highly impact cellular response to electrical signals. It should be noted that PPy has a higher surface roughness than gold coated mylar [575], which might explain the difference in vinculin expression pattern between the two substrates. It seems plausible to hypothesise that the roughness of the material affects the way these cells adhere to each substrate and, consequently, how they respond to the substrate-mediated applied electrical signals. It appears that when ES is applied via PPy, MCF10A cells respond by strengthening their focal adhesions. Conversely, when the signals are transmitted via smooth gold coat mylar the adhesion of these cells to the substrate is weakened. Importantly, these data should be confirmed with standard techniques to assess protein expression, such as Western blotting. In addition, it would be relevant to further characterise vinculin's activity and response when these cells are responding to electrical stimuli using

molecular constructs such as a fluorescence resonance energy transfer (FRET)-based vinculin tension sensor [589]. This could potentially shed light on the relationship between cytoskeletal tension with vinculin expression and activity in the experimental conditions of the present work.

4.6 Concluding Remarks and Future Work

In conclusion, the work presented in this chapter shows the use of PPy-mediated electrical stimulation applied to human mammary epithelial cells to characterise cellular mechanosensory events. To the best of found knowledge, this is the first time substrate-mediated direct ES has been used to investigate the way these cells respond to electrical stimuli both biophysically and biochemically, by synergistically combining SICM, AFM, immunostaining and gene expression analysis.

Elasticity measurements showed that these epithelial cells increase their apparent stiffness in response to direct electrical stimulation as measured by two independent methods - SICM and AFM. Even though YAP/TAZ have been shown to be activated when cellular tension is increased, the gene expression and protein subcellular localisation data gathered in this study do not show a clear role for this regulatory mechanotransduction pathway in controlling the way MCF10A cells respond to ES. Future research at the gene expression level should investigate changes occurring in the whole genome, particularly by employing techniques such as RNA sequencing, to more comprehensively understand the molecular and regulatory mechanisms underlying this mechanoresponse. This could be made possible by leveraging engineering and fabrication techniques that could produce cell culture formats to get a higher throughput.

Moving forward, even though no significant change was observed in terms of actin cytoskeletal rearrangement, it would be key to utilise more high-content imaging and computational modelling to more adequately extract and investigate the possible morphological changes happening within these cells after electrical stimulation. Finally, vinculin's contrasting response to gold coated mylar and to PPy not only highlights the complexity of such responsive mechanisms, but also the relevance of the conducting material itself. It would be important to complement these data with other standard techniques to assess protein expression, such as Western blotting, and employ other biomolecular tools to better investigate the tension sensed at the focal adhesion level.

5

Conclusions and Future Work

Contents

5.1 Outlook

Within tissues, cells are continuously exposed to physical and biochemical stimuli from the surrounding extracellular (ECM) and neighbouring cells. The extracellular environment plays a fundamental role in controlling and regulating all essential aspects of cell behaviour, including differentiation, proliferation, survival, polarisation and migration. In addition, far from being a static structure, the ECM is highly dynamic and under continuous remodelling, which involves biosynthesis, secretion, assembly, modification and degradation of its components. There is a bidirectional relationship between the cells and the ECM, and both cell behaviour and matrix structure are dependent on the constant biochemical and biophysical cues.

This thesis aimed at exploring and investigating different aspects of the response of human mammary epithelial cells when their surrounding environment is biochemically and/or biophysically manipulated. In Chapter 2, the crosstalk between ECM composition and epithelial-mesenchymal transition (EMT) was investigated using various biomolecular tools, such as gene and protein expression, microscopy and Raman spectroscopy. In Chapter 3, cells undergoing EMT were exposed to a biologically-active laminin-111 fragment and its potential to modulate EMT events was investigated via different strategies. In Chapter 4, mechanoresponsive elements in electrically-stimulated MCF10A cells were characterised using a comprehensive methodology. The following three sections will cover final considerations on each of these chapters.

5.2 Interplay between ECM composition and EMT - final considerations

The epithelial microenvironment is instrumental to maintain tissue homeostasis and to control epithelial cell phenotype, including cell polarity and controlled levels of proliferation and apoptosis. Epithelial tissues are tightly organised and maintained by the basement membrane (BM), mainly composed of collagen IV and laminin 111. Surrounding the BM there is stromal ECM, predominantly comprised of type I collagen. One of the hallmarks of malignant carcinomas is the breaching of the BM, in which cells acquire an invasive behaviour and migrate from the epithelial compartment to the stromal matrix, where they encounter type I collagen. In fact, abnormally high expression of type I collagen has been associated with metastasis [350]. In Chapter 2, the breaching of the BM by human mammary epithelial cells was modelled by using biological components cells encounter *in vivo* – reconstituted BM through the use of Matrigel and reconstituted type I collagen. It was observed that exposure of non-transformed human mammary epithelial cells to increasing concentrations of type I collagen in the matrix results in an invasive phenotype. This work provided direct evidence that an imbalanced ECM composition can result in a dysregulated epithelial phenotype, which can contribute to the development and progression of disease.

The observed morphological and behavioural changes highly resemble EMT, a process in which epithelial cells lose their apicobasal polarity and become migratory. Indeed, there was an increased expression of mesenchymal markers at gene and protein level. Even though the importance, or even existence, of EMT in the context of cancer is still controversial, it seems that this debate is more an issue of semantics than of biological mechanisms. EMT is a complex phenomenon that involves multiple transitional states and underlying mechanisms, as opposed to a binary cellular switch. Cells need to acquire features that allow them to migrate and invade other sites in the body in order to metastasise, and there is compelling evidence that the process EMT, being it partial or complete, is what allows them to do so. Hence, investigating EMT in the context of disease, particularly cancer, is of utmost importance and the development of physiologically relevant systems, particularly in 3D, is needed.

While making use of natural ECM components, including animal-derived type I collagen and BM components from Matrigel, has the advantage of providing physiologically relevant microenvironments when forming matrices for cell culture, it is imperative to recognise and acknowledge the caveats of such systems. Type I collagen can bind various cell surface receptors, namely integrins, and activate different signalling pathways, thereby controlling cell fate independently of matrix mechanics. Therefore, using type I collagen to study the effects of matrix mechanics, including stiffness, be-

comes limiting, as it is not possible to decouple biophysical from biochemical effects. In addition, despite its crucial role throughout decades of research, EHS sarcoma tumour derived Matrigel is a BM structure that is both chemically and physically heterogeneous, further convoluting the relative contribution of different signals and inputs. Thus, future research should focus on the development of (semi-)synthetic systems to allow decoupling of biochemical from biophysical effects when studying such changes in cell behaviour. To this end, the considerable advances in the biomaterials field should be leveraged when designing future experiments, particularly when using synthetic hydrogels with increased functionality and complexity that can recapitulate different aspects of native ECM and support cell culture.

Moreover, SICM was employed to map the mechanical stiffness of these cells on rBM/collagen I matrices. To the best of found knowledge, this was the first time SICM was employed using such soft matrices for cell culture. The results obtained here refuted the initial working hypothesis that foresaw a decrease in cellular stiffness with increased matrix stiffness, suggesting that these cells might stiffen when exhibiting an invasive phenotype within a stiffer matrix, with a higher type I collagen content. It should be noted, however, that no statistical significance can be drawn from these experiments due to the lack of sufficient biological replicates. In addition, it was not possible to eliminate matrix effects with this experimental setup. Future research should make use of techniques that measure intracellular stiffness without interacting with ECM components, such as microrheology using microbeads delivered intracellularly or Brillouin microscopy.

Raman spectroscopy (RS), a powerful molecular vibrational technique that can be used to obtain the biochemical fingerprint of any given sample, and the multivariate PLS-DA method were successfully employed to classify each phenotype within the EMT spectrum into distinct groups with high accuracy. In this experimental design, two 2D *in vitro* culture methods were used as EMT models to compare with the 3D morphogenesis assay using rBM/collagen I matrices. This was the first exploratory research work that aimed at analysing the Raman spectra of cells undergoing EMT via different *in vitro* methods. It is important to consider, however, that, even though RS is a versatile molecular spectroscopy technique to extract important biological information from various types of samples, there is no gold standard method to analyse and process these data yet. The conversion of each spectrum into variables that allow for interpretation of meaningful information has been a central part of RS data processing. Here, the employment of PLS-DA to classify different EMT states showed that they are indeed biochemically different. However, it was also clear that these differences are far more complex than what standard gene and protein expression studies lead to believe. In the future, proteomic studies and novel optical probes (e.g. Raman tags) should be carried out to better track these biochemical changes.

5.3 Towards modulating EMT using a cryptic ECM fragment - final considerations

Despite significant efforts having been put into understanding the mechanisms and the key events underlying cellular invasion, there are limited therapeutic approaches to prevent, limit or even reverse metastatic tumour progression [484]. In Chapter 3, a fragment (from the β1 arm of laminin 111) with cryptic activity was used to modulate EMT-like events in human mammary epithelial cells. Two different strategies of interfacing the recombinantly produced bioactive laminin β1 fragment with cells undergoing EMT (via TGF-β1 treatment and 3D morphogenesis assay with type I collagen) were applied – as a soluble factor and as tethered to a GelMA-based hydrogel. Tethering of the laminin fragment to a GelMA-based hydrogel system was carried out via a SPAAC copper-free click chemistry (via cysteine or lysine residues), a convenient and non-toxic strategy to synthesise biomaterials for various applications as it does not require the use of a metal catalyst. The click chemistry strategy can be employed to have a controlled chemical functionalisation of various biomaterials with any biomolecule, as long as their structures allow the addition of alkynes or azide groups. This could potentially enable the development of platforms that can be used for high-throughput screening of novel therapeutics.

The use of this fragment on its own as a soluble compound increased mesenchymal gene expression but showed a modest potential to downregulate the expression of some mesenchymal genes when EMT-inducer TGF-β1 was added to the medium. It is possible that this cryptic fragment can interfere with EMT events when it can act as a TFG-β inhibitor. When covalently tethered at a higher concentration to functionalised GelMA-based hydrogels, the fragment showed encouraging, albeit not significant, potential to inhibit invasion of cells from encapsulated spheroids. Future experiments should test higher concentrations of hydrogel-tethered recombinant fragment and evaluate longer time-points.

ELISA and BLI were used to study the possible interaction between the recombinant laminin fragment and α3β1 integrin, both of human and of murine origin, and also TGF-β1. These techniques confirmed that the fragment interacts with mouse α3β1 integrin and possibly human α3β1 integrin (only confirmed by ELISA). Previous reports showed supporting evidence of this interaction [473, 474], but its mechanistic and regulatory aspects, particularly how it affects the activity of the fragment, still remain elusive. SPAAC chemistry was also used to label the fragment with a fluorescent Cy5 dye (via cysteine or lysine residues). Interaction between Cy5-labelled fragment and α3 integrin knockdown MCF10A cells showed that the fluorescent intensity of cell-associated fragment is reduced 24 and 48 hours post-transfection with siRNA, further corroborating the existence of an interaction between this recombinant fragment and α3 integrin. However, more research is necessary to understand the

nature of this relationship and how it regulates the molecular mechanisms underlying the laminin fragment's activity. In addition, an interaction between the laminin fragment and TGF-β1 was confirmed both by BLI and ELISA. These results further built on the idea that the fragment might modulate certain EMT events when it can act as a TGF-β inhibitor. Moreover, it is also known that several integrins regulate TGF-β1-mediated signal transduction [505]. Hence, if this fragment can act as a TGF-β1 inhibitor and can directly or indirectly interact with α3β1 integrin, it will be imperative to further elucidate these molecular mechanisms and signalling pathways.

Some domains of full-length laminin 111 have been shown to promote malignancy [511, 512] and induce immune responses [513]. Several of the active sites identified within laminin 111 sequence have been shown to have opposing phenotypic effects, with some promoting tumour growth and metastasis, and others inhibiting these behaviours [515]. It is hoped that the work here presented will encourage a more comprehensive molecular characterisation not only of the laminin β1 here used, but also of other biologically-active ECM fragments to avoid unwanted effects.

5.4 Towards characterising the mechanoresponse of electrically-stimulated epithelial cells - final considerations

Epithelial cells, lining all surfaces in our bodies, continuously sense external chemical (ligands) or physical (mechanical or electrical) signals from their environment. Electrical signalling plays a fundamental role in maintaining physiological homeostasis, but the molecular mechanotransduction mechanisms underlying cell response to electrostimulation are very elusive. Chapter 4 shows an exploratory work that aimed at charactering the mechanoresponse of electrically stimulated human mammary epithelial cells. To do so, doped PPy, one of the most well studied conducting polymers in biomedical research, was used to apply direct, substrate-mediated electrical stimulation, and the cellular biophysical and biochemical response was investigated by synergistically combining SICM, AFM, immunostaining and gene expression analysis.

SICM and AFM were employed to measure cell elasticity upon electrical stimulation and both techniques showed that MCF10A cells increase their apparent cellular stiffness in response to these signals. Experimentally, more biological replicates are necessary to statistically confirm the observed differences using SICM. However, the agreement between the two independent methods provides fairly strong evidence that these cells rapidly respond to direct electrical stimulation by increasing their cellular tension. As it has been shown that YAP/TAZ are translocated into the nucleus and become activated when cells experience higher cytoskeletal tension [555], gene expression of YAP target genes and YAP subcellular localisation were assessed. However, these analyses did not show a clear role for the YAP/TAZ regulatory pathway in controlling the way MCF10A cells respond to ES and more research work is necessary. Future experimental work should make use of techniques such as RNA sequencing, which can provide an unparalleled look into the whole transcriptome of cells, to understand which genes are activated or downregulated by these cells upon direct ES.

The analysis carried out to investigate the cytoskeletal rearrangement of unstimulated and electrically stimulated MCF10A cells did not show any visible significant change. However, in order to adequately interrogate the morphological and structural changes occurring after ES, morphometric methodologies that utilise high-content imaging and computational modelling should be employed. When investigating these cells' response to electrical stimulation at the focal adhesion level by assessing the expression of vinculin, a key sensory element that binds to both talin and F-actin, it was observed that the changes varied according to the substrate used to mediate the electrical signal. Since PPy has a higher surface roughness than gold coated mylar [575], it is plausible to hypothesise that this parameter affects the way these cells adhere to each substrate and then how they respond to the substrate-mediated applied electrical signals. It seems that when ES is applied via PPy MCF10A

cells respond by strengthening their focal adhesions, but when the signals are transmitted via smooth gold coat mylar the adhesion of these cells to the substrate is weakened. These findings should be confirmed by independent biomolecular quantification methods, such as Western blotting.

5.5 Final Remarks

This body of work explored different aspects of human mammary epithelial cells' response to various external biochemical and biophysical cues. It showed an increase in mesenchymal gene expression with increased stiffness of the extracellular matrix, driven by the presence of type I collagen. The data gathered in this work supports the view of EMT as being a complex phenomenon that involves multiple transitional states and underlying mechanisms. In addition, the employment and analysis of Raman spectra for a more comprehensive investigation showed that the different EMT states are biochemically distinct and these differences are more complex than what standard gene and protein expression studies have led to believe thus far. In addition, it is hoped that the experimental work done with the laminin β1 fragment has highlighted the importance of understanding the mechanisms of such cryptic ECM fragments. It is likely that the fragment used in this work can modulate EMT in very specific biological contexts. Bioactive fragments from ECM components might hold a great potential to be used in clinical applications, but the possible presence of various active sites that can have opposing effects emphasises the need to have well characterised cryptic ECM information. Finally, these epithelial cells clearly respond to substrate-mediated electrical stimulation by increasing their apparent stiffness and by changing their vinculin expression pattern. In future research, it will be important to have a view of these cells' transcriptomic landscape to better understand the undergoing changes upon receiving such signals. Hopefully this work will inspire research that can leverage and capitalise on the use of advanced biological and analytical techniques with optimised biomaterials to exert control over various aspects of cell behaviour.

Bibliography

[1] L. E. O'Brien, M. M. Zegers, and K. E. Mostov, "Building epithelial architecture: Insights from three-dimensional culture models," *Nature Reviews Molecular Cell Biology*, vol. 3, no. 7, pp. 531–537, 2002.

[2] K. Shin, V. C. Fogg, and B. Margolis, "Tight Junctions and Cell Polarity," *Annual Review of Cell and Developmental Biology*, vol. 22, no. 1, pp. 207–235, 2006.

[3] Q. Wang and B. Margolis, "Apical junctional complexes and cell polarity," *Kidney International*, vol. 72, no. 12, pp. 1448–1458, 2007. [Online]. Available: http://dx.doi.org/10.1038/sj.ki.5002579

[4] J. Roignot, X. Peng, and K. Mostov, "Polarity in mammalian epithelial morphogenesis," *Cold Spring Harbor Perspectives in Biology*, vol. 5, no. 2, pp. 1–15, 2013.

[5] S. Tstlkita, M. Furuse, T. Hirase, M. Itoh, A. Nagafuchi, S. Yonemura, S. Tsukita, and S. Tsukita, "Occludin: A Novel Integral Membrane Protein Localizing at Tight Junctions," *Journal of Cell Biology*, vol. 123, no. 6, pp. 1777–1788, 1993.

[6] M. Furuse, K. Fujita, T. Hiiragi, K. Fujimoto, and S. Tsukita, "Claudin-1 and -2: Novel integral membrane proteins localizing at tight junctions with no sequence similarity to occludin," *Journal of Cell Biology*, vol. 141, no. 7, pp. 1539–1550, 1998.

[7] A. Stoppacciaro, L. Williams, I. Martìn-Padura, P. Fruscella, M. Romano, M. Schneemann, A. Villa, D. Simmons, E. Dejana, L. Ruco, S. Lostaglio, and C. Panzeri, "Junctional Adhesion Molecule, a Novel Member of the Immunoglobulin Superfamily That Distributes at Intercellular Junctions and Modulates Monocyte Transmigration," *The Journal of Cell Biology*, vol. 142, no. 1, pp. 117–127, 1998.

[8] P. R. Dragsten, R. Blumenthal, and J. S. Handler, "Membrane asymmetry in epithelia: Is the tight junction a barrier to diffusion in the plasma membrane?" *Nature*, vol. 294, no. 5843, pp. 718–722, 1981.

[9] P. Claude, "Morphological factors influencing transepithelial permeability: A model for the resistance of the Zonula Occludens," *The Journal of Membrane Biology*, vol. 39, no. 2-3, pp. 219–232, 1978.

[10] A. Hartsock and W. J. Nelson, “Adherens and tight junctions: Structure, function and connections to the actin cytoskeleton,” *Biochimica et Biophysica Acta (BBA) - Biomembranes*, vol. 1778, no. 3, pp. 660–669, mar 2008. [Online]. Available: https://linkinghub.elsevier.com/retrieve/pii/S0005273607002714

[11] R. O. Hynes and A. Naba, “Overview of the Matrisome–An Inventory of Extracellular Matrix Constituents and Functions,” *Cold Spring Harbor Perspectives in Biology*, vol. 4, no. 1, pp. a004 903–a004 903, jan 2012. [Online]. Available: http://cshperspectives.cshlp.org/lookup/doi/10.1101/cshperspect.a004903

[12] A. Naba, K. R. Clauser, S. Hoersch, H. Liu, S. A. Carr, and R. O. Hynes, “The Matrisome: In Silico Definition and In Vivo Characterization by Proteomics of Normal and Tumor Extracellular Matrices,” *Molecular & Cellular Proteomics*, vol. 11, no. 4, p. M111.014647, 2012. [Online]. Available: http://www.mcponline.org/content/11/4/M111.014647.full.pdf{%}0Ahttp://www.mcponline.org/lookup/doi/10.1074/mcp.M111.014647

[13] D. D. Roberts, “Emerging functions of matricellular proteins,” *Cellular and Molecular Life Sciences*, vol. 68, no. 19, pp. 3133–3136, oct 2011. [Online]. Available: http://link.springer.com/10.1007/s00018-011-0779-2

[14] W. P. Daley, S. B. Peters, and M. Larsen, “Extracellular matrix dynamics in development and regenerative medicine,” *Journal of Cell Science*, vol. 121, no. 3, pp. 255–264, 2008.

[15] S. Ricard-Blum, “The Collagen Family,” *Cold Spring Harbor Perspectives in Biology*, vol. 3, no. 1, pp. 1–19, 2011.

[16] H. Lodish, A. Berk, S. L. Zipursky, P. Matsudaira, D. Baltimore, and J. Darnell, *Molecular Cell Biology*. W. H. Freeman, 2000.

[17] M. K. Gordon and R. A. Hahn, “Collagens,” *Cell and Tissue Research*, vol. 339, pp. 247–257, 2009. [Online]. Available: https://linkinghub.elsevier.com/retrieve/pii/B9780123786302001699

[18] J. M. Muncie and V. M. Weaver, *The Physical and Biochemical Properties of the Extracellular Matrix Regulate Cell Fate*, 1st ed. Elsevier Inc., 2018, vol. 130. [Online]. Available: http://dx.doi.org/10.1016/bs.ctdb.2018.02.002

[19] J. K. Mouw, G. Ou, and V. M. Weaver, “Extracellular matrix assembly: A multiscale deconstruction,” *Nature Reviews Molecular Cell Biology*, vol. 15, no. 12, pp. 771–785, 2014. [Online]. Available: http://dx.doi.org/10.1038/nrm3902

[20] N. Saraswathy and P. Ramalingam, “16 - Glycoproteomics,” in *Woodhead Publishing Series in Biomedicine*, N. Saraswathy, P. B. T. C. Ramalingam, T. in Genomics, and Proteomics, Eds. Woodhead Publishing, 2011, pp. 213–218. [Online]. Available: http://www.sciencedirect.com/science/article/pii/B978190756810750016X

[21] R. Timpl and J. C. Brown, “The laminins,” *Matrix Biology*, vol. 14, no. 4, pp. 275–281, 1994.

[Online]. Available: http://www.sciencedirect.com/science/article/pii/0945053X94901929

[22] M. Aumailley, L. Brucknertuderman, W. Carter, R. Deutzmann, D. Edgar, P. Ekblom, J. Engel, E. Engvall, E. Hohenester, and J. Jones, "A simplified laminin nomenclature," *Matrix Biology*, vol. 24, no. 5, pp. 326–332, aug 2005. [Online]. Available: https://linkinghub.elsevier.com/retrieve/pii/S0945053X0500065X

[23] K. Sugawara, D. Tsuruta, M. Ishii, J. C. Jones, and H. Kobayashi, "Laminin-332 and -511 in skin," *Experimental Dermatology*, vol. 17, no. 6, pp. 473–480, 2008.

[24] E. Hohenester and P. D. Yurchenco, "Laminins in basement membrane assembly," *Cell Adhesion and Migration*, vol. 7, no. 1, pp. 56–63, 2013.

[25] T. R. Cox and J. T. Erler, "Remodeling and homeostasis of the extracellular matrix: implications for fibrotic diseases and cancer," *Disease Models & Mechanisms*, vol. 4, no. 2, pp. 165–178, 2011.

[26] C. Bonnans, J. Chou, and Z. Werb, "Remodelling the extracellular matrix in development and disease," *Nature Reviews Molecular Cell Biology*, vol. 15, no. 12, pp. 786–801, 2014. [Online]. Available: http://dx.doi.org/10.1038/nrm3904

[27] R. Timpl, S. Fujiwara, M. Dziaiiek, M. Aumailley, S. Webera, and J. Engel, "Laminin, Proteoglycan, Nidogen and Collagen IV: Structural Models and Molecular Interactions," in *Ciba Foundation Symposium 108 - Basement Membranes and Cell Movement*, may 1984, ch. 3, pp. 25–43.

[28] M. Paulsson, S. Fujiwara, M. Dziadek, R. Timpl, G. Pejler, G. Bäckström, U. Lindahl, and J. Engel, "Structure and function of basement membrane proteoglycans," *Ciba Foundation symposium*, vol. 124, pp. 189–203, feb 1986.

[29] R. Timpl and J. C. Brown, "Supramolecular assembly of basement membranes," *BioEssays*, vol. 18, no. 2, pp. 123–132, 1996.

[30] R. Kalluri, "Basement membranes: Structure, assembly and role in tumour angiogenesis," *Nature Reviews Cancer*, vol. 3, no. 6, pp. 422–433, 2003.

[31] R. O. Hynes, "The Extracellular Matrix: Not Just Pretty Fibrils," *Science*, vol. 326, no. 5957, pp. 1216–1219, nov 2009. [Online]. Available: http://www.sciencemag.org/cgi/doi/10.1126/science.1176009

[32] C. Frantz, K. M. Stewart, and V. M. Weaver, "The extracellular matrix at a glance," *Journal of Cell Science*, vol. 123, no. 24, pp. 4195–4200, 2010.

[33] X. Xian, S. Gopal, and J. R. Couchman, "Syndecans as receptors and organizers of the extracellular matrix," *Cell and Tissue Research*, vol. 339, no. 1, pp. 31–46, 2010.

[34] B. Leitinger and E. Hohenester, "Mammalian collagen receptors," *Matrix Biology*, vol. 26, no. 3, pp. 146–155, 2007.

[35] D. S. Harburger and D. A. Calderwood, "Integrin signalling at a glance." *Journal of cell science*,

vol. 122, no. Pt 2, pp. 159–63, 2009. [Online]. Available: http://www.ncbi.nlm.nih.gov/pubmed/19118207{%}0Ahttp://www.pubmedcentral.nih.gov/articlerender.fcgi?artid=PMC2714413

[36] R. O. Hynes, “Integrins : Bidirectional , Allosteric Signaling Machines In their roles as major adhesion receptors,” *Cell*, vol. 110, no. 6, pp. 673–687, 2002.

[37] C. Kim, F. Ye, and M. H. Ginsberg, “Regulation of Integrin Activation,” *Annual Review of Cell and Developmental Biology*, vol. 27, no. 1, pp. 321–345, 2011.

[38] D. A. Calderwood, I. D. Campbell, and D. R. Critchley, “Talins and kindlins: Partners in integrin-mediated adhesion,” *Nature Reviews Molecular Cell Biology*, vol. 14, no. 8, pp. 503–517, 2013. [Online]. Available: http://dx.doi.org/10.1038/nrm3624

[39] S. J. Shattil, C. Kim, and M. H. Ginsberg, “The final steps of integrin activation: The end game,” *Nature Reviews Molecular Cell Biology*, vol. 11, no. 4, pp. 288–300, 2010. [Online]. Available: http://dx.doi.org/10.1038/nrm2871

[40] N. Wang, J. D. Tytell, and D. E. Ingber, “Mechanotransduction at a distance: Mechanically coupling the extracellular matrix with the nucleus,” *Nature Reviews Molecular Cell Biology*, vol. 10, no. 1, pp. 75–82, 2009.

[41] N. Wang, K. Naruse, D. Stamenovic, J. J. Fredberg, S. M. Mijailovich, I. M. Tolic-Norrelykke, T. Polte, R. Mannix, and D. E. Ingber, “Mechanical behavior in living cells consistent with the tensegrity model,” *Proceedings of the National Academy of Sciences*, vol. 98, no. 14, pp. 7765–7770, 2001. [Online]. Available: http://www.pnas.org/cgi/doi/10.1073/pnas.141199598

[42] P. F. Davies, “Overview: Temporal and Spatial Relationships in Shear Stress-Mediated Endothelial Signalling,” *Journal of Vascular Research*, vol. 34, no. 3, pp. 208–211, 1997. [Online]. Available: https://www.karger.com/DOI/10.1159/000159224

[43] W. B. Kiosses, G. Cao, M. A. Schwartz, B. Engelhardt, E. Dejana, D. A. Schultz, E. Tzima, M. Irani-Tehrani, and H. DeLisser, “A mechanosensory complex that mediates the endothelial cell response to fluid shear stress,” *Nature*, vol. 437, no. 7057, pp. 426–431, 2005.

[44] S. Gudi, J. P. Nolan, and J. A. Frangos, “Modulation of GTPase activity of G proteins by fluid shear stress and phospholipid composition,” *Proceedings of the National Academy of Sciences*, vol. 95, no. 5, pp. 2515–2519, 2002.

[45] N. Wang, “Review of cellular mechanotransduction,” *Journal of Physics D: Applied Physics*, vol. 50, no. 23, 2017.

[46] N. Wang, J. Butler, and D. Ingber, “Mechanotransduction across the cell surface and through the cytoskeleton,” *Science*, vol. 260, no. 5111, pp. 1124–1127, may 1993. [Online]. Available: http://www.sciencemag.org/cgi/doi/10.1126/science.7684161

[47] Z. Sun, M. Costell, and R. Fässler, “Integrin activation by talin, kindlin and mechanical forces,” *Nature Cell Biology*, vol. 21, no. 1, pp. 25–31, 2019. [Online]. Available:

http://dx.doi.org/10.1038/s41556-018-0234-9

[48] E. R. Horton, P. Astudillo, M. J. Humphries, and J. D. Humphries, "Mechanosensitivity of integrin adhesion complexes: role of the consensus adhesome," *Experimental Cell Research*, vol. 343, no. 1, pp. 7–13, apr 2016. [Online]. Available: http://dx.doi.org/10.1016/j.yexcr.2015.10.025https://linkinghub.elsevier.com/retrieve/pii/S0014482715301300

[49] S. E. Winograd-Katz, R. Fässler, B. Geiger, and K. R. Legate, "The integrin adhesome: from genes and proteins to human disease," *Nature Reviews Molecular Cell Biology*, vol. 15, no. 4, pp. 273–288, apr 2014. [Online]. Available: http://www.nature.com/articles/nrm3769

[50] K. R. Legate and R. Fassler, "Mechanisms that regulate adaptor binding to β-integrin cytoplasmic tails," *Journal of Cell Science*, vol. 122, no. 2, pp. 187–198, jan 2009. [Online]. Available: http://jcs.biologists.org/cgi/doi/10.1242/jcs.041624

[51] M. H. Ginsberg, R. O. Hynes, D. J. G. Rees, R. Grant, R. Zent, and D. A. Calderwood, "The Talin Head Domain Binds to Integrin β Subunit Cytoplasmic Tails and Regulates Integrin Activation," *Journal of Biological Chemistry*, vol. 274, no. 40, pp. 28 071–28 074, 2002.

[52] D. T. Loo, S. B. Kanner, and A. Aruffo, "Filamin Binds to the Cytoplasmic Domain of the β1 -Integrin," *Journal of Biological Chemistry*, vol. 273, no. 36, pp. 23 304–23 312, sep 1998. [Online]. Available: http://www.jbc.org/lookup/doi/10.1074/jbc.273.36.23304

[53] E. Montanez, S. Ussar, M. Schifferer, M. Bösl, R. Zent, M. Moser, and R. Fässler, "Kindlin-2 controls bidirectional signaling of integrins," *Genes and Development*, vol. 22, no. 10, pp. 1325–1330, 2008.

[54] M. Moser, B. Nieswandt, S. Ussar, M. Pozgajova, and R. Fässler, "Kindlin-3 is essential for integrin activation and platelet aggregation," *Nature Medicine*, vol. 14, no. 3, pp. 325–330, 2008.

[55] L.-M. Chen, D. Bailey, and C. Fernandez-Valle, "Association of β1 Integrin with Focal Adhesion Kinase and Paxillin in Differentiating Schwann Cells," *The Journal of Neuroscience*, vol. 20, no. 10, pp. 3776–3784, 2018.

[56] B. P. Eliceiri, X. S. Puente, J. D. Hood, D. G. Stupack, D. D. Schlaepfer, X. Z. Huang, D. Sheppard, and D. A. Cheresh, "Src-mediated coupling of focal adhesion kinase to integrin αvβ5 in vascular endothelial growth factor signaling," *Journal of Cell Biology*, vol. 157, no. 1, pp. 149–159, 2002.

[57] E. G. Arias-Salgado, S. Lizano, S. Sarkar, J. S. Brugge, M. H. Ginsberg, and S. J. Shattil, "Src kinase activation by direct interaction with the integrin cytoplasmic domain," *Proceedings of the National Academy of Sciences*, vol. 100, no. 23, pp. 13 298–13 302, 2003.

[58] K. Bledzka, K. Bialkowska, K. Sossey-Alaoui, J. Vaynberg, E. Pluskota, J. Qin, and E. F. Plow, "Kindlin-2 directly binds actin and regulates integrin outside-in signaling," *Journal of Cell Biology*, vol. 213, no. 1, pp. 97–108, 2016.

[59] M. Crisp, Q. Liu, K. Roux, J. Rattner, C. Shanahan, B. Burke, P. D. Stahl, and D. Hodzic, "Coupling of the nucleus and cytoplasm," *The Journal of Cell Biology*, vol. 172, no. 1, pp. 41–53, jan 2006. [Online]. Available: http://www.jcb.org/lookup/doi/10.1083/jcb.200509124

[60] P. Lu, K. Takai, V. M. Weaver, and Z. Werb, "Extracellular Matrix Degradation and Remodeling in Development and Disease," *Cold Spring Harbor Perspectives in Biology*, vol. 3, no. 12, pp. a005 058–a005 058, dec 2011. [Online]. Available: http://www.mdpi.com/1422-0067/20/1/205http://cshperspectives.cshlp.org/lookup/doi/10.1101/cshperspect.a005058

[61] J. T. Oxford, J. C. Reeck, and M. J. Hardy, "Extracellular Matrix in Development and Disease," *International journal of molecular sciences*, vol. 20, no. 1, 2019.

[62] L. Li, Q. Zhao, and W. Kong, "Extracellular matrix remodeling and cardiac fibrosis," *Matrix Biology*, vol. 68-69, pp. 490–506, aug 2018. [Online]. Available: https://linkinghub.elsevier.com/retrieve/pii/S0945053X17303980

[63] J. Herrera, C. A. Henke, and P. B. Bitterman, "Extracellular matrix as a driver of progressive fibrosis," *Journal of Clinical Investigation*, vol. 128, no. 1, pp. 45–53, jan 2018. [Online]. Available: http://www.embase.com/search/results?subaction=viewrecord{&}from=export{&}id=L620167302{%}0Ahttp://dx.doi.org/10.1172/JCI93557https://www.jci.org/articles/view/93557

[64] P. Lu, V. M. Weaver, and Z. Werb, "The extracellular matrix: A dynamic niche in cancer progression," *Journal of Cell Biology*, vol. 196, no. 4, pp. 395–406, 2012.

[65] J. Gross and C. M. Lapiere, "Collagenolytic activity in amphibian tissues: a tissue culture assay." *Proceedings of the National Academy of Sciences of the United States of America*, vol. 48, no. 6, pp. 1014–22, jun 1962. [Online]. Available: https://www.ncbi.nlm.nih.gov/pubmed/13902219https://www.ncbi.nlm.nih.gov/pmc/PMC220898/http://www.ncbi.nlm.nih.gov/pubmed/13902219http://www.pubmedcentral.nih.gov/articlerender.fcgi?artid=PMC220898

[66] W. Bode, F.-X. Gomis-Rüth, and W. Stöckler, "Astacins, serralysins, snake venom and matrix metalloproteinases exhibit identical zinc-binding environments (HEXXHXXGXXH and Met-turn) and topologies and should be grouped into a common family, the 'metzincins'," *FEBS Letters*, vol. 331, no. 1-2, pp. 134–140, sep 1993. [Online]. Available: http://doi.wiley.com/10.1016/0014-5793{%}2893{%}2980312-I

[67] W. Stöcker, F. Grams, P. Reinemer, W. Bode, U. Baumann, F.-X. Gomis-Rüth, and D. B. Mckay, "The metzincins - Topological and sequential relations between the astacins, adamalysins, serralysins, and matrixins (collagenases) define a super family of zinc-peptidases," *Protein Science*, vol. 4, no. 5, pp. 823–840, dec 1995. [Online]. Available: http://doi.wiley.com/10.1002/pro.5560040502

[68] E. S. Radisky, M. Raeeszadeh-Sarmazdeh, and D. C. Radisky, "Therapeutic Potential of Matrix

Metalloproteinase Inhibition in Breast Cancer," *Journal of Cellular Biochemistry*, vol. 118, no. 11, pp. 3531–3548, 2017.

[69] V. S. Golubkov, P. Cieplak, A. V. Chekanov, B. I. Ratnikov, A. E. Aleshin, N. V. Golubkova, T. I. Postnova, I. A. Radichev, D. V. Rozanov, W. Zhu, K. Motamedchaboki, and A. Y. Strongin, "Internal Cleavages of the Autoinhibitory Prodomain Are Required for Membrane Type 1 Matrix Metalloproteinase Activation, although Furin Cleavage Alone Generates Inactive Proteinase," *Journal of Biological Chemistry*, vol. 285, no. 36, pp. 27 726–27 736, sep 2010. [Online]. Available: http://www.jbc.org/lookup/doi/10.1074/jbc.M110.135442

[70] H. E. Van Wart and H. Birkedal-Hansen, "The cysteine switch: a principle of regulation of metalloproteinase activity with potential applicability to the entire matrix metalloproteinase gene family." *Proceedings of the National Academy of Sciences*, vol. 87, no. 14, pp. 5578–5582, jul 1990. [Online]. Available: http://www.pnas.org/cgi/doi/10.1073/pnas.87.14.5578

[71] I. Yana and S. J. Weiss, "Regulation of Membrane Type-1 Matrix Metalloproteinase Activation by Proprotein Convertases," *Molecular Biology of the Cell*, vol. 11, no. 7, pp. 2387–2401, jul 2000. [Online]. Available: http://www.molbiolcell.org/doi/10.1091/mbc.11.7.2387

[72] A. Page-McCaw, A. J. Ewald, and Z. Werb, "Matrix metalloproteinases and the regulation of tissue remodelling," *Nature Reviews Molecular Cell Biology*, vol. 8, no. 3, pp. 221–233, mar 2007. [Online]. Available: http://www.nature.com/articles/nrm2125

[73] C. M. Overall, "Molecular Determinants of Metalloproteinase Substrate Specificity: Matrix Metalloproteinase Substrate Binding Domains, Modules, and Exosites," *Molecular Biotechnology*, vol. 22, no. 1, pp. 051–086, sep 2002. [Online]. Available: http://link.springer.com/10.1385/MB:22:1:051https://linkinghub.elsevier.com/retrieve/pii/S0891584904004617

[74] K. K. Nelson and J. A. Melendez, "Mitochondrial redox control of matrix metalloproteinases," *Free Radical Biology and Medicine*, vol. 37, no. 6, pp. 768–784, 2004.

[75] M. D. Sternlicht, M. J. Bissell, and Z. Werb, "The matrix metalloproteinase stromelysin-1 acts as a natural mammary tumor promoter," *Oncogene*, vol. 19, no. 8, pp. 1102–1113, feb 2000. [Online]. Available: http://www.nature.com/articles/1203347

[76] D. Rodríguez, C. J. Morrison, and C. M. Overall, "Matrix metalloproteinases: What do they not do? New substrates and biological roles identified by murine models and proteomics," *Biochimica et Biophysica Acta (BBA) - Molecular Cell Research*, vol. 1803, no. 1, pp. 39–54, jan 2010. [Online]. Available: http://dx.doi.org/10.1016/j.bbamcr.2009.09.015https://linkinghub.elsevier.com/retrieve/pii/S0167488909002407

[77] S. Ricard-Blum and R. Salza, "Matricryptins and matrikines: biologically active fragments of the extracellular matrix," *Experimental Dermatology*, vol. 23, no. 7, pp. 457–463, jul 2014. [Online]. Available: http://doi.wiley.com/10.1111/exd.12435

[78] M. D. Sternlicht and Z. Werb, “How Matrix Metalloproteinases Regulate Cell Behavior,” *Annual Review of Cell and Developmental Biology*, vol. 17, no. 1, pp. 463–516, nov 2001. [Online]. Available: http://www.annualreviews.org/doi/10.1146/annurev.cellbio.17.1.463

[79] P. Cieplak and A. Y. Strongin, “Matrix metalloproteinases – From the cleavage data to the prediction tools and beyond,” *Biochimica et Biophysica Acta (BBA) - Molecular Cell Research*, vol. 1864, no. 11, pp. 1952–1963, nov 2017. [Online]. Available: http://dx.doi.org/10.1016/j.bbamcr.2017.03.010https://linkinghub.elsevier.com/retrieve/pii/S0167488917300642

[80] L. A. Hite, J. D. Shannon, J. B. Bjarnason, and J. W. Fox, “Sequence of a cDNA clone encoding the zinc metalloproteinase hemorrhagic toxin e from Crotalus atrox: evidence for signal, zymogen and disintegrin-like structures,” *Biochemistry*, vol. 31, no. 27, pp. 6203–6211, jul 1992. [Online]. Available: http://pubs.acs.org/doi/abs/10.1021/bi00142a005

[81] N. Giebeler and P. Zigrino, “A Disintegrin and Metalloprotease (ADAM): Historical Overview of Their Functions,” *Toxins*, vol. 8, no. 4, p. 122, apr 2016. [Online]. Available: http://www.mdpi.com/2072-6651/8/4/122

[82] K. Kuno, N. Kanada, E. Nakashima, F. Fujiki, F. Ichimura, and K. Matsushima, “Molecular Cloning of a Gene Encoding a New Type of Metalloproteinase-disintegrin Family Protein with Thrombospondin Motifs as an Inflammation Associated Gene,” *Journal of Biological Chemistry*, vol. 272, no. 1, pp. 556–562, jan 1997. [Online]. Available: http://www.jbc.org/lookup/doi/10.1074/jbc.272.1.556

[83] T. G. Wolfsberg, P. Primakoff, D. G. Myles, and M. White, Judith, “ADAM, a novel family of membrane proteins containing A Disintegrin And Metalloprotease domain: multipotential functions in cell-cell and cell- matrix interactions,” *The Journal of Cell Biology*, vol. 131, no. 2, pp. 275–278, oct 1995. [Online]. Available: http://www.jcb.org/cgi/doi/10.1083/jcb.131.2.275

[84] J. M. White, “ADAMs: modulators of cell–cell and cell–matrix interactions,” *Current Opinion in Cell Biology*, vol. 15, no. 5, pp. 598–606, oct 2003. [Online]. Available: https://linkinghub.elsevier.com/retrieve/pii/S0955067403001108

[85] R. Kelwick, I. Desanlis, G. N. Wheeler, and D. R. Edwards, “The ADAMTS (A Disintegrin and Metalloproteinase with Thrombospondin motifs) family,” *Genome Biology*, vol. 16, no. 1, p. 113, dec 2015. [Online]. Available: http://genomebiology.com/2015/16/1/113

[86] J. S. Bond, K. Rojas, J. Overhauser, H. Y. Zoghbi, and W. Jiang, “The structural genes, MEP1A and MEP1B, for the α and β subunits of the metalloendopeptidase meprin map to human chromosomes 6p and 18q, respectively,” *Genomics*, vol. 25, no. 1, pp. 300–303, jan 1995. [Online]. Available: http://linkinghub.elsevier.com/retrieve/pii/0888754395801429

[87] P. Marchand, J. Tang, and J. S. Bond, “Membrane association and oligomeric organization of the α and β subunits of mouse meprin A,” *Journal of Biological Chemistry*, vol. 269, no. 21, pp.

15 388–15 393, 1994.

[88] J. S. Bond and R. J. Beynon, “The astacin family of metalloendopeptidases,” *Protein Science*, vol. 4, no. 7, pp. 1247–1261, 1995.

[89] J. Tang and J. S. Bond, “Maturation of Secreted Meprin α during Biosynthesis: Role of the Furin Site and Identification of the COOH-Terminal Amino Acids of the Mouse Kidney Metalloprotease Subunit,” *Archives of Biochemistry and Biophysics*, vol. 349, no. 1, pp. 192–200, jan 1998. [Online]. Available: http://linkinghub.elsevier.com/retrieve/pii/S0003986197904537

[90] J. L. Arolas, C. Broder, T. Jefferson, T. Guevara, E. E. Sterchi, W. Bode, W. Stocker, C. Becker-Pauly, and F. X. Gomis-Ruth, “Structural basis for the sheddase function of human meprin metalloproteinase at the plasma membrane,” *Proceedings of the National Academy of Sciences*, vol. 109, no. 40, pp. 16 131–16 136, oct 2012. [Online]. Available: http://www.pnas.org/cgi/doi/10.1073/pnas.1211076109

[91] T. Jefferson, U. auf dem Keller, C. Bellac, V. V. Metz, C. Broder, J. Hedrich, A. Ohler, W. Maier, V. Magdolen, E. Sterchi, J. S. Bond, A. Jayakumar, H. Traupe, A. Chalaris, S. Rose-John, C. U. Pietrzik, R. Postina, C. M. Overall, and C. Becker-Pauly, “The substrate degradome of meprin metalloproteases reveals an unexpected proteolytic link between meprin β and ADAM10,” *Cellular and Molecular Life Sciences*, vol. 70, no. 2, pp. 309–333, jan 2013. [Online]. Available: http://link.springer.com/10.1007/s00018-012-1106-2

[92] C. Broder, P. Arnold, S. Vadon-Le Goff, M. A. Konerding, K. Bahr, S. Muller, C. M. Overall, J. S. Bond, T. Koudelka, A. Tholey, D. J. S. Hulmes, C. Moali, and C. Becker-Pauly, “Metalloproteases meprin and meprin are C- and N-procollagen proteinases important for collagen assembly and tensile strength,” *Proceedings of the National Academy of Sciences*, vol. 110, no. 35, pp. 14 219–14 224, aug 2013. [Online]. Available: http://www.pnas.org/cgi/doi/10.1073/pnas.1305464110

[93] C. Broder and C. Becker-Pauly, “The metalloproteases meprin α and meprin β: unique enzymes in inflammation, neurodegeneration, cancer and fibrosis,” *Biochemical Journal*, vol. 450, no. 2, pp. 253–264, mar 2013. [Online]. Available: http://www.biochemj.org/cgi/doi/10.1042/BJ20121751

[94] R. Khokha, A. Murthy, and A. Weiss, “Metalloproteinases and their natural inhibitors in inflammation and immunity,” *Nature Reviews Immunology*, vol. 13, no. 9, pp. 649–665, sep 2013. [Online]. Available: http://dx.doi.org/10.1038/nri3499http://www.nature.com/articles/nri3499

[95] A. Winer, S. Adams, and P. Mignatti, “Matrix Metalloproteinase Inhibitors in Cancer Therapy: Turning Past Failures Into Future Successes,” *Molecular Cancer Therapeutics*, vol. 17, no. 6, pp. 1147–1155, jun 2018. [Online]. Available: http://mct.aacrjournals.org/lookup/doi/10.1158/

1535-7163.MCT-17-0646

[96] J. Hedrich, D. Lottaz, K. Meyer, I. Yiallouros, W. Jahnen-Dechent, W. Stocker, and C. Becker-Pauly, “Fetuin-A and Cystatin C Are Endogenous Inhibitors of Human Meprin Metalloproteases,” *Biochemistry*, vol. 49, no. 39, pp. 8599–8607, oct 2010. [Online]. Available: https://pubs.acs.org/doi/10.1021/bi1004238

[97] M. Berman, E. Manseau, M. Law, and D. Aiken, “Ulceration is correlated with degradation of fibrin and fibronectin at the corneal surface,” *Investigative Ophthalmology and Visual Science*, vol. 24, no. 10, pp. 1358–1366, 1983. [Online]. Available: http://ovidsp.ovid.com/ovidweb.cgi?T=JS{&}PAGE=reference{&}D=emed1a{&}NEWS=N{&}AN=1983246827

[98] B. Shenkman, T. Livnat, I. Budnik, I. Tamarin, Y. Einav, and U. Martinowitz, “Plasma tissue-type plasminogen activator increases fibrinolytic activity of exogenous urokinase-type plasminogen activator,” *Blood Coagulation & Fibrinolysis*, vol. 23, no. 8, pp. 729–733, dec 2012. [Online]. Available: http://content.wkhealth.com/linkback/openurl?sid=WKPTLP:landingpage{&}an=00001721-201212000-00009

[99] Z.-L. Chen and S. Strickland, “Neuronal Death in the Hippocampus Is Promoted by Plasmin-Catalyzed Degradation of Laminin,” *Cell*, vol. 91, no. 7, pp. 917–925, dec 1997. [Online]. Available: https://linkinghub.elsevier.com/retrieve/pii/S0092867400804833

[100] M. Fonović and B. Turk, “Cysteine cathepsins and extracellular matrix degradation,” *Biochimica et Biophysica Acta (BBA) - General Subjects*, vol. 1840, no. 8, pp. 2560–2570, aug 2014. [Online]. Available: https://linkinghub.elsevier.com/retrieve/pii/S0304416514001214

[101] V. Turk, V. Stoka, O. Vasiljeva, M. Renko, T. Sun, B. Turk, and D. Turk, “Cysteine cathepsins: From structure, function and regulation to new frontiers,” *Biochimica et Biophysica Acta (BBA) - Proteins and Proteomics*, vol. 1824, no. 1, pp. 68–88, jan 2012. [Online]. Available: https://linkinghub.elsevier.com/retrieve/pii/S1570963911002706

[102] E. Hammond, A. Khurana, V. Shridhar, and K. Dredge, “The Role of Heparanase and Sulfatases in the Modification of Heparan Sulfate Proteoglycans within the Tumor Microenvironment and Opportunities for Novel Cancer Therapeutics,” *Frontiers in Oncology*, vol. 4, no. July, pp. 1–15, jul 2014. [Online]. Available: http://journal.frontiersin.org/article/10.3389/fonc.2014.00195/abstract

[103] A. Ochoa-Espinosa and M. Affolter, “Branching Morphogenesis: From Cells to Organs and Back,” *Cold Spring Harbor Perspectives in Biology*, vol. 4, no. 10, pp. a008 243–a008 243, oct 2012. [Online]. Available: http://cshperspectives.cshlp.org/lookup/doi/10.1101/cshperspect.a008243

[104] D. G. Brownfield, G. Venugopalan, A. Lo, H. Mori, K. Tanner, D. A. Fletcher, and M. J. Bissell, “Patterned Collagen Fibers Orient Branching Mammary Epithelium through

Distinct Signaling Modules," *Current Biology*, vol. 23, no. 8, pp. 703–709, apr 2013. [Online]. Available: http://dx.doi.org/10.1016/j.cub.2013.03.032https://linkinghub.elsevier.com/retrieve/pii/S0960982213003345

[105] W. P. Daley and K. M. Yamada, "ECM-modulated cellular dynamics as a driving force for tissue morphogenesis," *Current Opinion in Genetics & Development*, vol. 23, no. 4, pp. 408–414, aug 2013. [Online]. Available: http://dx.doi.org/10.1016/j.gde.2013.05.005https://linkinghub.elsevier.com/retrieve/pii/S0959437X13000828

[106] H. Y. Kim and C. M. Nelson, "Extracellular matrix and cytoskeletal dynamics during branching morphogenesis," *Organogenesis*, vol. 8, no. 2, pp. 56–64, apr 2012. [Online]. Available: http://www.tandfonline.com/doi/abs/10.4161/org.19813

[107] J. E. Fata, A. T. Ho, K. J. Leco, R. A. Moorehead, and R. Khokha, "Cellular turnover and extracellular matrix remodeling in female reproductive tissues: functions of metalloproteinases and their inhibitors," *Cellular and Molecular Life Sciences (CMLS)*, vol. 57, no. 1, pp. 77–95, jan 2000. [Online]. Available: http://link.springer.com/10.1007/s000180050500

[108] J. E. Fata, K. J. Leco, E. B. Voura, H.-y. E. Yu, P. Waterhouse, G. Murphy, R. A. Moorehead, and R. Khokha, "Accelerated apoptosis in the Timp-3–deficient mammary gland," *Journal of Clinical Investigation*, vol. 108, no. 6, pp. 831–841, sep 2001. [Online]. Available: http://www.jci.org/articles/view/13171

[109] L. Szabova, S. S. Yamada, H. Birkedal-Hansen, and K. Holmbeck, "Expression pattern of four membrane-type matrix metalloproteinases in the normal and diseased mouse mammary gland," *Journal of Cellular Physiology*, vol. 205, no. 1, pp. 123–132, oct 2005. [Online]. Available: http://doi.wiley.com/10.1002/jcp.20385

[110] J. P. Witty, J. H. Wright, and L. M. Matrisian, "Matrix metalloproteinases are expressed during ductal and alveolar mammary morphogenesis, and misregulation of stromelysin-1 in transgenic mice induces unscheduled alveolar development." *Molecular Biology of the Cell*, vol. 6, no. 10, pp. 1287–1303, oct 1995. [Online]. Available: http://www.molbiolcell.org/doi/10.1091/mbc.6.10.1287

[111] R. S. Talhouk, J. R. Chin, E. N. Unemori, Z. Werb, and M. J. Bissell, "Proteinases of the mammary gland: developmental regulation in vivo and vectorial secretion in culture," *Development - Supplement*, vol. 112, no. 2, pp. 439–449, 1991.

[112] K. A. Green and L. R. Lund, "ECM degrading proteases and tissue remodelling in the mammary gland," *BioEssays*, vol. 27, no. 9, pp. 894–903, sep 2005. [Online]. Available: http://doi.wiley.com/10.1002/bies.20281

[113] M. Simian, Y. Hirai, M. Navre, Z. Werb, A. Lochter, and M. J. Bissell, "The interplay of matrix metalloproteinases, morphogens and growth factors is necessary for branching

of mammary epithelial cells," *Development*, vol. 128, pp. 3117–3131, jun 2001. [Online]. Available: https://linkinghub.elsevier.com/retrieve/pii/S0048357511000411

[114] B. S. Wiseman, M. D. Sternlicht, L. R. Lund, C. M. Alexander, J. Mott, M. J. Bissell, P. Soloway, S. Itohara, and Z. Werb, "Site-specific inductive and inhibitory activities of MMP-2 and MMP-3 orchestrate mammary gland branching morphogenesis," *The Journal of Cell Biology*, vol. 162, no. 6, pp. 1123–1133, sep 2003. [Online]. Available: http://www.jcb.org/lookup/doi/10.1083/jcb.200302090

[115] X. Zhang, G. Qiao, and P. Lu, "Modulation of Fibroblast Growth Factor Signaling Is Essential for Mammary Epithelial Morphogenesis," *PLoS ONE*, vol. 9, no. 4, p. e92735, apr 2014. [Online]. Available: https://dx.plos.org/10.1371/journal.pone.0092735

[116] H. P. Makarenkova, M. P. Hoffman, A. Beenken, A. V. Eliseenkova, R. Meech, C. Tsau, V. N. Patel, R. A. Lang, and M. Mohammadi, "Differential Interactions of FGFs with Heparan Sulfate Control Gradient Formation and Branching Morphogenesis," *Science Signaling*, vol. 2, no. 88, pp. ra55–ra55, sep 2009. [Online]. Available: http://stke.sciencemag.org/cgi/doi/10.1126/scisignal.2000304

[117] X. Zhang, D. Martinez, Z. Koledova, G. Qiao, C. H. Streuli, and P. Lu, "FGF ligands of the postnatal mammary stroma regulate distinct aspects of epithelial morphogenesis," *Development*, vol. 141, no. 17, pp. 3352–3362, sep 2014. [Online]. Available: http://dev.biologists.org/cgi/doi/10.1242/dev.106732

[118] X. Zhang, O. A. Ibrahimi, S. K. Olsen, H. Umemori, M. Mohammadi, and D. M. Ornitz, "Receptor Specificity of the Fibroblast Growth Factor Family," *Journal of Biological Chemistry*, vol. 281, no. 23, pp. 15 694–15 700, jun 2006. [Online]. Available: http://www.jbc.org/lookup/doi/10.1074/jbc.M601252200

[119] A. C. Goldstrohm, A. L. Greenleaf, and M. A. Garcia-Blanco, "Co-transcriptional splicing of pre-messenger RNAs: considerations for the mechanism of alternative splicing," *Gene*, vol. 277, no. 1-2, pp. 31–47, oct 2001. [Online]. Available: http://linkinghub.elsevier.com/retrieve/pii/S0378111901006953

[120] B. K. Yeh, M. Igarashi, A. V. Eliseenkova, A. N. Plotnikov, I. Sher, D. Ron, S. A. Aaronson, and M. Mohammadi, "Structural basis by which alternative splicing confers specificity in fibroblast growth factor receptors," *Proceedings of the National Academy of Sciences*, vol. 100, no. 5, pp. 2266–2271, mar 2003. [Online]. Available: http://www.pnas.org/cgi/doi/10.1073/pnas.0436500100

[121] M. Xue and C. J. Jackson, "Extracellular Matrix Reorganization During Wound Healing and Its Impact on Abnormal Scarring," *Advances in Wound Care*, vol. 4, no. 3, pp. 119–136, mar 2015. [Online]. Available: http://www.liebertpub.com/doi/10.1089/wound.2013.0485

[122] T. Rozario and D. W. DeSimone, "The extracellular matrix in development and morphogenesis: A dynamic view," *Developmental Biology*, vol. 341, no. 1, pp. 126–140, may 2010. [Online]. Available: http://dx.doi.org/10.1016/j.ydbio.2009.10.026https://linkinghub.elsevier.com/retrieve/pii/S0012160609012858

[123] P. P. Provenzano, D. R. Inman, K. W. Eliceiri, J. G. Knittel, L. Yan, C. T. Rueden, J. G. White, and P. J. Keely, "Collagen density promotes mammary tumor initiation and progression," *BMC Medicine*, vol. 6, no. 1, p. 11, dec 2008. [Online]. Available: http://bmcmedicine.biomedcentral.com/articles/10.1186/1741-7015-6-11

[124] B. Hinz, "The role of myofibroblasts in wound healing," *Current Research in Translational Medicine*, vol. 64, no. 4, pp. 171–177, oct 2016. [Online]. Available: http://dx.doi.org/10.1016/j.retram.2016.09.003https://linkinghub.elsevier.com/retrieve/pii/S2452318616300393

[125] T. Wynn, "Cellular and molecular mechanisms of fibrosis," *The Journal of Pathology*, vol. 214, no. 2, pp. 199–210, jan 2008. [Online]. Available: http://doi.wiley.com/10.1002/path.2277

[126] G. Gabbiani, "The myofibroblast in wound healing and fibrocontractive diseases," *The Journal of Pathology*, vol. 200, no. 4, pp. 500–503, jul 2003. [Online]. Available: http://doi.wiley.com/10.1002/path.1427

[127] X.-m. Meng, D. J. Nikolic-Paterson, and H. Y. Lan, "TGF-β: the master regulator of fibrosis," *Nature Reviews Nephrology*, vol. 12, no. 6, pp. 325–338, jun 2016. [Online]. Available: http://dx.doi.org/10.1038/nrneph.2016.48http://www.nature.com/articles/nrneph.2016.48

[128] T. A. Wynn and K. M. Vannella, "Macrophages in Tissue Repair, Regeneration, and Fibrosis," *Immunity*, vol. 44, no. 3, pp. 450–462, mar 2016. [Online]. Available: http://dx.doi.org/10.1016/j.immuni.2016.02.015https://linkinghub.elsevier.com/retrieve/pii/S107476131630053X

[129] B. Hinz, S. H. Phan, V. J. Thannickal, A. Galli, M.-L. Bochaton-Piallat, and G. Gabbiani, "The Myofibroblast," *The American Journal of Pathology*, vol. 170, no. 6, pp. 1807–1816, jun 2007. [Online]. Available: https://insights.ovid.com/crossref?an=00000372-198100310-00010https://linkinghub.elsevier.com/retrieve/pii/S0002944010613909

[130] F. Verrecchia, M.-l. Chu, and A. Mauviel, "Identification of Novel TGF-β/Smad Gene Targets in Dermal Fibroblasts using a Combined cDNA Microarray/Promoter Transactivation Approach," *Journal of Biological Chemistry*, vol. 276, no. 20, pp. 17 058–17 062, may 2001. [Online]. Available: http://www.jbc.org/lookup/doi/10.1074/jbc.M100754200

[131] T. A. Wynn and T. R. Ramalingam, "Mechanisms of fibrosis: therapeutic translation for fibrotic disease," *Nature Medicine*, vol. 18, no. 7, pp. 1028–1040, jul 2012. [Online]. Available: http://dx.doi.org/10.1038/nm.2807http://www.nature.com/articles/nm.2807

[132] K. L. Walton, K. E. Johnson, and C. A. Harrison, "Targeting TGF-β Mediated SMAD Signaling for the Prevention of Fibrosis," *Frontiers in Pharmacology*, vol. 8, no. JUL, jul 2017. [Online].

Available: http://journal.frontiersin.org/article/10.3389/fphar.2017.00461/full

[133] M. C. Fleisch, C. A. Maxwell, and M.-H. Barcellos-Hoff, “The pleiotropic roles of transforming growth factor beta in homeostasis and carcinogenesis of endocrine organs,” *Endocrine-Related Cancer*, vol. 13, no. 2, pp. 379–400, jun 2006. [Online]. Available: https://erc.bioscientifica.com/view/journals/erc/13/2/0130379.xml

[134] M. W. Parker, D. Rossi, M. Peterson, K. Smith, K. Sikström, E. S. White, J. E. Connett, C. A. Henke, O. Larsson, and P. B. Bitterman, “Fibrotic extracellular matrix activates a profibrotic positive feedback loop,” *Journal of Clinical Investigation*, vol. 124, no. 4, pp. 1622–1635, apr 2014. [Online]. Available: http://www.jci.org/articles/view/71386

[135] A. Santos and D. Lagares, “Matrix Stiffness: the Conductor of Organ Fibrosis,” *Current Rheumatology Reports*, vol. 20, no. 1, p. 2, jan 2018. [Online]. Available: http://link.springer.com/10.1007/s11926-018-0710-z

[136] J. Solon, I. Levental, K. Sengupta, P. C. Georges, and P. A. Janmey, “Fibroblast Adaptation and Stiffness Matching to Soft Elastic Substrates,” *Biophysical Journal*, vol. 93, no. 12, pp. 4453–4461, dec 2007. [Online]. Available: https://linkinghub.elsevier.com/retrieve/pii/S000634950771696X

[137] F. Liu, J. D. Mih, B. S. Shea, A. T. Kho, A. S. Sharif, A. M. Tager, and D. J. Tschumperlin, “Feedback amplification of fibrosis through matrix stiffening and COX-2 suppression,” *The Journal of Cell Biology*, vol. 190, no. 4, pp. 693–706, aug 2010. [Online]. Available: http://www.jcb.org/lookup/doi/10.1083/jcb.201004082

[138] M. J. Bissell and W. C. Hines, “Why don’t we get more cancer? A proposed role of the microenvironment in restraining cancer progression,” *Nature Medicine*, vol. 17, no. 3, pp. 320–329, mar 2011. [Online]. Available: http://dx.doi.org/10.1038/nm.2328http://www.nature.com/articles/nm.2328

[139] A. Bergamaschi, E. Tagliabue, T. Sørlie, B. Naume, T. Triulzi, R. Orlandi, H. Russnes, J. Nesland, R. Tammi, P. Auvinen, V.-M. Kosma, S. Ménard, and A.-L. Børresen-Dale, “Extracellular matrix signature identifies breast cancer subgroups with different clinical outcome,” *The Journal of Pathology*, vol. 214, no. 3, pp. 357–367, feb 2008. [Online]. Available: http://doi.wiley.com/10.1002/path.2278

[140] M. J. Bissell and D. Radisky, “Putting tumours in context,” *Nature Reviews Cancer*, vol. 1, no. 1, pp. 46–54, oct 2001. [Online]. Available: https://www.jmbfs.org/jmbfs-210-rasamiravaka/?issue{_}id=4690{&}article{_}id=6http://www.nature.com/articles/35094059

[141] J. N. Skhinas and T. R. Cox, “The interplay between extracellular matrix remodelling and kinase signalling in cancer progression and metastasis,” *Cell Adhesion & Migration*, vol. 12, no. 6, pp. 529–537, nov 2018. [Online]. Available: https://doi.org/10.1080/19336918.2017.1405208https:

//www.tandfonline.com/doi/full/10.1080/19336918.2017.1405208

[142] F. Spill, D. S. Reynolds, R. D. Kamm, and M. H. Zaman, "Impact of the physical microenvironment on tumor progression and metastasis," *Current Opinion in Biotechnology*, vol. 40, pp. 41–48, aug 2016. [Online]. Available: http://dx.doi.org/10.1016/j.copbio.2016.02.007https://linkinghub.elsevier.com/retrieve/pii/S0958166916300301

[143] H. Yu, J. K. Mouw, and V. M. Weaver, "Forcing form and function: biomechanical regulation of tumor evolution," *Trends in Cell Biology*, vol. 21, no. 1, pp. 47–56, jan 2011. [Online]. Available: http://dx.doi.org/10.1016/j.tcb.2010.08.015https://linkinghub.elsevier.com/retrieve/pii/S0962892410001832

[144] M. R. Junttila and F. J. de Sauvage, "Influence of tumour micro-environment heterogeneity on therapeutic response," *Nature*, vol. 501, no. 7467, pp. 346–354, sep 2013. [Online]. Available: http://www.nature.com/articles/nature12626

[145] H. Miyamoto, T. Murakami, K. Tsuchida, H. Sugino, H. Miyake, and S. Tashiro, "Tumor-Stroma Interaction of Human Pancreatic Cancer: Acquired Resistance to Anticancer Drugs and Proliferation Regulation Is Dependent on Extracellular Matrix Proteins," *Pancreas*, vol. 28, no. 1, pp. 38–44, jan 2004. [Online]. Available: http://content.wkhealth.com/linkback/openurl?sid=WKPTLP:landingpage{&}an=00006676-200401000-00006

[146] M. J. Oudin and V. M. Weaver, "Physical and Chemical Gradients in the Tumor Microenvironment Regulate Tumor Cell Invasion, Migration, and Metastasis," *Cold Spring Harbor Symposia on Quantitative Biology*, vol. 81, no. 1, pp. 189–205, 2016. [Online]. Available: http://symposium.cshlp.org/lookup/doi/10.1101/sqb.2016.81.030817

[147] F. Kai, H. Laklai, and V. M. Weaver, "Force Matters: Biomechanical Regulation of Cell Invasion and Migration in Disease," *Trends in Cell Biology*, vol. 26, no. 7, pp. 486–497, jul 2016. [Online]. Available: http://dx.doi.org/10.1016/j.tcb.2016.03.007https://linkinghub.elsevier.com/retrieve/pii/S0962892416000507

[148] K. Csiszar, "Lysyl oxidases: A novel multifunctional amine oxidase family," 2001, vol. 70, pp. 1–32. [Online]. Available: https://linkinghub.elsevier.com/retrieve/pii/S0079660301700128

[149] A. Herchenhan, F. Uhlenbrock, P. Eliasson, M. Weis, D. Eyre, K. E. Kadler, S. P. Magnusson, and M. Kjaer, "Lysyl Oxidase Activity Is Required for Ordered Collagen Fibrillogenesis by Tendon Cells," *Journal of Biological Chemistry*, vol. 290, no. 26, pp. 16 440–16 450, jun 2015. [Online]. Available: http://www.jbc.org/lookup/doi/10.1074/jbc.M115.641670

[150] M. R. Ng and J. S. Brugge, "A Stiff Blow from the Stroma: Collagen Crosslinking Drives Tumor Progression," *Cancer Cell*, vol. 16, no. 6, pp. 455–457, dec 2009. [Online]. Available: http://dx.doi.org/10.1016/j.ccr.2009.11.013https://linkinghub.elsevier.com/retrieve/pii/S1535610809003912

[151] K. R. Levental, H. Yu, L. Kass, J. N. Lakins, M. Egeblad, J. T. Erler, S. F. Fong, K. Csiszar, A. Giaccia, W. Weninger, M. Yamauchi, D. L. Gasser, and V. M. Weaver, "Matrix Crosslinking Forces Tumor Progression by Enhancing Integrin Signaling," *Cell*, vol. 139, no. 5, pp. 891–906, nov 2009. [Online]. Available: http://dx.doi.org/10.1016/j.cell.2009.10.027https://linkinghub.elsevier.com/retrieve/pii/S0092867409013531

[152] S.-P. Huang, J. Chiou, Y.-H. Jan, T.-C. Lai, Y.-L. Yu, M. Hsiao, and Y.-F. Lin, "Over-expression of lysyl oxidase is associated with poor prognosis and response to therapy of patients with lower grade gliomas," *Biochemical and Biophysical Research Communications*, vol. 501, no. 3, pp. 619–627, jun 2018. [Online]. Available: https://doi.org/10.1016/j.bbrc.2018.04.228https://linkinghub.elsevier.com/retrieve/pii/S0006291X1831026X

[153] J. T. Erler, K. L. Bennewith, M. Nicolau, N. Dornhöfer, C. Kong, Q.-T. Le, J.-T. A. Chi, S. S. Jeffrey, and A. J. Giaccia, "Lysyl oxidase is essential for hypoxia-induced metastasis," *Nature*, vol. 440, no. 7088, pp. 1222–1226, apr 2006. [Online]. Available: http://www.nature.com/articles/nature04695

[154] A.-M. Baker, D. Bird, J. C. Welti, M. Gourlaouen, G. Lang, G. I. Murray, A. R. Reynolds, T. R. Cox, and J. T. Erler, "Lysyl Oxidase Plays a Critical Role in Endothelial Cell Stimulation to Drive Tumor Angiogenesis," *Cancer Research*, vol. 73, no. 2, pp. 583–594, jan 2013. [Online]. Available: http://cancerres.aacrjournals.org/cgi/doi/10.1158/0008-5472.CAN-12-2447

[155] H. E. Barker, T. R. Cox, and J. T. Erler, "The rationale for targeting the LOX family in cancer," *Nature Reviews Cancer*, vol. 12, no. 8, pp. 540–552, aug 2012. [Online]. Available: http://dx.doi.org/10.1038/nrc3319http://www.nature.com/articles/nrc3319

[156] ClinicalTrials.gov, "First-in-human Study of AB0024 to Evaluate Safety and Tolerability in Adults With Advanced Solid Tumors," 2011. [Online]. Available: https://clinicaltrials.gov/ct2/show/NCT01323933

[157] G. M. Cooper and R. E. Hausman, "The Development and Causes of Cancer," in *The Cell: A Molecular Approach*, 2nd ed. Sunderland (MA): Sinauer Associates, Inc., 2000.

[158] M. J. Roskelley, C. D., Srebrow, A. and Bissell, "A hierarchy of ECM mediated signalling regulates tissue-specific gene expression," *Current Opinion in Cell Biology*, vol. 7, pp. 736–747, 1995.

[159] K. Wolf and P. Friedl, "Extracellular matrix determinants of proteolytic and non-proteolytic cell migration," *Trends in Cell Biology*, vol. 21, no. 12, pp. 736–744, dec 2011. [Online]. Available: http://dx.doi.org/10.1016/j.tcb.2011.09.006https://linkinghub.elsevier.com/retrieve/pii/S0962892411001966

[160] P. A. Kenny and M. J. Bissell, "Tumor reversion: Correction of malignant behavior by microenvironmental cues," *International Journal of Cancer*, vol. 107, no. 5, pp. 688–695, dec

2003. [Online]. Available: http://doi.wiley.com/10.1002/ijc.11491

[161] D. E. Ingber, J. A. Madri, and J. D. Jamieson, “Basement membrane as a spatial organizer of polarized epithelia. Exogenous basement membrane reorients pancreatic epithelial tumor cells in vitro.” *Am J Pathol*, vol. 122, no. 1, pp. 129–139, 1986.

[162] A. P. Cooper, *On the anatomy of the breast*, 1840, vol. I.

[163] J. S. Lowe and P. G. Anderson, “Chapter 18 - skin and breast,” in *Stevens & Lowe’s Human Histology*, fourth edition ed., J. S. Lowe and P. G. Anderson, Eds. Philadelphia: Mosby, 2015, pp. 363 – 384. [Online]. Available: http://www.sciencedirect.com/science/article/pii/B9780723435020000188

[164] M. D. Sternlicht, “Key stages in mammary gland development: The cues that regulate ductal branching morphogenesis,” *Breast Cancer Research*, vol. 8, no. 1, p. 201, feb 2005. [Online]. Available: http://breast-cancer-research.biomedcentral.com/articles/10.1186/bcr1368

[165] J. Russo and I. H. Russo, “Development of the human breast,” *Maturitas*, vol. 49, no. 1, pp. 2–15, sep 2004. [Online]. Available: http://www.thieme-connect.de/DOI/DOI?10.1055/s-0033-1343989https://linkinghub.elsevier.com/retrieve/pii/S037851220400204X

[166] S. Jindal, D. Gao, P. Bell, G. Albrektsen, S. M. Edgerton, C. B. Ambrosone, A. D. Thor, V. F. Borges, and P. Schedin, “Postpartum breast involution reveals regression of secretory lobules mediated by tissue-remodeling,” *Breast Cancer Research*, vol. 16, no. 2, p. R31, apr 2014. [Online]. Available: http://breast-cancer-research.biomedcentral.com/articles/10.1186/bcr3633

[167] J. E. Ferguson, A. M. Schor, A. Howell, and M. W. J. Ferguson, “Changes in the extracellular matrix of the normal human breast during the menstrual cycle,” *Cell & Tissue Research*, vol. 268, no. 1, pp. 167–177, apr 1992. [Online]. Available: http://link.springer.com/10.1007/BF00338066

[168] World Health Organisation, “Press Release No 263. Latest global cancer data: Cancer burden rises to 18.1 million new cases and 9.6 million cancer deaths in 2018,” Tech. Rep., 2018. [Online]. Available: http://gco.iarc.fr/,

[169] E. A. El-Abd, A. S. Sultan, E. A. Shalaby, and F. Matalkah, “Animal Models of Breast Cancer,” in *Omics Approaches in Breast Cancer*. New Delhi: Springer India, 2014, no. April, pp. 297–314. [Online]. Available: http://link.springer.com/10.1007/978-81-322-0843-3{_}15

[170] S. J. Jackson and G. J. Thomas, “Human tissue models in cancer research: looking beyond the mouse,” *Disease Models & Mechanisms*, vol. 10, no. 8, pp. 939–942, aug 2017. [Online]. Available: http://dmm.biologists.org/lookup/doi/10.1242/dmm.031260

[171] C. R. Gaush, W. L. Hard, and T. F. Smith, “Characterization of an Established Line of Canine Kidney Cells (MDCK).” *Proceedings of the Society for Experimental Biology and Medicine*, vol. 122, no. 3, pp. 931–935, jul 1966. [Online]. Available:

https://journals.sagepub.com/doi/abs/10.3181/00379727-122-31293

[172] K. M. McCarthy, S. A. Francis, J. M. McCormack, J. Lai, R. A. Rogers, I. B. Skare, R. D. Lynch, and E. E. Schneeberger, “Inducible expression of claudin-1-myc but not occludin-VSV-G results in aberrant tight junction strand formation in MDCK cells,” *Journal of Cell Science*, vol. 113, no. 19, pp. 3387 LP – 3398, oct 2000. [Online]. Available: http://jcs.biologists.org/content/113/19/3387.abstract

[173] K. Takaishi, T. Sasaki, H. Kotani, H. Nishioka, and Y. Takai, “Regulation of Cell–Cell Adhesion by Rac and Rho Small G Proteins in MDCK Cells,” *The Journal of Cell Biology*, vol. 139, no. 4, pp. 1047–1059, nov 1997. [Online]. Available: http://www.jcb.org/lookup/doi/10.1083/jcb.139.4.1047

[174] S. Tsukita and M. Furuse, “Claudin-based barrier in simple and stratified cellular sheets,” *Current Opinion in Cell Biology*, vol. 14, no. 5, pp. 531–536, oct 2002. [Online]. Available: http://linkinghub.elsevier.com/retrieve/pii/S0955067402003629

[175] B. A. E. Hartemink, S. Science, and A. Hartemink, “Hartemink, B. A. E., Science, S., & Hartemink, A. (2003). Book reviews, 114, 139–140. doi:10.1016/S,” vol. 114, pp. 139–140, 2003.

[176] A. Z. Wang, G. K. Ojakian, and W. J. Nelson, “Steps in the morphogenesis of a polarized epithelium. I. Uncoupling the roles of cell-cell and cell-substratum contact in establishing plasma membrane polarity in multicellular epithelial (MDCK) cysts,” *Journal of Cell Science*, vol. 95, no. 1, pp. 137 LP – 151, jan 1990. [Online]. Available: http://jcs.biologists.org/content/95/1/137.abstract

[177] ——, “Steps in the morphogenesis of a polarized epithelium. II. Disassembly and assembly of plasma membrane domains during reversal of epithelial cell polarity in multicellular epithelial (MDCK) cysts,” *Journal of Cell Science*, vol. 95, no. 1, pp. 153 LP – 165, jan 1990. [Online]. Available: http://jcs.biologists.org/content/95/1/153.abstract

[178] J. Debnath and J. S. Brugge, “Modelling glandular epithelial cancers in three-dimensional cultures,” *Nature Reviews Cancer*, vol. 5, no. 9, pp. 675–688, 2005.

[179] L. E. O’Brien, T.-S. Jou, A. L. Pollack, Q. Zhang, S. H. Hansen, P. Yurchenco, and K. E. Mostov, “Rac1 orientates epithelial apical polarity through effects on basolateral laminin assembly,” *Nature Cell Biology*, vol. 3, no. 9, pp. 831–838, sep 2001. [Online]. Available: http://www.nature.com/articles/ncb0901-831

[180] H. D. Soule, T. M. Maloney, S. R. Wolman, W. D. Peterson, R. Brenz, C. M. Mcgrath, J. Russo, R. J. Pauley, R. F. Jones, and S. C. Brooks, “Isolation and Characterization of a Spontaneously Immortalized Isolation and Characterization of a Spontaneously Immortalized Human Breast,” *Cancer Research*, vol. 50, pp. 6075–6086, 1990.

[181] G. R. Merlo, F. Basolo, L. Fiore, L. Duboc, and N. E. Hynes, “p53-dependent and p53-independent activation of apoptosis in mammary epithelial cells reveals a survival function of EGF and insulin,” *The Journal of Cell Biology*, vol. 128, no. 6, pp. 1185–1196, mar 1995. [Online]. Available: http://www.jcb.org/cgi/doi/10.1083/jcb.128.6.1185

[182] J. Debnath, K. R. Mills, N. L. Collins, M. J. Reginato, S. K. Muthuswamy, and J. S. Brugge, “The Role of Apoptosis in Creating and Maintaining Luminal Space within Normal and Oncogene-Expressing Mammary Acini,” *Cell*, vol. 111, no. 1, pp. 29–40, oct 2002. [Online]. Available: https://linkinghub.elsevier.com/retrieve/pii/S0092867402010012

[183] S. K. Muthuswamy, D. Li, S. Lelievre, M. J. Bissell, and J. S. Brugge, “ErbB2, but not ErbB1, reinitiates proliferation and induces luminal repopulation in epithelial acini,” *Nature Cell Biology*, vol. 3, no. 9, pp. 785–792, sep 2001. [Online]. Available: http://www.ingentaconnect.com/content/10.1166/nnl.2017.2324http://www.nature.com/articles/ncb0901-785

[184] B. W. Futscher, “Epigenetic Changes During Cell Transformation,” in *Advances in experimental medicine and biology*, 2013, vol. 754, pp. 179–194. [Online]. Available: https://www.ncbi.nlm.nih.gov/pubmed/22956502https://www.ncbi.nlm.nih.gov/pmc/PMC3594783/http://link.springer.com/10.1007/978-1-4419-9967-2{_}9

[185] B. Elenbaas, “Human breast cancer cells generated by oncogenic transformation of primary mammary epithelial cells,” *Genes & Development*, vol. 15, no. 1, pp. 50–65, jan 2001. [Online]. Available: http://www.genesdev.org/cgi/doi/10.1101/gad.828901

[186] M. R. Stampfer and P. Yaswen, “Culture models of human mammary epithelial cell transformation,” *Journal of Mammary Gland Biology and Neoplasia*, vol. 5, no. 4, pp. 365–378, 2000.

[187] J. Debnath, S. K. Muthuswamy, and J. S. Brugge, “Morphogenesis and oncogenesis of MCF-10A mammary epithelial acini grown in three-dimensional basement membrane cultures,” *Methods*, vol. 30, no. 3, pp. 256–268, 2003.

[188] D. H. Janss, E. A. Hillman, L. B. Malan-Shibley, and T. L. Ben, “Chapter 5 Methods for the Isolation and Culture of Normal Human Breast Epithelial Cells11Suppored by NCI Contracts NO1-CO-75380 and NO1-CP-43237.” in *Normal Human Tissue and Cell Culture B. Endocrine, Urogenital, and Gastrointestinal Systems*, C. C. Harris, B. F. Trump, and G. D. B. T. M. i. C. B. Stoner, Eds. Academic Press, 1980, vol. 21, pp. 107–134. [Online]. Available: http://www.sciencedirect.com/science/article/pii/S0091679X08606809

[189] G. C. Easty, D. M. Easty, P. Monaghan, M. G. Ormerod, and A. M. Neville, “Preparation and identification of human breast epithelial cells in culture,” *International Journal of Cancer*, vol. 26, no. 5, pp. 577–584, nov 1980. [Online]. Available: https://doi.org/10.1002/ijc.2910260509

[190] D. Tosoni, P. P. Di Fiore, and S. Pece, “Functional Purification of Human and Mouse Mammary Stem Cells,” in *Progenitor Cells: Methods and Protocols*, K. A. Mace and

K. M. Braun, Eds. Totowa, NJ: Humana Press, 2012, pp. 59–79. [Online]. Available: https://doi.org/10.1007/978-1-61779-980-8{_}6

[191] A. Raouf and Y. J. Sun, “In Vitro Methods to Culture Primary Human Breast Epithelial Cells BT - Basic Cell Culture Protocols,” C. D. Helgason and C. L. Miller, Eds. Totowa, NJ: Humana Press, 2013, pp. 363–381. [Online]. Available: https://doi.org/10.1007/978-1-62703-128-8{_}23

[192] M. A. LaBarge, J. C. Garbe, and M. R. Stampfer, “Processing of Human Reduction Mammoplasty and Mastectomy Tissues for Cell Culture,” *JoVE*, no. 71, p. e50011, 2013. [Online]. Available: https://www.jove.com/video/50011

[193] J. Stingl, J. T. Emerman, and C. J. Eaves, “Enzymatic Dissociation and Culture of Normal Human Mammary Tissue to Detect Progenitor Activity,” in *Basic Cell Culture Protocols. Methods in Molecular Biology*, C. D. Helgason and C. L. Miller, Eds. Totowa, NJ: Humana Press, 2005, pp. 249–263. [Online]. Available: https://doi.org/10.1385/1-59259-838-2:249

[194] P. Berthon, G. Pancino, P. de Cremoux, A. Roseto, C. Gespach, and F. Calvo, “Characterization of normal breast epithelial cells in primary cultures: Differentiation and growth factor receptors studies,” *In Vitro Cellular & Developmental Biology - Animal*, vol. 28, no. 11, pp. 716–724, 1992. [Online]. Available: https://doi.org/10.1007/BF02631059

[195] P. S. Rudland, C. M. Hughes, S. A. Ferns, and M. J. Warburton, “Characterization of human mammary cell types in primary culture: Immunofluorescent and immunocytochemical indicators of cellular heterogeneity,” *In Vitro Cellular & Developmental Biology*, vol. 25, no. 1, pp. 23–36, 1989. [Online]. Available: https://doi.org/10.1007/BF02624407

[196] P. Yaswen and M. R. Stampfer, “Molecular changes accompanying senescence and immortalization of cultured human mammary epithelial cells,” *The International Journal of Biochemistry & Cell Biology*, vol. 34, no. 11, pp. 1382–1394, 2002. [Online]. Available: http://www.sciencedirect.com/science/article/pii/S135727250200047X

[197] A. Zubeldia-Plazaola, E. Ametller, M. Mancino, M. Prats de Puig, A. López-Plana, F. Guzman, L. Vinyals, E. M. Pastor-Arroyo, V. Almendro, G. Fuster, and P. Gascón, “Comparison of methods for the isolation of human breast epithelial and myoepithelial cells,” *Frontiers in cell and developmental biology*, vol. 3, p. 32, may 2015. [Online]. Available: https://www.ncbi.nlm.nih.gov/pubmed/26052514https://www.ncbi.nlm.nih.gov/pmc/PMC4440402/

[198] K. Rao, Ö. Alper, K. E. Opheim, G. Bonnet, K. Wolfe, E. Bryant, S. O. Larivee, P. Porter, and J. K. McDougall, “Cytogenetic characterization and H-ras associated transformation of immortalized human mammary epithelial cells,” *Cancer Cell International*, vol. 6, no. 1, p. 15, 2006. [Online]. Available: https://doi.org/10.1186/1475-2867-6-15

[199] M. R. Stampfer and P. Yaswen, “Human epithelial cell immortalization as a step in carcinogenesis,” *Cancer Lett*, vol. 194, 2003. [Online]. Available: https://doi.org/10.1016/

S0304-3835(02)00707-3

[200] K. Rao, E. Bryant, S. O'Hara Larivee, and J. K. McDougall, "Production of spindle cell carcinoma by transduction of H-Ras 61L into immortalized human mammary epithelial cells," *Cancer Lett*, vol. 201, 2003. [Online]. Available: https://doi.org/10.1016/S0304-3835(03)00423-3

[201] T. Gudjonsson, R. Villadsen, L. Rønnov-Jessen, and O. W. Petersen, "Immortalization protocols used in cell culture models of human breast morphogenesis," *Cellular and Molecular Life Sciences CMLS*, vol. 61, no. 19, pp. 2523–2534, 2004. [Online]. Available: https://doi.org/10.1007/s00018-004-4167-z

[202] W. Roux, "Beiträge zur Entwickelungsmechanik des Embryo," *Archiv für mikroskopische Anatomie*, vol. 29, no. 1, pp. 157–212, 1887.

[203] R. G. Harrison, M. J. Greenman, F. P. Mall, and C. M. Jackson, "Observations of the living developing nerve fiber," *The Anatomical Record*, vol. 1, no. 5, pp. 116–128, jun 1907. [Online]. Available: https://doi.org/10.1002/ar.1090010503

[204] G. Stacey, "Primary Cell Cultures and Immortal Cell Lines," in *Encyclopedia of Life Sciences*. Chichester: John Wiley & Sons, Ltd, apr 2001, pp. 1–6. [Online]. Available: http://doi.wiley.com/10.1038/npg.els.0002564

[205] A. Abbott, "Biology's new dimension," *Nature*, vol. 424, no. 6951, pp. 870–872, aug 2003. [Online]. Available: https://doi.org/10.1038/424870ahttp://www.nature.com/articles/424870a

[206] S. Breslin and L. O'Driscoll, "Three-dimensional cell culture: The missing link in drug discovery," *Drug Discovery Today*, vol. 18, no. 5-6, pp. 240–249, 2013. [Online]. Available: http://dx.doi.org/10.1016/j.drudis.2012.10.003

[207] K. Duval, H. Grover, L.-H. Han, Y. Mou, A. F. Pegoraro, J. Fredberg, and Z. Chen, "Modeling Physiological Events in 2D vs. 3D Cell Culture," *Physiology*, vol. 32, no. 4, pp. 266–277, jul 2017. [Online]. Available: http://www.physiology.org/doi/10.1152/physiol.00036.2016

[208] J. J. Campbell and C. J. Watson, "Three-dimensional culture models of mammary gland," *Organogenesis*, vol. 5, no. 2, pp. 43–49, apr 2009. [Online]. Available: http://www.tandfonline.com/doi/abs/10.4161/org.5.2.8321

[209] J. B. Kim, R. Stein, and M. J. O'Hare, "Three-dimensional in vitro tissue culture models of breast cancer — a review," *Breast Cancer Research and Treatment*, vol. 85, no. 3, pp. 281–291, jun 2004. [Online]. Available: http://link.springer.com/10.1023/B:BREA.0000025418.88785.2b

[210] M. Kapałczyńska, T. Kolenda, W. Przybyła, M. Zajączkowska, A. Teresiak, V. Filas, M. Ibbs, R. Bliźniak, Ł. Łuczewski, and K. Lamperska, "2D and 3D cell cultures – a comparison of different types of cancer cell cultures," *Archives of Medical Science*, vol. 14, no. 4, pp. 910–919, 2016. [Online]. Available: https://www.termedia.pl/doi/10.5114/aoms.2016.63743

[211] N. Torras, M. García-Díaz, V. Fernández-Majada, and E. Martínez, "Mimicking Epithelial

Tissues in Three-Dimensional Cell Culture Models," *Frontiers in Bioengineering and Biotechnology*, vol. 6, no. December, pp. 1–7, dec 2018. [Online]. Available: https://www.frontiersin.org/article/10.3389/fbioe.2018.00197/full

[212] K. M. Yamada and E. Cukierman, "Modeling Tissue Morphogenesis and Cancer in 3D," *Cell*, vol. 130, no. 4, pp. 601–610, aug 2007. [Online]. Available: https://linkinghub.elsevier.com/retrieve/pii/S0092867407010288

[213] M. J. Bissell, A. Rizki, and I. S. Mian, "Tissue architecture: the ultimate regulator of breast epithelial function," *Current Opinion in Cell Biology*, vol. 15, no. 6, pp. 753–762, dec 2003. [Online]. Available: https://linkinghub.elsevier.com/retrieve/pii/S0955067403001431

[214] E. Cukierman, R. Pankov, and K. M. Yamada, "Cell interactions with three-dimensional matrices," *Current Opinion in Cell Biology*, vol. 14, no. 5, pp. 633–640, oct 2002. [Online]. Available: http://eutils.ncbi.nlm.nih.gov/entrez/eutils/elink.fcgi?dbfrom=pubmed{&}id=12231360{&}retmode=ref{&}cmd=prlinks{%}0Apapers3://publication/uuid/200A5308-2EF9-42B5-B2FE-7CC84785AEA1http://linkinghub.elsevier.com/retrieve/pii/S0955067402003642

[215] L. G. Griffith and M. A. Swartz, "Capturing complex 3D tissue physiology in vitro," *Nature Reviews Molecular Cell Biology*, vol. 7, no. 3, pp. 211–224, 2006.

[216] A. Birgersdotter, R. Sandberg, and I. Ernberg, "Gene expression perturbation in vitro - A growing case for three-dimensional (3D) culture systems," *Seminars in Cancer Biology*, vol. 15, no. 5 SPEC. ISS., pp. 405–412, 2005.

[217] S. Ghosh, G. C. Spagnoli, I. Martin, S. Ploegert, P. Demougin, M. Heberer, and A. Reschner, "Three-dimensional culture of melanoma cells profoundly affects gene expression profile: A high density oligonucleotide array study," *Journal of Cellular Physiology*, vol. 204, no. 2, pp. 522–531, aug 2005. [Online]. Available: http://doi.wiley.com/10.1002/jcp.20320

[218] S. Li, J. Lao, B. P. C. Chen, Y.-S. Li, Y. Zhao, J. Chu, K.-D. Chen, T.-C. Tsou, K. Peck, and S. CHIEN, "Genomic analysis of smooth muscle cells in 3-dimensional collagen matrix," *The FASEB Journal*, vol. 17, no. 1, pp. 97–99, jan 2003. [Online]. Available: http://www.fasebj.org/doi/10.1096/fj.02-0256fje

[219] M. Itoh, C. M. Nelson, C. A. Myers, and M. J. Bissell, "Rap1 Integrates Tissue Polarity, Lumen Formation, and Tumorigenic Potential in Human Breast Epithelial Cells," *Cancer Research*, vol. 67, no. 10, pp. 4759–4766, may 2007. [Online]. Available: http://cancerres.aacrjournals.org/cgi/doi/10.1158/0008-5472.CAN-06-4246

[220] V. Aranda, T. Haire, M. E. Nolan, J. P. Calarco, A. Z. Rosenberg, J. P. Fawcett, T. Pawson, and S. K. Muthuswamy, "Par6–aPKC uncouples ErbB2 induced disruption of polarized epithelial organization from proliferation control," *Nature Cell Biology*, vol. 8, no. 11, pp. 1235–1245, nov

2006. [Online]. Available: http://www.nature.com/articles/ncb1485

[221] E. Cukierman, “Taking Cell-Matrix Adhesions to the Third Dimension,” *Science*, vol. 294, no. 5547, pp. 1708–1712, nov 2001. [Online]. Available: http://www.sciencemag.org/cgi/doi/10.1126/science.1064829

[222] F. Grinnell, “Fibroblast biology in three-dimensional collagen matrices,” *Trends in Cell Biology*, vol. 13, no. 5, pp. 264–269, may 2003. [Online]. Available: https://linkinghub.elsevier.com/retrieve/pii/S0962892403000576

[223] K. Sugawara, D. Tsuruta, M. Ishii, J. C. Jones, and H. Kobayashi, “Laminin-332 and -511 in skin,” *Experimental Dermatology*, vol. 17, no. 6, pp. 473–480, 2008.

[224] H. Y. Irie, R. V. Pearline, D. Grueneberg, M. Hsia, P. Ravichandran, N. Kothari, S. Natesan, and J. S. Brugge, “Distinct roles of Akt1 and Akt2 in regulating cell migration and epithelial–mesenchymal transition,” *The Journal of Cell Biology*, vol. 171, no. 6, pp. 1023–1034, dec 2005. [Online]. Available: http://www.jcb.org/lookup/doi/10.1083/jcb.200505087

[225] B. Fallica, J. S. Maffei, S. Villa, G. Makin, and M. Zaman, “Alteration of Cellular Behavior and Response to PI3K Pathway Inhibition by Culture in 3D Collagen Gels,” *PLoS ONE*, vol. 7, no. 10, p. e48024, oct 2012. [Online]. Available: https://dx.plos.org/10.1371/journal.pone.0048024

[226] J. E. Barralet, L. Wang, M. Lawson, J. T. Triffitt, P. R. Cooper, and R. M. Shelton, “Comparison of bone marrow cell growth on 2D and 3D alginate hydrogels,” *Journal of Materials Science: Materials in Medicine*, vol. 16, no. 6, pp. 515–519, jun 2005. [Online]. Available: http://link.springer.com/10.1007/s10856-005-0526-z

[227] E. L. Baker, J. Srivastava, D. Yu, R. T. Bonnecaze, and M. H. Zaman, “Cancer Cell Migration: Integrated Roles of Matrix Mechanics and Transforming Potential,” *PLoS ONE*, vol. 6, no. 5, p. e20355, may 2011. [Online]. Available: https://dx.plos.org/10.1371/journal.pone.0020355

[228] S. Even-Ram and K. M. Yamada, “Cell migration in 3D matrix,” *Current Opinion in Cell Biology*, vol. 17, no. 5, pp. 524–532, oct 2005. [Online]. Available: https://linkinghub.elsevier.com/retrieve/pii/S0955067405001183

[229] K. E. Fisher, A. Pop, W. Koh, N. J. Anthis, W. B. Saunders, and G. E. Davis, “Tumor cell invasion of collagen matrices requires coordinate lipid agonist-induced G-protein and membrane-type matrix metalloproteinase-1-dependent signaling,” *Molecular Cancer*, vol. 5, pp. 1–23, 2006.

[230] R. Pankov, Y. Endo, S. Even-Ram, M. Araki, K. Clark, E. Cukierman, K. Matsumoto, and K. M. Yamada, “A Rac switch regulates random versus directionally persistent cell migration,” *The Journal of Cell Biology*, vol. 170, no. 5, pp. 793–802, aug 2005. [Online]. Available: http://www.jcb.org/lookup/doi/10.1083/jcb.200503152

[231] N. S. Hwang, S. Varghese, P. Theprungsirikul, A. Canver, and J. Elisseeff, “Enhanced chondrogenic differentiation of murine embryonic stem cells in hydrogels with glucosamine,”

Biomaterials, vol. 27, no. 36, pp. 6015–6023, dec 2006. [Online]. Available: https://linkinghub.elsevier.com/retrieve/pii/S0142961206005898

[232] E. G. Z. Centeno, H. Cimarosti, and A. Bithell, "2D versus 3D human induced pluripotent stem cell-derived cultures for neurodegenerative disease modelling," *Molecular Neurodegeneration*, vol. 13, no. 1, p. 27, dec 2018. [Online]. Available: https://molecularneurodegeneration.biomedcentral.com/articles/10.1186/s13024-018-0258-4

[233] A. S. Ribeiro, E. M. Powell, and J. B. Leach, "Neural Stem Cell Differentiation in 2D and 3D Microenvironments," in *26th Southern Biomedical Engineering Conference SBEC 2010, April 30 - May 2, 2010, College Park, Maryland, USA*, K. E. Herold, J. Vossoughi, and W. E. Bentley, Eds. Berlin, Heidelberg: Springer Berlin Heidelberg, 2010, pp. 422–425.

[234] D. E. Discher, P. Janmey, and Y.-l. Wang, "Tissue Cells Feel and Respond to the Stiffness of Their Substrate," *Science*, vol. 310, no. 5751, pp. 1139–1143, nov 2005. [Online]. Available: http://www.sciencemag.org/cgi/doi/10.1126/science.1116995

[235] C. M. Nelson and M. J. Bissell, "Of Extracellular Matrix, Scaffolds, and Signaling: Tissue Architecture Regulates Development, Homeostasis, and Cancer," *Annual Review of Cell and Developmental Biology*, vol. 22, no. 1, pp. 287–309, nov 2006. [Online]. Available: http://www.annualreviews.org/doi/10.1146/annurev.cellbio.22.010305.104315

[236] S. R. Caliari and J. A. Burdick, "A practical guide to hydrogels for cell culture," *Nature Methods*, vol. 13, no. 5, pp. 405–414, may 2016. [Online]. Available: http://dx.doi.org/10.1038/nmeth.3839http://www.nature.com/articles/nmeth.3839

[237] A. J. Engler, S. Sen, H. L. Sweeney, and D. E. Discher, "Matrix Elasticity Directs Stem Cell Lineage Specification," *Cell*, vol. 126, no. 4, pp. 677–689, aug 2006. [Online]. Available: https://linkinghub.elsevier.com/retrieve/pii/S0092867406009615

[238] K. Kolind, K. W. Leong, F. Besenbacher, and M. Foss, "Guidance of stem cell fate on 2D patterned surfaces," *Biomaterials*, vol. 33, no. 28, pp. 6626–6633, oct 2012. [Online]. Available: http://dx.doi.org/10.1016/j.biomaterials.2012.05.070https://linkinghub.elsevier.com/retrieve/pii/S0142961212006345

[239] M. Thery, "Micropatterning as a tool to decipher cell morphogenesis and functions," *Journal of Cell Science*, vol. 123, no. 24, pp. 4201–4213, dec 2010. [Online]. Available: http://jcs.biologists.org/cgi/doi/10.1242/jcs.075150

[240] M. Ghibaudo, L. Trichet, J. Le Digabel, A. Richert, P. Hersen, and B. Ladoux, "Substrate Topography Induces a Crossover from 2D to 3D Behavior in Fibroblast Migration," *Biophysical Journal*, vol. 97, no. 1, pp. 357–368, jul 2009. [Online]. Available: https://linkinghub.elsevier.com/retrieve/pii/S0006349509008546

[241] V. Weaver, O. Petersen, F. Wang, C. Larabell, P. Briand, C. Damsky, and M. Bissell, "Reversion

of the Malignant Phenotype of Human Breast Cells in Three-Dimensional Culture and In Vivo by Integrin Blocking Antibodies," *The Journal of Cell Biology*, vol. 137, no. 1, pp. 231–245, apr 1997. [Online]. Available: http://www.jcb.org/lookup/doi/10.1083/jcb.137.1.231

[242] T. Gudjonsson, L. Rønnov-Jessen, R. Villadsen, F. Rank, M. J. Bissell, and O. W. Petersen, "Normal and tumor-derived myoepithelial cells differ in their ability to interact with luminal breast epithelial cells for polarity and basement membrane deposition." *Journal of cell science*, vol. 115, no. 1, pp. 39–50, 2002. [Online]. Available: http://www.ncbi.nlm.nih.gov/pubmed/11801722{%}0Ahttp://www.pubmedcentral.nih.gov/articlerender.fcgi?artid=PMC2933194

[243] G. Y. Lee, P. A. Kenny, E. H. Lee, and M. J. Bissell, "Three-dimensional culture models of normal and malignant breast epithelial cells," *Nature Methods*, vol. 4, no. 4, pp. 359–365, apr 2007. [Online]. Available: http://www.nature.com/articles/nmeth1015

[244] B. Muz, P. de la Puente, F. Azab, and A. K. Azab, "The role of hypoxia in cancer progression, angiogenesis, metastasis, and resistance to therapy," *Hypoxia*, p. 83, dec 2015. [Online]. Available: https://www.dovepress.com/the-role-of-hypoxia-in-cancer-progression-angiogenesis-metastasis-and--peer-reviewed-article-HP

[245] S. Däster, N. Amatruda, D. Calabrese, R. Ivanek, E. Turrini, R. A. Droeser, P. Zajac, C. Fimognari, G. C. Spagnoli, G. Iezzi, V. Mele, and M. G. Muraro, "Induction of hypoxia and necrosis in multicellular tumor spheroids is associated with resistance to chemotherapy treatment," *Oncotarget*, vol. 8, no. 1, pp. 1725–1736, jan 2017. [Online]. Available: http://www.oncotarget.com/abstract/13857http://www.oncotarget.com/fulltext/13857

[246] L. M. Brown, R. L. Cowen, C. Debray, A. Eustace, J. T. Erler, F. C. D. Sheppard, C. A. Parker, I. J. Stratford, and K. J. Williams, "Reversing Hypoxic Cell Chemoresistance in Vitro Using Genetic and Small Molecule Approaches Targeting Hypoxia Inducible Factor-1," *Molecular Pharmacology*, vol. 69, no. 2, pp. 411–418, nov 2005. [Online]. Available: http://molpharm.aspetjournals.org/cgi/doi/10.1124/mol.105.015743

[247] J. Y. Kim and J. Y. Lee, "Targeting Tumor Adaption to Chronic Hypoxia: Implications for Drug Resistance, and How It Can Be Overcome," *International Journal of Molecular Sciences*, vol. 18, no. 9, p. 1854, aug 2017. [Online]. Available: http://www.mdpi.com/1422-0067/18/9/1854

[248] N. Rohwer and T. Cramer, "Hypoxia-mediated drug resistance: Novel insights on the functional interaction of HIFs and cell death pathways," *Drug Resistance Updates*, vol. 14, no. 3, pp. 191–201, 2011. [Online]. Available: http://dx.doi.org/10.1016/j.drup.2011.03.001

[249] S. A. Langhans, "Three-Dimensional in Vitro Cell Culture Models in Drug Discovery and Drug Repositioning," *Frontiers in Pharmacology*, vol. 9, no. JAN, pp. 1–14, jan 2018. [Online]. Available: http://journal.frontiersin.org/article/10.3389/fphar.2018.00006/full

[250] R. Z. Lin and H. Y. Chang, "Recent advances in three-dimensional multicellular spheroid culture

for biomedical research," *Biotechnology Journal*, vol. 3, no. 9-10, pp. 1172–1184, 2008.

[251] H. Liu, Y. Han, L.-L. Ye, Z.-L. Chen, X.-M. Liu, S.-C. Li, B.-C. Wu, and Q.-W. Wang, "Cultivation of Recombinant Chinese hamster ovary cells grown as suspended aggregates in stirred vessels," *Journal of Bioscience and Bioengineering*, vol. 102, no. 5, pp. 430–435, 2006.

[252] B. K. Jong, "Three-dimensional tissue culture models in cancer biology," *Seminars in Cancer Biology*, vol. 15, no. 5 SPEC. ISS., pp. 365–377, 2005.

[253] M. Ingram, G. B. Techy, R. Saroufeem, O. Yazan, K. S. Narayan, T. J. Goodwin, and G. F. Spaulding, "Three-dimensional growth patterns of various human tumor cell lines in simulated microgravity of a NASA bioreactor," *In Vitro Cellular & Developmental Biology - Animal*, vol. 33, no. 6, pp. 459–466, jun 1997. [Online]. Available: http://link.springer.com/10.1007/s11626-997-0064-8

[254] R. L. Carpenedo, C. Y. Sargent, and T. C. McDevitt, "Rotary Suspension Culture Enhances the Efficiency, Yield, and Homogeneity of Embryoid Body Differentiation," *STEM CELLS*, vol. 25, no. 9, pp. 2224–2234, sep 2007. [Online]. Available: http://doi.wiley.com/10.1634/stemcells.2006-0523

[255] T. J. Goodwin, T. L. Prewett, D. A. Wolf, and G. F. Spaulding, "Reduced shear stress: A major component in the ability of mammalian tissues to form three-dimensional assemblies in simulated microgravity," *Journal of Cellular Biochemistry*, vol. 51, no. 3, pp. 301–311, mar 1993. [Online]. Available: http://doi.wiley.com/10.1002/jcb.240510309

[256] M. Shri, H. Agrawal, P. Rani, D. Singh, and S. K. Onteru, "Hanging drop, a best three-dimensional (3D) culture method for primary buffalo and sheep hepatocytes," *Scientific Reports*, vol. 7, no. 1, pp. 1–13, 2017. [Online]. Available: http://dx.doi.org/10.1038/s41598-017-01355-6

[257] S. Wang, X. Wang, J. Boone, J. Wie, K. P. Yip, J. Zhang, L. Wang, and R. Liu, "Application of Hanging Drop Technique for Kidney Tissue Culture," *Kidney and Blood Pressure Research*, vol. 42, no. 2, pp. 220–231, 2017.

[258] N. E. Timmins and L. K. Nielsen, "Generation of Multicellular Tumor Spheroids by the Hanging-Drop Method BT - Tissue Engineering," H. Hauser and M. Fussenegger, Eds. Totowa, NJ: Humana Press, 2007, pp. 141–151. [Online]. Available: https://doi.org/10.1007/978-1-59745-443-8{_}8

[259] D. Del Duca, T. Werbowetski, and R. F. Del Maestro, "Spheroid preparation from hanging drops: Characterization of a model of brain tumor invasion," *Journal of Neuro-Oncology*, vol. 67, no. 3, pp. 295–303, 2004.

[260] A. Ivascu and M. Kubbies, "Rapid generation of single-tumor spheroids for high-throughput cell function and toxicity analysis," *Journal of Biomolecular Screening*, vol. 11, no. 8, pp. 922–932, 2006.

[261] A. L. Howes, R. D. Richardson, D. Finlay, and K. Vuori, “3-Dimensional Culture Systems for Anti-Cancer Compound Profiling and High-Throughput Screening Reveal Increases in EGFR Inhibitor-Mediated Cytotoxicity Compared to Monolayer Culture Systems,” *PLoS One*, vol. 9, no. 9, p. e108283, sep 2014. [Online]. Available: https://dx.plos.org/10.1371/journal.pone.0108283

[262] M. T. Cook, D. Y. S. Chau, S. Shafaie, V. Hutter, and M. B. Brown, “Influence of surface geometry on the culture of human cell lines: A comparative study using flat, round-bottom and v-shaped 96 well plates,” *Plos One*, vol. 12, no. 10, p. e0186799, 2017.

[263] A. Nagelkerke, J. Bussink, F. C. Sweep, and P. N. Span, “Generation of multicellular tumor spheroids of breast cancer cells: How to go three-dimensional,” *Analytical Biochemistry*, vol. 437, no. 1, pp. 17–19, jun 2013. [Online]. Available: http://dx.doi.org/10.1016/j.ab.2013.02.004https://linkinghub.elsevier.com/retrieve/pii/S0003269713000766

[264] Y. Li and E. Kumacheva, “Hydrogel microenvironments for cancer spheroid growth and drug screening,” *Science Advances*, vol. 4, no. 4, p. eaas8998, apr 2018. [Online]. Available: http://advances.sciencemag.org/lookup/doi/10.1126/sciadv.aas8998

[265] A. Zuchowska, E. Jastrzebska, M. Chudy, A. Dybko, and Z. Brzozka, “3D lung spheroid cultures for evaluation of photodynamic therapy (PDT) procedures in microfluidic Lab-on-a-Chip system,” *Analytica Chimica Acta*, vol. 990, pp. 110–120, oct 2017. [Online]. Available: https://doi.org/10.1016/j.aca.2017.07.009https://linkinghub.elsevier.com/retrieve/pii/S0003267017307948

[266] Y. Abe, A. Tada, J. Isoyama, S. Nagayama, R. Yao, J. Adachi, and T. Tomonaga, “Improved phosphoproteomic analysis for phosphosignaling and active-kinome profiling in Matrigel-embedded spheroids and patient-derived organoids,” *Scientific Reports*, vol. 8, no. 1, pp. 1–12, 2018.

[267] K. M. Charoen, B. Fallica, Y. L. Colson, M. H. Zaman, and M. W. Grinstaff, “Embedded multicellular spheroids as a biomimetic 3D cancer model for evaluating drug and drug-device combinations,” *Biomaterials*, vol. 35, no. 7, pp. 2264–2271, 2014. [Online]. Available: http://dx.doi.org/10.1016/j.biomaterials.2013.11.038

[268] G. Cheng, J. Tse, R. K. Jain, and L. L. Munn, “Micro-environmental mechanical stress controls tumor spheroid size and morphology by suppressing proliferation and inducing apoptosis in cancer cells,” *PLoS One*, vol. 4, no. 2, 2009.

[269] A. Aung, J. Theprungsirikul, H. L. Lim, and S. Varghese, “Chemotaxis-driven assembly of endothelial barrier in a tumor-on-a-chip platform,” *Lab on a Chip*, vol. 16, no. 10, pp. 1886–1898, 2016.

[270] E. Y. Tokuda, C. E. Jones, and K. S. Anseth, “PEG–peptide hydrogels reveal differential

effects of matrix microenvironmental cues on melanoma drug sensitivity," *Integrative Biology*, vol. 9, no. 1, pp. 76–87, 2017. [Online]. Available: http://dx.doi.org/10.1039/C6IB00229Chttps://academic.oup.com/ib/article/9/1/76-87/5096888

[271] T.-M. Achilli, J. Meyer, and J. R. Morgan, "Advances in the formation, use and understanding of multi-cellular spheroids," *Expert Opinion on Biological Therapy*, vol. 12, no. 10, pp. 1347–1360, 2012.

[272] A. Dongre and R. A. Weinberg, "New insights into the mechanisms of epithelial–mesenchymal transition and implications for cancer," *Nature Reviews Molecular Cell Biology*, vol. 20, no. 2, pp. 69–84, feb 2019. [Online]. Available: http://dx.doi.org/10.1038/s41580-018-0080-4http://www.nature.com/articles/s41580-018-0080-4

[273] J. P. Thiery and J. P. Sleeman, "Complex networks orchestrate epithelial-mesenchymal transitions," *Nature Reviews Molecular Cell Biology*, vol. 7, no. 2, pp. 131–142, 2006.

[274] J. P. Thiery, H. Acloque, R. Y. Huang, and M. A. Nieto, "Epithelial-Mesenchymal Transitions in Development and Disease," *Cell*, vol. 139, no. 5, pp. 871–890, 2009.

[275] J. M. Lee, S. Dedhar, R. Kalluri, and E. W. Thompson, "The epithelial-mesenchymal transition: New insights in signaling, development, and disease," *Journal of Cell Biology*, vol. 172, no. 7, pp. 973–981, 2006.

[276] G. Greenburg and E. D. Hay, "Epithelia suspended in collagen gels can lose polarity and express characteristics of migrating mesenchymal cells," *The Journal of Cell Biology*, vol. 95, no. 1, pp. 333–339, oct 1982. [Online]. Available: http://www.jcb.org/cgi/doi/10.1083/jcb.95.1.333

[277] E. D. Hay, "An overview of epithelio-mesenchymal transformation." pp. 8–20, 1995. [Online]. Available: http://www.ncbi.nlm.nih.gov/pubmed/8714286

[278] M. A. Nieto, R. Y. Y. Huang, R. A. A. Jackson, and J. P. P. Thiery, "Emt: 2016," *Cell*, vol. 166, no. 1, pp. 21–45, 2016.

[279] D. Tarin, "The Fallacy of Epithelial Mesenchymal Transition in Neoplasia," *Cancer Research*, vol. 65, no. 14, pp. 5996–6001, jul 2005. [Online]. Available: http://cancerres.aacrjournals.org/lookup/doi/10.1158/0008-5472.CAN-05-0699

[280] J. W. O'Connor and E. W. Gomez, "Biomechanics of TGFβ-induced epithelial-mesenchymal transition: implications for fibrosis and cancer," *Clinical and Translational Medicine*, vol. 3, no. 1, p. 23, 2014.

[281] G. Moreno-Bueno, F. Portillo, and A. Cano, "Transcriptional regulation of cell polarity in EMT and cancer," *Oncogene*, vol. 27, no. 55, pp. 6958–6969, nov 2008. [Online]. Available: http://www.nature.com/articles/onc2008346

[282] L. Sun and J. Fang, "Epigenetic regulation of epithelial–mesenchymal transition," *Cellular*

and Molecular Life Sciences, vol. 73, no. 23, pp. 4493–4515, dec 2016. [Online]. Available: http://link.springer.com/10.1007/s00018-016-2303-1

[283] T. Kiesslich, M. Pichler, and D. Neureiter, "Epigenetic control of epithelial-mesenchymal-transition in human cancer," *Molecular and Clinical Oncology*, vol. 1, no. 1, pp. 3–11, jan 2013. [Online]. Available: https://www.spandidos-publications.com/10.3892/mco.2012.28

[284] V. M. Díaz, R. Viñas-Castells, and A. G. De Herreros, "Regulation of the protein stability of EMT transcription factors," *Cell Adhesion and Migration*, vol. 8, no. 4, pp. 418–428, 2014.

[285] I. M. Shapiro, A. W. Cheng, N. C. Flytzanis, M. Balsamo, J. S. Condeelis, M. H. Oktay, C. B. Burge, and F. B. Gertler, "An EMT–Driven Alternative Splicing Program Occurs in Human Breast Cancer and Modulates Cellular Phenotype," *PLoS Genetics*, vol. 7, no. 8, p. e1002218, aug 2011. [Online]. Available: http://dx.plos.org/10.1371/journal.pgen.1002218

[286] Y. Yang, J. W. Park, T. W. Bebee, C. C. Warzecha, Y. Guo, X. Shang, Y. Xing, and R. P. Carstens, "Determination of a Comprehensive Alternative Splicing Regulatory Network and Combinatorial Regulation by Key Factors during the Epithelial-to-Mesenchymal Transition," *Molecular and Cellular Biology*, vol. 36, no. 11, pp. 1704–1719, jun 2016. [Online]. Available: http://mcb.asm.org/lookup/doi/10.1128/MCB.00019-16

[287] D. Pradella, C. Naro, C. Sette, and C. Ghigna, "EMT and stemness: flexible processes tuned by alternative splicing in development and cancer progression," *Molecular Cancer*, vol. 16, no. 1, p. 8, dec 2017. [Online]. Available: http://dx.doi.org/10.1186/s12943-016-0579-2http://molecular-cancer.biomedcentral.com/articles/10.1186/s12943-016-0579-2

[288] B. P. Zhou, J. Deng, W. Xia, J. Xu, Y. M. Li, M. Gunduz, and M.-C. Hung, "Dual regulation of Snail by GSK-3β-mediated phosphorylation in control of epithelial–mesenchymal transition," *Nature Cell Biology*, vol. 6, no. 10, pp. 931–940, oct 2004. [Online]. Available: http://www.nature.com/articles/ncb1173

[289] Z. Yang, S. Rayala, D. Nguyen, R. K. Vadlamudi, S. Chen, and R. Kumar, "Pak1 Phosphorylation of Snail, a Master Regulator of Epithelial-to-Mesenchyme Transition, Modulates Snail's Subcellular Localization and Functions," *Cancer Research*, vol. 65, no. 8, pp. 3179–3184, apr 2005. [Online]. Available: http://cancerres.aacrjournals.org/lookup/doi/10.1158/0008-5472.CAN-04-3480

[290] R. Kalluri and R. A. Weinberg, "The basics of epithelial-mesenchymal transition," *Journal of Clinical Investigation*, vol. 119, no. 6, pp. 1420–1428, jun 2009. [Online]. Available: http://www.jci.org/articles/view/39104

[291] J. P. Thiery, "Epithelial–mesenchymal transitions in tumour progression," *Nature Reviews Cancer*, vol. 2, no. 6, pp. 442–454, jun 2002. [Online]. Available: http://www.nature.com/articles/nrc822

[292] H. Peinado, D. Olmeda, and A. Cano, “Snail, Zeb and bHLH factors in tumour progression: an alliance against the epithelial phenotype?” *Nature Reviews Cancer*, vol. 7, no. 6, pp. 415–428, jun 2007. [Online]. Available: http://www.nature.com/articles/nrc2131

[293] A. Cano, M. A. Pérez-Moreno, I. Rodrigo, A. Locascio, M. J. Blanco, M. G. del Barrio, F. Portillo, and M. A. Nieto, “The transcription factor Snail controls epithelial–mesenchymal transitions by repressing E-cadherin expression,” *Nature Cell Biology*, vol. 2, no. 2, pp. 76–83, feb 2000. [Online]. Available: http://www.nature.com/articles/ncb0200{_}76

[294] E. Batlle, E. Sancho, C. Francí, D. Domínguez, M. Monfar, J. Baulida, and A. García de Herreros, “The transcription factor Snail is a repressor of E-cadherin gene expression in epithelial tumour cells,” *Nature Cell Biology*, vol. 2, no. 2, pp. 84–89, feb 2000. [Online]. Available: http://www.nature.com/articles/ncb0200{_}84

[295] E. Sánchez-Tilló, A. Lázaro, R. Torrent, M. Cuatrecasas, E. C. Vaquero, A. Castells, P. Engel, and A. Postigo, “ZEB1 represses E-cadherin and induces an EMT by recruiting the SWI/SNF chromatin-remodeling protein BRG1,” *Oncogene*, vol. 29, no. 24, pp. 3490–3500, jun 2010. [Online]. Available: http://www.nature.com/articles/onc2010102

[296] R. Y.-J. Huang, P. Guilford, and J. P. Thiery, “Early events in cell adhesion and polarity during epithelial-mesenchymal transition,” *Journal of Cell Science*, vol. 125, no. 19, pp. 4417–4422, 2012.

[297] S. Lamouille, J. Xu, and R. Derynck, “Molecular mechanisms of epithelial-mesenchymal transition,” *Nature Reviews Molecular Cell Biology*, vol. 15, no. 3, pp. 178–196, 2014. [Online]. Available: http://dx.doi.org/10.1038/nrm3758

[298] M. J. Wheelock, Y. Shintani, M. Maeda, Y. Fukumoto, and K. R. Johnson, “Cadherin switching,” *Journal of Cell Science*, vol. 121, no. 6, pp. 727–735, feb 2008. [Online]. Available: http://jcs.biologists.org/cgi/doi/10.1242/jcs.000455

[299] A. Satelli and S. Li, “Vimentin in cancer and its potential as a molecular target for cancer therapy,” *Cellular and Molecular Life Sciences*, vol. 68, no. 18, pp. 3033–3046, sep 2011. [Online]. Available: http://link.springer.com/10.1007/s00018-011-0735-1

[300] V. Cantemir, D. Cai, M. Reedy, and P. Brauer, “Tissue inhibitor of metalloproteinase-2 (TIMP-2) expression during cardiac neural crest cell migration and its role in proMMP-2 activation,” *Developmental Dynamics*, vol. 231, no. 4, pp. 709–719, dec 2004. [Online]. Available: http://doi.wiley.com/10.1002/dvdy.20171

[301] D. Cai and P. Brauer, “Synthetic matrix metalloproteinase inhibitor decreases early cardiac neural crest migration in chicken embryos,” *Developmental Dynamics*, vol. 224, no. 4, pp. 441–449, aug 2002. [Online]. Available: http://doi.wiley.com/10.1002/dvdy.10129

[302] J. E. Fata, Z. Werb, and M. J. Bissell, “Regulation of mammary gland branching morphogenesis

by the extracellular matrix and its remodeling enzymes," *Breast Cancer Research*, vol. 6, no. 1, p. 1, feb 2003. [Online]. Available: http://breast-cancer-research.biomedcentral.com/articles/10.1186/bcr634

[303] E. S. Radisky and D. C. Radisky, "Matrix Metalloproteinase-Induced Epithelial-Mesenchymal Transition in Breast Cancer," *Journal of Mammary Gland Biology and Neoplasia*, vol. 15, no. 2, pp. 201–212, jun 2010. [Online]. Available: http://link.springer.com/10.1007/s10911-010-9177-x

[304] H. Kouros-Mehr and Z. Werb, "Candidate regulators of mammary branching morphogenesis identified by genome-wide transcript analysis," *Developmental Dynamics*, vol. 235, no. 12, pp. 3404–3412, dec 2006. [Online]. Available: http://doi.wiley.com/10.1002/dvdy.20978

[305] C. J. Simpson, R. S. Talhouk, C. M. Alexander, J. R. Chin, S. M. Clift, M. J. Bissell, and Z. Werb, "Targeted expression of stromelysin-1 in mammary gland provides evidence for a role of proteinases in branching morphogenesis and the requirement for an intact basement membrane for tissue-specific gene expression," *The Journal of Cell Biology*, vol. 125, no. 3, pp. 681–693, may 1994. [Online]. Available: http://www.jcb.org/cgi/doi/10.1083/jcb.125.3.681

[306] L. S. Orlichenko and D. C. Radisky, "Matrix metalloproteinases stimulate epithelial-mesenchymal transition during tumor development," *Clinical & Experimental Metastasis*, vol. 25, no. 6, pp. 593–600, oct 2008. [Online]. Available: http://link.springer.com/10.1007/s10585-008-9143-9

[307] M. Giannandrea and W. C. Parks, "Diverse functions of matrix metalloproteinases during fibrosis," *Disease Models & Mechanisms*, vol. 7, no. 2, pp. 193–203, feb 2014. [Online]. Available: http://dmm.biologists.org/cgi/doi/10.1242/dmm.012062

[308] C. Gialeli, A. D. Theocharis, and N. K. Karamanos, "Roles of matrix metalloproteinases in cancer progression and their pharmacological targeting," *FEBS Journal*, vol. 278, no. 1, pp. 16–27, jan 2011. [Online]. Available: http://doi.wiley.com/10.1111/j.1742-4658.2010.07919.x

[309] D. C. Radisky and J. A. Przybylo, "Matrix Metalloproteinase-induced Fibrosis and Malignancy in Breast and Lung," *Proceedings of the American Thoracic Society*, vol. 5, no. 3, pp. 316–322, apr 2008. [Online]. Available: http://pats.atsjournals.org/cgi/doi/10.1513/pats.200711-166DR

[310] J. Xu, S. Lamouille, and R. Derynck, "TGF-β-induced epithelial to mesenchymal transition," *Cell Research*, vol. 19, no. 2, pp. 156–172, feb 2009. [Online]. Available: http://www.nature.com/articles/cr20095

[311] Z. Wang, Y. Li, D. Kong, and F. H. Sarkar, "The Role of Notch Signaling Pathway in Epithelial-Mesenchymal Transition (EMT) During Development and Tumor Aggressiveness," *Current Drug Targets*, vol. 11, no. 6, pp. 745–751, jun 2010. [Online]. Available: http://www.ncbi.nlm.nih.gov/pubmed/20041844{%}0Ahttp://www.pubmedcentral.nih.

gov/articlerender.fcgi?artid=PMC3084452http://www.eurekaselect.com/openurl/content.php?genre=article{&}issn=1389-4501{&}volume=11{&}issue=6{&}spage=745

[312] N. M. Ghahhari and S. Babashah, “Interplay between microRNAs and WNT/β-catenin signalling pathway regulates epithelial–mesenchymal transition in cancer,” *European Journal of Cancer*, vol. 51, no. 12, pp. 1638–1649, aug 2015. [Online]. Available: http://dx.doi.org/10.1016/j.ejca.2015.04.021https://linkinghub.elsevier.com/retrieve/pii/S0959804915003834

[313] U. Valcourt, M. Kowanetz, H. Niimi, C.-H. Heldin, and A. Moustakas, “TGF-β and the Smad Signaling Pathway Support Transcriptomic Reprogramming during Epithelial-Mesenchymal Cell Transition,” *Molecular Biology of the Cell*, vol. 16, no. 4, pp. 1987–2002, apr 2005. [Online]. Available: http://www.molbiolcell.org/cgi/doi/10.1091/mbc.E04?10?0867http://www.molbiolcell.org/doi/10.1091/mbc.e04-08-0658

[314] X.-H. Feng and R. Derynck, “Specificity and Versatility in TGF-β Signaling Through Smads,” *Annual Review of Cell and Developmental Biology*, vol. 21, no. 1, pp. 659–693, nov 2005. [Online]. Available: http://www.annualreviews.org/doi/10.1146/annurev.cellbio.21.022404.142018

[315] D. Peng, L. Fu, and G. Sun, “Expression analysis of the TGF-β/SMAD target genes in adenocarcinoma of esophagogastric junction,” *Open Medicine (Poland)*, vol. 11, no. 1, pp. 83–86, 2016.

[316] A. Dhasarathy, D. Phadke, D. Mav, R. R. Shah, and P. A. Wade, “The Transcription Factors Snail and Slug Activate the Transforming Growth Factor-Beta Signaling Pathway in Breast Cancer,” *PLoS ONE*, vol. 6, no. 10, p. e26514, oct 2011. [Online]. Available: https://dx.plos.org/10.1371/journal.pone.0026514

[317] S. Grelet, L. A. Link, B. Howley, C. Obellianne, V. Palanisamy, V. K. Gangaraju, J. A. Diehl, and P. H. Howe, “A regulated PNUTS mRNA to lncRNA splice switch mediates EMT and tumour progression,” *Nature Cell Biology*, vol. 19, no. 9, pp. 1105–1115, sep 2017. [Online]. Available: http://www.nature.com/articles/ncb3595

[318] A. Chaudhury, G. S. Hussey, P. S. Ray, G. Jin, P. L. Fox, and P. H. Howe, “TGF-β-mediated phosphorylation of hnRNP E1 induces EMT via transcript-selective translational induction of Dab2 and ILEI,” *Nature Cell Biology*, vol. 12, no. 3, pp. 286–293, mar 2010. [Online]. Available: http://dx.doi.org/10.1038/ncb2029http://www.nature.com/articles/ncb2029

[319] X. Ye and R. A. Weinberg, “The SUMO guards for SNAIL,” *Oncotarget*, vol. 8, no. 58, pp. 97 701–97 702, nov 2017. [Online]. Available: http://www.oncotarget.com/fulltext/22432

[320] C. Scheel, E. N. Eaton, S. H. J. Li, C. L. Chaffer, F. Reinhardt, K. J. Kah, G. Bell, W. Guo, J. Rubin, A. L. Richardson, and R. A. Weinberg, “Paracrine and autocrine signals induce and maintain mesenchymal and stem cell states in the breast,” *Cell*, vol. 145, no. 6, pp. 926–940,

2011. [Online]. Available: http://dx.doi.org/10.1016/j.cell.2011.04.029

[321] D. E. Jaalouk and J. Lammerding, “Mechanotransduction gone awry,” *Nature Reviews Molecular Cell Biology*, vol. 10, no. 1, pp. 63–73, 2009.

[322] S. C. Wei and J. Yang, “Forcing through Tumor Metastasis: The Interplay between Tissue Rigidity and Epithelial-Mesenchymal Transition,” *Trends in Cell Biology*, vol. 26, no. 2, pp. 111–120, 2016. [Online]. Available: http://dx.doi.org/10.1016/j.tcb.2015.09.009

[323] J. Fenner, A. C. Stacer, F. Winterroth, T. D. Johnson, K. E. Luker, and G. D. Luker, “Macroscopic Stiffness of Breast Tumors Predicts Metastasis,” *Scientific Reports*, vol. 4, no. 1, p. 5512, may 2015. [Online]. Available: http://www.nature.com/articles/srep05512

[324] N. F. Boyd, L. J. Martin, M. J. Yaffe, and S. Minkin, “Mammographic density and breast cancer risk: current understanding and future prospects,” *Breast Cancer Research*, vol. 13, no. 6, p. 223, dec 2011. [Online]. Available: http://breast-cancer-research.biomedcentral.com/articles/10.1186/bcr2942

[325] M. J. Paszek, N. Zahir, K. R. Johnson, J. N. Lakins, G. I. Rozenberg, A. Gefen, C. A. Reinhart-King, S. S. Margulies, M. Dembo, D. Boettiger, D. A. Hammer, and V. M. Weaver, “Tensional homeostasis and the malignant phenotype,” *Cancer Cell*, vol. 8, no. 3, pp. 241–254, 2005.

[326] S. C. Wei, L. Fattet, J. H. Tsai, Y. Guo, V. H. Pai, H. E. Majeski, A. C. Chen, R. L. Sah, S. S. Taylor, A. J. Engler, and J. Yang, “Matrix stiffness drives epithelial–mesenchymal transition and tumour metastasis through a TWIST1–G3BP2 mechanotransduction pathway,” *Nature Cell Biology*, vol. 17, no. 5, pp. 678–688, may 2015. [Online]. Available: http://www.nature.com/articles/ncb3157

[327] S. P. Carey, K. E. Martin, and C. A. Reinhart-King, “Three-dimensional collagen matrix induces a mechanosensitive invasive epithelial phenotype,” *Scientific Reports*, vol. 7, no. February, pp. 1–14, 2017. [Online]. Available: http://dx.doi.org/10.1038/srep42088

[328] J. L. Leight, M. A. Wozniak, S. Chen, M. L. Lynch, and C. S. Chen, “Matrix rigidity regulates a switch between TGF-β1–induced apoptosis and epithelial–mesenchymal transition,” *Molecular Biology of the Cell*, vol. 23, no. 5, pp. 781–791, mar 2012. [Online]. Available: http://www.molbiolcell.org/doi/10.1091/mbc.e11-06-0537

[329] M. A. Nieto, “Epithelial-Mesenchymal Transitions in development and disease: Old views and new perspectives,” *International Journal of Developmental Biology*, vol. 53, no. 8-10, pp. 1541–1547, 2009.

[330] R. Bellairs, “The primitive streak,” *Anatomy and Embryology*, vol. 174, no. 1, pp. 1–14, apr 1986. [Online]. Available: https://doi.org/10.1007/BF00318331http://link.springer.com/10.1007/BF00318331

[331] J. P. Thiery, “Mechanisms of cell migration in the vertebrate embryo,” *Cell Differentiation*,

vol. 15, no. 1, pp. 1–15, nov 1984. [Online]. Available: http://www.sciencedirect.com/science/article/pii/0045603984900241https://linkinghub.elsevier.com/retrieve/pii/0045603984900241

[332] R. C. Stone, I. Pastar, N. Ojeh, V. Chen, S. Liu, K. I. Garzon, and M. Tomic-Canic, "Epithelial-mesenchymal transition in tissue repair and fibrosis," *Cell and Tissue Research*, vol. 365, no. 3, pp. 495–506, sep 2016. [Online]. Available: http://dx.doi.org/10.1007/s00441-016-2464-0http://link.springer.com/10.1007/s00441-016-2464-0

[333] P. A. Coulombe, "Wound Epithelialization: Accelerationg the Pace of Discovery," *Journal of Investigative Dermatology*, vol. 121, no. 2, pp. 219–230, aug 2003. [Online]. Available: https://linkinghub.elsevier.com/retrieve/pii/S0022202X15303511

[334] V. Arnoux, C. Côme, D. F. Kusewitt, L. G. Hudson, and P. Savagner, "Cutaneous Wound Reepithelialization: A Partial and Reversible EMT," in *Rise and Fall of Epithelial Phenotype: Concepts of Epithelial-Mesenchymal Transition*, P. Savagner, Ed. Boston, MA: Springer US, 2005, pp. 111–134. [Online]. Available: https://doi.org/10.1007/0-387-28671-3{_}8

[335] P. Nistico, M. J. Bissell, and D. C. Radisky, "Epithelial-Mesenchymal Transition: General Principles and Pathological Relevance with Special Emphasis on the Role of Matrix Metalloproteinases," *Cold Spring Harbor Perspectives in Biology*, vol. 4, no. 2, pp. a011 908–a011 908, feb 2012. [Online]. Available: http://cshperspectives.cshlp.org/lookup/doi/10.1101/cshperspect.a011908

[336] M. Iwano, D. Plieth, T. M. Danoff, C. Xue, H. Okada, and E. G. Neilson, "Evidence that fibroblasts derive from epithelium during tissue fibrosis," *Journal of Clinical Investigation*, vol. 110, no. 3, pp. 341–350, aug 2002. [Online]. Available: http://www.jci.org/articles/view/15518

[337] M. Yáñez-Mó, E. Lara-Pezzi, R. Selgas, M. Ramírez-Huesca, C. Domínguez-Jiménez, J. A. Jiménez-Heffernan, A. Aguilera, J. A. Sánchez-Tomero, M. A. Bajo, V. Álvarez, M. A. Castro, G. del Peso, A. Cirujeda, C. Gamallo, F. Sánchez-Madrid, and M. López-Cabrera, "Peritoneal Dialysis and Epithelial-to-Mesenchymal Transition of Mesothelial Cells," *New England Journal of Medicine*, vol. 348, no. 5, pp. 403–413, jan 2003. [Online]. Available: http://www.nejm.org/doi/abs/10.1056/NEJMoa020809

[338] K. K. Kim, M. C. Kugler, P. J. Wolters, L. Robillard, M. G. Galvez, A. N. Brumwell, D. Sheppard, and H. A. Chapman, "Alveolar epithelial cell mesenchymal transition develops in vivo during pulmonary fibrosis and is regulated by the extracellular matrix," *Proceedings of the National Academy of Sciences*, vol. 103, no. 35, pp. 13 180–13 185, aug 2006. [Online]. Available: http://www.pnas.org/cgi/doi/10.1073/pnas.0605669103

[339] E. M. Zeisberg, O. Tarnavski, M. Zeisberg, A. L. Dorfman, J. R. McMullen, E. Gustafsson, A. Chandraker, X. Yuan, W. T. Pu, A. B. Roberts, E. G. Neilson, M. H. Sayegh, S. Izumo, and R. Kalluri, "Endothelial-to-mesenchymal transition contributes to cardiac

fibrosis," *Nature Medicine*, vol. 13, no. 8, pp. 952–961, aug 2007. [Online]. Available: http://www.nature.com/articles/nm1613

[340] E. M. Zeisberg, S. E. Potenta, H. Sugimoto, M. Zeisberg, and R. Kalluri, "Fibroblasts in Kidney Fibrosis Emerge via Endothelial-to-Mesenchymal Transition," *Journal of the American Society of Nephrology*, vol. 19, no. 12, pp. 2282–2287, dec 2008. [Online]. Available: http://www.jasn.org/lookup/doi/10.1681/ASN.2008050513

[341] M. J. Blanco, G. Moreno-Bueno, D. Sarrio, A. Locascio, A. Cano, J. Palacios, and M. A. Nieto, "Correlation of Snail expression with histological grade and lymph node status in breast carcinomas," *Oncogene*, vol. 21, no. 20, pp. 3241–3246, may 2002. [Online]. Available: http://www.nature.com/articles/1205416

[342] K. Gravdal, O. J. Halvorsen, S. A. Haukaas, and L. A. Akslen, "A Switch from E-Cadherin to N-Cadherin Expression Indicates Epithelial to Mesenchymal Transition and Is of Strong and Independent Importance for the Progress of Prostate Cancer," *Clinical Cancer Research*, vol. 13, no. 23, pp. 7003–7011, dec 2007. [Online]. Available: http://clincancerres.aacrjournals.org/cgi/doi/10.1158/1078-0432.CCR-07-1263

[343] L. Prudkin, D. D. Liu, N. C. Ozburn, M. Sun, C. Behrens, X. Tang, K. C. Brown, B. N. Bekele, C. Moran, and I. I. Wistuba, "Epithelial-to-mesenchymal transition in the development and progression of adenocarcinoma and squamous cell carcinoma of the lung," *Modern Pathology*, vol. 22, no. 5, pp. 668–678, may 2009. [Online]. Available: http://dx.doi.org/10.1038/modpathol.2009.19http://www.nature.com/articles/modpathol200919

[344] X. Yan, L. Yan, S. Liu, Z. Shan, Y. Tian, and Z. Jin, "N-cadherin, a novel prognostic biomarker, drives malignant progression of colorectal cancer," *Molecular medicine reports*, vol. 12, no. 2, pp. 2999–3006, 2015.

[345] J. Huang, H. Li, and G. Ren, "Epithelial-mesenchymal transition and drug resistance in breast cancer (Review)," *International Journal of Oncology*, vol. 47, no. 3, pp. 840–848, 2015.

[346] S. Lim, A. Becker, A. Zimmer, J. Lu, R. Buettner, and J. Kirfel, "SNAI1-Mediated Epithelial-Mesenchymal Transition Confers Chemoresistance and Cellular Plasticity by Regulating Genes Involved in Cell Death and Stem Cell Maintenance," *PLoS ONE*, vol. 8, no. 6, pp. 1–12, 2013.

[347] K. Kuwada, S. Kagawa, R. Yoshida, S. Sakamoto, A. Ito, M. Watanabe, T. Ieda, S. Kuroda, S. Kikuchi, H. Tazawa, and T. Fujiwara, "The epithelial-to-mesenchymal transition induced by tumor-associated macrophages confers chemoresistance in peritoneally disseminated pancreatic cancer," *Journal of Experimental and Clinical Cancer Research*, vol. 37, no. 1, pp. 1–10, 2018.

[348] J. Wang, Q. Wei, X. Wang, S. Tang, H. Liu, F. Zhang, M. K. Mohammed, J. Huang, D. Guo, M. Lu, F. Liu, J. Liu, C. Ma, X. Hu, R. C. Haydon, T. C. He, and H. H. Luu, "Transition to

resistance: An unexpected role of the EMT in cancer chemoresistance," *Genes and Diseases*, vol. 3, no. 1, pp. 3–6, 2016.

[349] S. Ramaswamy, K. N. Ross, E. S. Lander, and T. R. Golub, "A molecular signature of metastasis in primary solid tumors," *Nature Genetics*, vol. 33, no. 1, pp. 49–54, 2003.

[350] N. A. van Huizen, R. R. Coebergh van den Braak, M. Doukas, L. J. Dekker, J. N. IJzermans, and T. M. Luider, "Up-regulation of collagen proteins in colorectal liver metastasis compared with normal liver tissue," *Journal of Biological Chemistry*, vol. 294, no. 1, pp. 281–289, 2019.

[351] A. Kaur, B. L. Ecker, S. M. Douglass, C. H. Kugel, M. R. Webster, F. V. Almeida, R. Somasundaram, J. Hayden, E. Ban, H. Ahmadzadeh, J. Franco-Barraza, N. Shah, I. A. Mellis, F. Keeney, A. Kossenkov, H. Y. Tang, X. Yin, Q. Liu, X. Xu, M. Fane, P. Brafford, M. Herlyn, D. W. Speicher, J. A. Wargo, M. T. Tetzlaff, L. E. Haydu, A. Raj, V. Shenoy, E. Cukierman, and A. T. Weeraratna, "Remodeling of the collagen matrix in aging skin promotes melanoma metastasis and affects immune cell motility," *Cancer Discovery*, vol. 9, no. 1, pp. 64–81, 2019.

[352] P. P. Provenzano, K. W. Eliceiri, J. M. Campbell, D. R. Inman, J. G. White, and P. J. Keely, "Collagen reorganization at the tumor-stromal interface facilitates local invasion," *BMC Medicine*, vol. 4, pp. 1–15, 2006.

[353] T. T. Chang, D. Thakar, and V. M. Weaver, "Force-dependent breaching of the basement membrane," *Matrix Biology*, vol. 57-58, pp. 178–189, 2017. [Online]. Available: http://dx.doi.org/10.1016/j.matbio.2016.12.005

[354] M. Zeisberg, E. G. Neilson, M. Zeisberg, and E. G. Neilson, "Biomarkers for epithelial-mesenchymal transitions," *J Clin Invest.*, vol. 119, no. 6, pp. 1429–1437, 2009.

[355] Z. Movasaghi, S. Rehman, and I. U. Rehman, "Raman spectroscopy of biological tissues," *Applied Spectroscopy Reviews*, vol. 42, no. 5, pp. 493–541, 2007.

[356] Y. Q. Chen, H. Y. Lan, Y. C. Wu, W. H. Yang, A. Chiou, and M. H. Yang, "Epithelial-mesenchymal transition softens head and neck cancer cells to facilitate migration in 3D environments," *Journal of Cellular and Molecular Medicine*, vol. 22, no. 8, pp. 3837–3846, 2018.

[357] J. L. Puetzer and L. J. Bonassar, "High density type I collagen gels for tissue engineering of whole menisci," *Acta Biomaterialia*, vol. 9, no. 8, pp. 7787–7795, aug 2013. [Online]. Available: http://dx.doi.org/10.1016/j.actbio.2013.05.002https://linkinghub.elsevier.com/retrieve/pii/S1742706113002341

[358] A. R. Massensini, H. Ghuman, L. T. Saldin, C. J. Medberry, T. J. Keane, F. J. Nicholls, S. S. Velankar, S. F. Badylak, and M. Modo, "Concentration-dependent rheological properties of ECM hydrogel for intracerebral delivery to a stroke cavity," *Acta Biomaterialia*, vol. 27, pp. 116–130, nov 2015. [Online]. Available: http://dx.doi.org/10.1016/j.actbio.2015.08.040https://linkinghub.elsevier.com/retrieve/pii/S1742706115300842

[359] J. M. Zuidema, C. J. Rivet, R. J. Gilbert, and F. A. Morrison, “A protocol for rheological characterization of hydrogels for tissue engineering strategies,” *Journal of Biomedical Materials Research Part B: Applied Biomaterials*, vol. 102, no. 5, pp. 1063–1073, jul 2014. [Online]. Available: http://doi.wiley.com/10.1002/jbm.b.33088

[360] D. Sánchez, N. Johnson, C. Li, P. Novak, J. Rheinlaender, Y. Zhang, U. Anand, P. Anand, J. Gorelik, G. I. Frolenkov, C. Benham, M. Lab, V. P. Ostanin, T. E. Schäffer, D. Klenerman, and Y. E. Korchev, “Noncontact measurement of the local mechanical properties of living cells using pressure applied via a pipette,” *Biophysical Journal*, vol. 95, no. 6, pp. 3017–3027, 2008.

[361] R. W. Clarke, P. Novak, A. Zhukov, E. J. Tyler, M. Cano-Jaimez, A. Drews, O. Richards, K. Volynski, C. Bishop, and D. Klenerman, “Low Stress Ion Conductance Microscopy of Sub-Cellular Stiffness,” *Soft Matter*, vol. 12, no. 38, pp. 7953–7958, 2016. [Online]. Available: http://dx.doi.org/10.1039/C6SM01106Chttp://xlink.rsc.org/?DOI=C6SM01106C

[362] J. Rheinlaender and T. E. Schäffer, “Mapping the mechanical stiffness of live cells with the scanning ion conductance microscope,” *Soft Matter*, vol. 9, no. 12, p. 3230, 2013. [Online]. Available: http://xlink.rsc.org/?DOI=c2sm27412d

[363] Zeger, Scott L. and Liang, Kung-Yee, “Longitudinal Data Analysis for Discrete and Continuous Outcomes,” *Biometrics*, vol. 42, no. 1, pp. 121–130, 1986.

[364] C. Li, J. P. Armstrong, I. J. Pence, W. Kit-Anan, J. L. Puetzer, S. Correia Carreira, A. C. Moore, and M. M. Stevens, “Glycosylated superparamagnetic nanoparticle gradients for osteochondral tissue engineering,” *Biomaterials*, vol. 176, pp. 24–33, 2018. [Online]. Available: https://doi.org/10.1016/j.biomaterials.2018.05.029

[365] J. A. Hanley, A. Negassa, M. D. B. Edwardes, and J. E. Forrester, “Statistical analysis of correlated data using generalized estimating equations: An orientation,” *American Journal of Epidemiology*, vol. 157, no. 4, pp. 364–375, 2003.

[366] C. M. O’Brien, J. L. Herington, N. Brown, I. J. Pence, B. C. Paria, J. C. Slaughter, J. Reese, and A. Mahadevan-Jansen, “In vivo Raman spectral analysis of impaired cervical remodeling in a mouse model of delayed parturition,” *Scientific Reports*, vol. 7, no. 1, pp. 1–14, 2017.

[367] M. Plodinec, M. Loparic, C. A. Monnier, E. C. Obermann, R. Zanetti-Dallenbach, P. Oertle, J. T. Hyotyla, U. Aebi, M. Bentires-Alj, R. Y. H. Lim, and C.-A. Schoenenberger, “The nanomechanical signature of breast cancer,” *Nature Nanotechnology*, vol. 7, no. 11, pp. 757–765, nov 2012. [Online]. Available: http://www.nature.com/articles/nnano.2012.167

[368] D. Sarrió, S. M. Rodriguez-Pinilla, D. Hardisson, A. Cano, G. Moreno-Bueno, and J. Palacios, “Epithelial-Mesenchymal Transition in Breast Cancer Relates to the Basal-like Phenotype,” *Cancer Research*, vol. 68, no. 4, pp. 989–997, feb 2008. [Online]. Available: http://cancerres.aacrjournals.org/lookup/doi/10.1158/0008-5472.CAN-07-2017

[369] P. J. Miettinen, “TGF-beta induced transdifferentiation of mammary epithelial cells to mesenchymal cells: involvement of type I receptors,” *The Journal of Cell Biology*, vol. 127, no. 6, pp. 2021–2036, dec 1994. [Online]. Available: http://www.jcb.org/cgi/doi/10.1083/jcb.127.6.2021

[370] K. Gasior, N. J. Wagner, J. Cores, R. Caspar, A. Wilson, S. Bhattacharya, and M. L. Hauck, “The role of cellular contact and TGF-beta signaling in the activation of the epithelial mesenchymal transition (EMT),” *Cell Adhesion and Migration*, vol. 00, no. 00, pp. 1–13, 2018. [Online]. Available: https://doi.org/10.1080/19336918.2018.1526597

[371] J. Choi, Y. P. Sun, and C. K. Joo, “Transforming growth factor-β1 represses E-cadherin production via Slug expression in lens epithelial cells,” *Investigative Ophthalmology and Visual Science*, vol. 48, no. 6, pp. 2708–2718, 2007.

[372] R. Vogelmann, M.-D. Nguyen-tat, K. Giehl, G. Adler, D. Wedlich, and A. Menke, “TGF -induced downregulation of E-cadherin-based cell-cell adhesion depends on PI3-kinase and PTEN,” *Journal of Cell Science*, vol. 118, no. 20, pp. 4901–4912, oct 2005. [Online]. Available: http://jcs.biologists.org/cgi/doi/10.1242/jcs.02594

[373] J. De Gelder, K. De Gussem, P. Vandenabeele, and L. Moens, “Reference database of Raman spectra of biological molecules,” *Journal of Raman Spectroscopy*, vol. 38, no. 9, pp. 1133–1147, 2007.

[374] M. Egeblad, M. G. Rasch, and V. M. Weaver, “Dynamic interplay between the collagen scaffold and tumor evolution,” *Current Opinion in Cell Biology*, vol. 22, no. 5, pp. 697–706, 2010. [Online]. Available: http://dx.doi.org/10.1016/j.ceb.2010.08.015

[375] O. Chaudhuri, S. T. Koshy, C. Branco Da Cunha, J. W. Shin, C. S. Verbeke, K. H. Allison, and D. J. Mooney, “Extracellular matrix stiffness and composition jointly regulate the induction of malignant phenotypes in mammary epithelium,” *Nature Materials*, vol. 13, no. 10, pp. 970–978, 2014.

[376] C. Viebahn, E. Lane, and F. Ramaekers, “Keratin and vimentin expression in early organogenesis of the rabbit embryo,” *Cell and Tissue Research*, vol. 253, no. 3, pp. 553–562, sep 1988. [Online]. Available: http://link.springer.com/10.1007/BF00219746

[377] J.-E. Fléchon, J. Degrouard, and B. Fléchon, “Gastrulation events in the prestreak pig embryo: Ultrastructure and cell markers,” *genesis*, vol. 38, no. 1, pp. 13–25, 2004. [Online]. Available: http://doi.wiley.com/10.1002/gene.10244

[378] A. Kishi, M. Yamamoto, A. Kikuchi, O. Iwanuma, Y. Watanabe, Y. Ide, and S. Abe, “Gene and protein expressions of vimentin and desmin during embryonic development of the mylohyoid muscle,” *Anatomical Science International*, vol. 87, no. 3, pp. 126–131, sep 2012. [Online]. Available: http://link.springer.com/10.1007/s12565-012-0132-3

[379] V. Kommata and C. R. Dermon, “Transient vimentin expression during the embryonic development of the chicken cerebellum,” *International Journal of Developmental Neuroscience*, vol. 65, no. May 2017, pp. 11–20, apr 2018. [Online]. Available: https://doi.org/10.1016/j.ijdevneu.2017.10.003https://linkinghub.elsevier.com/retrieve/pii/S073657481730151X

[380] C. Gilles, M. Polette, J.-M. Zahm, J.-M. Tournier, L. Volders, J.-M. Foidart, and P. Birembaut, “Vimentin contributes to human mammary epithelial cell migration,” *Journal of cell science*, vol. 112 (Pt 2, pp. 4615–25, 1999. [Online]. Available: http://www.ncbi.nlm.nih.gov/pubmed/10574710

[381] R. A. Whipple, E. M. Balzer, E. H. Cho, M. A. Matrone, J. R. Yoon, and S. S. Martin, “Vimentin Filaments Support Extension of Tubulin-Based Microtentacles in Detached Breast Tumor Cells,” *Cancer Research*, vol. 68, no. 14, pp. 5678–5688, jul 2008. [Online]. Available: http://cancerres.aacrjournals.org/cgi/doi/10.1158/0008-5472.CAN-07-6589

[382] G. M. Calaf, A. S. Balajee, M. T. Montalvo-Villagra, M. Leon, D. N. M., R. G. Alvarez, D. Roy, G. Narayan, and J. Abarca-Quinones, “Vimentin and Notch as biomarkers for breast cancer progression,” *Oncology Letters*, vol. 7, no. 3, pp. 721–727, mar 2014. [Online]. Available: https://www.spandidos-publications.com/10.3892/ol.2014.1781

[383] W. Birchmeier, “E-cadherin as a tumor (invasion) suppressor gene,” *BioEssays*, vol. 17, no. 2, pp. 97–99, 1995.

[384] A. Hollestelle, J. K. Peeters, M. Smid, M. Timmermans, L. C. Verhoog, P. J. Westenend, A. A. J. Heine, A. Chan, A. M. Sieuwerts, E. A. C. Wiemer, J. G. M. Klijn, P. J. van der Spek, J. A. Foekens, M. Schutte, M. A. den Bakker, and J. W. M. Martens, “Loss of E-cadherin is not a necessity for epithelial to mesenchymal transition in human breast cancer,” *Breast Cancer Research and Treatment*, vol. 138, no. 1, pp. 47–57, feb 2013. [Online]. Available: http://link.springer.com/10.1007/s10549-013-2415-3

[385] M. Wang, D. Ren, W. Guo, S. Huang, Z. Wang, Q. Li, H. Du, L. Song, and X. Peng, “N-cadherin promotes epithelial-mesenchymal transition and cancer stem cell-like traits via ErbB signaling in prostate cancer cells,” *International Journal of Oncology*, vol. 48, no. 2, pp. 595–606, 2016.

[386] C. Vogel and E. M. Marcotte, “Insights into the regulation of protein abundance from proteomic and transcriptomic analyses,” *Nature Reviews Genetics*, vol. 13, no. 4, pp. 227–232, apr 2012. [Online]. Available: http://dx.doi.org/10.1038/nrg3185http://www.nature.com/articles/nrg3185

[387] A. Sakamoto, K. Murata, H. Suzuki, M. Yatabe, and M. Kikuchi, “Immunohistochemical Observation of Co-expression of E- and N-cadherins in Rat Organogenesis,” *Acta Histochemica Et Cytochemica*, vol. 41, no. 5, pp. 143–147, 2008.

[388] S. Monaco, V. Sparano, M. Gioia, D. Sbardella, D. Di Pierro, S. Marini, and M. Coletta, “Enzymatic processing of collagen IV by MMP-2 (gelatinase A) affects neutrophil migration and

it is modulated by extracatalytic domains," *Protein Science*, vol. 15, no. 12, pp. 2805–2815, dec 2006. [Online]. Available: http://doi.wiley.com/10.1110/ps.062430706

[389] R. T. Aimes and J. P. Quigley, "Matrix metalloproteinase-2 is an interstitial collagenase. Inhibitor-free enzyme catalyzes the cleavage of collagen fibrils and soluble native type I collagen generating the specific 3/4- and 1/4-length fragments." *Journal of Biological Chemistry*, vol. 270, no. 11, pp. 5872–5876, mar 1995. [Online]. Available: http://www.jbc.org/lookup/doi/10.1074/jbc.270.11.5872

[390] M. L. Patterson, S. J. Atkinson, V. Knäuper, and G. Murphy, "Specific collagenolysis by gelatinase A, MMP-2, is determined by the hemopexin domain and not the fibronectin-like domain," *FEBS Letters*, vol. 503, no. 2-3, pp. 158–162, aug 2001. [Online]. Available: http://doi.wiley.com/10.1016/S0014-5793{%}2801{%}2902723-5

[391] E.-S. Kim, Y.-W. Sohn, and A. Moon, "TGF-β-induced transcriptional activation of MMP-2 is mediated by activating transcription factor (ATF)2 in human breast epithelial cells," *Cancer Letters*, vol. 252, no. 1, pp. 147–156, jul 2007. [Online]. Available: https://linkinghub.elsevier.com/retrieve/pii/S0304383506006902

[392] J. Park and J. E. Schwarzbauer, "Mammary epithelial cell interactions with fibronectin stimulate epithelial-mesenchymal transition," *Oncogene*, vol. 33, no. 13, pp. 1649–1657, mar 2014. [Online]. Available: http://dx.doi.org/10.1038/onc.2013.118http://www.nature.com/articles/onc2013118

[393] A. G. de Herreros, S. Peiró, M. Nassour, and P. Savagner, "Snail Family Regulation and Epithelial Mesenchymal Transitions in Breast Cancer Progression," *Journal of Mammary Gland Biology and Neoplasia*, vol. 15, no. 2, pp. 135–147, jun 2010. [Online]. Available: http://link.springer.com/10.1007/s10911-010-9179-8

[394] I. Boraschi-Diaz, J. Wang, J. S. Mort, and S. V. Komarova, "Collagen Type I as a Ligand for Receptor-Mediated Signaling," *Frontiers in Physics*, vol. 5, no. May, pp. 1–11, 2017.

[395] A. Engler, L. Bacakova, C. Newman, A. Hategan, M. Griffin, and D. Discher, "Substrate Compliance versus Ligand Density in Cell on Gel Responses," *Biophysical Journal*, vol. 86, no. 1, pp. 617–628, jan 2004. [Online]. Available: http://dx.doi.org/10.1016/S0006-3495(04)74140-5https://linkinghub.elsevier.com/retrieve/pii/S0006349504741405

[396] M. A. Wozniak, R. Desai, P. A. Solski, C. J. Der, and P. J. Keely, "ROCK-generated contractility regulates breast epithelial cell differentiation in response to the physical properties of a three-dimensional collagen matrix," *Journal of Cell Biology*, vol. 163, no. 3, pp. 583–595, 2003.

[397] B. N. Mason, A. Starchenko, R. M. Williams, L. J. Bonassar, and C. A. Reinhart-King, "Tuning three-dimensional collagen matrix stiffness independently of collagen concentration modulates endothelial cell behavior," *Acta Biomaterialia*, vol. 9, no. 1, pp. 4635–4644, 2013. [Online].

Available: http://dx.doi.org/10.1016/j.actbio.2012.08.007

[398] R. Roy, A. Boskey, and L. J. Bonassar, "Processing of type I collagen gels using nonenzymatic glycation," *Journal of Biomedical Materials Research Part A*, vol. 9999A, no. 3, pp. NA–NA, 2009. [Online]. Available: http://doi.wiley.com/10.1002/jbm.a.32231

[399] G. Thoelking, B. Reiss, J. Wegener, H. Oberleithner, H. Pavenstaedt, and C. Riethmuller, "Nanotopography follows force in TGF-β1 stimulated epithelium," *Nanotechnology*, vol. 21, no. 26, p. 265102, jul 2010. [Online]. Available: http://stacks.iop.org/0957-4484/21/i=26/a=265102?key=crossref.c72d14923e21eeb15c3cad73c9332ec9

[400] S. T. Buckley, C. Medina, A. M. Davies, and C. Ehrhardt, "Cytoskeletal re-arrangement in TGF-β1-induced alveolar epithelial-mesenchymal transition studied by atomic force microscopy and high-content analysis," *Nanomedicine: Nanotechnology, Biology and Medicine*, vol. 8, no. 3, pp. 355–364, apr 2012. [Online]. Available: http://dx.doi.org/10.1016/j.nano.2011.06.021https://linkinghub.elsevier.com/retrieve/pii/S1549963411002747

[401] D. Schneider, T. Baronsky, A. Pietuch, J. Rother, M. Oelkers, D. Fichtner, D. Wedlich, and A. Janshoff, "Tension Monitoring during Epithelial-to-Mesenchymal Transition Links the Switch of Phenotype to Expression of Moesin and Cadherins in NMuMG Cells," *PLoS ONE*, vol. 8, no. 12, p. e80068, dec 2013. [Online]. Available: https://dx.plos.org/10.1371/journal.pone.0080068

[402] A. V. Nguyen, K. D. Nyberg, M. B. Scott, A. M. Welsh, A. H. Nguyen, N. Wu, S. V. Hohlbauch, N. A. Geisse, E. A. Gibb, A. G. Robertson, T. R. Donahue, and A. C. Rowat, "Stiffness of pancreatic cancer cells is associated with increased invasive potential," *Integrative Biology*, vol. 8, no. 12, pp. 1232–1245, 2016. [Online]. Available: https://academic.oup.com/ib/article/8/12/1232-1245/5115325

[403] R. Smith, K. L. Wright, and L. Ashton, "Raman spectroscopy: An evolving technique for live cell studies," *Analyst*, vol. 141, no. 12, pp. 3590–3600, 2016.

[404] L. Zhang and W. Min, "Bioorthogonal chemical imaging of metabolic changes during epithelial–mesenchymal transition of cancer cells by stimulated Raman scattering microscopy," *Journal of Biomedical Optics*, vol. 22, no. 10, p. 1, 2017. [Online]. Available: https://www.spiedigitallibrary.org/journals/journal-of-biomedical-optics/volume-22/issue-10/106010/Bioorthogonal-chemical-imaging-of-metabolic-changes-during-epithelialmesenchymal-transition-of/10.1117/1.JBO.22.10.106010.full

[405] X. Cao, X. Chen, C. Shi, M. Zhang, W. Lu, L. Li, J. Dong, X. Han, and W. Qian, "Process characterization of epithelial–mesenchymal transition in alveolar epithelial type II cells using surface-enhanced Raman scattering spectroscopy," *RSC Advances*, vol. 6, no. 17, pp. 14 321–14 328, 2016. [Online]. Available: http://xlink.rsc.org/?DOI=C5RA17022B

[406] M. Marro, C. Nieva, R. Sanz-Pamplona, and A. Sierra, “Molecular monitoring of epithelial-to-mesenchymal transition in breast cancer cells by means of Raman spectroscopy,” *Biochimica et Biophysica Acta - Molecular Cell Research*, vol. 1843, no. 9, pp. 1785–1795, 2014. [Online]. Available: http://dx.doi.org/10.1016/j.bbamcr.2014.04.012

[407] K. A. Brown, M. E. Aakre, A. E. Gorska, J. O. Price, S. E. Eltom, J. A. Pietenpol, and H. L. Moses, “Induction by transforming growth factor-β1 of epithelial to mesenchymal transition is a rare event in vitro,” *Breast Cancer Research*, vol. 6, pp. 215–231, 2004.

[408] H. J. Byrne, P. Knief, M. E. Keating, and F. Bonnier, “Spectral pre and post processing for infrared and Raman spectroscopy of biological tissues and cells,” *Chemical Society Reviews*, vol. 45, no. 7, pp. 1865–1878, 2016. [Online]. Available: http://xlink.rsc.org/?DOI=C5CS00440C

[409] H. J. Butler, L. Ashton, B. Bird, G. Cinque, K. Curtis, J. Dorney, K. Esmonde-White, N. J. Fullwood, B. Gardner, P. L. Martin-Hirsch, M. J. Walsh, M. R. McAinsh, N. Stone, and F. L. Martin, “Using Raman spectroscopy to characterize biological materials,” *Nature Protocols*, vol. 11, no. 4, pp. 664–687, mar 2016. [Online]. Available: http://dx.doi.org/10.1038/nprot.2016.036http://www.nature.com/doifinder/10.1038/nprot.2016.036

[410] A. Biancolillo and F. Marini, “Chemometric Methods for Spectroscopy-Based Pharmaceutical Analysis,” *Frontiers in Chemistry*, vol. 6, no. November, pp. 1–14, nov 2018. [Online]. Available: https://www.frontiersin.org/article/10.3389/fchem.2018.00576/full

[411] C. Nieva, M. Marro, N. Santana-Codina, S. Rao, D. Petrov, and A. Sierra, “The Lipid Phenotype of Breast Cancer Cells Characterized by Raman Microspectroscopy: Towards a Stratification of Malignancy,” *PLoS ONE*, vol. 7, no. 10, 2012.

[412] B. M. Baker and C. S. Chen, “Deconstructing the third dimension – how 3D culture microenvironments alter cellular cues,” *Journal of Cell Science*, vol. 125, no. 13, pp. 3015–3024, jul 2012. [Online]. Available: http://jcs.biologists.org/lookup/doi/10.1242/jcs.079509

[413] M. Jermyn, J. Desroches, K. Aubertin, K. St-Arnaud, W. J. Madore, E. De Montigny, M. C. Guiot, D. Trudel, B. C. Wilson, K. Petrecca, and F. Leblond, “A review of Raman spectroscopy advances with an emphasis on clinical translation challenges in oncology,” *Physics in Medicine and Biology*, vol. 61, no. 23, pp. R370–R400, 2016.

[414] I. P. Santos, E. M. Barroso, T. C. Bakker Schut, P. J. Caspers, C. G. Van Lanschot, D. H. Choi, M. F. Van Der Kamp, R. W. Smits, R. Van Doorn, R. M. Verdijk, V. Noordhoek Hegt, J. H. Von Der Thüsen, C. H. Van Deurzen, L. B. Koppert, G. J. Van Leenders, P. C. Ewing-Graham, H. C. Van Doorn, C. M. Dirven, M. B. Busstra, J. Hardillo, A. Sewnaik, I. Ten Hove, H. Mast, D. A. Monserez, C. Meeuwis, T. Nijsten, E. B. Wolvius, R. J. Baatenburg De Jong, G. J. Puppels, and S. Koljenović, “Raman spectroscopy for cancer detection and cancer surgery guidance: Translation to the clinics,” *Analyst*, vol. 142, no. 17, pp. 3025–3047, 2017.

[415] M. G. Ramírez-Elías, E. S. Kolosovas-Machuca, D. Kershenobich, C. Guzmán, G. Escobedo, and F. J. González, "Evaluation of liver fibrosis using Raman spectroscopy and infrared thermography: A pilot study," *Photodiagnosis and Photodynamic Therapy*, vol. 19, no. June, pp. 278–283, 2017.

[416] A. M. Giudetti, S. De Domenico, A. Ragusa, P. Lunetti, A. Gaballo, J. Franck, P. Simeone, G. Nicolardi, F. De Nuccio, A. Santino, L. Capobianco, P. Lanuti, I. Fournier, M. Salzet, M. Maffia, and D. Vergara, "A specific lipid metabolic profile is associated with the epithelial mesenchymal transition program," *Biochimica et Biophysica Acta (BBA) - Molecular and Cell Biology of Lipids*, vol. 1864, no. 3, pp. 344–357, mar 2019. [Online]. Available: https://linkinghub.elsevier.com/retrieve/pii/S1388198118303743

[417] E. A. Phelps, N. O. Enemchukwu, V. F. Fiore, J. C. Sy, N. Murthy, T. A. Sulchek, T. H. Barker, and A. J. García, "Maleimide cross-linked bioactive PEG hydrogel exhibits improved reaction kinetics and cross-linking for cell encapsulation and in situ delivery," *Advanced Materials*, vol. 24, no. 1, pp. 64–70, 2012.

[418] L. A. Gurski, A. K. Jha, C. Zhang, X. Jia, and M. C. Farach-Carson, "Hyaluronic acid-based hydrogels as 3D matrices for in vitro evaluation of chemotherapeutic drugs using poorly adherent prostate cancer cells," *Biomaterials*, vol. 30, no. 30, pp. 6076–6085, 2009. [Online]. Available: http://dx.doi.org/10.1016/j.biomaterials.2009.07.054

[419] B. J. Klotz, D. Gawlitta, A. J. Rosenberg, J. Malda, and F. P. Melchels, "Gelatin-Methacryloyl Hydrogels: Towards Biofabrication-Based Tissue Repair," *Trends in Biotechnology*, vol. 34, no. 5, pp. 394–407, 2016. [Online]. Available: http://dx.doi.org/10.1016/j.tibtech.2016.01.002

[420] J. A. Rowley, G. Madlambayan, and D. J. Mooney, "Alginate hydrogels as synthetic extracellular matrix materials," *Biomaterials*, vol. 20, no. 1, pp. 45–53, jan 1999. [Online]. Available: https://linkinghub.elsevier.com/retrieve/pii/S0142961298001070

[421] N. Huebsch, P. R. Arany, A. S. Mao, D. Shvartsman, O. A. Ali, S. A. Bencherif, J. Rivera-feliciano, and D. J. Mooney, "Cell / Matrix Interface To Control Stem-Cell Fate," *Nature Materials*, vol. 9, no. 6, pp. 518–526, 2010. [Online]. Available: http://dx.doi.org/10.1038/nmat2732

[422] Y. Fang and R. M. Eglen, "Three-Dimensional Cell Cultures in Drug Discovery and Development," *SLAS Discovery*, vol. 22, no. 5, pp. 456–472, 2017.

[423] S. Rodin, L. Antonsson, C. Niaudet, O. E. Simonson, E. Salmela, E. M. Hansson, A. Domogatskaya, Z. Xiao, P. Damdimopoulou, M. Sheikhi, J. Inzunza, A. S. Nilsson, D. Baker, R. Kuiper, Y. Sun, E. Blennow, M. Nordenskjöld, K. H. Grinnemo, J. Kere, C. Betsholtz, O. Hovatta, and K. Tryggvason, "Clonal culturing of human embryonic stem cells on laminin-521/E-cadherin matrix in defined and xeno-free environment," *Nature Communications*, vol. 5, pp. 1–13, 2014.

[424] E. L. Baker, J. Lu, D. Yu, R. T. Bonnecaze, and M. H. Zaman, "Cancer Cell Stiffness: Integrated

Roles of Three-Dimensional Matrix Stiffness and Transforming Potential," *Biophysical Journal*, vol. 99, no. 7, pp. 2048–2057, oct 2010. [Online]. Available: http://dx.doi.org/10.1016/j.bpj.2010.07.051https://linkinghub.elsevier.com/retrieve/pii/S0006349510009239

[425] G. Antonacci and S. Braakman, "Biomechanics of subcellular structures by non-invasive Brillouin microscopy," *Scientific Reports*, vol. 6, no. 1, p. 37217, dec 2016. [Online]. Available: http://dx.doi.org/10.1038/srep37217http://www.nature.com/articles/srep37217

[426] R. Jayadev and D. R. Sherwood, "Basement membranes," *Current Biology*, vol. 27, no. 6, pp. R207–R211, 2017. [Online]. Available: http://dx.doi.org/10.1016/j.cub.2017.02.006

[427] H. K. Kleinman, M. L. McGarvey, L. A. Liotta, P. G. Robey, K. Tryggvason, and G. R. Martin, "Isolation and characterization of type IV procollagen, laminin, and heparan sulfate proteoglycan from the EHS sarcoma," *Biochemistry*, vol. 21, no. 24, pp. 6188–6193, nov 1982. [Online]. Available: http://pubs.acs.org/doi/abs/10.1021/bi00267a025

[428] A. Domogatskaya, S. Rodin, and K. Tryggvason, "Functional Diversity of Laminins," *Annual Review of Cell and Developmental Biology*, vol. 28, no. 1, pp. 523–553, 2012.

[429] J. H. Miner and P. D. Yurchenco, "LAMININ FUNCTIONS IN TISSUE MORPHOGENESIS," *Annual Review of Cell and Developmental Biology*, vol. 20, no. 1, pp. 255–284, nov 2004. [Online]. Available: http://www.annualreviews.org/doi/10.1146/annurev.cellbio.20.010403.094555

[430] P. R. Macdonald, A. Lustig, M. O. Steinmetz, and R. A. Kammerer, "Laminin chain assembly is regulated by specific coiled-coil interactions," *Journal of Structural Biology*, vol. 170, no. 2, pp. 398–405, may 2010. [Online]. Available: http://dx.doi.org/10.1016/j.jsb.2010.02.004https://linkinghub.elsevier.com/retrieve/pii/S1047847710000390

[431] P. Tunggal, N. Smyth, M. Paulsson, and M. C. Ott, "Laminins: Structure and genetic regulation," *Microscopy Research and Technique*, vol. 51, no. 3, pp. 214–227, 2000.

[432] J. Muschler and C. H. Streuli, "Cell-matrix interactions in mammary gland development and breast cancer." *Cold Spring Harbor perspectives in biology*, vol. 2, no. 10, 2010.

[433] R. Timpl, H. Wiedemann, V. Delden, H. Furthmayr, and K. Kuhn, "A Network Model for the Organization of Type IV Collagen Molecules in Basement Membranes," *European Journal of Biochemistry*, vol. 120, no. 2, pp. 203–211, nov 1981. [Online]. Available: http://doi.wiley.com/10.1111/j.1432-1033.1981.tb05690.x

[434] B. G. Hudson, T. R. Stephen, and K. Tryggvason, "Type IV collagen: structure, gene organization, and role in human diseases," *Journal of Biological Chemistry*, vol. 268, no. 35, pp. 26 033–26 036, 1993.

[435] A. Boutaud, D.-b. Borza, O. Bondar, S. Gunwar, K.-o. Netzer, N. Singh, Y. Ninomiya, Y. Sado, M. E. Noelken, and B. G. Hudson, "Type IV Collagen of the Glomerular Basement Membrane,"

Journal of Biological Chemistry, vol. 275, no. 39, pp. 30 716–30 724, sep 2000. [Online]. Available: http://www.jbc.org/lookup/doi/10.1074/jbc.M004569200

[436] R. Vanacore, A.-J. L. Ham, M. Voehler, C. R. Sanders, T. P. Conrads, T. D. Veenstra, K. B. Sharpless, P. E. Dawson, and B. G. Hudson, "A Sulfilimine Bond Identified in Collagen IV," *Science*, vol. 325, no. 5945, pp. 1230–1234, sep 2009. [Online]. Available: http://www.sciencemag.org/cgi/doi/10.1126/science.1176811

[437] P. D. Yurchenco, "Basement Membranes: Cell Scaffoldings and Signaling Platforms," *Cold Spring Harbor Perspectives in Biology*, vol. 3, no. 2, pp. a004 911–a004 911, feb 2011. [Online]. Available: http://cshperspectives.cshlp.org/lookup/doi/10.1101/cshperspect.a004911

[438] J. Ishihara, A. Ishihara, K. Fukunaga, K. Sasaki, M. J. V. White, P. S. Briquez, and J. A. Hubbell, "Laminin heparin-binding peptides bind to several growth factors and enhance diabetic wound healing," *Nature Communications*, vol. 9, no. 1, p. 2163, dec 2018. [Online]. Available: http://dx.doi.org/10.1038/s41467-018-04525-whttp://www.nature.com/articles/s41467-018-04525-w

[439] P. Vandenberg, "Characterization of a type IV collagen major cell binding site with affinity to the alpha 1 beta 1 and the alpha 2 beta 1 integrins," *The Journal of Cell Biology*, vol. 113, no. 6, pp. 1475–1483, jun 1991. [Online]. Available: http://www.jcb.org/cgi/doi/10.1083/jcb.113.6.1475

[440] D. Harrison, S.-a. Hussain, A. C. Combs, J. M. Ervasti, P. D. Yurchenco, and E. Hohenester, "Crystal Structure and Cell Surface Anchorage Sites of Laminin α1LG4-5," *Journal of Biological Chemistry*, vol. 282, no. 15, pp. 11 573–11 581, apr 2007. [Online]. Available: http://www.jbc.org/lookup/doi/10.1074/jbc.M610657200

[441] P. Chiarugi and E. Giannoni, "Anoikis: A necessary death program for anchorage-dependent cells," *Biochemical Pharmacology*, vol. 76, no. 11, pp. 1352–1364, 2008.

[442] J. S. Desgrosellier and D. A. Cheresh, "Integrins in cancer: biological implications and therapeutic opportunities," *Nature Reviews Cancer*, vol. 10, no. 1, pp. 9–22, jan 2010. [Online]. Available: http://dx.doi.org/10.1038/nrc2748http://www.nature.com/articles/nrc2748

[443] P. M. Carpenter, A. Ziogas, E. M. Markham, A. S. Cantillep, R. Yan, and H. Anton-Culver, "Laminin 332 expression and prognosis in breast cancer," *Human Pathology*, vol. 82, pp. 289–296, 2018. [Online]. Available: https://doi.org/10.1016/j.humpath.2018.08.003

[444] J. Chia, N. Kusuma, R. Anderson, B. Parker, B. Bidwell, L. Zamurs, E. Nice, and N. Pouliot, "Evidence for a role of tumor-derived laminin-511 in the metastatic progression of breast cancer," *American Journal of Pathology*, vol. 170, no. 6, pp. 2135–2148, 2007. [Online]. Available: http://dx.doi.org/10.2353/ajpath.2007.060709

[445] A. Glentis, V. Gurchenkov, and D. M. Vignjevic, "Assembly, heterogeneity, and breaching of the basement membranes," *Cell Adhesion and Migration*, vol. 8, no. 3, pp. 236–245, 2014.

[446] M. Williams, C. Burdsal, A. Periasamy, M. Lewandoski, and A. Sutherland, “Mouse primitive streak forms in situ by initiation of epithelial to mesenchymal transition without migration of a cell population,” *Developmental Dynamics*, vol. 241, no. 2, pp. 270–283, feb 2012. [Online]. Available: http://doi.wiley.com/10.1002/dvdy.23711

[447] R. Yadav, K. Larbi, R. Young, and S. Nourshargh, “Migration of leukocytes through the vessel wall and beyond,” *Thrombosis and Haemostasis*, vol. 90, no. 10, pp. 598–606, dec 2003. [Online]. Available: http://www.thieme-connect.de/DOI/DOI?10.1160/TH03-04-0220

[448] D. R. Sherwood, “Cell invasion through basement membranes: an anchor of understanding,” *Trends in Cell Biology*, vol. 16, no. 5, pp. 250–256, may 2006. [Online]. Available: https://linkinghub.elsevier.com/retrieve/pii/S0962892406000845

[449] L. C. Kelley, L. L. Lohmer, E. J. Hagedorn, and D. R. Sherwood, “Traversing the basement membrane in vivo: A diversity of strategies,” *The Journal of Cell Biology*, vol. 204, no. 3, pp. 291–302, feb 2014. [Online]. Available: http://www.jcb.org/lookup/doi/10.1083/jcb.201311112

[450] C.-M. Horejs, “Basement membrane fragments in the context of the epithelial-to-mesenchymal transition,” *European Journal of Cell Biology*, vol. 95, no. 11, pp. 427–440, nov 2016. [Online]. Available: http://dx.doi.org/10.1016/j.ejcb.2016.06.002https://linkinghub.elsevier.com/retrieve/pii/S0171933516300930

[451] P. Friedl and S. Alexander, “Cancer Invasion and the Microenvironment: Plasticity and Reciprocity,” *Cell*, vol. 147, no. 5, pp. 992–1009, nov 2011. [Online]. Available: http://dx.doi.org/10.1016/j.cell.2011.11.016https://linkinghub.elsevier.com/retrieve/pii/S0092867411013547

[452] R. G. Rowe and S. J. Weiss, “Breaching the basement membrane: who, when and how?” *Trends in Cell Biology*, vol. 18, no. 11, pp. 560–574, nov 2008. [Online]. Available: http://www.ncbi.nlm.nih.gov/pubmed/18848450https://linkinghub.elsevier.com/retrieve/pii/S0962892408002353

[453] R. Hiramatsu, T. Matsuoka, C. Kimura-Yoshida, S.-W. Han, K. Mochida, T. Adachi, S. Takayama, and I. Matsuo, “External Mechanical Cues Trigger the Establishment of the Anterior-Posterior Axis in Early Mouse Embryos,” *Developmental Cell*, vol. 27, no. 2, pp. 131–144, oct 2013. [Online]. Available: http://dx.doi.org/10.1016/j.devcel.2013.09.026https://linkinghub.elsevier.com/retrieve/pii/S1534580713005741

[454] J. Lohi, J. Oivula, E. Kivilaakso, T. Kiviluoto, K. Fröjdman, Y. Yamada, R. E. Burgeson, I. Leivo, and I. Virtanen, “Basement membrane laminin-5 is deposited in colorectal adenomas and carcinomas and serves as a ligand for alpha3 beta1 integrinNote,” *APMIS*, vol. 108, no. 3, pp. 161–172, mar 2000. [Online]. Available: http://doi.wiley.com/10.1034/j.1600-0463.2000.d01-40.x

[455] F.-X. Maquart, S. Pasco, L. Ramont, W. Hornebeck, and J.-C. Monboisse, “An introduction

to matrikines: extracellular matrix-derived peptides which regulate cell activity," *Critical Reviews in Oncology/Hematology*, vol. 49, no. 3, pp. 199–202, mar 2004. [Online]. Available: https://linkinghub.elsevier.com/retrieve/pii/S1040842803002750

[456] P. C. Colorado, A. Torre, G. Kamphaus, Y. Maeshima, H. Hopfer, K. Takahashi, R. Volk, E. D. Zamborsky, S. Herman, P. K. Sarkar, M. B. Ericksen, M. Dhanabal, M. Simons, M. Post, D. W. Kufe, R. R. Weichselbaum, V. P. Sukhatme, and R. Kalluri, "Anti-angiogenic cues from vascular basement membrane collagen," *Cancer Research*, vol. 60, no. 9, pp. 2520–2526, 2000.

[457] A. Sudhakar, P. Nyberg, V. G. Keshamouni, A. P. Mannam, J. Li, H. Sugimoto, D. Cosgrove, and R. Kalluri, "Human α1 type IV collagen NC1 domain exhibits distinct antiangiogenic activity mediated by $\alpha 1\beta 1$ integrin," *Journal of Clinical Investigation*, vol. 115, no. 10, pp. 2801–2810, oct 2005. [Online]. Available: http://www.ncbi.nlm.nih.gov/entrez/query.fcgi?cmd=Retrieve{&}db=PubMed{&}dopt=Citation{&}list{_}uids=16151532http://www.jci.org/cgi/doi/10.1172/JCI24813

[458] H. E. Yong, P. Murthi, M. H. Wong, B. Kalionis, S. P. Brennecke, and R. J. Keogh, "Anti-angiogenic collagen fragment arresten is increased from 16 weeks' gestation in pre-eclamptic plasma," *Placenta*, vol. 36, no. 11, pp. 1300–1309, nov 2015. [Online]. Available: http://dx.doi.org/10.1016/j.placenta.2015.08.013https://linkinghub.elsevier.com/retrieve/pii/S0143400415300400

[459] G. D. Kamphaus, P. C. Colorado, D. J. Panka, H. Hopfer, R. Ramchandran, A. Torre, Y. Maeshima, J. W. Mier, V. P. Sukhatme, and R. Kalluri, "Canstatin, a Novel Matrix-derived Inhibitor of Angiogenesis and Tumor Growth," *Journal of Biological Chemistry*, vol. 275, no. 2, pp. 1209–1215, jan 2000. [Online]. Available: http://www.jbc.org/cgi/doi/10.1074/jbc.275.2.1209

[460] C. Magnon, A. Galaup, B. Mullan, V. Rouffiac, J.-M. Bidart, F. Griscelli, P. Opolon, and M. Perricaudet, "Canstatin Acts on Endothelial and Tumor Cells via Mitochondrial Damage Initiated through Interaction with α v β 3 and α v β 5 Integrins," *Cancer Research*, vol. 65, no. 10, pp. 4353–4361, may 2005. [Online]. Available: http://cancerres.aacrjournals.org/lookup/doi/10.1158/0008-5472.CAN-04-3536

[461] H. Kanazawa, K. Imoto, M. Okada, and H. Yamawaki, "Canstatin inhibits hypoxia-induced apoptosis through activation of integrin/focal adhesion kinase/Akt signaling pathway in H9c2 cardiomyoblasts," *PLOS ONE*, vol. 12, no. 2, p. e0173051, feb 2017. [Online]. Available: https://dx.plos.org/10.1371/journal.pone.0173051

[462] Y. Maeshima, "Tumstatin, an Endothelial Cell-Specific Inhibitor of Protein Synthesis," *Science*, vol. 295, no. 5552, pp. 140–143, jan 2002. [Online]. Available: http://www.sciencemag.org/cgi/doi/10.1126/science.1065298

[463] Y. Hamano, M. Zeisberg, H. Sugimoto, J. C. Lively, Y. Maeshima, C. Yang, R. O. Hynes, Z. Werb, A. Sudhakar, and R. Kalluri, "Physiological levels of tumstatin,

a fragment of collagen IV α3 chain, are generated by MMP-9 proteolysis and suppress angiogenesis via αVβ3 integrin," *Cancer Cell*, vol. 3, no. 6, pp. 589–601, jun 2003. [Online]. Available: http://www.ncbi.nlm.nih.gov/pubmed/2775452https://linkinghub.elsevier.com/retrieve/pii/S1535610803001338

[464] Y.-Q. Luo, Li-JuanYao, L. Zhao, A.-y. Sun, H. Dong, J.-P. Du, S.-Z. Wu, and W. Hu, "Development of an ELISA for quantification of tumstatin in serum samples and tissue extracts of patients with lung carcinoma," *Clinica Chimica Acta*, vol. 411, no. 7-8, pp. 510–515, apr 2010. [Online]. Available: http://dx.doi.org/10.1016/j.cca.2010.01.001https://linkinghub.elsevier.com/retrieve/pii/S0009898110000148

[465] J. Van der Velden, L. M. Harkness, D. M. Barker, G. J. Barcham, C. L. Ugalde, E. Koumoundouros, H. Bao, L. A. Organ, A. Tokanovic, J. K. Burgess, and K. J. Snibson, "The Effects of Tumstatin on Vascularity, Airway Inflammation and Lung Function in an Experimental Sheep Model of Chronic Asthma," *Scientific Reports*, vol. 6, no. 1, p. 26309, sep 2016. [Online]. Available: http://dx.doi.org/10.1038/srep26309http://www.nature.com/articles/srep26309

[466] S. Brassart-Pasco, K. Sénéchal, J. Thevenard, L. Ramont, J. Devy, L. Di Stefano, A. Dupont-Deshorgue, S. Brézillon, J. Feru, J.-F. Jazeron, M.-D. Diebold, S. Ricard-Blum, F.-X. Maquart, and J. C. Monboisse, "Tetrastatin, the NC1 Domain of the α4(IV) Collagen Chain: A Novel Potent Anti-Tumor Matrikine," *PLoS ONE*, vol. 7, no. 4, p. e29587, apr 2012. [Online]. Available: https://dx.plos.org/10.1371/journal.pone.0029587

[467] E. Lambert, E. Fuselier, L. Ramont, B. Brassart, S. Dukic, J.-B. Oudart, A. Dupont-Deshorgue, C. Sellier, C. Machado, M. Dauchez, J.-C. Monboisse, F.-X. Maquart, S. Baud, and S. Brassart-Pasco, "Conformation-dependent binding of a Tetrastatin peptide to αvβ3 integrin decreases melanoma progression through FAK/PI3K/Akt pathway inhibition," *Scientific Reports*, vol. 8, no. 1, p. 9837, dec 2018. [Online]. Available: http://www.nature.com/articles/s41598-018-28003-x

[468] G. Giannelli, "Induction of Cell Migration by Matrix Metalloprotease-2 Cleavage of Laminin-5," *Science*, vol. 277, no. 5323, pp. 225–228, jul 1997. [Online]. Available: http://www.sciencemag.org/cgi/doi/10.1126/science.277.5323.225

[469] N. Koshikawa, G. Giannelli, V. Cirulli, K. Miyazaki, and V. Quaranta, "Role of Cell Surface Metalloprotease Mt1-Mmp in Epithelial Cell Migration over Laminin-5," *The Journal of Cell Biology*, vol. 148, no. 3, pp. 615–624, feb 2000. [Online]. Available: http://www.embase.com/search/results?subaction=viewrecord{&}from=export{&}id=L30682572{%}0Ahttp://dx.doi.org/10.1083/jcb.148.3.615http://www.jcb.org/lookup/doi/10.1083/jcb.148.3.615

[470] E. Pirilä, A. Sharabi, T. Salo, V. Quaranta, H. Tu, R. Heljasvaara, N. Koshikawa, T. Sorsa, and P. Maisi, "Matrix metalloproteinases process the laminin-5 γ2-chain and regulate

epithelial cell migration," *Biochemical and Biophysical Research Communications*, vol. 303, no. 4, pp. 1012–1017, apr 2003. [Online]. Available: https://linkinghub.elsevier.com/retrieve/pii/S0006291X03004522

[471] N. Koshikawa, T. Minegishi, A. Sharabi, V. Quaranta, and M. Seiki, "Membrane-type Matrix Metalloproteinase-1 (MT1-MMP) Is a Processing Enzyme for Human Laminin γ2 Chain," *Journal of Biological Chemistry*, vol. 280, no. 1, pp. 88–93, jan 2005. [Online]. Available: http://www.jbc.org/lookup/doi/10.1074/jbc.M411824200

[472] T. S. Udayakumar, M. L. Chen, E. L. Bair, D. C. V. Bredow, A. E. Cress, R. B. Nagle, and G. T. Bowden, "Membrane Type-1-Matrix Metalloproteinase Expressed by Prostate Carcinoma," *Cancer Research*, vol. 63, no. 9, pp. 2292–2299, 2003.

[473] C.-M. Horejs, A. Serio, A. Purvis, A. J. Gormley, S. Bertazzo, A. Poliniewicz, A. J. Wang, P. DiMaggio, E. Hohenester, and M. M. Stevens, "Biologically-active laminin-111 fragment that modulates the epithelial-to-mesenchymal transition in embryonic stem cells," *Proceedings of the National Academy of Sciences*, vol. 111, no. 16, pp. 5908–5913, 2014. [Online]. Available: http://www.pnas.org/cgi/doi/10.1073/pnas.1403139111

[474] C. M. Horejs, J. P. St-Pierre, J. R. Ojala, J. A. Steele, P. B. Da Silva, A. Rynne-Vidal, S. A. Maynard, C. S. Hansel, C. Rodríguez-Fernández, M. M. Mazo, A. Y. You, A. J. Wang, T. Von Erlach, K. Tryggvason, M. López-Cabrera, and M. M. Stevens, "Preventing tissue fibrosis by local biomaterials interfacing of specific cryptic extracellular matrix information," *Nature Communications*, vol. 8, 2017.

[475] E. L. Bair, M. L. Chen, K. McDaniel, K. Sekiguchi, A. E. Cress, R. B. Nagle, and G. T. Bowden, "Membrane Type 1 Matrix Metalloprotease Cleaves Laminin-10 and Promotes Prostate Cancer Cell Migration," *Neoplasia*, vol. 7, no. 4, pp. 380–389, apr 2005. [Online]. Available: http://dx.doi.org/10.1593/neo.04619https://linkinghub.elsevier.com/retrieve/pii/S1476558605800697

[476] S. Ricard-Blum and S. D. Vallet, "Fragments generated upon extracellular matrix remodeling: Biological regulators and potential drugs," *Matrix Biology*, vol. 75-76, pp. 170–189, jan 2019. [Online]. Available: https://doi.org/10.1016/j.matbio.2017.11.005https://linkinghub.elsevier.com/retrieve/pii/S0945053X17302779

[477] T. L. Adair-Kirk and R. M. Senior, "Fragments of extracellular matrix as mediators of inflammation," *The International Journal of Biochemistry & Cell Biology*, vol. 40, no. 6-7, pp. 1101–1110, jun 2008. [Online]. Available: https://linkinghub.elsevier.com/retrieve/pii/S1357272507004098

[478] S. Ricard-Blum and S. D. Vallet, "Matricryptins network with matricellular receptors at the surface of endothelial and tumor cells," *Frontiers in Pharmacology*, vol. 7, no. FEB, pp. 1–14, 2016.

[479] Z. Wang, Z. Li, Y. Wang, D. Cao, X. Wang, M. Jiang, M. Li, X. Yan, Y. Li,

Y. Liu, and F. Luo, “Versican silencing improves the antitumor efficacy of endostatin by alleviating its induced inflammatory and immunosuppressive changes in the tumor microenvironment,” *Oncology Reports*, vol. 33, no. 6, pp. 2981–2991, jun 2015. [Online]. Available: https://www.spandidos-publications.com/10.3892/or.2015.3903

[480] I. Alahuhta, M. Aikio, O. Väyrynen, S. Nurmenniemi, J. Suojanen, S. Teppo, T. Pihlajaniemi, R. Heljasvaara, T. Salo, and P. Nyberg, “Endostatin induces proliferation of oral carcinoma cells but its effect on invasion is modified by the tumor microenvironment,” *Experimental Cell Research*, vol. 336, no. 1, pp. 130–140, aug 2015. [Online]. Available: http://dx.doi.org/10.1016/j.yexcr.2015.06.012https://linkinghub.elsevier.com/retrieve/pii/S0014482715300215

[481] I. Celik, O. Sürücü, C. Dietz, J. V. Heymach, J. Force, I. Höschele, C. M. Becker, J. Folkman, and O. Kisker, “Therapeutic Efficacy of Endostatin Exhibits a Biphasic Dose-Response Curve,” *Cancer Research*, vol. 65, no. 23, pp. 11 044–11 050, dec 2005. [Online]. Available: http://cancerres.aacrjournals.org/lookup/doi/10.1158/0008-5472.CAN-05-2617

[482] K. Javaherian, T.-Y. Lee, R. M. T. T. Sjin, G. E. Parris, and L. Hlatky, “Two Endogenous Antiangiogenic Inhibitors, Endostatin and Angiostatin, Demonstrate Biphasic Curves in their Antitumor Profiles,” *Dose-Response*, vol. 9, no. 3, pp. dose–response.1, jul 2011. [Online]. Available: http://journals.sagepub.com/doi/10.2203/dose-response.10-020.Javaherian

[483] L. Morbidelli, S. Donnini, F. Chillemi, A. Giachetti, and M. Ziche, “Angiosuppressive and Angiostimulatory Effects Exerted by Synthetic Partial Sequences of Endostatin,” *Clinical Cancer Research*, vol. 9, no. 14, pp. 5358–5369, 2003.

[484] N. Riggi, M. Aguet, and I. Stamenkovic, “Cancer Metastasis: A Reappraisal of Its Underlying Mechanisms and Their Relevance to Treatment,” *Annual Review of Pathology: Mechanisms of Disease*, vol. 13, no. 1, pp. 117–140, jan 2018. [Online]. Available: http://www.annualreviews.org/doi/10.1146/annurev-pathol-020117-044127

[485] K. Polyak and R. A. Weinberg, “Transitions between epithelial and mesenchymal states: Acquisition of malignant and stem cell traits,” *Nature Reviews Cancer*, vol. 9, no. 4, pp. 265–273, 2009.

[486] T. Shibue and R. A. Weinberg, “EMT, CSCs, and drug resistance: the mechanistic link and clinical implications,” *Nature Reviews Clinical Oncology*, vol. 14, no. 10, pp. 611–629, oct 2017. [Online]. Available: http://dx.doi.org/10.1038/nrclinonc.2017.44http://www.nature.com/articles/nrclinonc.2017.44

[487] F. Marcucci, G. Stassi, and R. De Maria, “Epithelial-mesenchymal transition: A new target in anticancer drug discovery,” *Nature Reviews Drug Discovery*, vol. 15, no. 5, pp. 311–325, 2016. [Online]. Available: http://dx.doi.org/10.1038/nrd.2015.13

[488] D. Loessner, C. Meinert, E. Kaemmerer, L. C. Martine, K. Yue, P. A. Levett, T. J. Klein,

F. P. W. Melchels, A. Khademhosseini, and D. W. Hutmacher, “Functionalization, preparation and use of cell-laden gelatin methacryloyl–based hydrogels as modular tissue culture platforms,” *Nature Protocols*, vol. 11, no. 4, pp. 727–746, apr 2016. [Online]. Available: http://dx.doi.org/10.1038/nprot.2016.037http://www.nature.com/articles/nprot.2016.037

[489] S. Yazdani, R. Bansal, and J. Prakash, “Drug targeting to myofibroblasts: Implications for fibrosis and cancer,” *Advanced Drug Delivery Reviews*, vol. 121, pp. 101–116, nov 2017. [Online]. Available: https://doi.org/10.1016/j.addr.2017.07.010https://linkinghub.elsevier.com/retrieve/pii/S0169409X17301072

[490] V. J. Craig, L. Zhang, J. S. Hagood, and C. A. Owen, “Matrix Metalloproteinases as Therapeutic Targets for Idiopathic Pulmonary Fibrosis,” *American Journal of Respiratory Cell and Molecular Biology*, vol. 53, no. 5, pp. 585–600, nov 2015. [Online]. Available: http://www.atsjournals.org/doi/10.1165/rcmb.2015-0020TR

[491] J. Concepcion, K. Witte, C. Wartchow, S. Choo, D. Yao, H. Persson, J. Wei, P. Li, B. Heidecker, W. Ma, R. Varma, L.-S. Zhao, D. Perillat, G. Carricato, M. Recknor, K. Du, H. Ho, T. Ellis, J. Gamez, M. Howes, J. Phi-Wilson, S. Lockard, R. Zuk, and H. Tan, “Label-Free Detection of Biomolecular Interactions Using BioLayer Interferometry for Kinetic Characterization,” *Combinatorial Chemistry & High Throughput Screening*, vol. 12, no. 8, pp. 791–800, sep 2009. [Online]. Available: http://www.eurekaselect.com/openurl/content.php?genre=article{&}issn=1386-2073{&}volume=12{&}issue=8{&}spage=791

[492] J. Yu, Y. Hai, G. Liu, T. Fang, S. K. P. Kung, and J. Xie, “The Heterogeneous Nuclear Ribonucleoprotein L Is an Essential Component in the Ca 2+ /Calmodulin-dependent Protein Kinase IV-regulated Alternative Splicing through Cytidine-Adenosine Repeats,” *Journal of Biological Chemistry*, vol. 284, no. 3, pp. 1505–1513, jan 2009. [Online]. Available: http://www.jbc.org/lookup/doi/10.1074/jbc.M805113200

[493] N. Mahmood and J. Xie, “An endogenous ‘non-specific’ protein detected by a His-tag antibody is human transcription regulator YY1,” *Data in Brief*, vol. 2, pp. 52–55, mar 2015. [Online]. Available: https://linkinghub.elsevier.com/retrieve/pii/S2352340914000328

[494] M. Barbosa, M. Martins, and P. Gomes, “Grafting Techniques towards Production of Peptide-Tethered Hydrogels, a Novel Class of Materials with Biomedical Interest,” *Gels*, vol. 1, no. 2, pp. 194–218, oct 2015. [Online]. Available: http://www.mdpi.com/2310-2861/1/2/194

[495] M. Tamura, F. Yanagawa, S. Sugiura, T. Takagi, K. Sumaru, and T. Kanamori, “Click-crosslinkable and photodegradable gelatin hydrogels for cytocompatible optical cell manipulation in natural environment,” *Scientific Reports*, vol. 5, no. 1, p. 15060, dec 2015. [Online]. Available: http://dx.doi.org/10.1038/srep15060http://www.nature.com/articles/srep15060

[496] Y. Zou, L. Zhang, L. Yang, F. Zhu, M. Ding, F. Lin, Z. Wang, and Y. Li, ""Click" chemistry in polymeric scaffolds: Bioactive materials for tissue engineering," *Journal of Controlled Release*, vol. 273, no. January, pp. 160–179, mar 2018. [Online]. Available: https://doi.org/10.1016/j.jconrel.2018.01.023https://linkinghub.elsevier.com/retrieve/pii/S0168365918300397

[497] G. A. Howe and C. L. Addison, "β1 integrin," *Cell Adhesion & Migration*, vol. 6, no. 2, pp. 71–77, mar 2012. [Online]. Available: http://www.tandfonline.com/doi/abs/10.4161/cam.20077

[498] M. Morini, M. Mottolese, N. Ferrari, F. Ghiorzo, S. Buglioni, R. Mortarini, D. M. Noonan, P. G. Natali, and A. Albini, "The $\alpha 3\beta 1$ integrin is associated with mammary carcinoma cell metastasis, invasion, and gelatinase B (mmp-9) activity," *International Journal of Cancer*, vol. 87, no. 3, pp. 336–342, aug 2000. [Online]. Available: http://doi.wiley.com/10.1002/1097-0215{%}2820000801{%}2987{%}3A3{%}3C336{%}3A{%}3AAID-IJC5{%}3E3.0.CO{%}3B2-3

[499] Z. Borok, "Role for $\alpha 3$ integrin in EMT and pulmonary fibrosis," *Journal of Clinical Investigation*, vol. 119, no. 1, pp. 7–10, dec 2009. [Online]. Available: http://www.jci.org/articles/view/38084

[500] T. Shirakihara, T. Kawasaki, A. Fukagawa, K. Semba, R. Sakai, K. Miyazono, K. Miyazawa, and M. Saitoh, "Identification of integrin $\alpha 3$ as a molecular marker of cells undergoing epithelial-mesenchymal transition and of cancer cells with aggressive phenotypes," *Cancer Science*, vol. 104, no. 9, pp. 1189–1197, sep 2013. [Online]. Available: http://doi.wiley.com/10.1111/cas.12220

[501] B. Zhou, K. N. Gibson-Corley, M. E. Herndon, Y. Sun, E. Gustafson-Wagner, M. Teoh-Fitzgerald, F. E. Domann, M. D. Henry, and C. S. Stipp, "Integrin $\alpha 3\beta 1$ Can Function to Promote Spontaneous Metastasis and Lung Colonization of Invasive Breast Carcinoma," *Molecular Cancer Research*, vol. 12, no. 1, pp. 143–154, jan 2014. [Online]. Available: http://mcr.aacrjournals.org/lookup/doi/10.1158/1541-7786.MCR-13-0184

[502] S. Cagnet, M. M. Faraldo, M. Kreft, A. Sonnenberg, K. Raymond, and M. A. Glukhova, "Signaling events mediated by $\alpha 3\beta 1$ integrin are essential for mammary tumorigenesis," *Oncogene*, vol. 33, no. 34, pp. 4286–4295, aug 2014. [Online]. Available: http://www.nature.com/articles/onc2013391

[503] K. Mitchell, K. B. Svenson, W. M. Longmate, K. Gkirtzimanaki, R. Sadej, X. Wang, J. Zhao, A. G. Eliopoulos, F. Berditchevski, and C. M. DiPersio, "Suppression of Integrin $\alpha 3\beta 1$ in Breast Cancer Cells Reduces Cyclooxygenase-2 Gene Expression and Inhibits Tumorigenesis, Invasion, and Cross-Talk to Endothelial Cells," *Cancer Research*, vol. 70, no. 15, pp. 6359–6367, aug 2010. [Online]. Available: http://cancerres.aacrjournals.org/cgi/doi/10.1158/0008-5472.CAN-09-4283

[504] V. Ramovs, P. Secades, J.-Y. Song, B. Thijssen, M. Kreft, and A. Sonnenberg, "Absence of integrin $\alpha 3\beta 1$ promotes the progression of HER2-driven breast cancer in

vivo," *Breast Cancer Research*, vol. 21, no. 1, p. 63, dec 2019. [Online]. Available: https://breast-cancer-research.biomedcentral.com/articles/10.1186/s13058-019-1146-8

[505] C. Margadant and A. Sonnenberg, "Integrin-TGF-B crosstalk in fibrosis, cancer and wound healing," *EMBO Reports*, vol. 11, no. 2, pp. 97–105, 2010.

[506] S. Li, D. Edgar, R. Fässler, W. Wadsworth, and P. D. Yurchenco, "The Role of Laminin in Embryonic Cell Polarization and Tissue Organization," *Developmental Cell*, vol. 4, no. 5, pp. 613–624, may 2003. [Online]. Available: https://linkinghub.elsevier.com/retrieve/pii/S153458070300128X

[507] F. Pedrosa-Domellöf, C.-F. Tiger, I. Virtanen, L.-E. Thornell, and D. Gullberg, "Laminin Chains in Developing and Adult Human Myotendinous Junctions," *Journal of Histochemistry & Cytochemistry*, vol. 48, no. 2, pp. 201–209, feb 2000. [Online]. Available: http://journals.sagepub.com/doi/10.1177/002215540004800205

[508] J. E. Rooney, P. B. Gurpur, and D. J. Burkin, "Laminin-111 protein therapy prevents muscle disease in the mdx mouse model for Duchenne muscular dystrophy," *Proceedings of the National Academy of Sciences*, vol. 106, no. 19, pp. 7991–7996, sep 2009. [Online]. Available: http://www.pnas.org/cgi/doi/10.1073/pnas.0908785106

[509] J. E. Rooney, J. R. Knapp, B. L. Hodges, R. D. Wuebbles, and D. J. Burkin, "Laminin-111 Protein Therapy Reduces Muscle Pathology and Improves Viability of a Mouse Model of Merosin-Deficient Congenital Muscular Dystrophy," *The American Journal of Pathology*, vol. 180, no. 4, pp. 1593–1602, apr 2012. [Online]. Available: http://dx.doi.org/10.1016/j.ajpath.2011.12.019https://linkinghub.elsevier.com/retrieve/pii/S0002944012000223

[510] P. Barraza-Flores, T. M. Fontelonga, R. D. Wuebbles, H. J. Hermann, A. M. Nunes, J. N. Kornegay, and D. J. Burkin, "Laminin-111 protein therapy enhances muscle regeneration and repair in the GRMD dog model of Duchenne muscular dystrophy," *Human Molecular Genetics*, vol. 28, no. 16, pp. 2686–2695, aug 2019. [Online]. Available: https://academic.oup.com/hmg/article/28/16/2686/5479258

[511] S. H. Jun, E. W. Thompson, M. Gottardis, J. Torri, K. Yamamura, M. C. Kibbey, W. H. Kim, and H. K. Kleinman, "Laminin adhesion-selected primary human colon cancer cells are more tumorigenic than the parental and non adherent cells," *International Journal of Oncology*, vol. 4, no. 1, pp. 55–60, 1994.

[512] J. A. Engbring and H. K. Kleinman, "The basement membrane matrix in malignancy," *The Journal of Pathology*, vol. 200, no. 4, pp. 465–470, jul 2003. [Online]. Available: http://doi.wiley.com/10.1002/path.1396

[513] T. Simon and J. S. Bromberg, "Regulation of the Immune System by Laminins," *Trends in Immunology*, vol. 38, no. 11, pp. 858–871, nov 2017. [Online]. Available: http://dx.doi.org/10.

1016/j.it.2017.06.002https://linkinghub.elsevier.com/retrieve/pii/S1471490617301059

[514] Y. Yamada and H. K. Kleinman, “Functional domains of cell adhesion molecules,” *Current Opinion in Cell Biology*, vol. 4, no. 5, pp. 819–823, oct 1992. [Online]. Available: https://linkinghub.elsevier.com/retrieve/pii/095506749290105L

[515] Y. Kikkawa, K. Hozumi, F. Katagiri, M. Nomizu, H. K. Kleinman, and J. E. Koblinski, “Laminin-111-derived peptides and cancer,” *Cell Adhesion & Migration*, vol. 7, no. 1, pp. 150–159, jan 2013. [Online]. Available: http://www.tandfonline.com/doi/abs/10.4161/cam.22827

[516] B. Han, X.-H. Bai, M. Lodyga, J. Xu, B. B. Yang, S. Keshavjee, M. Post, and M. Liu, “Conversion of Mechanical Force into Biochemical Signaling,” *Journal of Biological Chemistry*, vol. 279, no. 52, pp. 54 793–54 801, dec 2004. [Online]. Available: http://www.jbc.org/lookup/doi/10.1074/jbc.M406880200

[517] D. E. Ingber, “Cellular mechanotransduction: Putting all the pieces together again,” *FASEB Journal*, vol. 20, no. 7, pp. 811–827, 2006.

[518] D. Discher, C. Dong, J. J. Fredberg, F. Guilak, D. Ingber, P. Janmey, R. D. Kamm, G. W. Schmid-Schönbein, and S. Weinbaum, “Biomechanics: Cell research and applications for the next decade,” *Annals of Biomedical Engineering*, vol. 37, no. 5, pp. 847–859, 2009.

[519] B. D. Hoffman, C. Grashoff, and M. A. Schwartz, “Dynamic molecular processes mediate cellular mechanotransduction,” *Nature*, vol. 475, no. 7356, pp. 316–323, jul 2011. [Online]. Available: http://www.nature.com/articles/nature10316

[520] F. Martino, A. R. Perestrelo, V. Vinarský, S. Pagliari, and G. Forte, “Cellular mechanotransduction: From tension to function,” *Frontiers in Physiology*, vol. 9, no. JUL, pp. 1–21, 2018.

[521] B. Martinac, “The ion channels to cytoskeleton connection as potential mechanism of mechanosensitivity,” *Biochimica et Biophysica Acta - Biomembranes*, vol. 1838, no. 2, pp. 682–691, 2014. [Online]. Available: http://dx.doi.org/10.1016/j.bbamem.2013.07.015

[522] N. D. Gallant, K. E. Michael, and A. J. García, “Cell Adhesion Strengthening: Contributions of Adhesive Area, Integrin Binding, and Focal Adhesion Assembly,” *Molecular Biology of the Cell*, vol. 16, no. 9, pp. 4329–4340, sep 2005. [Online]. Available: https://www.molbiolcell.org/doi/10.1091/mbc.e05-02-0170

[523] J. D. Humphries, P. Wang, C. Streuli, B. Geiger, M. J. Humphries, and C. Ballestrem, “Vinculin controls focal adhesion formation by direct interactions with talin and actin,” *The Journal of Cell Biology*, vol. 179, no. 5, pp. 1043–1057, dec 2007. [Online]. Available: http://www.jcb.org/lookup/doi/10.1083/jcb.200703036

[524] P. Kanchanawong, G. Shtengel, A. M. Pasapera, E. B. Ramko, M. W. Davidson, H. F. Hess, and C. M. Waterman, “Nanoscale architecture of integrin-based cell adhesions,” *Nature*, vol. 468, no. 7323, pp. 580–584, nov 2010. [Online]. Available:

http://www.nature.com/articles/nature09621

[525] G. Giannone, “Super-resolution links vinculin localization to function in focal adhesions,” *Nature Cell Biology*, vol. 17, no. 7, pp. 845–847, jul 2015. [Online]. Available: http://dx.doi.org/10.1038/ncb3196http://www.nature.com/articles/ncb3196

[526] D. W. Dumbauld, T. T. Lee, A. Singh, J. Scrimgeour, C. A. Gersbach, E. A. Zamir, J. Fu, C. S. Chen, J. E. Curtis, S. W. Craig, and A. J. Garcia, “How vinculin regulates force transmission,” *Proceedings of the National Academy of Sciences*, vol. 110, no. 24, pp. 9788–9793, jun 2013. [Online]. Available: http://www.pnas.org/cgi/doi/10.1073/pnas.1216209110

[527] D. A. Fletcher and R. D. Mullins, “Cell mechanics and the cytoskeleton,” *Nature*, vol. 463, no. 7280, pp. 485–492, jan 2010. [Online]. Available: http://www.nature.com/articles/nature08908

[528] D. M. Toivola, G.-Z. Tao, A. Habtezion, J. Liao, and M. B. Omary, “Cellular integrity plus: organelle-related and protein-targeting functions of intermediate filaments,” *Trends in Cell Biology*, vol. 15, no. 11, pp. 608–617, nov 2005. [Online]. Available: https://linkinghub.elsevier.com/retrieve/pii/S096289240500228X

[529] H. Kubitschke, J. Schnauss, K. D. Nnetu, E. Warmt, R. Stange, and J. Kaes, “Actin and microtubule networks contribute differently to cell response for small and large strains,” *New Journal of Physics*, vol. 19, no. 9, p. 093003, sep 2017. [Online]. Available: http://stacks.iop.org/1367-2630/19/i=9/a=093003?key=crossref.d1462c9c2b6753cb71524db4c3c33fd7

[530] A. R. Harris, P. Jreij, and D. A. Fletcher, “Mechanotransduction by the Actin Cytoskeleton: Converting Mechanical Stimuli into Biochemical Signals,” *Annual Review of Biophysics*, vol. 47, no. 1, pp. 617–631, may 2018. [Online]. Available: https://www.annualreviews.org/doi/10.1146/annurev-biophys-070816-033547

[531] A. Desai and T. J. Mitchison, “Microtubule polymerization dynamics,” *Annual Review of Cell and Developmental Biology*, vol. 13, no. 1, pp. 83–117, nov 1997. [Online]. Available: http://www.annualreviews.org/doi/10.1146/annurev.cellbio.13.1.83

[532] J. Zhang, W.-H. Guo, and Y.-L. Wang, “Microtubules stabilize cell polarity by localizing rear signals,” *Proceedings of the National Academy of Sciences*, vol. 111, no. 46, pp. 16 383–16 388, nov 2014. [Online]. Available: http://www.pnas.org/lookup/doi/10.1073/pnas.1410533111

[533] S. Meunier and I. Vernos, “Microtubule assembly during mitosis – from distinct origins to distinct functions?” *Journal of Cell Science*, vol. 125, no. 12, pp. 2805–2814, jun 2012. [Online]. Available: http://jcs.biologists.org/lookup/doi/10.1242/jcs.092429

[534] K. Barlan and V. I. Gelfand, “Microtubule-Based Transport and the Distribution, Tethering, and Organization of Organelles,” *Cold Spring Harbor Perspectives in Biology*, vol. 9, no. 5, p. a025817, may 2017. [Online]. Available: http://cshperspectives.cshlp.org/lookup/doi/10.1101/cshperspect.a025817

[535] C. P. Brangwynne, F. C. MacKintosh, S. Kumar, N. A. Geisse, J. Talbot, L. Mahadevan, K. K. Parker, D. E. Ingber, and D. A. Weitz, “Microtubules can bear enhanced compressive loads in living cells because of lateral reinforcement,” *The Journal of Cell Biology*, vol. 173, no. 5, pp. 733–741, jun 2006. [Online]. Available: http://www.jcb.org/lookup/doi/10.1083/jcb.200601060

[536] Z. Qin, M. J. Buehler, and L. Kreplak, “A multi-scale approach to understand the mechanobiology of intermediate filaments,” *Journal of Biomechanics*, vol. 43, no. 1, pp. 15–22, jan 2010. [Online]. Available: http://dx.doi.org/10.1016/j.jbiomech.2009.09.004https://linkinghub.elsevier.com/retrieve/pii/S0021929009004953

[537] R. Sanghvi-Shah and G. F. Weber, “Intermediate Filaments at the Junction of Mechanotransduction, Migration, and Development,” *Frontiers in Cell and Developmental Biology*, vol. 5, no. SEP, pp. 1–19, sep 2017. [Online]. Available: http://journal.frontiersin.org/article/10.3389/fcell.2017.00081/full

[538] D. Tsuruta, “The vimentin cytoskeleton regulates focal contact size and adhesion of endothelial cells subjected to shear stress,” *Journal of Cell Science*, vol. 116, no. 24, pp. 4977–4984, dec 2003. [Online]. Available: http://jcs.biologists.org/cgi/doi/10.1242/jcs.00823

[539] S. Sivaramakrishnan, J. V. DeGiulio, L. Lorand, R. D. Goldman, and K. M. Ridge, “Micromechanical properties of keratin intermediate filament networks,” *Proceedings of the National Academy of Sciences*, vol. 105, no. 3, pp. 889–894, jan 2008. [Online]. Available: http://www.pnas.org/cgi/doi/10.1073/pnas.0710728105

[540] S. Sivaramakrishnan, J. L. Schneider, A. Sitikov, R. D. Goldman, and K. M. Ridge, “Shear Stress Induced Reorganization of the Keratin Intermediate Filament Network Requires Phosphorylation by Protein Kinase C ζ,” *Molecular Biology of the Cell*, vol. 20, no. 11, pp. 2755–2765, jun 2009. [Online]. Available: https://www.molbiolcell.org/doi/10.1091/mbc.e08-10-1028

[541] P. Hotulainen and P. Lappalainen, “Stress fibers are generated by two distinct actin assembly mechanisms in motile cells,” *The Journal of Cell Biology*, vol. 173, no. 3, pp. 383–394, may 2006. [Online]. Available: http://www.jcb.org/lookup/doi/10.1083/jcb.200511093

[542] E. Kassianidou and S. Kumar, “A biomechanical perspective on stress fiber structure and function,” *Biochimica et Biophysica Acta - Molecular Cell Research*, vol. 1853, no. 11, pp. 3065–3074, 2015. [Online]. Available: http://dx.doi.org/10.1016/j.bbamcr.2015.04.006

[543] M. Yoshigi, L. M. Hoffman, C. C. Jensen, H. J. Yost, and M. C. Beckerle, “Mechanical force mobilizes zyxin from focal adhesions to actin filaments and regulates cytoskeletal reinforcement,” *The Journal of Cell Biology*, vol. 171, no. 2, pp. 209–215, oct 2005. [Online]. Available: http://www.jcb.org/lookup/doi/10.1083/jcb.200505018

[544] J. Colombelli, A. Besser, H. Kress, E. G. Reynaud, P. Girard, E. Caussinus, U. Haselmann, J. V. Small, U. S. Schwarz, and E. H. K. Stelzer, “Mechanosensing in actin stress

fibers revealed by a close correlation between force and protein localization," *Journal of Cell Science*, vol. 122, no. 10, pp. 1665–1679, may 2009. [Online]. Available: http://jcs.biologists.org/cgi/doi/10.1242/jcs.042986

[545] K. N. Dahl, A. J. Ribeiro, and J. Lammerding, "Nuclear Shape, Mechanics, and Mechanotransduction," *Circulation Research*, vol. 102, no. 11, pp. 1307–1318, jun 2008. [Online]. Available: https://www.ahajournals.org/doi/10.1161/CIRCRESAHA.108.173989

[546] F. Guilak, "Compression-induced changes in the shape and volume of the chondrocyte nucleus," *Journal of Biomechanics*, vol. 28, no. 12, pp. 1529–1541, dec 1995. [Online]. Available: https://linkinghub.elsevier.com/retrieve/pii/002192909500100X

[547] M. Crisp, Q. Liu, K. Roux, J. Rattner, C. Shanahan, B. Burke, P. D. Stahl, and D. Hodzic, "Coupling of the nucleus and cytoplasm," *The Journal of Cell Biology*, vol. 172, no. 1, pp. 41–53, jan 2006. [Online]. Available: http://www.jcb.org/lookup/doi/10.1083/jcb.200509124

[548] M. J. Stroud, I. Banerjee, J. Veevers, and J. Chen, "Linker of Nucleoskeleton and Cytoskeleton Complex Proteins in Cardiac Structure, Function, and Disease," *Circulation Research*, vol. 114, no. 3, pp. 538–548, jan 2014. [Online]. Available: https://www.ahajournals.org/doi/10.1161/CIRCRESAHA.114.301236

[549] G. Uzer, C. T. Rubin, and J. Rubin, "Cell Mechanosensitivity Is Enabled by the LINC Nuclear Complex," *Current Molecular Biology Reports*, vol. 2, no. 1, pp. 36–47, mar 2016. [Online]. Available: http://link.springer.com/10.1007/s40610-016-0032-8

[550] J. A. Mellad, D. T. Warren, and C. M. Shanahan, "Nesprins LINC the nucleus and cytoskeleton," *Current Opinion in Cell Biology*, vol. 23, no. 1, pp. 47–54, 2011. [Online]. Available: http://dx.doi.org/10.1016/j.ceb.2010.11.006

[551] B. A. Sosa, A. Rothballer, U. Kutay, and T. U. Schwartz, "LINC Complexes Form by Binding of Three KASH Peptides to Domain Interfaces of Trimeric SUN Proteins," *Cell*, vol. 149, no. 5, pp. 1035–1047, may 2012. [Online]. Available: http://dx.doi.org/10.1016/j.cell.2012.03.046https://linkinghub.elsevier.com/retrieve/pii/S0092867412005247

[552] F. Haque, D. Mazzeo, J. T. Patel, D. T. Smallwood, J. A. Ellis, C. M. Shanahan, and S. Shackleton, "Mammalian SUN Protein Interaction Networks at the Inner Nuclear Membrane and Their Role in Laminopathy Disease Processes," *Journal of Biological Chemistry*, vol. 285, no. 5, pp. 3487–3498, jan 2010. [Online]. Available: http://www.jbc.org/lookup/doi/10.1074/jbc.M109.071910

[553] M. L. Lombardi and J. Lammerding, "Keeping the LINC: the importance of nucleocytoskeletal coupling in intracellular force transmission and cellular function," *Biochemical Society Transactions*, vol. 39, no. 6, pp. 1729–1734, dec 2011. [Online]. Available: http://www.biochemsoctrans.org/cgi/doi/10.1042/BST20110686

[554] A. Elosegui-Artola, I. Andreu, A. E. Beedle, A. Lezamiz, M. Uroz, A. J. Kosmalska, R. Oria, J. Z. Kechagia, P. Rico-Lastres, A.-L. Le Roux, C. M. Shanahan, X. Trepat, D. Navajas, S. Garcia-Manyes, and P. Roca-Cusachs, "Force Triggers YAP Nuclear Entry by Regulating Transport across Nuclear Pores," *Cell*, vol. 171, no. 6, pp. 1397–1410.e14, nov 2017. [Online]. Available: http://dx.doi.org/10.1016/j.cell.2017.10.008https://linkinghub.elsevier.com/retrieve/pii/S0092867417311923

[555] S. Dupont, L. Morsut, M. Aragona, E. Enzo, S. Giulitti, M. Cordenonsi, F. Zanconato, J. Le Digabel, M. Forcato, S. Bicciato, N. Elvassore, and S. Piccolo, "Role of YAP/TAZ in mechanotransduction," *Nature*, vol. 474, no. 7350, pp. 179–184, 2011.

[556] F. Calvo, N. Ege, A. Grande-Garcia, S. Hooper, R. P. Jenkins, S. I. Chaudhry, K. Harrington, P. Williamson, E. Moeendarbary, G. Charras, and E. Sahai, "Mechanotransduction and YAP-dependent matrix remodelling is required for the generation and maintenance of cancer-associated fibroblasts," *Nature Cell Biology*, vol. 15, no. 6, pp. 637–646, jun 2013. [Online]. Available: http://dx.doi.org/10.1038/ncb2756http://www.nature.com/articles/ncb2756

[557] C. G. Hansen, T. Moroishi, and K. L. Guan, "YAP and TAZ: A nexus for Hippo signaling and beyond," *Trends in Cell Biology*, vol. 25, no. 9, pp. 499–513, 2015. [Online]. Available: http://dx.doi.org/10.1016/j.tcb.2015.05.002

[558] A. Totaro, T. Panciera, and S. Piccolo, "YAP/TAZ upstream signals and downstream responses," *Nature Cell Biology*, vol. 20, no. 8, pp. 888–899, 2018. [Online]. Available: http://dx.doi.org/10.1038/s41556-018-0142-z

[559] T. Panciera, L. Azzolin, M. Cordenonsi, and S. Piccolo, "Mechanobiology of YAP and TAZ in physiology and disease," *Nature Reviews Molecular Cell Biology*, vol. 18, no. 12, pp. 758–770, 2017. [Online]. Available: http://dx.doi.org/10.1038/nrm.2017.87

[560] G. Halder, S. Dupont, and S. Piccolo, "Transduction of mechanical and cytoskeletal cues by YAP and TAZ," *Nature Reviews Molecular Cell Biology*, vol. 13, no. 9, pp. 591–600, sep 2012. [Online]. Available: http://www.nature.com/articles/nrm3416

[561] J. Pu, C. D. McCaig, L. Cao, Z. Zhao, J. E. Segall, and M. Zhao, "EGF receptor signalling is essential for electric-field-directed migration of breast cancer cells," *Journal of Cell Science*, vol. 120, no. 19, pp. 3395–3403, oct 2007. [Online]. Available: http://jcs.biologists.org/cgi/doi/10.1242/jcs.002774

[562] C. D. McCaig, B. Song, and A. M. Rajnicek, "Electrical dimensions in cell science," *Journal of Cell Science*, vol. 122, no. 23, pp. 4267–4276, dec 2009. [Online]. Available: http://jcs.biologists.org/cgi/doi/10.1242/jcs.023564

[563] C. Li, S. Rezania, S. Kammerer, A. Sokolowski, T. Devaney, A. Gorischek, S. Jahn, H. Hackl, K. Groschner, C. Windpassinger, E. Malle, T. Bauernhofer, and W. Schreibmayer, "Piezo1 forms

mechanosensitive ion channels in the human MCF-7 breast cancer cell line," *Scientific Reports*, vol. 5, pp. 1–9, 2015.

[564] I. Titushkin and M. Cho, "Regulation of cell cytoskeleton and membrane mechanics by electric field: Role of linker proteins," *Biophysical Journal*, vol. 96, no. 2, pp. 717–728, 2009. [Online]. Available: http://dx.doi.org/10.1016/j.bpj.2008.09.035

[565] S. Mobini, U.-L. Talts, R. Xue, N. J. Cassidy, and S. H. Cartmell, "Electrical stimulation changes human mesenchymal stem cells orientation and cytoskeleton organization," *Journal of Biomaterials and Tissue Engineering*, vol. 7, no. 9, 2017.

[566] R. Balint, N. J. Cassidy, and S. H. Cartmell, "Electrical stimulation: A novel tool for tissue engineering," *Tissue Engineering - Part B: Reviews*, vol. 19, no. 1, pp. 48–57, 2013.

[567] ——, "Conductive polymers: Towards a smart biomaterial for tissue engineering," *Acta Biomaterialia*, vol. 10, no. 6, pp. 2341–2353, jun 2014. [Online]. Available: http://dx.doi.org/10.1016/j.actbio.2014.02.015https://linkinghub.elsevier.com/retrieve/pii/S1742706114000671

[568] G. Kaur, R. Adhikari, P. Cass, M. Bown, and P. Gunatillake, "Electrically conductive polymers and composites for biomedical applications," *RSC Advances*, vol. 5, no. 47, pp. 37 553–37 567, 2015. [Online]. Available: http://xlink.rsc.org/?DOI=C5RA01851J

[569] A. Kaynak, L. Rintoul, and G. A. George, "Change of mechanical and electrical properties of polypyrrole films with dopant concentration and oxidative aging," *Materials Research Bulletin*, vol. 35, no. 6, pp. 813–824, 2000.

[570] N. K. Guimard, N. Gomez, and C. E. Schmidt, "Conducting polymers in biomedical engineering," *Progress in Polymer Science (Oxford)*, vol. 32, no. 8-9, pp. 876–921, 2007.

[571] Z.-B. Huang, G.-F. Yin, X.-M. Liao, and J.-W. Gu, "Conducting polypyrrole in tissue engineering applications," *Frontiers of Materials Science*, vol. 8, no. 1, pp. 39–45, mar 2014. [Online]. Available: http://link.springer.com/10.1007/s11706-014-0238-8

[572] P. M. George, A. W. Lyckman, D. A. LaVan, A. Hegde, Y. Leung, R. Avasare, C. Testa, P. M. Alexander, R. Langer, and M. Sur, "Fabrication and biocompatibility of polypyrrole implants suitable for neural prosthetics," *Biomaterials*, vol. 26, no. 17, pp. 3511–3519, jun 2005. [Online]. Available: https://linkinghub.elsevier.com/retrieve/pii/S014296120400866X

[573] X. Wang, X. Gu, C. Yuan, S. Chen, P. Zhang, T. Zhang, J. Yao, F. Chen, and G. Chen, "Evaluation of biocompatibility of polypyrrolein vitro andin vivo," *Journal of Biomedical Materials Research*, vol. 68A, no. 3, pp. 411–422, mar 2004. [Online]. Available: http://doi.wiley.com/10.1002/jbm.a.20065

[574] A. Yussuf, M. Al-Saleh, S. Al-Enezi, and G. Abraham, "Synthesis and Characterization of Conductive Polypyrrole: The Influence of the Oxidants and Monomer on the Electrical, Thermal, and Morphological Properties," *International Journal of Polymer Science*, vol. 2018,

pp. 1–8, jul 2018. [Online]. Available: https://www.hindawi.com/journals/ijps/2018/4191747/

[575] A. Fahlgren, C. Bratengeier, A. Gelmi, C. M. Semeins, J. Klein-Nulend, E. W. H. Jager, and A. D. Bakker, “Biocompatibility of Polypyrrole with Human Primary Osteoblasts and the Effect of Dopants,” *PLOS ONE*, vol. 10, no. 7, p. e0134023, jul 2015. [Online]. Available: https://dx.plos.org/10.1371/journal.pone.0134023

[576] H. Castano, E. A. O’Rear, P. S. McFetridge, and V. I. Sikavitsas, “Polypyrrole Thin Films Formed by Admicellar Polymerization Support the Osteogenic Differentiation of Mesenchymal Stem Cells,” *Macromolecular Bioscience*, vol. 4, no. 8, pp. 785–794, aug 2004. [Online]. Available: http://doi.wiley.com/10.1002/mabi.200300123

[577] C. Puckert, A. Gelmi, M. K. Ljunggren, M. Rafat, and E. W. Jager, “Optimisation of conductive polymer biomaterials for cardiac progenitor cells,” *RSC Advances*, vol. 6, no. 67, pp. 62 270–62 277, 2016. [Online]. Available: http://dx.doi.org/10.1039/C6RA11682E

[578] K. Svennersten, M. Berggren, A. Richter-Dahlfors, and E. W. Jager, “Mechanical stimulation of epithelial cells using polypyrrole microactuators,” *Lab on a Chip*, vol. 11, no. 19, pp. 3287–3293, 2011.

[579] Q. Zhang, D. Esrafilzadeh, J. M. Crook, R. Kapsa, E. M. Stewart, E. Tomaskovic-Crook, G. G. Wallace, and X.-F. Huang, “Electrical Stimulation Using Conductive Polymer Polypyrrole Counters Reduced Neurite Outgrowth of Primary Prefrontal Cortical Neurons from NRG1-KO and DISC1-LI Mice,” *Scientific Reports*, vol. 7, no. 1, p. 42525, mar 2017. [Online]. Available: http://www.nature.com/articles/srep42525

[580] A. Gelmi, M. K. Ljunggren, M. Rafat, and E. W. Jager, “Influence of conductive polymer doping on the viability of cardiac progenitor cells,” *Journal of Materials Chemistry B*, vol. 2, no. 24, pp. 3860–3867, 2014.

[581] D. C. Lin, E. K. Dimitriadis, and F. Horkay, “Robust Strategies for Automated AFM Force Curve Analysis—I. Non-adhesive Indentation of Soft, Inhomogeneous Materials,” *Journal of Biomechanical Engineering*, vol. 129, no. 3, pp. 430–440, jun 2007. [Online]. Available: https://asmedigitalcollection.asme.org/biomechanical/article/129/3/430/469880/Robust-Strategies-for-Automated-AFM-Force-Curve

[582] E. Spanjaard and J. de Rooij, “Mechanotransduction: Vinculin Provides Stability when Tension Rises,” *Current Biology*, vol. 23, no. 4, pp. R159–R161, feb 2013. [Online]. Available: http://dx.doi.org/10.1016/j.cub.2013.01.020https://linkinghub.elsevier.com/retrieve/pii/S0960982213000237

[583] K. Haase and A. E. Pelling, “Investigating cell mechanics with atomic force microscopy,” *Journal of The Royal Society Interface*, vol. 12, no. 104, p. 20140970, mar 2015. [Online]. Available: https://royalsocietypublishing.org/doi/10.1098/rsif.2014.0970

[584] G. S. Zoubiane, “A role for the cytoskeleton in prolactin-dependent mammary epithelial cell differentiation,” *Journal of Cell Science*, vol. 117, no. 2, pp. 271–280, jan 2004. [Online]. Available: http://jcs.biologists.org/cgi/doi/10.1242/jcs.00855

[585] M. L. Lalli and A. R. Asthagiri, “Investigating electrotaxis of the non-transformed MCF-10A mammary epithelial cell line,” *Proceedings of the IEEE Annual Northeast Bioengineering Conference, NEBEC*, vol. 2014-Decem, no. April 2014, pp. 5–7, 2014.

[586] M. D. Treiser, E. H. Yang, S. Gordonov, D. M. Cohen, I. P. Androulakis, J. Kohn, C. S. Chen, and P. V. Moghe, “Cytoskeleton-based forecasting of stem cell lineage fates,” *Proceedings of the National Academy of Sciences of the United States of America*, vol. 107, no. 2, pp. 610–615, 2010.

[587] W. H. Goldmann, “Role of vinculin in cellular mechanotransduction,” *Cell Biology International*, vol. 40, no. 3, pp. 241–256, mar 2016. [Online]. Available: http://doi.wiley.com/10.1002/cbin.10563

[588] W. H. Goldmann, R. Galneder, M. Ludwig, W. Xu, E. D. Adamson, N. Wang, and R. M. Ezzell, “Differences in Elasticity of Vinculin-Deficient F9 Cells Measured by Magnetometry and Atomic Force Microscopy,” *Experimental Cell Research*, vol. 239, no. 2, pp. 235–242, mar 1998. [Online]. Available: https://linkinghub.elsevier.com/retrieve/pii/S001448279793915X

[589] C. Grashoff, B. D. Hoffman, M. D. Brenner, R. Zhou, M. Parsons, M. T. Yang, M. A. McLean, S. G. Sligar, C. S. Chen, T. Ha, and M. A. Schwartz, “Measuring mechanical tension across vinculin reveals regulation of focal adhesion dynamics,” *Nature*, vol. 466, no. 7303, pp. 263–266, jul 2010. [Online]. Available: http://dx.doi.org/10.1038/nature09198http://www.nature.com/articles/nature09198

Appendix with supplementary information for Chapter 2

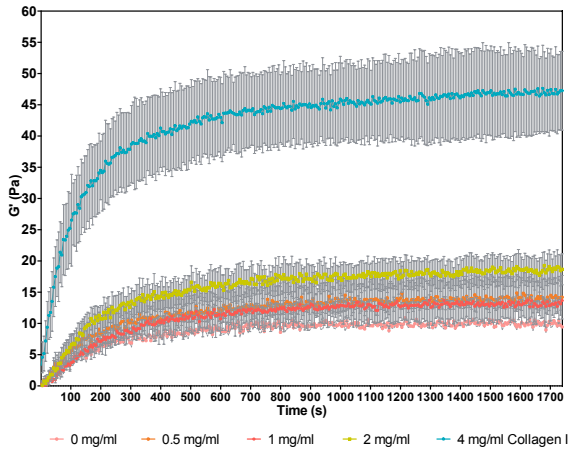

Figure A.1: Rheological measurements of matrices composed for rBM and type I collagen (0, 0.5, 1, 2, and 4 mg/ml). Plot shows a oscillatory time sweep that was performed at 37℃ using a 0.2% constant strain (within the linear viscoelastic region) and at a frequency of 3.14 rad/s. *y* axis: shear modulus G' in Pa.

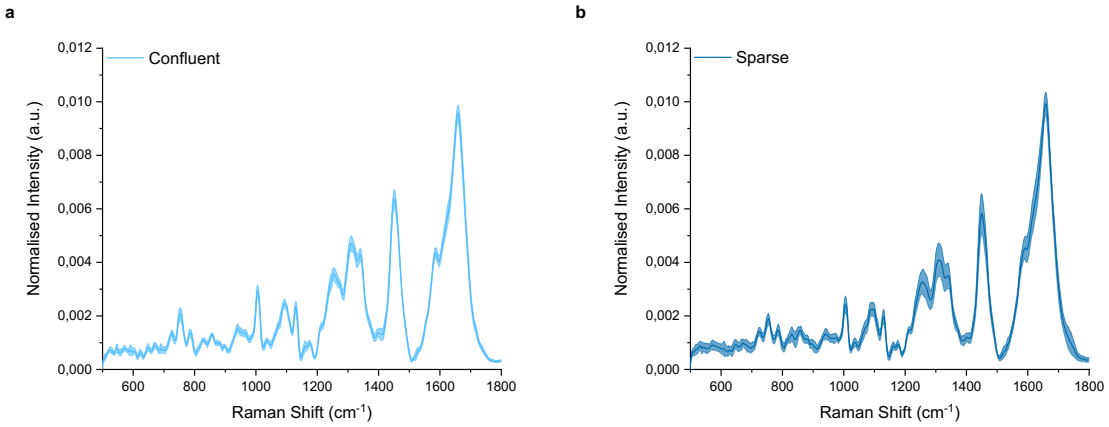

Figure A.2: Raman spectra from MCF10A cells cultured at different densities (a confluent, and b sparse) 24 hours post seeding. Mean ± SD (represented by the shaded area). Raman spectra were collected by Conor Horgan and Fergus O'Brien.

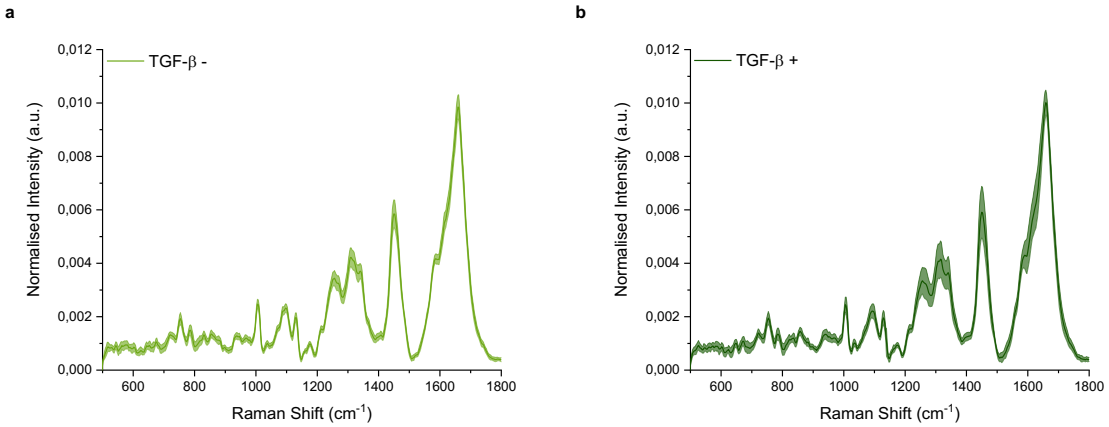

Figure A.3: Raman spectra from MCF10A cells 24 hours post TGF-β treatment (a control, and b 10 ng/ml TGF-β), 48 hours post seeding. Mean ± SD (represented by the shaded area). Raman spectra were collected by Conor Horgan and Fergus O'Brien.

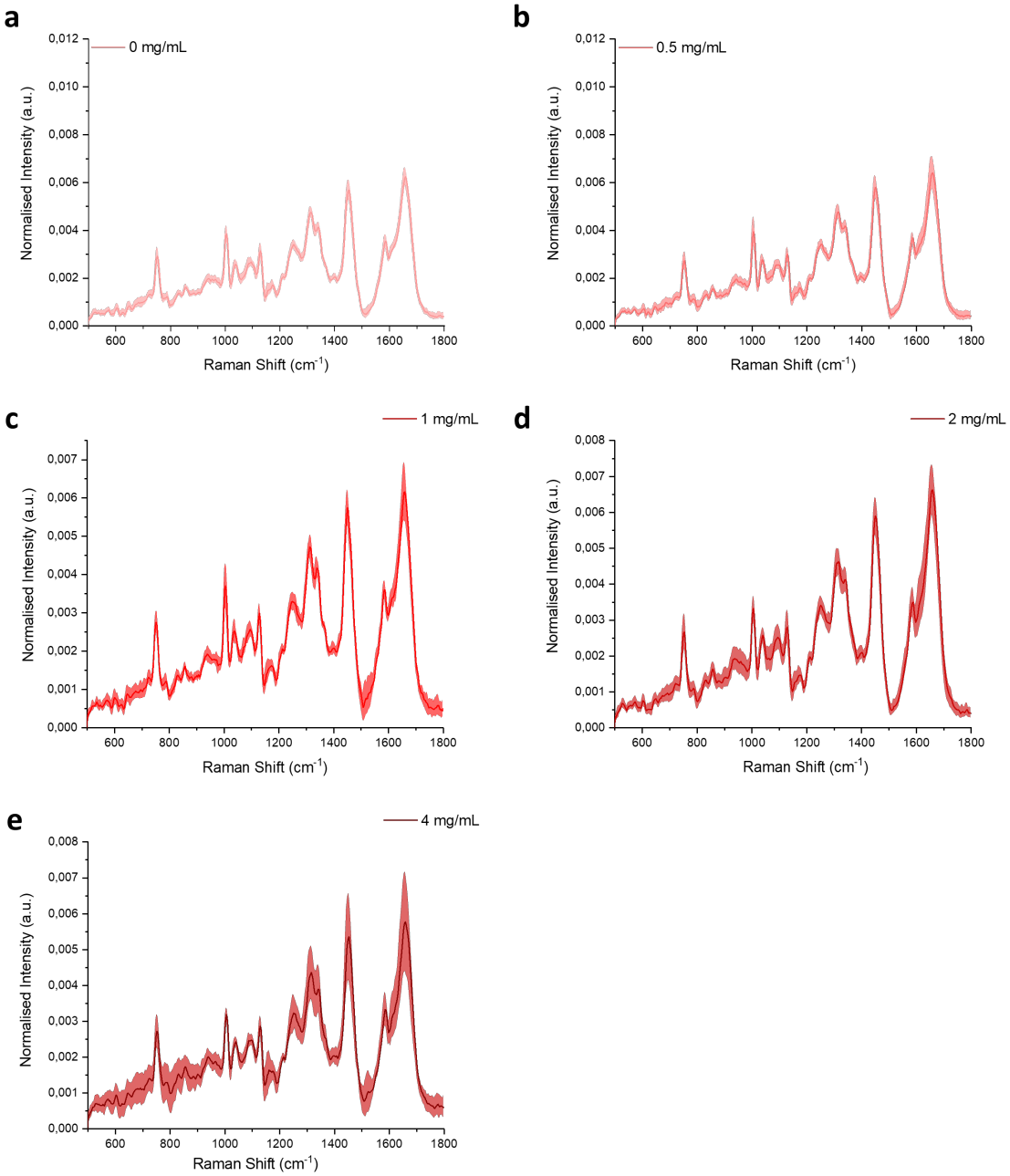

Figure A.4: Raman spectra from MCF10A cells on rBM/collagen I matrices, 1 week post seeding. **a** 0, **b** 0.5, **c** 1, **d** 2, **e** mg/ml collagen I. Mean ± SD (represented by the shaded area). Raman spectra were collected by Conor Horgan and Fergus O'Brien.

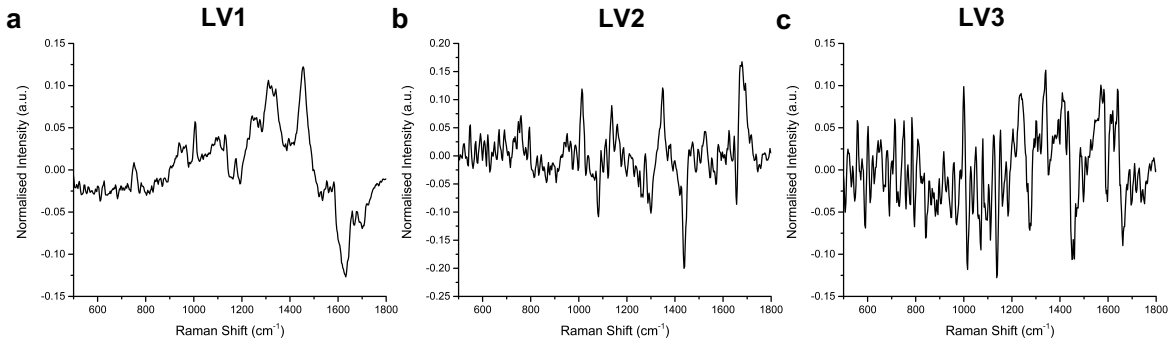

Figure A.5: Latent variable plots for PLS-DA model from MCF10A cells cultured at different densities (confluent and sparse) 24 hours post seeding. a LV1, **b** LV2, and **c** LV3. LV - latent variable.

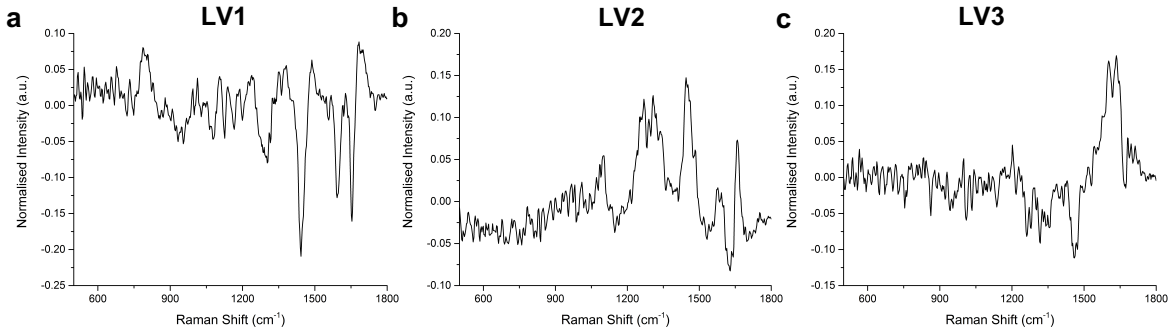

Figure A.6: Latent variable plots for PLS-DA model from MCF10A cells 24 hours post TGF-β treatment, 48 hours post seeding. a LV1, **b** LV2, and **c** LV3. LV - latent variable.

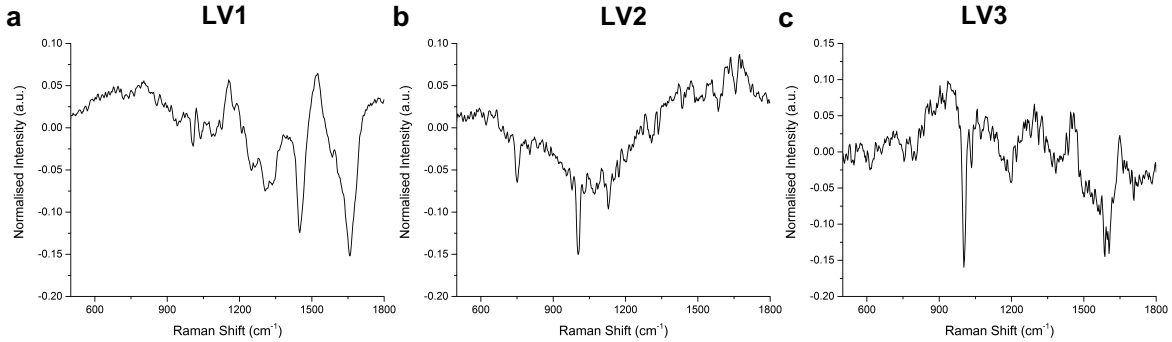

Figure A.7: Latent variable plots for PLS-DA model from MCF10A cells on rBM/collagen I matrices (0, 0.5, 1, 2, and 4 mg/ml collagen I), 1 week post seeding. a LV1, **b** LV2, and **c** LV3. LV - latent variable.

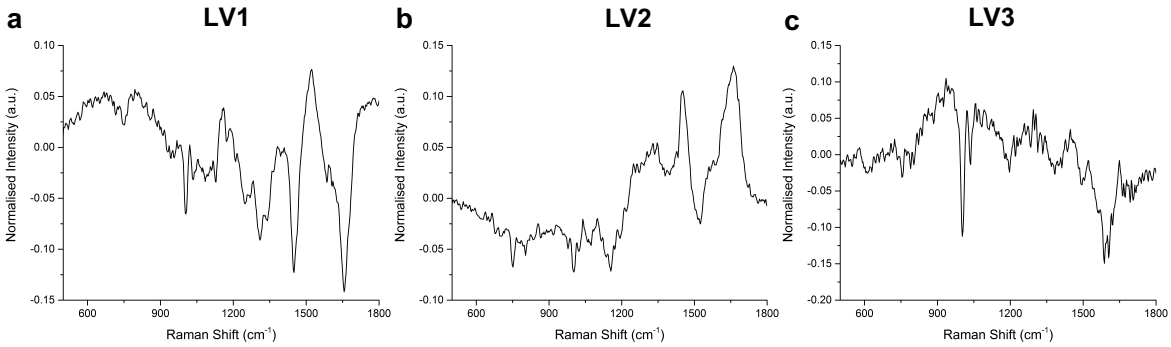

Figure A.8: Latent variable plots for PLS-DA model from MCF10A cells on rBM/collagen I matrices (0, 0.5, 2, and 4 mg/ml collagen I), 1 week post seeding. a LV1, **b** LV2, and **c** LV3. LV - latent variable.

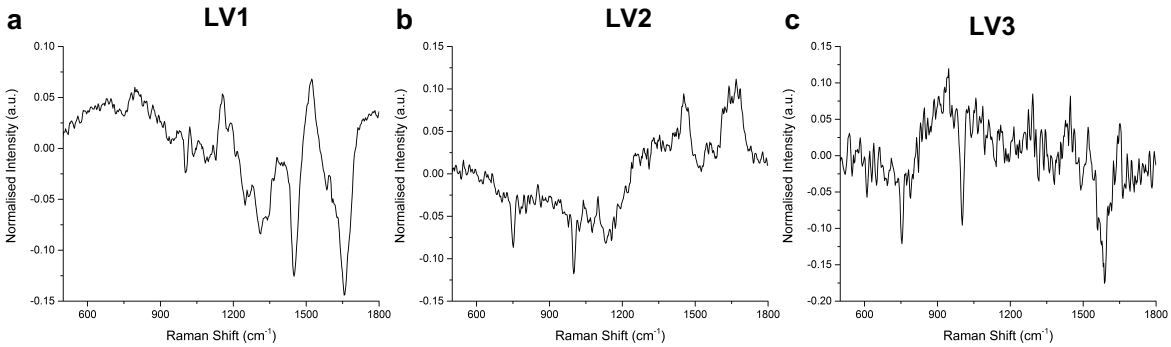

Figure A.9: Latent variable plots for PLS-DA model from MCF10A cells on rBM/collagen I matrices (0, and 4 mg/ml collagen I), 1 week post seeding. a LV1, **b** LV2, and **c** LV3. LV - latent variable.

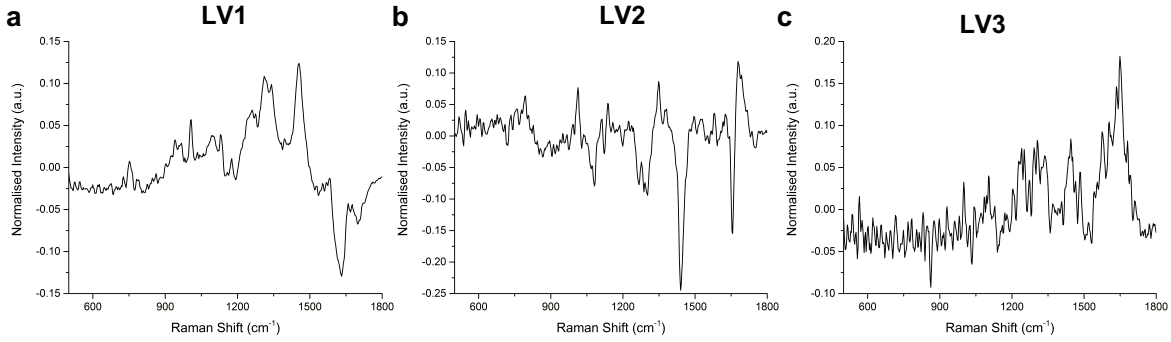

Figure A.10: Latent variable plots for PLS-DA model from MCF10A cells 2D culture - sparse versus confluent and TGF-β1 treatment. From PLS-DA model to classify the spectra of epithelial (confluent and TGF-β1-) and (quasi-)mesenchymal states (sparse and TGF-β1+) **a** LV1, **b** LV2, and **c** LV3. LV - latent variable.

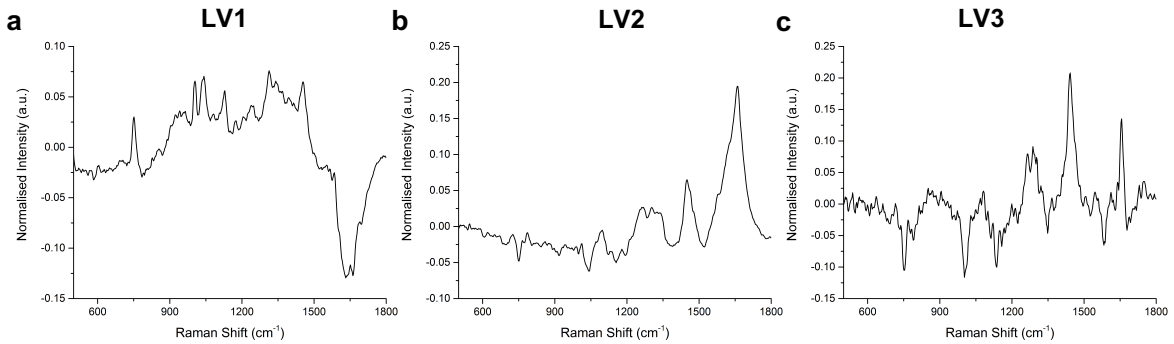

Figure A.11: Latent variable plots for PLS-DA model from MCF10A cells 2D and 3D culture. From PLS-DA model to classify the spectra of epithelial (confluent, TGF-β1-, and 0 mg/ml collagen I matrix) and (quasi-)mesenchymal states (sparse, TGF-β1+, and 4 mg/ml collagen I matrix) **a** LV1, **b** LV2, and **c** LV3. LV - latent variable.

B

Appendix with supplementary information for Chapter 3

a

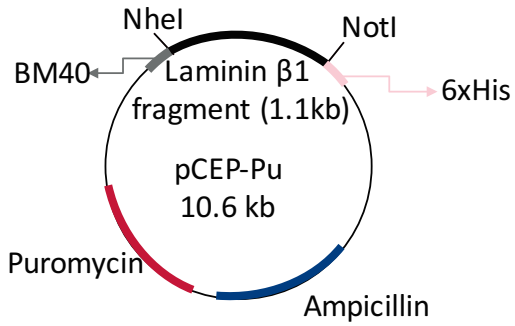

b

Laminin β1 fragment amino acid sequence

```
EPEFSYGC AEGSCYPATG DLLIGRAQKL SVTSTCGLHK PEPYCIVSHL QEDKKCFICD
SRDPYHETLN PDSHLIENVV TTFAPNRLKI WWQSENGVEN VTIQLDLEAE FHFTHLIMTF
KTFRPAAMLI ERSSDFGKAW GVYRYFAYDC ESSFPGISTG PMKKVDDIIC DSRYSDIEPS
TEGEVIFRAL DPAFKIEDPY SPRIQNLLKI TNLRIKFVKL HTLGDNLLDS RMEIREKYYY
AVYDMVVRGN CFCYGHASEC APVDGVNEEV EGMVHGHCMC RHNTKGLNCE LCMDFYHDLP
WRPAEGRNSN ACKKCNCNEH SSSCHFDMAV FLATGNVSGG VCDNCQHNTM GRNCEQCKPF
YFQHPERDIR DPNLCEPCTC DPAGSENGGI CDGYTDFSVG LIAGQCRCKL HVEGERCDVC
KEGFYDLSAE DPYGCKSCAC NPLGTIPGGN PCDSETGYCY CKRLVTGQRC DQCLPQHWGL
SNDLDGCRP
```

Figure B.1: Laminin β1 fragment - plasmid structure and amino acid sequence. **a** general structure of the plasmid carrying the laminin fragment gene for transfection of 293F HEK cells in suspension. As depicted in the figure, the fragment is produced with two flanking tags, one being a BM40 secretory peptide and the other a 6XHistidine tag for downstream purification. **b** amino acid sequence of the laminin fragment used in this study, which corresponds to a molecular weight of approximately 60kDa.

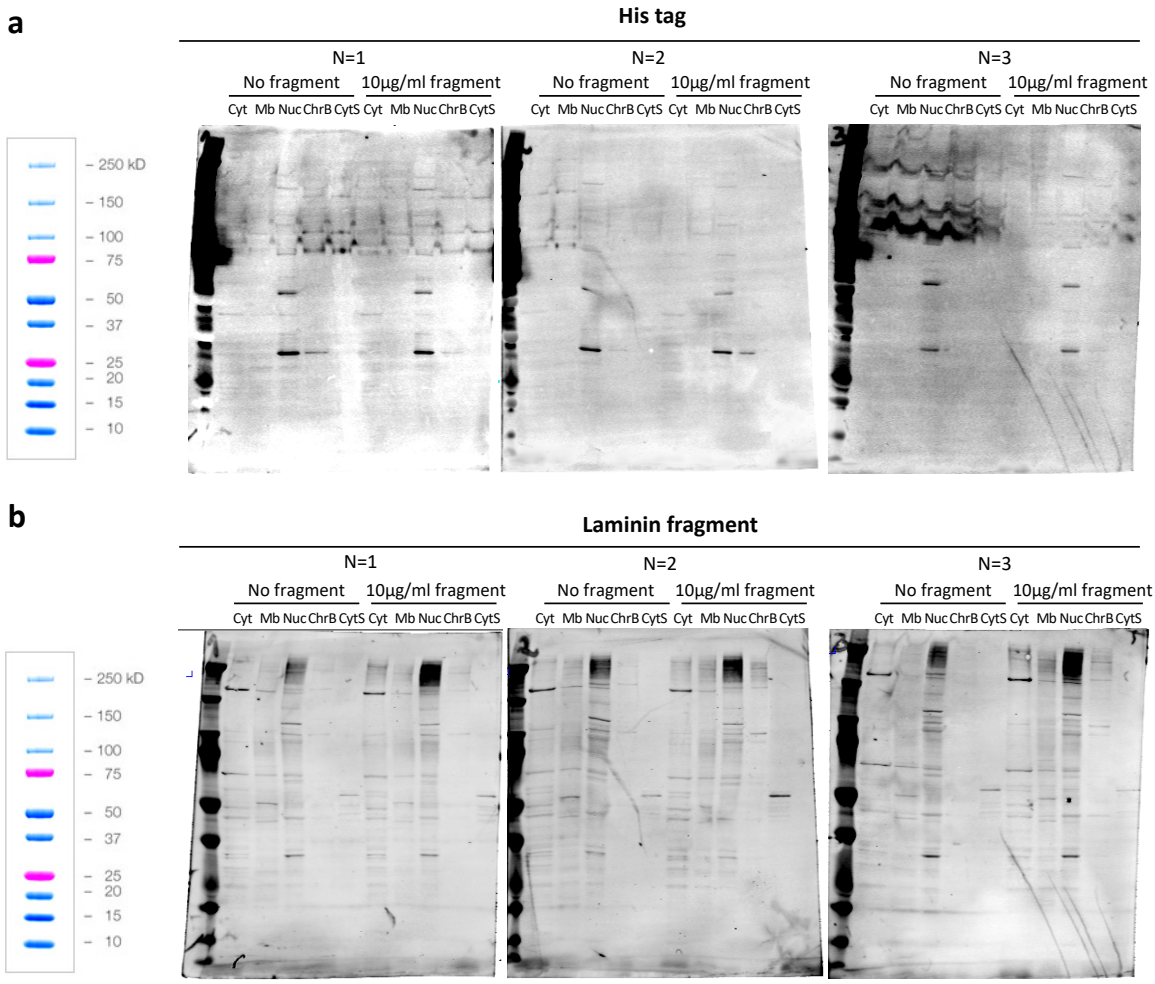

Figure B.2: Western blotting analysis of subcellular fractions from MCF10A cells treated with soluble laminin fragment. a His tag antibody, and **b** laminin fragment custom-made antibody. Cyt - cytoplasmic fraction; Mb - membrane fraction; Nuc - nuclear fraction; ChrB - chromatin-bound fraction; CytS - cytoskeletal fraction. Precision Plus Protein Dual Color Standards from Bio-Rad are shown to aid visualisation and analysis of the membranes.

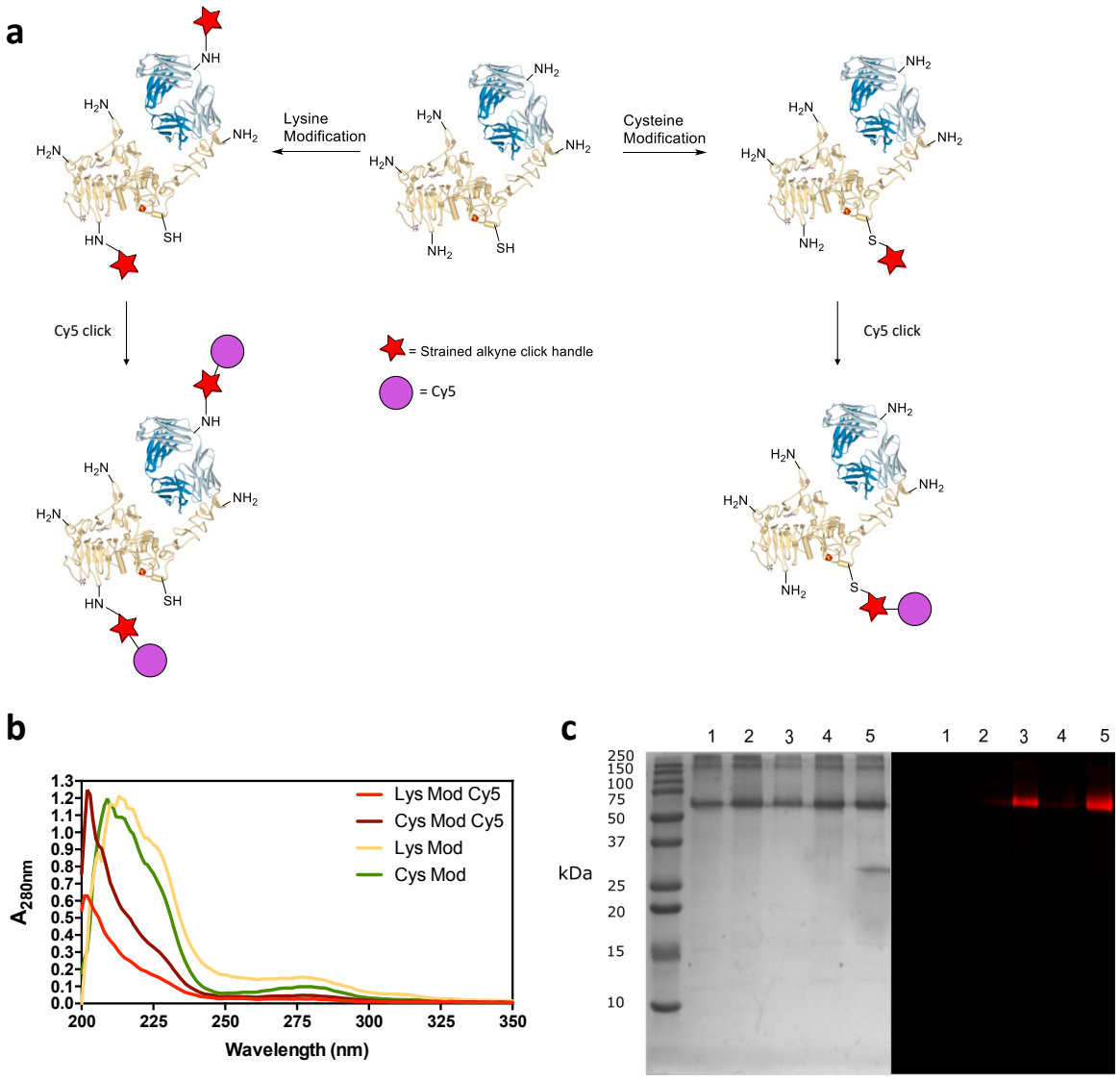

Figure B.3: Laminin Fragment Chemical Modification. **a** schematic representation of the laminin fragment chemical modification, using a SPAAC click chemistry strategy. Due to the chemical nature of the sequence of the fragment, the modification via lysine results in more fluorophore covalently attached. **b** UV-Vis curves. Lys Mod and Cys Mod mean lysine modified and cysteine modified, respectively. **c** SDS-PAGE with chemically modified fragment. Lanes: 1 - native laminin fragment, 2 - lysine modified fragment, 3 - lysine modified fragment with Cy5, 4 - cysteine modified, 5 - cysteine modified with Cy5. Chemical modification of the fragment was carried out by Dr. Daniel Richards.

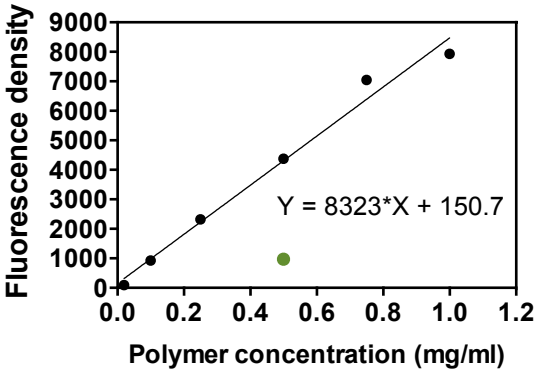

Figure B.4: Fluoraldehyde assay raw data and linear fit to determine the degree of functionalisation of GelMA. GelMA solution was prepared in PBS at 0.5 mg/ml (green datapoint). Known solutions of GelMA were prepared in PBS at different concentrations (0, 0.02, 0.1, 0.25, 0.5, 0.75 and 1 mg/ml; black datapoints). A linear equation was obtained from the known standards.

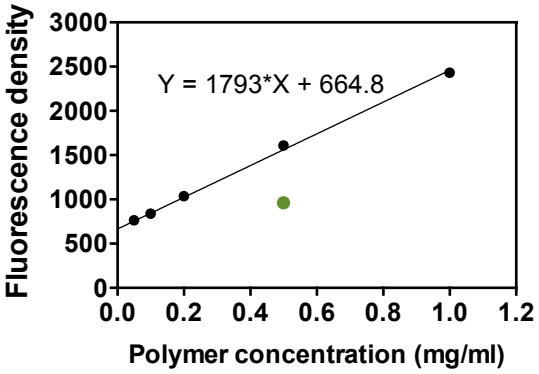

Figure B.5: Fluoraldehyde assay raw data and linear fit to determine the degree of functionalisation of GelMA-Azide. GelMA-Azide solution was prepared in PBS at 0.5 mg/ml (green datapoint). Known solutions of unmodified GelMA were prepared in PBS at different concentrations (0, 0.05, 0.1, 0.2, 0.5, and 1 mg/ml; black datapoints). A linear equation was obtained from the known standards.

C

Appendix with supplementary information for Chapter 4

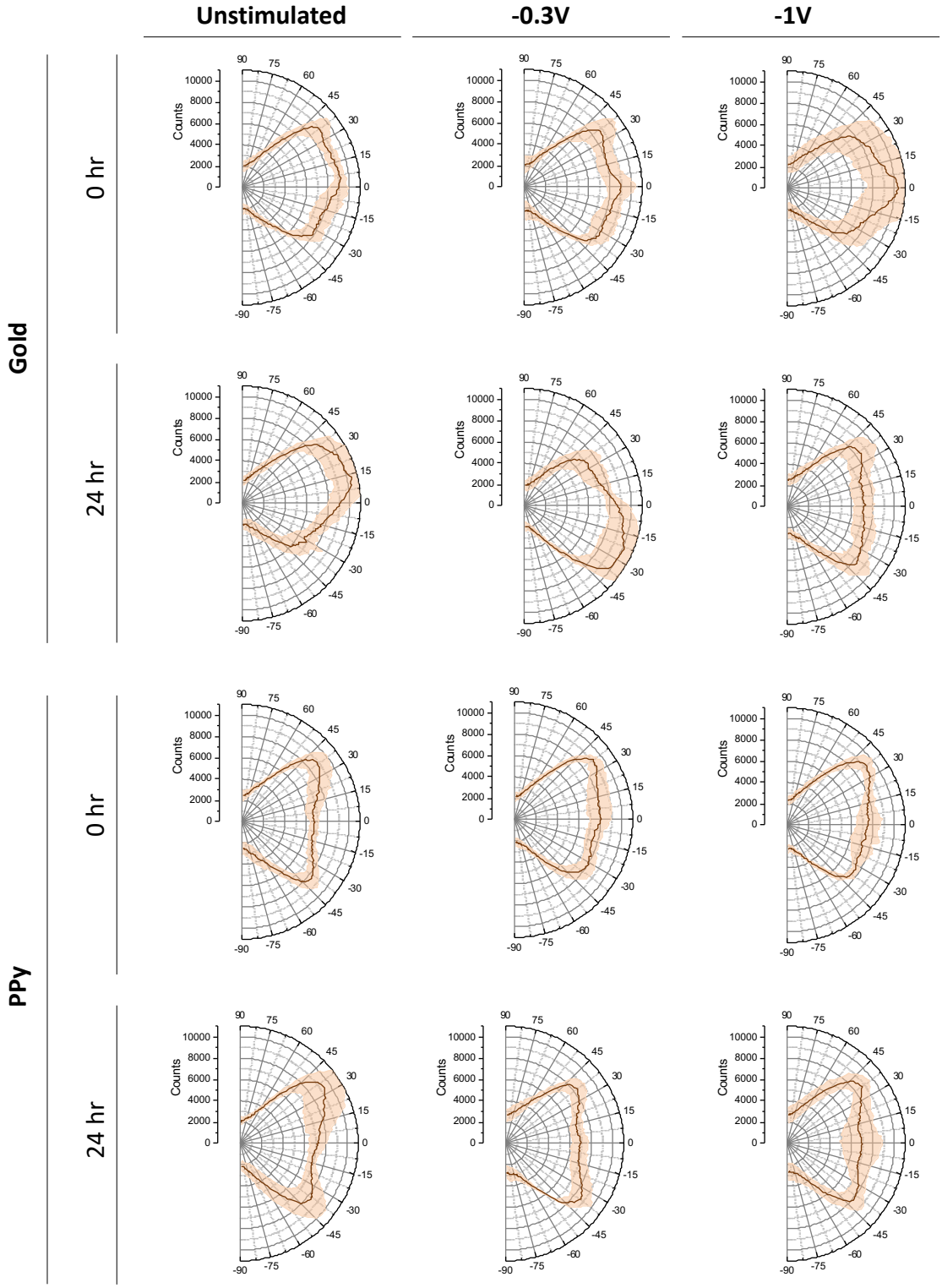

Figure C.1: Circular histogram of local orientation of actin fibers of electrically-stimulated MCF10A cells. Plots show the distribution of orientations of actin fibres (obtained from OrientationJ). Mean $\pm$ SD (represented by the shaded area).